Pharmacological and biophysical characteristics of voltage-dependent calcium channels in rat cerebellar granule neurones.

John Russell Burley

A thesis submitted in fulfilment of the
requirements for the degree of
Doctor of Philosophy
at the
University of London

February, 1997
The Royal Free Hospital School of Medicine,
Rowland Hill Street,
London NW3 2PF

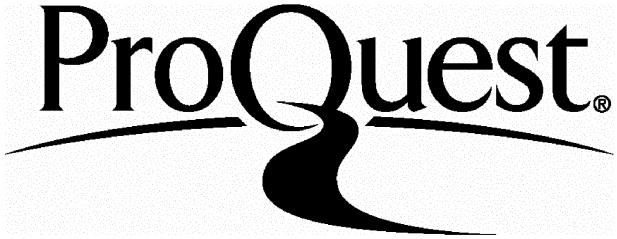

09779.

Abstract

Voltage-dependent Ca^{2+} channels were investigated in rat cerebellar granule neurones using the whole-cell variant of the patch-clamp technique. Some biophysical properties were studied and a pharmacological approach was used to characterise the component parts of the whole-cell Ca^{2+} channel current using a selection of naturally occurring toxins, Ca^{2+} channel agonists, and antagonists. The ω-CTx MVIIC-, ω-Aga IVA- and ω-CgTx GVIA-sensitive components were found to account for 45% of the total whole-cell current and these toxins exhibited overlapping sensitivity to subtypes of the Ca^{2+} channel current in these cells.

Low doses (1 μM) of the DHP antagonists nicardipine inhibited a component of the current insensitive to the toxins used and accounted for 16% of the total current, whereas high doses (100 μM) caused inhibition of a greater proportion of the current than could be solely attributed to L-type Ca^{2+} channels.

The current blocked by nicardipine in granule cells may be largely the result of L-type current, alternatively it may be blocking a non-L-type, DHP-sensitive channel. Experiments were conducted on a relatively recently cloned Ca^{2+} channel known to be expressed in granule cells. Transient expression of the α_{1E} subunit was studied in the mammalian cell line COS-7. The sensitivity of $\alpha_{1E}\backslash\beta_{1b}\backslash\alpha_2\delta$ channels to the DHP antagonist nicardipine and the agonist *s*-(-)-BayK8644 was determined. These channels were found to be inhibited by nicardipine but insensitive to *s*-(-)-BayK8644. The biophysical and pharmacological profile of this channel clone suggest that it has properties that do not fall into the existing classification of Ca^{2+} channel types. The α_{1E} channel shares some features of both LVA and HVA Ca^{2+} channels.

Changes in intracellular free Mg^{2+} caused a concentration-dependent reduction in whole-cell conductance. Some properties of currents were studied in the presence of different $[Mg^{2+}]_i$ and changes in the pharmacological components of the current were apparent. A selective, but incomplete reduction in the ω-CgTx GVIA-sensitive current was shown.

An estimation of the resting $[Mg^{2+}]_i$ in cerebellar granule cells using the Mg^{2+}-sensitive indicator MagFURA2 was 0.49 mM. A glutamate-induced increase in $[Mg^{2+}]_i$ was studied in granule cells loaded with MagFURA2.

Contents

Title 1

Abstract 2

Abbreviations 11

Chapter 1

Introduction 14

Beginnings 14
Early electrophysiology 14
Excitability depends on ion channels 15
Ca^{2+} homeostasis 16

Discovery of voltage-dependent Ca^{2+} channels 17

Three types of voltage-dependent Ca^{2+} channel with different properties 17
P-type Ca^{2+} channels isolated in Purkinje cells 20
A fourth class of Ca^{2+} current 20
A resistant component of current in cerebellar granule neurones 21

Cloning of a voltage-dependent Ca^{2+} channel from skeletal muscle 21

The structure of the Ca^{2+} channel 23

Purification of the cardiac Ca^{2+} channel 24
A DHP-sensitive Ca^{2+} channel in brain 26
Cloning of a neuronal α_1 subunit 27
DHP-sensitivity can be transferred to the α_{1A} Ca^{2+} channel 28
ω-CgTx GVIA was used to purify a neuronal Ca^{2+} channel 28
α_{1E}, a sixth class of Ca^{2+} channel 29

Accessory subunits 30

The β subunit 32
The β binding region of the α_1 subunit 33
The $\alpha_2\delta$ subunit is a single transmembrane extracellular protein 33
The γ-subunit 35

Modulation of Ca^{2+} channels 36

Modulation can occur via G-proteins 36
Phosphorylation of Ca^{2+} channels 38

Intracellular Mg^{2+} 40

A regulatory role for $[Mg^{2+}]_i$? 40
Effects on Na^+ channels 41
K^+ channels of several classes have been reported to be blocked by Mg^{2+} 41
Pumps and transporters are modulated by changes in Mg^{2+} concentration 42
Mg^{2+} alters Ca^{2+} channel function 42
Surface potential considerations 43

Cerebellar granule neurones 45

The role of the cerebellum 45
Structure of the cerebellum 45
Development of granule cells 46
Ca^{2+} channels in cerebellar granule neurones 47
$[Mg^{2+}]_i$ and $[Mg.ATP]_i$ in cerebellar granule neurones 49

Aims 50

Chapter 2

Methods 53

Culture of neonatal rat cerebellar granule neurones 53

Preparation of coverslips 53
Dissociation of granule neurones 53

Preparation of COS-7 cells 54

Transfection by electroporation 57
Replating of COS-7 cells 57
Preparation of cDNA 57
Transfection 58

Electrophysiology 58

Theory of voltage-clamp 58
Patch-clamp electronics 60
Pipette capacitance compensation 62
Whole-cell capacitance compensation 62
Series resistance compensation 63
Voltage error 64
Junction potential 64
Problems with space clamp 65
Recording 65

Voltage protocols 67
Data analysis 67

Recording solutions 72

Cerebellar granule neurones 72
COS-7 cells 74

Fluorescence-*in vivo* measurements of cell chemistry 78

Theory 79
Fluorescence microscopy 81
Magnesium imaging 83

Chapter 3

General properties of Ca^{2+} channel currents in cerebellar granule neurones 86

Results 87

Development of currents 87
Current transients 87
Ca^{2+} and Ba^{2+} currents 91
Activation, inactivation and tail current deactivation 91
Voltage-dependence of activation and steady-state inactivation 94

Discussion 98

Chapter 4

Pharmacological dissection of the Ca^{2+} channel current in rat cerebellar granule neurones using naturally occurring peptide toxins 101

Results 102

Inhibition of Ca^{2+} channel currents by ω-CTx MVIIC 102
Inhibition of Ca^{2+} channel currents by ω-Aga IVA 104
Inhibition of Ca^{2+} channel currents by ω-CgTx GVIA 106
ω-CTx MVIIC exhibits overlapping sensitivity with ω-Aga IVA and ω-CgTx GVIA 108
ω-Aga IVA and ω-CgTx GVIA exhibit overlapping selectivity 110
No evidence of a Q-type current was found in granule cells under these conditions 110

Discussion 114

Chapter 5

Effect of 1,4-dihydropyridines on Ca^{2+} channel currents in rat cerebellar granule neurones 124

Results

Inhibition of Ca^{2+} channel currents by nicardipine 125
1 μM nicardipine blocks a component of the current that is insensitive to toxins 127
Inhibition of Ca^{2+} channel currents by 10 μM nicardipine 129
Effect of BayK8644 on Ca^{2+} currents in cerebellar granule neurones. 132
Recovery from inhibition by 1 μM nicardipine 135

Discussion 139

Chapter 6

Functional expression of a rat brain cloned α_{1E} Ca^{2+} channel in COS-7 cells 147

Results

COS-7 cells are an effective expression system 148
Expression of $\alpha_{1E}/\beta_{1b}/\alpha_2\delta$ 149
Pharmacology of $\alpha_{1E}/\beta_{1b}/\alpha_2\delta$ currents 152

Discussion 155

Chapter 7

Measurements of intracellular free Mg^{2+} and the effect of this ion on Ca^{2+} channel currents in rat cerebellar granule neurones 161

Results

Characteristics of currents recorded with 0.1, 0.5 or 1.0 mM $[Mg^{2+}]_i$ 162
Effects of $[Mg^{2+}]_i$ on ω-CgTx GVIA-sensitive components of the Ca^{2+} channel current 166
The effect of ω-Aga IVA and ω-CTx MVIIC was not affected by $[Mg^{2+}]_i$. 167
$[Mg^{2+}]_i$ and DHP activity 169

Use of fluorescent probes to measure $[Mg^{2+}]_i$ 174
Determination of the resting $[Mg^{2+}]_i$ in cerebellar granule neurones by fluorescence microscopy 174
Magnesium imaging: stimulation of cerebellar granule neurones with glutamate 175

Discussion 180

Intracellular free Mg^{2+} 180
Measurements of intracellular $[Mg^{2+}]_i$ 184

Concluding remarks..... 187

Abstracts and Publications arising from this work..... 194

Acknowledgements..... 195

References..... 196

Figures

Chapter 1

Figure 1.1 Illustration of the 2-dimensional arrangement of calcium..... 31
channel subunits across the cell membrane.

Chapter 2

Figure 2.1 Electronic design of the patch-clamp amplifier..... 61
Figure 2.2 Example of current activation, inactivation and deactivation..... 69
kinetics fit by exponential functions.
Figure 2.3 A diagram of the experimental arrangement used to measure..... 84
MagFURA2 fluorescence.

Chapter 3

Figure 3.1 Photomicrograph showing cerebellar granule neurones (×400)..... 88
grown in culture for 14 days
Figure 3.2 Development of Ca^{2+} channel currents in cerebellar granule..... 89
neurones over 14 days in culture.
Figure 3.3 Analysis of current transients in cerebellar granule neurones..... 90
Figure 3.4 Comparison of Ca^{2+} channel currents carried by 10 mM..... 92
Ca^{2+} or Ba^{2+} and block by Cd^{2+}.
Figure 3.5 Activation of Ca^{2+} channel currents in cerebellar..... 93
granule neurones.
Figure 3.6 Comparison of inactivation and current-voltage relationships..... 95
in Ca^{2+} channel currents carried by Ba^{2+} and Ca^{2+}.
Figure 3.7 Steady-state inactivation properties of Ca^{2+} channel..... 97
currents in cerebellar granule neurones.

Chapter 4

Figure 4.1 Effect of ω-CTx MVIIC on Ca^{2+} channel currents in..... 103
cerebellar granule neurones.
Figure 4.2 Effect of ω-Aga IVA on Ca^{2+} channel currents in..... 105
cerebellar granule neurones.
Figure 4.3 Effect of ω-CgTx GVIA on Ca^{2+} channel currents in..... 107
cerebellar granule neurones.
Figure 4.4 Effect of the coapplication of ω-CTx MVIIC and..... 109
ω-CgTx GVIA or ω-Aga IVA on Ca^{2+} channel currents.
Figure 4.5 Time course showing the effect of consecutive application..... 111
of ω-Aga IVA and ω-CgTx GVIA on Ca^{2+} channel currents.
Figure 4.6 Effect of the application of ω-CTx MVIIC following block..... 112
of Ca^{2+} channel currents by ω-Aga IVA and ω-CgTx GVIA
Figure 4.7 Comparison of toxin-sensitive components of the Ca^{2+}..... 118
channel current in cerebellar granule cells.
Figure 4.8 Summary of the effects of ω-CTx MVIIC, ω-CgTx GVIA..... 120
and ω-Aga IVA applied singularly or in combination
to cerebellar granule cells.

Chapter 5

Figure 5.1 Effect of nicardipine on Ca^{2+} channel currents in cerebellar..... 126
granule neurones.
Figure 5.2 Block of Ca^{2+} channel currents by ω-CTx MVIIC and..... 128
1 μM nicardipine in cerebellar granule neurones.
Time course of inhibition, and effect on
current-voltage relationships.
Figure 5.3 Effect on Ca^{2+} channel currents of 10 μM nicardipine applied..... 130
to cerebellar granule neurones and effect of application of
ω-CTx MVIIC after block by 10 μM nicardipine.
Figure 5.4 Effect of 10 μM nicardipine on steady-state inactivation of..... 131
Ca^{2+} channel currents and effect of holding potential on
nicardipine block.
Figure 5.5 Sensitivity of Ca^{2+} channel currents in cerebellar granule..... 133
neurones to the DHPs *s*-(-)-BayK8644, and *r*-(+)-BayK8644.
Figure 5.6 Change in Ca^{2+} channel current kinetics in cells exposed to..... 136
s-(-)-BayK8644.
Figure 5.7 Time course of block by nicardipine and recovery from block..... 138
facilitated by a control perfusion or *s*-(-)-BayK8644.
Figure 5.8 Summary of the effects of nicardipine on Ca^{2+} channel currents.... 145
applied alone or in combination with various toxins to
cerebellar granule neurones.

Chapter 6

Figure 6.1 Ca^{2+} channel currents in COS-7 cells transiently transfected..... 150
with $\alpha_{1E}/\beta_{1b}/\alpha_2\delta$ Ca^{2+} channel subunits.

Figure 6.2 Sensitivity of Ca^{2+} channel currents in COS-7 cells expressing..... 151
$\alpha_{1E}/\beta_{1b}/\alpha_2\delta$ to the DHP antagonist nicardipine. Time course
of block and effect on the current-voltage relationship in
a single cell.

Figure 6.3 Voltage-dependence of nicardipine block in COS-7 cells..... 153
expressing $\alpha_{1E}/\beta_{1b}/\alpha_2\delta$

Figure 6.4 Some characteristics of DHP activity in COS-7 cells..... 154
expressing $\alpha_{1E}/\beta_{1b}/\alpha_2\delta$. Effect of test potential on
percentage inhibition and activation kinetics, and
application of *s*-(-)-BayK8644.

Chapter 7

Figure 7.1 Comparison of Ca^{2+} channel currents in cerebellar granule..... 164
neurones with different $[Mg^{2+}]_i$. Differences in current-voltage
relationships and steady-state inactivation.

Figure 7.2 Effect of $[Mg^{2+}]_i$ on inhibition of Ca^{2+} channel currents in..... 167
cerebellar granule neurones by ω-CgTx GVIA.

Figure 7.3 Comparison of the effect of ω-CTx MVIIC and ω-Aga IVA on..... 168
Ca^{2+} channel currents in cerebellar granule neurones with
different $[Mg^{2+}]_i$.

Figure 7.4 Comparison of the effect of DHP compounds on Ca^{2+} channel..... 170
currents in cerebellar granule neurones with different $[Mg^{2+}]_i$.

Figure 7.5 Features of *s*-(-)-BayK8644-potentiated currents in cerebellar..... 172
granule neurones recorded with different $[Mg^{2+}]_i$.

Figure 7.6 Change in MagFURA2 fluorescence (340/380 nm) in example..... 176
cells challenged with glutamate.

Figure 7.7 Phase picture and sequence of pseudocolour images showing..... 177
fluorescence (340:380 nm) before and after application of
glutamate to a region of granule cells loaded with MagFURA2.

Figure 7.8 Changes in MagFURA2 fluorescence (340:380 nm) in granule..... 179
cells in the presence or absence of extracellular Ca^{2+}.

Tables

Chapter 1

Table 1.1 Classification and some properties of calcium channel types..... 19

Table 1.2 Cloning, localisation and expression of calcium channel α_1..... 25
subunits.

Table 1.3 Cloning, localisation and properties of accessory calcium..... 34
channel subunits.

Chapter 2

Table 2.1	Composition of BSA in Earle's salts	55
Table 2.2	Composition of modified MEM used in the culture of cerebellar granule neurones.	56
Table 2.3	Intracellular solutions used for recordings from cerebellar granule neurones.	73
Table 2.4	Composition of extracellular solution used in recordings from cerebellar granule neurones.	75
Table 2.5	Extracellular and intracellular recording solutions used to record Ca^{2+} channel currents from COS-7 cells.	76
Table 2.6	Storage and supply of drugs and toxins	77
Table 2.7	Composition of Hank's Balanced Salt Solution	82

Chapter 7

Table 7.1	Summary of parameter values describing current-voltage relationships and steady-state inactivation in cells with different $[Mg^{2+}]_i$.	163

Abbreviations and symbols

A/D	analogue to digital
ADP	adenosine triphosphate
ω-Aga IA	ω-agatoxin IA
ω-Aga IIIA	ω-agatoxin IIIA
ω-Aga IVA	ω-agatoxin IVA
cAMP	cyclic adenosine monophosphate
ATP	adenosine diphosphate
ATPase	adenosine triphosphatase
BSA	bovine serum albumin
$[Ca^{2+}]_i$	intracellular free calcium concentration
C_f	feedback capacitance
C_m	whole-cell capacitance
C_p	pipette capacitance
CCD	charged coupled device
CEE	chick embryo extract
ω-CgTx GVIA	ω-conotoxin GVIA
ω-CTx MVIIA	ω-conotoxin MVIIA
ω-CTx MVIIC	ω-conotoxin MVIIC
ω-CTx MVIID	ω-conotoxin MVIID
ω-CTx SVIA	ω-conotoxin SVIA
CNS	central nervous system
DAG	diacyl glycerol
DHP	1,4-dihydropyridine
DIV	days *in vitro*
DMSO	dimethyl sulphoxide
DNA	deoxyribonucleic acid
cDNA	complementary deoxyribonucleic acid
DNase	deoxyribonuclease
DRG	dorsal root ganglion
E_{null}	null potential
EBSS	Earle's balanced salt solution
E-C	excitation-contraction
ECACC	Euoropean Collection of Animal Cell Cultures
EC_{50}	concentration for half-maximal effect
EDTA	ethylenediaminetetra acetic acid
EGTA	ethyleneglycol-bis(β-aminoethylether) N,N,N',N',-tetraacetate
FCS	foetal calf serum
FTX	extract of funnel web spider toxin
FUDR	flurodeoxyuridine
G-protein	guanosine triphosphate-binding protein
GABA	γ-aminobutyric acid
GFP	green fluorescent protein
GTP	guanosine triphosphate
GTPase	guanosine triphosphatase
GDP-β-S	guanosine-o-(2-thiodiphosphate)
HBSS	Hank's balanced salt solution
HEPES	*N*-(2 hydroxyethyl) piperazine-*N*'-(2 ethane sulphonic acid)
HS	horse serum
HVA	high voltage-activated
$I_{10\,ms}$	current 10 ms after repolarisation
I_{inst}	instantaneous tail current amplitude
IP_3	inositol trisphosphate
IP_4	inositol tetra *kis*phosphate
I-V	current-voltage

K_D	dissociation constant
kDa	kilo Daltons
LVA	low voltage-activated
$[Mg^{2+}]_i$	intracellular free magnesium
$[Mg.ATP]_i$	magnesium bound adenosine triphosphate
MEM	minimum essential medium
MW	molecular weight
NMDA	*N*-methyl-D-aspartate
NMDG	*N*-methyl-D-glucamine
P*n*	post-natal day *n*
PBS	phosphate buffered saline
PC	personal computer
PCR	polymerase chain reaction
Pen/Strep	penicillin/streptomycin
PKA	cAMP-dependent protein kinase
PKC	protein kinase C
PLC	phopholipase C
PTX	pertussis toxin
R_{acc}	access resistance
R_f	feedback resistance
R_m	input resistance
R_s	series resistance
RNA	ribonucleic acid
cRNA	complementary ribonulcleic acid
mRNA	messenger ribonucleic acid
rpm	revolutions per minute
RT-PCR	reverse transcription-polymerase chain reaction
SBTI	soybean trypsin inhibitor
s.e.m.	standard error of the mean
$\tau_{(act)}$	time constant of activation
$\tau_{(inact)}$	time constant of inactivation
$\tau_{(deact)}$	time constant of tail deactivation
TBA	tetra butylammonium salt
TEA	tetra ethylammonium salt
TTX	tetrodotoxin
$V_{50(act)}$	voltage for half activation
$V_{50(inact)}$	voltage for half inactivation

Chapter 1

Introduction

Beginnings

Three billion years after simple replicating life forms developed a lipid envelope separating the organism from its environment man has begun to understand its structure and function in the precise control of cellular constituents. This bimolecular diffusional barrier, although preventing the loss of vital cellular components also prevents the entry of essential ionised substances and the removal of ionised waste products. Evolution found solutions to this problem in the development of new transport mechanisms. Water-filled pores in the membrane allow the passage of ions at rates approaching their speed of diffusion through free solution, whose permeability can be intricately controlled by numerous processes such as the electric field across the membrane, or occupancy of a receptor site in the channel protein by a diffusible messenger molecule. In addition, numerous carrier molecules are found within the cell membrane to specifically transport ions and small molecules, sometimes against their electrical or concentration gradients.

Early electrophysiology

More than 100 years ago saw the beginning of studies that demonstrated the central role of ions in the excitability of nerve and muscle. The solutions used to perfuse the frog heart and maintain beating were investigated by Sidney Ringer (1882, 1883a,b) and found to require salts of potassium (K^+), sodium (Na^+) and calcium (Ca^{2+}) in exact proportions. This work led to investigations by Nernst (1888) into the electrical potentials that arise from solutions separated by a semi-permeable, and selectively permeable barrier. Shortly after this, Bernstein (1902, 1912) was able to propose that the membrane of excitable cells was, at rest selectively permeable to K^+ ions and during excitation became permeable to other ionic species. The 'membrane hypothesis' set the scene for the rapid development of theory during the 20^{th} century. For each physiological ion there is at least one specific role for it in the metabolic machinery. Every ion is distributed across the cell membrane precisely to give tightly controlled intracellular and extracellular

concentrations, and for every ion there is at least one carrier-like transport system coupled to the movement of another ion. These ionic pumps and co-transporters are responsible for setting up the ionic gradients that exist across the cell membrane, but their role in the excitability of the cell ends there. Excitation depends on the movement of ions through ionic channels. Most important amongst these are Na^+, K^+, Ca^{2+}, and chloride (Cl^-). Each of these ions has its own species of channel that possesses a selectivity filter restricting ion flow through it to a small class of ionic species. For example, the Ca^{2+} channel is 1000 times more selective for Ca^{2+} than for other ions.

Excitability depends on ion channels

The roles of each of the classes of ion channel can be demonstrated by considering the part they play in the conduction of impulses along nerve fibres, and the end effect of an incoming signal at the nerve ending. Pulsatile electrical impulses called action potentials are propagated along nerve axons by transient changes in ionic permeability of the cell membrane, resulting in changes in the membrane potential. The first preparation that allowed these basic changes to be studied was the squid giant axon, whose components are so large that they allow the membrane potential of the axon to be voltage-clamped, whilst the extracellular solutions are manipulated (see Hille, 1992). Experiments by Hodgkin and Huxley in the 1950's (1952a,b,c,d) showed that the action potential was propagated by a local regenerative increase in the permeability of the membrane to Na^+. As a sufficiently depolarising impulse arrives, Na^+ channels open adding to the depolarising effect. These channels are however, rapidly inactivated and the resulting Na^+ current is only transient. Depolarisation then leads to the slower opening of the delayed K^+ current, K^+ floods out of the cell down the steep concentration gradient that is maintained by the various ion pumps and transporters in the cell membrane and the cell repolarises. As the wave of depolarisation-repolarisation propagates along the axon, it arrives at the cell terminal. Depolarisation at the synaptic ending results in the opening of voltage-dependent Ca^{2+} channels (Katz and Miledi, 1967; also see Llinas, 1982). The resulting influx of Ca^{2+} leads to mobilisation of the mechanisms of neurotransmitter release, secreting onto the post-synaptic cell membrane. The

ultimate response in any excitable tissue is brought about by a rise in intracellular free Ca^{2+} ions $[Ca^{2+}]_i$. A huge range of biological responses are triggered by increasing $[Ca^{2+}]_i$. Contraction of muscle tissue, secretion of neurotransmitters, enzymes and neurohormones, and the modulation of other channel activity are all directly affected by Ca^{2+} concentration. As Ca^{2+} is of such a central importance in the integration of the activities of the cell it is not surprising that multiple mechanisms operate simultaneously to regulate its movement and concentration.

Ca^{2+} homeostasis

The regulation of $[Ca^{2+}]_i$ within carefully controlled limits is essential to the normal functioning of every cell. The $[Ca^{2+}]_i$ in neuronal cells is extremely low, around 100 nM. Extracellular Ca^{2+}, and the levels of Ca^{2+} bound in the organelles, such as the endoplasmic reticulum and the mitocondria are in the millimolar range. This high gradient is brought about by the combined actions of the Na^+/Ca^{2+} exchanger, and adenosine 5'-triphosphate (ATP)-dependent pumps on the plasma membrane and the membrane of the intracellular organelles. Buffering of $[Ca^{2+}]_i$ is also affected by Ca^{2+} binding proteins within the cell eg. calbindin, calmodulin, calcineurin, calsequestrin, calreticulin and parvalbumin. Transient elevations in Ca^{2+} can be achieved by a number of mechanisms. Extracellular Ca^{2+} can enter the cell via voltage-dependent Ca^{2+} channels, or via receptor-operated ion channels, such as the *N*-methyl-D-aspartate (NMDA) receptor. Intracellularly stored Ca^{2+} may also be released to contribute to elevations in Ca^{2+}. Two distinct pools of Ca^{2+} exist within the organelles that are released by independent mechanisms (see Berridge, 1993). The first can be stimulated to release by the binding of inositol phosphates to receptors located on the membrane of the endoplasmic reticulum. The second store is released by increases in Ca^{2+} itself. Ca^{2+}-induced Ca^{2+} release is brought about by activation of the ryanodine receptor, an important source of the massive release of Ca^{2+} from the sarcoplasmic reticulum required for contraction of muscle (Lai *et al.*, 1988a). Evidence also suggests that the inositol 1,4,5-trisphosphate (IP_3) receptor seems to have a Ca^{2+}-induced Ca^{2+} release mechanism which may contribute to the mechanism of repetitive Ca^{2+} spiking (Finch *et al.*, 1991; Iino and Endo, 1992). Sustained increases in Ca^{2+} are often deleterious to the cell. Ischaemia, and several

neurodegenerative diseases result in cell death due to failure of the corrective processes necessary to restore $[Ca^{2+}]_i$ to within normal limits (see Manev *et al.*, 1989).

Discovery of voltage-dependent Ca^{2+} channels

The first evidence for the existence of Ca^{2+} channels came shortly after the establishment of the Na^+ theory of the action potential. Fatt and Katz (1953) found by accident that in the large diameter muscle fibres of crab legs, when Na^+ ions were replaced by choline ions or tetraethylammonium acetate (TEA) the action potentials became larger and were able to propagate along the length of the fibre whereas they were weak and unable to propagate in the presence of Na^+. Excitation in crustacean muscle did not use Na^+ ions.

In 1958, Fatt and Ginsborg working with crayfish muscle showed that the TEA-induced action potential was based on the inflow of Ca^{2+}, Ba^{2+}, or Sr^{2+} ions and the higher the concentration of the divalent ion in the medium the steeper the rate of rise of the action potential and the higher the peak. We now know that the effect of the TEA, like many quaternary ammonium ions and Ba^{2+} was caused by their blocking effect on K^+ channels, preventing their repolarising action and allowing a weak Ca^{2+} influx to depolarise the membrane regeneratively.

Subsequent to these important early experiments voltage-gated Ca^{2+} channels have been found in nearly all excitable cells. Na^+ and delayed rectifier K^+ channels share several features with Ca^{2+} channels including a common evolutionary background. All have a steep voltage-dependence of and open with a delay after depolarisation. Each closes rapidly after repolarisation and shows some inactivation during a prolonged depolarisation. They also share much of their amino acid sequence with one another. The particularly interesting feature of the Ca^{2+} channel is however that they serve to translate an electrical signal into a chemical signal. Ca^{2+} influx into the cell interior controls numerous intracellular events.

Three types of voltage-dependent Ca^{2+} channel with different properties

The realisation that Ca^{2+} currents were carried by different kinds of ion channels began in 1984 when Carbone and Lux demonstrated the distinction of two classes on the basis of their voltage-dependence of activation. A low voltage activated

(LVA) current, which activated at relatively hyperpolarised potentials and inactivated rapidly could be differentiated from a high voltage activated (HVA) current that lacked rapid inactivation and could be isolated from the LVA component on the basis of these differences (Carbone and Lux 1984a,b; Kostyuk, 1986). In 1985(a), Nowycky *et al.* showed the coexistence of three types of neuronal Ca^{2+} channel in chick dorsal root ganglion (DRG) cells, and introduced a new classification. The three components were distinguished kinetically by applying depolarising test pulses from different holding potentials. From a holding potential of -40 mV, strong depolarisations were necessary to evoke an inward current. The resulting current-voltage (I-V) relationship was typical of only one current component. This current decayed very slowly and was designated 'L' for long lasting. From a holding potential of -100 mV a different picture emerged. Weak depolarisations evoked a rapidly decaying current that was maximal in amplitude at -40 mV. Due to its transient nature this component was labelled 'T'. The third component, 'N' (neither L nor T), appeared with strong depolarisations from -100 mV and showed substantial decay over 100 ms. Characterisation of the different components continued (Fox *et al.*, 1987a,b). Single channel studies in DRGs showed the T-type channels to have a conductance of 8 pS, L-type channels 25 pS, and N-type an intermediate 13 pS. Later a higher conductance of 18 pS was reported for the N-type channel (Plummer *et al.*, 1989). Each channel was also distinguishable pharmacologically. T-type currents were highly sensitive to Ni^{2+}, whereas Cd^{2+} blocked L- and N-types, sparing the T-type. The dihydropyridine (DHP) agonist BayK8644 shifted the voltage-dependence of L-type activation towards more negative potentials, and increased the probability of long channel openings (Nowycky *et al.*, 1985b). Conversely DHP antagonists, such as nifedipine strongly inhibited channel activity. The N-type component was found to be blocked irreversibly by the ω-toxin, type GVIA (ω-CgTx GVIA), from the venom of the cone snail *Conus geographus* (Kasai *et al.*, 1987; see Table 1.1). Recent evidence has prompted the re-evaluation of single N-channels in cell-attached patches from frog sympathetic neurones which were initially identified with the ω-CgTx GVIA-sensitive whole-cell N-current by Tsien *et al.* (1988). Elmslie *et al.*, (1994) recognised a novel current in these cells recorded in high Ba^{2+}, equivalent to the conditions used by Tsien *et al.* (1988) were a 40 mV shift

Classification	Kinetics	Activation threshold	Steady-state inactivation ($V_{50(inact)}$)	Single channel conductance/kinetics	Sensitivity to inorganic ions		Pharmacology	References
					Ni^{2+}	Cd^{2+}		
					EC_{50}	EC_{50}	EC_{50} or single concentration used	
T	rapid $\tau_{(inact)}$=20-50 ms	-70 mV	-70 mV	8 pS Brief burst, inactivation	✓ 30-780 µM	✓ 15-650 µM	ocatanol, non-selective block 1 µM amiloride, relatively specific 50 µM carbamazepine phenytoin flunarazine, non-selective block 1-3 µM	Fox *et al.*, 1987a.b see Huguenard, 1996
L	very slow $\tau_{(inact)}$ >500 ms	-10 mV	-20 mV	20-25 pS Continual reopening, no inactivation 3-100 ms open time	×	✓ ~1 µM	1,4-DHPs, 0.2-2 µM (-80), 0.1-5 nM (-30) Phenylalkylamines, 4 µM (-80), 1 nM (-30) Benzothiazepines, 40 µM (-80) (numbers in parentheses represent V_H)	Fox *et al.*, 1987a.b Tsien *et al.*, 1988 Catterall *et al.*, 1988 Glossman *et al.*, 1985 Hamilton *et al.*, 1987
N	moderate $\tau_{(inact)}$=50-80 ms	-30 mV	-50 mV	10-22 pS Long burst, inactivation 1 ms open time	×	✓ ~1 µM	ω-CgTx GVIA, 10 nM ω-CTx MVIIC, 18 nM rapid, reversible K_{on}=1×10^6 M^{-1}s^{-1}, K_{off}=0.04 s^{-1}	Fox *et al.*, 1987a.b Hillyard *et al.*, 1992 McDonough *et al.*, 1996 DeWaard *et al.*, 1991
P	slow	-20 mV	-5 mV	10-18 pS	×	✓ ~1 µM	ω-Aga IVA, 1-3 nM, slow on/off rates τ_{on}=13 s, τ_{off}=46 mins ω-CTx MVIIC, 100 nM, very slow on/off rates K_{on}=1.5×10^3 M^{-1}s^{-1}, τ_{off}=200 mins	Llinas *et al.*, 1989 Usowicz *et al.*, 1992 Mintz *et al.*, 1992a,b Randall *et al.*, 1995 Pearson *et al.*, 1995
G1	slow	-10 (90 Ba^{2+})	-40 mV complete	21 pS			50 nM Aga-IVA full block 3 µM ω-CTx MVIIC full block	Tottene *et al.*, 1996
Q	moderate	-20 mV	-45 mV		×	✓ ~1 µM	ω-Aga IVA, 90 nM ω-CTx MVIIC, 100 nM	Hillyard *et al.*,1992 Zhang *et al.*, 1993 Wheeler *et al.*, 1994 Randall *et al.*, 1995
R	rapid $\tau_{(inact)}$=20-30 ms	-40 mV	-15 mV		✓ 50 µM	✓ ~1 µM		Zhang *et al.*, 1993 Randall *et al.*, 1995
G2 G3	rapid rapid	-40 (90 Ba^{2+}) -30 (90 Ba^{2+})	-90 mV -90 mV	15 pS 20 pS	✓ 4 and 153 µM	✓ ~1 µM		Tottene *et al.*, 1996

Table 1.1 Some biophysical and pharmacological properties of identified Ca^{2+} channel types. Species shown under the broken line represent subtypes of Ca^{2+} channel identified in cerebellar granule neurones.

was expected between whole-cell and cell-attached recordings due to surface charge effects (see later). This current which was more likely to be carried by the 'N-channels' and not the 'ω-CgTx GVIA-sensitive N-current' on the basis of activation range, inactivation properties and the voltage-dependence of the modulatory effect of noradrenaline, was similar to the ω-CgTx GVIA-resistant novel current and showed many discrepancies to the macroscopic ω-CgTx GVIA-sensitive N-current.

P-type Ca^{2+} channels isolated in Purkinje cells

With an ever increasing number of investigations into Ca^{2+} currents in other cell types it soon became apparent that this classification was insufficient to describe the currents seen in all cases. Llinas *et al.*, (1989) isolated a new class of Ca^{2+} channel from Purkinje cells of the cerebellum. In tissue slices Ca^{2+}-dependent spikes were blocked by an extract from the venom of the American funnel web spider *Agelenopsis aperta*, (FTX). After isolation of the protein and incorporation into black lipid membranes, the channel was seen to exhibit a single channel conductance of 10-12 pS. The new channel was termed 'P'-type, as it was first described in Purkinje cells. The P-type current in Purkinje cells activated at -45 mV, and showed little time-dependent inactivation and little voltage-dependent inactivation (Usowicz *et al.*, 1992). As well as being insensitive to DHPs and ω-CgTx GVIA the P-type current was blocked by a toxin fraction from the funnel web spider, ω-Agatoxin IVA (ω-Aga IVA) (Mintz *et al.*, 1992a,b).

A fourth class of Ca^{2+} current

A number of cell types have also been shown to display current characteristics that are unlike those already discussed. A new peptide isolated from the piscivorous marine snail *Conus magus*, namely ω-conotoxin MVIIC (ω-CTx MVIIC), inhibited depolarisation-induced $^{45}Ca^{2+}$ uptake in synaptosomes, inhibited Ca^{2+} currents in cerebellar Purkinje cells, and inhibited a subset of ω-CgTx GVIA-resistant currents in CA1 hippocampal pyramidal cells (Hillyard *et al.*, 1992). In cerebellar granule neurones a current component was described that could be blocked by ω-CTx MVIIC following application of ω-Aga IVA, which it was

presumed would completely block the P-type current contribution (Randall *et al.*, 1995). Similarly, a novel component of Ca^{2+} current supporting synaptic transmission in the hippocampus from CA3 to CA1 neurones was reported to be inhibited by ω-CTx MVIIC, and to be distinct from the P-type current, but blocked by ω-Aga IVA at concentrations in excess of those required to completely block P-type channels (Wheeler *et al.*, 1994). This novel component was termed 'Q'-type (Zhang *et al.*, 1993). In binding studies, rat brain has been shown to contain a high affinity binding site for ω-CTx MVIIC, which binds with a much higher affinity than ω-CTx MVIICs affinity for the N- or P-type Ca^{2+} channels (Hillyard *et al.*, 1992; Adams *et al.*, 1993). This putative 'O'-type Ca^{2+} channel may be closely related to the proposed Q-type channel of cerebellar granule cells or the P-type channel of Purkinje cells since they are both blocked by ω-Aga IVA and ω-CTx MVIIC though with differing affinities (Olivera *et al.*, 1994). Adams *et al.*, (1993) proposed that these channel types may form an 'OPQ' superfamily.

A resistant component of current in cerebellar granule neurones

A sixth channel type was suggested by Zhang *et al.* (1993) which represented a component of current remaining in cerebellar granule cells after pharmacologically removing the other components. This current, termed 'R'-type because of its resistance to conventional Ca^{2+} antagonists, was rapidly decaying and sensitive to Ni^{2+}.

Cloning of a voltage-dependent Ca^{2+} channel from skeletal muscle

Isolation and structural determination of voltage-dependent Ca^{2+} channels was primarily hindered by the low density of ion channels in the membrane of excitable cells. Initially, studies were limited to tissues where a high localised expression of channels occurred. Skeletal muscle has a particularly high density of Ca^{2+} channels restricted to the transverse tubule system (Sanchez and Stefani, 1978) and the skeletal muscle DHP-sensitive Ca^{2+} channel was the first subtype to be purified. High affinity binding sites for three groups of Ca^{2+} channel antagonists were found to be present in high concentration in transverse tubule membranes (Glossman *et al.*, 1983; Galizzi *et al.*, 1984) and inhibited Ca^{2+}

channels in skeletal muscle fibres (see Almers *et al.*, 1985). These were for the 1,4-DHPs e.g. nicardipine, the phenylalkylamines e.g. verapamil, and the benzothiazepines e.g. diltiazem. Data from binding studies supported a model of the Ca^{2+} antagonist receptor having three separate, allosterically linked binding sites for Ca^{2+} antagonist drugs (Glossman *et al.*, 1985; Garcia *et al.*, 1986). Curtis and Catterall (1984) and Borsotto (1984, 1985) independently developed purification techniques based on the finding that the DHP receptor was a glycoprotein and could be purified by affinity chromatography on immobilised lectin columns. Analysis of these preparations by several laboratories revealed three non-covalently associated subunits which comigrated with DHP binding activity. These were the α polypeptide of 162 kDa which shifted to a lower apparent size after reduction of disulphide bonds indicating heterogeneity, the β of 50 kDa, and the γ of 33 kDa (Curtis and Catterall, 1984; Striessnig *et al.*, 1986; Flockerzi *et al.*, 1986). The purified receptors could be incorporated into phospholipid vesicles and acted as functional Ca^{2+} channels. BayK8644 increased the rate of $^{45}Ca^{2+}$ uptake into the vesicles 2- to 3-fold, and PN200-110, a DHP inhibited the response in concentrations that blocked Ca^{2+} currents in transverse tubule membranes (Curtis and Caterall, 1986). The heterogeneous α band from the purification process was more recently resolved after reduction of disulphide bonds into two distinctly different proteins (Vaghy *et al.*, 1987). The α_1 subunit had an apparent size of 175 kDa after reduction of disulphide bonds and contained binding sites for DHPs and verapamil. Binding of a hydrophobic photoaffinity probe indicated it had multiple transmembrane domains (Takahashi *et al.*, 1987). In contrast, the α_2 had an apparent size of 135-150 kDa after reduction, and contained no receptor sites for Ca^{2+} channel antagonists. The α_2 subunit was found to be linked by a disulphide bond to a 24-29 kDa δ subunit. The $\alpha_2\delta$ subunit was shown to be extensively glycosylated and contained few transmembrane regions (Takahashi *et al.*, 1987; Barhanin *et al.*, 1987; Schramm *et al.*, 1983). The remaining subunits, designated β and γ, were found to be associated with the α_1 subunit. The β subunit was not glycosylated and not labelled by photoaffinity probes, suggesting that it was located intracellularly. The γ subunit however was

shown to be both heavily labelled by photoaffinity probes and glycosylated, suggesting a transmembrane location (Takahashi *et al.*, 1987).

An important study was performed by Tanabe *et al.* (1988) showing that an expression plasmid carrying complementary deoxyribonucleic acid (cDNA) encoding the DHP receptor of skeletal muscle could restore excitation-contraction (E-C) coupling and slow Ca^{2+} currents when microinjected into cultured muscle cells from mice with muscular dysgenesis. This showed that muscular dysgenesis results from a mutation altering the function of the DHP receptor and that in the transverse tubule membrane this protein functions both as the voltage-sensor for E-C coupling and as a slow Ca^{2+} channel.

Expression studies using stably transfected mouse L-cells, (microinjection of complementary ribonucleic acid (cRNA) into *Xenopus* oocytes failed to produce functional Ca^{2+} channels, even when coinjected with auxiliary subunits), showed that in the absence of other subunits, the α_{1S} led to the appearance of functional ion channels whose kinetics were surprisingly slow (Perez-Reyes *et al.*, 1989). When the skeletal muscle β subunit was coexpressed, the current was normalised in terms of kinetics (Lacerda *et al.*, 1991). Additionally a five-fold increase in the number of DHP binding sites was observed, without a corresponding increase in current density.

The structure of the Ca^{2+} channel

The Na^+ channel and the DHP-sensitive Ca^{2+} channel were the first two voltage-operated ion channels to be purified and characterised. Tanabe *et al.* (1987) isolated cDNA clones coding for the α_1 subunit of the Ca^{2+} channel and deduced its primary structure, which was seen to be 55% homologous to the Na^+ channel α subunits in terms of sequence, and shared much similarity with K^+ channel subunits. Both the Na^+ and Ca^{2+} channel subunits contain four homologous domains (I-IV), containing multiple hydrophobic, membrane spanning α-helical sequences (S1-S6), the fourth transmembrane was found to contain a positively charged amino acid at every third or fourth position which led to a hypothetical role being assigned to this region as a voltage sensor (see Catterall *et al.*, 1993), and it has been possible to measure the movement of gating charge through the

membrane as an outward current (Armstrong, 1981). The prediction that these positive charges serve as a gating current has been tested by mutugenesis and expression studies of both Na^+ and K^+ channels. Neutralisation of the positively charged residues in the fourth transmembrane domain has major effects on the voltage-dependence of activation (Stühmer *et al.*, 1989). For the S4 segments to move through the protein structure during activation, the size and shape of the hydrophobic residues would also be assumed to be important. Mutation of hydrophobic residues can cause dramatic shifts in the voltage-dependence of gating. In the voltage-dependent Na^+ channel encoded by the rat IIa clone a single change in the S4 region caused a 20 mV shift (Auld *et al.*, 1991). Similarly, mutation of residues in the S4 segments of the Shaker K^+ channel can cause up to a 80 mV change in the voltage dependence (McCormack *et al.*, 1991).

Computer modelling of the voltage-dependent ion channel α_1 subunit predicts that in all four homologous repeats a putative extracellular loop between transmembrane domains S5 and S6 forms a α-helical hairpin loop (SS1) connected to a β-structure (SS2), which bends back into the membrane via strictly conserved regions (Guy and Conti, 1990; Varadi *et al.*, 1995). The SS1-SS2 loop, or P-loop is thought to form the lining of the pore and interact directly with the permeant ions, even small alterations in the amino acid residues in this region have crucial effects on ion conductance and selectivity. Mutation of only two highly conserved amino acid residues at the mouth of the pore region, amongst areas of predominantly negative charge in the Na^+ channel is sufficient to confer Ca^{2+} channel-like permeability properties, suggesting this region has importance as the ion selectivity filter of the channel (Heinemann *et al.*, 1992). The equivalent positions in the Ca^{2+} channel sequence are also highly conserved and are presumed to have a similar role. Replacement of glutamate residues within the SS2 region of the S5-S6 linker in motif I or III produced a mutant Ca^{2+} channel that was 10-fold more permeable to Na^+, and the resulting Na^+ currents could be modulated by DHPs (Tang *et al.*, 1993b).

Purification of the cardiac Ca^{2+} channel

Purification of the cardiac Ca^{2+} channel was hindered by the lower density of DHP binding sites in the sarcolemmal membrane from the heart. These studies

Clone	cDNA	Localisation	References	Expression	Pharmacology	References
α_{1A}	CaCh 4 BI rbA	brain, esp. cerebellum, hippocampus, olfactory, cortex heart, kidney GH4C1, PC12, C-cells	Starr *et al.*, 1991 Mori *et al.*, 1991 Stea *et al.*, 1994 Westernbroek *et al.*, 1995	*Xenopus* oocytes	Cd^{2+} ω-Aga IVA, ω-CTx MVIIC BayK8644 crude A. *aperta* venom	Stea *et al.*, 1994 Mori *et al.*, 1991 Sather *et al.*, 1993
α_{1B}	CaCh 5 rbB BIII doe-II	brain, esp. dorsal cerebral cortex, forebrain, midbrain, hippocampus, hypothalamus, thalamus, olfactory bulb PC12, C-cells marine ray	McEnery *et al.*, 1991 Horne *et al.*, 1991 Dubel *et al.*, 1992 Witcher *et al.*, 1993 Westernbroek *et al.*, 1992	Hek 293 cells Skeletal muscle myotubes *Xenopus* oocytes	Cd^{2+} ω-CgTx GVIA ω-CTx MVIIC	Williams *et al.*, 1992a Fujita *et al.*, 1993 Stea *et al.*, 1993 Brust *et al.*, 1993
α_{1C}	CaCh 2 pCARD3 psCal rbC Vsmα_1	cardiac brain, esp. cerebrum, cerebellum, olfactory aorta, trachea, lung, kidney GH4C1, PC12, C-cells	Mikami *et al.*, 1989 Biel *et al.*, 1990 Koch *et al.*, 1990 Snutch *et al.*, 1991 Hell *et al.*, 1993a	*Xenopus* oocytes	Cd^{2+} DHP agonists DHP antagonists	Mikami *et al.*, 1989 Biel *et al.*, 1990 Wei *et al.*, 1991
α_{1D}	CaCh 3 CACN4 RBα_1	brain, esp. cerebrum, cerebellum, hippocampus pancreas, kidney, ovary cardiac/skeletal muscle (trace) GH4C1, PC12, C-cells	Perez-Reyes *et al.*, 1989 Hui *et al.*, 1991 Seino *et al.*, 1992 Williams *et al.*, 1992b Yu *et al.*, 1992 Hell *et al.*, 1993a	*Xenopus* oocytes	Cd^{2+} DHP agonists DHP antagonists (ω-CgTx GVIA?)	Williams *et al.*, 1992
α_{1S}	CaCh 1	skeletal muscle	Tanabe *et al.*, 1987 Perez-Reyes *et al.*, 1989 Lacerda *et al.*, 1991 Varadi *et al.*, 1991	L cells	Cd^{2+} DHP agonists DHP antagonists	Perez-Reyes *et al.*,1989
α_{1E}	CaCh 6 rbEII BII doe-1	brain, esp. olfactory bulb, cerebellum marine ray	Soong *et al.*, 1993 Horne *et al.*, 1993 Williams *et al.*, 1994 Schneider *et al.*, 1994 Niidomoe *et al.*, 1992 Yokoyama *et al.*, 1995	*Xenopus* oocytes COS-7 cells	Cd^{2+} Ni^{2+} ω-Aga IVA amiloride methoxyverapamil/diltiazem D-600 crude A. *aperta* venom	Ellinor *et al.*, 1993 Williams *et al.*, 1994 Wakamori *et al.*, 1994 Soong *et al.*, 1993 Schneider *et al.*, 1994 Stephens *et al.*, 1997

Table 1.2. Cloning and expression of calcium channel α_1 subunits.

identified three subunits similar in molecular weight to the α_1, $\alpha_2\delta$, and β subunits from skeletal muscle. cDNA was cloned from rabbit heart cDNA libraries using low stringency hybridisation with a skeletal muscle cDNA probe (Mikami *et al.*, 1989). The α_{1C} channel protein was 66 % similar to the α_{1S} subunit. Additionally, it was also expressed in a number of other tissues, (see Table 1.2). On comparison of the published sequences, it appears that the α_{1C} gene is alternatively spliced in six regions and both variants of particular forms are expressed in numerous tissues (Perez-Reyes *et al.*, 1990). However, a long form of the amino terminus is a cardiac specific feature (Biel *et al.*, 1991).

Injection of α_{1C} cRNA into *Xenopus* oocytes led to the appearance of Ca^{2+} channel currents that were sensitive to DHPs, in contrast with the stable transfection system first used required to express α_{1S}, oocytes provided an easy method of investigating the effect of auxiliary subunits. Mikami *et al.* (1989) showed that the $\alpha_2\delta$ increased currents two-fold, without change in the channel properties. Similar findings were described for the lung variant of α_{1C} (Biel *et al.*, 1990). Coexpression with all βs not only caused an increase in the amplitude of currents, but shifted the voltage-dependence of activation, and accelerated the rate of activation (Wei *et al.*, 1991). Coexpression of the γ subunit had no effect in oocytes.

A DHP-sensitive Ca^{2+} channel in brain

A third DHP-sensitive Ca^{2+} channel was cloned by various methods by several groups (Hui *et al.*, 1991; Williams *et al.*, 1992b; Seino *et al.*, 1992; Perez-Reyes *et al.*, 1990; Yaney *et al.*, 1992). The deduced sequence was found to be 70% identical to α_{1C}, and showed similarities in the location of alternatively spliced regions. A novel splice variant of the carboxy terminus was discovered which was considerably shorter than any other to have been cloned, (the carboxy terminus can make up to 30% of the channel protein). As well as being expressed in pancreas (Seino *et al.*, 1992; Yaney *et al.*, 1992), it was also seen in brain (Hui *et al.*, 1991; Williams *et al.*, 1992b), kidney (Yu *et al.*, 1992) and ovary (Perez-Reyes *et al.*, 1990).

Expression of a human α_{1D} in *Xenopus* oocytes (Willliams *et al.*, 1992) did not lead to detectable currents. However, coinjection with $\alpha_2\delta$ and β led to DHP-sensitive currents being expressed. Surprisingly, when $\alpha_2\delta$ and β subunits were injected alone DHP-insensitive currents were seen suggestive of the presence of endogenous currents that can be boosted by overexpression of accessory subunits. In addition, currents resulting from expression of α_{1D}, $\alpha_2\delta$ and β were partially inhibited by ω-CgTx GVIA. A likely explanation for this anomalous result is that ω-CgTx GVIA was blocking the endogenous oocyte channel (Lacerda *et al.*, 1994). Oocytes appear to express both an N-type and a T-like channel (Lacerda *et al.*, 1994).

Cloning of a neuronal α_1 subunit

The skeletal muscle α_{1S} sequence was also used to clone a fourth Ca^{2+} channel from rabbit and rat brain cDNA libraries (Mori *et al.*, 1991; Starr *et al.*, 1991). The α_{1A} shared 40 % sequence identity with the α_{1S}. Generally, membrane spanning regions were well conserved, but connecting loops were not. The distribution of α_{1A} is largely limited to the brain, where it occurs at high density in the cerebellum, in particular the Purkinje cells, and much lower levels in the kidney and heart (Mori *et al.*, 1991; Starr *et al.*, 1991). Functional expression in oocytes led to small currents that were increased three-fold by $\alpha_2\delta$, twenty-fold by β, or over two hundred-fold by coexpression with both $\alpha_2\delta$ and β (Mori *et al.*, 1991), indicating a synergy between the subunits. The pharmacology of the α_{1A}-induced currents was unusual in that they were insensitive to DHPs and ω-CgTx GVIA, but could be blocked by a crude extract from the venom of the funnel web spider. Sather *et al.* (1993) later showed that the expressed channel was inhibited by ω-Aga IVA which was thought to be specific for P-type channels. This result, together with its distribution in cerebellar Purkinje cells suggested that α_{1A} may correlate to the P-type Ca^{2+} channel. However, P-type channels in Purkinje cells were one hundred-fold more sensitive to ω-Aga IVA than α_{1A} currents in oocytes, and had differing kinetics, inactivating far more slowly (Sather *et al.*, 1993). Secondly, α_{1A} currents were shown to be ten-fold more sensitive to ω-CTx MVIIC. These differences may be accounted for as a result of other differences,

such as post-translational modifications, splice variation, or subunit coexpression, or the clone may represent a new, or different class of channel.

DHP-sensitivity can be transferred to the α_{1A} Ca^{2+} channel

Elucidation of the structural details of the DHP binding domains was carried out by Grabner *et al.* (1996) in experiments were they constructed chimeric Ca^{2+} channels based on the sequence from the α_{1A} subunit. The sensitivity to both DHP agonists and antagonists was successfully transferred to the otherwise insensitive class A Ca^{2+} channel. The minimum sequences for agonist/antagonist sensitivity were shown to be slightly different. For DHP agonist activity domains IIIS5 and IIIS6 together with the IIIS5-6 loop, and the IVS5-6 loop and the IVS6 transmembrane domain were essential. For DHP antagonist activity the IIIS5 and IIIS6 regions with the IIIS5-6 loop, and the IVS5-6 loop alone were necessary. Sequence analysis within these minimum motifs showed clusters of residues that are conserved in all L-type channels and are also identical within all non-L-type channels. Mutational analysis will undoubtedly reveal more exact sequence points involved in DHP interactions. In addition to DHP effects in these chimeric Ca^{2+} channels the effects of ω-Aga IVA were also studied. The class A subunit expressed in oocytes gives rise to currents that are blocked by ω-Aga IVA (Sather *et al.*, 1993; Stea *et al.*, 1994). Introduction of L-type sequence into the α_{1A} sequence did not effect the sensitivity to this toxin suggesting that the two pore-forming linkers of α_{1A} which were replaced by L-type sequences to produce DHP sensitivity are insignificant for toxin binding.

ω-CgTx GVIA was used to purify a neuronal Ca^{2+} channel

The high affinity of ω-CgTx GVIA for the N-type Ca^{2+} channel was used as a tool in its purification (McEnery *et al.*, 1991; Witcher *et al.*, 1993). Like the L-type channels α_{1B} purified with $\alpha_2\delta$ and β (β_3). Other proteins also purified with the ω-CgTx GVIA receptor, namely syntaxin and synaptotagmin (Leveque *et al.*, 1994), and the α subunit of guanosine triphosphatase (GTPase)-binding protein (G-protein) G_o (McEnery *et al.*, 1991). A similar cDNA has also been cloned from the marine ray *Discopyge ommata* (Horne *et al.*, 1991).

In situ hybridisation and polymerase chain reaction (PCR) analysis has shown a complete absence from peripheral tissues. In the brain it occurs at highest density in the dorsal cerebral cortex, hypothalamus, thalamus, hippocampus and olfactory, although species differences exist (Fujita *et al.*, 1993; Dubel *et al.*, 1992).

Expression of α_{1B} has been carried out in numerous systems. In oocytes, expression of the rbB-I clone from the rat produced currents that activated and inactivated extremely slowly (τ_{act}=65 ms, 15-20% inactivation over 800 ms expressed with $\alpha_2\delta$ and β_{1b}, Stea *et al.*, 1993). In the mammalian HEK293 cell line, expression of a human α_{1B} produced currents whose kinetics were much faster (τ_{act}~2 ms, half inactivation occurred in ~150 ms, Williams *et al.*, 1992a), as did expression of the rabbit BIII clone in cultured skeletal muscle myotubes from the mouse (Fujita *et al.*, 1993). Although similar differences have been noted between oocytes and other expression systems for other channel subtypes which maybe due to post-translational modification there appear to be species-specific differences in the kinetic properties of Ca^{2+} channel clones. In agreement with other coexpression studies $\alpha_2\delta$ and β subunit coexpression produced the largest currents and the most ω-CgTx GVIA receptors (Brust *et al.*, 1993).

<u>α_{1E}, a sixth class of Ca^{2+} channel</u>

A sixth class of Ca^{2+} channel was cloned by using PCR with primers based on conserved sequences (Soong *et al.*, 1993; Schneider *et al.*, 1994), or by screening a rat brain cDNA library with α_{1A} cDNA as a probe (Niidome *et al.*, 1992). A similar cDNA was also cloned from marine ray (Horne *et al.*, 1993). As with the other clones, a number of alternative splice variants of the carboxy terminus and intracellular loops have been cloned (Niidome *et al.*, 1992). The II-III loop contained a number of insertion/deletion sites and a motif also found in the α_{1B}. This particular motif may well have a role in channel inactivation since a similar sequence occurs in the Shaker K^+ channel inactivation ball. This loop is also the site of many consensus phosphorylation sites and two putative EF-hand Ca^{2+} binding domains (Schneider *et al.*, 1994). The α_{1E} gene appears to be exclusive to the central nervous system (CNS), significant expression occurs in the olfactory bulb, cortex, hippocampus, and cerebellum (Niidome *et al.*, 1992; Soong *et al.*,

1993). Expression studies showed that injection of α_{1E} alone was sufficient to produce robust Ca^{2+} channel currents (Schneider *et al.*, 1994). The coexpression of the β subunit had little effect on the peak currents but caused a shift in the voltage-dependence of activation, and inactivation towards more negative potentials. Currents activated and inactivated more rapidly (Ellinor *et al.*, 1993). Under the same conditions and employing the same charge carrier, α_{1E} activated 15 mV more negative than α_{1C} (Soong *et al.*, 1993). This led to suggestions that α_{1E} was a LVA channel. However, the single channel conductance of the α_{1E} currents was 14 pS (Schneider *et al.*, 1994), compared to 8 pS for the T-type channel (Tsien *et al.*, 1988). Secondly, T-type currents activate around 50 mV more negative than L-type channels. The pharmacology of α_{1E} was found to be strikingly different to other channels already characterised. DHPs and conotoxins had no effect on the currents (Schneider *et al.*, 1994; Williams *et al.*, 1994; Soong *et al.*, 1993). Ni^{2+} blocked the channel at concentrations that caused little or no block of the HVA Ca^{2+} currents (Schneider *et al.*, 1994; Williams *et al.*, 1994), but unlike other LVA Ca^{2+} channels, Cd^{2+} also caused potent block (Soong *et al.*, 1993; Ellinor *et al.*, 1993; Schneider *et al.*, 1994). Amiloride was able to inhibit currents at high concentrations (Schneider *et al.*, 1994), as was the L-type blocker D-600 (Schneider *et al.*, 1994). In addition crude extract of the venom from the funnel web spider blocked the channel (Schneider *et al.*, 1994).

Certain characteristics of the α_{1E} currents have been correlated to the R-type current on the basis of its kinetics and resistance to conventional blockers (Zhang *et al.*, 1993).

Accessory subunits of the voltage-dependent Ca^{2+} channel

The currently proposed model of the Ca^{2+} channel is illustrated in Fig. 1.1. The pore forming α_1 subunit has already been discussed but as can be seen the Ca^{2+} channel is a complex of four (or five in the case of the skeletal muscle clone) proteins with unique roles. It must be remembered that although the transmembrane regions are very highly conserved and general features of the channel protein remain similar between channel types, the intracellular terminals

Fig. 1.1 A 2-dimensional representation of the calcium channel showing the arrangement of subunits across the cell membrane.

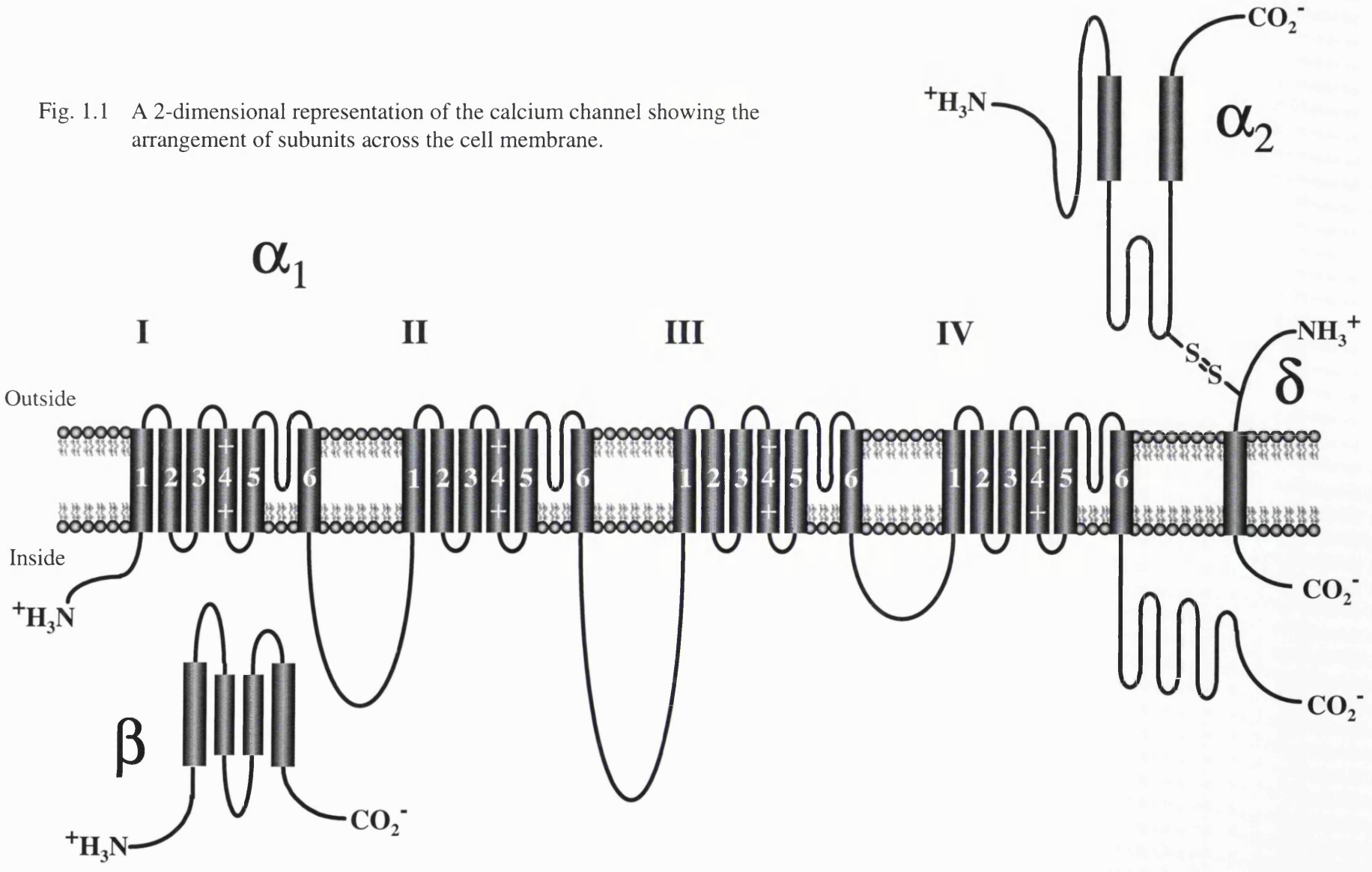

and loops contain a high degree of variation and lead to the differences in functional properties.

The β subunit

The β subunit from skeletal muscle was the first to be cloned in 1989 by Ruth *et al.* Secondary structural analysis predicted that the protein contained four α-helical domains. The presence of many charged amino acid residues suggested the absence of membrane spanning regions. The amino acid sequence showed that three of the four of these domains contained heptad repeats where the first and fourth residues were often hydrophobic. These kind of repeating sequences have been linked to interactions of the protein with other cytoskeletal elements (Fuchs and Hanakoglu, 1983), and it is possible that they serve a similar role in linking the α_1 subunit to the cytoskeleton. In addition to the heptad repeats each α-helical domain also contains a stretch of eight amino acids rich in negatively charged side chains suggested to function in the binding of divalent ions (Ruth *et al.*, 1989). The current classification and localisation of β subunits is shown in Table 1.3. Coexpression studies already discussed seemed to point to a role for the βs to increase the number of functional channels since most studies show an increase in current density with a correlating increase in high affinity DHP binding sites (Lacerda *et al.*, 1991; Perez-Reyes *et al.*, 1992). Neely *et al.* (1993) however, arrived at a different conclusion based on studies of gating movement. They found that the half-activation potential for charge movement of the voltage sensor of the α_{1C} subunit expressed in *Xenopus* oocytes was 35 mV more negative than that for pore opening. Coexpression with the β subunit reduced this difference without affecting charge movement. This demonstrated that intramolecular coupling between the voltage sensor and the channel pore opening was facilitated by a regulatory subunit.

The converse also applies. Antisense depletion of the β subunit from DRGs resulted in a reduction in the amplitude of the Ca^{2+} channel currents and slowed their kinetics of activation (Berrow *et al.*, 1995; Campbell *et al.*, 1995b).

The β binding region of the α_1 subunit

The site of interaction between the α_1 and β subunits has been identified as a sequence of residues on the cytoplasmic loop between domains I and II of the α_1 subunit (Pragnell *et al.*, 1994). In all of the cloned Ca^{2+} channels this region is conserved. Mutations within this region alter the interactions between the two subunits reducing the increase in current density and the shift in voltage-dependence. De Waard *et al.* (1994a) identified the corresponding critical sequence for this interaction as a conserved 30 amino acid stretch on the β subunit close to the N-terminus. Similarly, mutations in this region prevented β subunit induced kinetic changes normally seen.

The $\alpha_2\delta$ subunit is a single transmembrane extracellular protein

Rabbit skeletal muscle and human brain $\alpha_2\delta$ subunits have been cloned and found to be essentially identical, disregarding species differences (see Table 1.3). The δ-subunit sequence was found to be identical in sequence to the C-terminal region of the α_2 cDNA, indicating the α_2 and δ-subunits to be products of the same gene, separated by a post-translational modification. Their membrane arrangement has been the subject of some debate, but the currently accepted model is illustrated in Fig. 1.1. Ellis *et al.* (1988) suggested that the subunit contained two transmembrane regions, an intracellular loop, and large extracellular N- and C-terminals. The more likely model explored by Jay *et al.* (1991) put the entire α_2 polypeptide on the external surface of the membrane, anchored to the membrane spanning δ subunit by disulphide bonds. This model was supported by recent evidence which identified the transmembrane domain as necessary for functional interaction with the α_1 subunit (Gurnett *et al.*, 1996). As this model would have only five amino acids on the intracellular side, no direct interaction with cytoplasmic regulatory proteins such as the β subunit could be possible. In addition to the necessity of the transmembrane domain for subunit interaction, the structural integrity of the extracellular glycosylated domain was shown to be critical for the enhancement of current amplitude. Brickley *et al.*, (1995) supported this model by employing polyclonal antibodies against the $\alpha_2\delta$ translation product as membrane impermeant topological probes. Comparison of the antibodies

Accessory subunit	Localisation	Properties	References
β_{1a}	skeletal muscle	↑ peak current accelerate kinetics of α_{1C} but not α_{1A} accelerate inactivation hyperporarising shift in voltage-dependence of activation ↑ DHP binding sites of α_{1C}	Ruth *et al.*, 1989
β_{1b}	brain		Pragnell *et al.*, 1991
β_2	heart, lung, brain		Perez-Reyes *et al.*, 1992
β_3	brain, smooth muscle		Castellano *et al.*, 1993a
β_4	brain, esp. cerebellum		Castellano *et al.*, 1993b
$\alpha_2\delta$	skeletal muscle brain	↑ current in presence of β ↑ $\tau_{(inact)}$ in presence of β	Ellis *et al.*, 1988 Williams *et al.*, 1992
γ	skeletal muscle only	E-C coupling	Bosse *et al.*, 1990

Table 1.3. Cloning, localisation and functional properties of accessory calcium channel subunits.

binding ability in intact or detergent permeabilised rat DRGs showed that the N-termini of both the α_2 and δ subunits were located exofacially. In addition, the linking region in between the two hydrophobic domains proposed as being an intracellular loop by Ellis *et al.* (1988) was also found to be extracellular, thus agreeing with the model of Jay *et al.*, (1991). The role of the $\alpha_2\delta$ may depend on the α_1 subunit with which it is coexpressed. Coexpression studies have shown that $\alpha_2\delta$ with some α_1s cause little change to the properties of the channel, but may increase current amplitude when coexpressed with others (Biel *et al.*, 1990; Mikami *et al.*, 1990; Stea *et al.*, 1993). A synergistic increase appears to occur when it is coexpressed with β (Brust *et al.*, 1993; Stephens *et al.*, in press). Furthermore, results by Wiser *et al.* (1996), not only support the extracellular location of the α_2 subunit but also show that the $\alpha_2\delta$ subunit may play an additional role in regulating depolarisation-mediated secretion.

The γ-subunit

The γ-subunit appears to be exclusive to skeletal muscle. The deduced sequence contains four putative transmembrane regions (Bosse *et al.*, 1990). The role the γ-subunit plays in the Ca^{2+} channel complex remains to be elucidated, although its role in skeletal muscle may be in excitation-contraction coupling.

Modulation of Ca^{2+} channels

A broad range of messenger pathways can lead to alterations in channel function. When this results from the activation of a pathway containing intermediaries rather than a direct action of the stimulus on the channel molecule itself the stimulus is said to be modulating the channel function. It always follows the stimulus with a delay, and often outlasts the duration of stimulation since it involves the production of second messenger molecules and may lead to covalent modification of the channel. Where the second messenger cascade leads to the changes in gene expression the effects may last considerably longer.

Modulation can occur via G-proteins

Stimuli inducing these responses are usually neurotransmitters and hormones acting via G-proteins. For instance, noradrenaline and γ-aminobutyric acid (GABA) were found to cause a reduction in the amplitude of Ca^{2+} currents via a G-protein that could be blocked by intracellular administration of guanosine 5'-O-(2-thiodiphosphate) (GDP-β-S) (Holz *et al.*, 1986). Particularly common to neuronal cells is a pathway sensitive to a bacterial exotoxin from *Bordetella pertussis*. Pertussis toxin (PTX)-sensitive membrane-delimited G-protein inhibition of Ca^{2+} currents by a host of different neurotransmitters is often attributable to an effect on the N-type channel (Menon-Johansson *et al.*, 1993), but studies have also shown this type of modulation of the P-type channel by $GABA_B$ receptor activation (Mintz and Bean, 1993b). Hescheler *et al.* (1987) was able to reconstitute the inhibition of currents in PTX-treated neuroblastoma×glioma hybrids by perfusing the cells with purified G-protein heterotrimers. $G\alpha_o$ was found in these and other experiments (Ewald *et al.*, 1988) to be most effective in restoring current inhibition, and $G\beta\gamma$ was ineffective. Antisense depletion of G-proteins supported the role of $G\alpha_o$ in L- and N-type inhibition (Campbell *et al.*, 1993). Some studies began to suggest an additional role for the βγ subunit of the G-protein in modulating ion channels. Diverse-Pierluissi *et al.* (1995) showed that the βγ subunit was involved in the steady-state inhibition caused by α_2 adrenoceptor activation in DRG cells, and that the activation cascade involved the stimulation of phospholipase C (PLC) and protein kinase C (PKC) in turn. These

observations led other groups to investigate the involvement of Gβγ in modulation and found that transiently overexpressing Gβγ in neuronal cells mimicked and occluded the voltage-dependent inhibition produced by neurotransmitters but overexpression of Gα did not (Ikeda, 1996; Herlitze *et al.*, 1996). Recently, the intracellular loop between domains I and II has been demonstrated to be involved with binding of the G-protein βγ complex, which interacts with the cytoplasmic linker at two different positions (De Waard *et al.*, 1997). Also, within the Gβγ binding region is a site phosphorylated by PKC which antagonises the Gβγ-induced inhibition (Zamponi *et al.*, 1997) illustrating another level of control of Ca^{2+} channel activity.

In many neurones modulation by Gβγ of Ca^{2+} currents is tonically present. This can be seen in the above studies by the delivery of a depolarising pre-pulse to the cell. Control cells were seen to be only slightly 'facilitated' by a conditioning pulse. However, cells overexpressing Gβγ had currents comparable to control cells after relieving Gβγ inhibition by the delivery of a pre-pulse. There are many similarities between facilitation that occurs by this means and enhancement of current by other routes such as phosphorylation. Voltage-dependent facilitation has been investigated in a number of tissues expressing Ca^{2+} channels. Fenwick *et al.* (1982) first showed facilitation by depolarising prepulses in bovine chromaffin cells, and this has since been studied by other groups (Artalejo *et al.*, 1990, 1991a,b) who report that the depolarisation-induced increase in current is probably due to the phosphorylation of a normally silent L-type Ca^{2+} channel that occurs during the depolarisation. In muscle tissue the mechanism of facilitation has been studied. Some suggest that the large depolarisation during the prepulse activated a 'reluctant' voltage sensor in one of the domains that was responsible for the slower activation kinetics of currents in skeletal muscle, and was unable to deactivate before the test-pulse (Feldmeyer *et al.*, 1992). Phosphorylation may also be involved. Sculptoreanu *et al.* (1993) put forward the hypothesis that during depolarisation a phosphorylation site is exposed, becomes phosphorylated, and slowly dephosphorylates as the membrane potential is repolarised leading to the increase in current amplitude.

Phosphorylation of Ca^{2+} channels

In studies of L-type channels in skeletal muscle, Rohrkasten *et al.* (1988) showed that the channel protein could be phosphorylated at two sites by cyclic adenosine monophosphate (cAMP)-dependent protein kinase (PKA), one area on the large intracellular loop between transmembrane domains II and III, the other on the cytoplasmic C-terminal. The C-tail contains up to seven putative PKA phosphorylation sites, with fewer on truncated forms of the α_1. Increasing levels of cAMP in the myocyte seem only to cause phosphorylation of the β subunit (Catterall *et al.*, 1993) which has a number of consensus sites for phosphorylation by PKA, although a long form of the α_{1C} is a substrate for PKA (Yoshida *et al.*, 1992). Both size forms of the channel can be phosphorylated by other kinases and in contrast to the cardiac channel, both the short and long forms of the α_{1B} subunit have PKA phosphorylation sites (Hell *et al.*, 1994a,b).

Some investigations suggest that there is a minimum requirement of phosphorylation necessary for the Ca^{2+} channel to function. The loss of activity in excised patches from GH3 cells can be restored by PKA phosphorylation (Hymel *et al.*, 1988). In skeletal muscle, purified channels show a linear increase in activity according to their degree of phosphorylation (Nunoki *et al.*, 1989), and the purified channel expressed in lipid bilayers has no activity unless phosphorylated by PKA (Hymel *et al.*, 1988).

Enhancement of Ca^{2+} channels by PKC has been demonstrated in smooth muscle (Vivaudou *et al.*, 1988), and PKC has been shown to exert either inhibitory or excitatory effects on DHP-sensitive channels in cardiac cells (Lacerda *et al.*, 1988). Some contradiction occurs in vertebrate neurones concerning PKC-mediated modulation by neurotransmitters. Inhibition of Ca^{2+} currents in sensory neurones by noradrenaline and diacylglycerol (DAG) analogues is mediated by PKC (Rane *et al.*, 1989) as is the inhibition produced by bradykinin in DRGs (Boland *et al.*, 1991). Phorbol ester stimulation of PKC suppresses an LVA, T-type Ca^{2+} current in rat sensory neurones (Schroeder *et al.*, 1990) and a HVA current in hippocampal pyramidal neurones (Doerner *et al.*, 1990). Conversely, phorbol esters have also caused a reduction in Ca^{2+} currents via pathways independent of PKC (Hockberger *et al.*, 1989; Doerner *et al.*, 1990), and can stimulate currents in rat and frog sympathetic neurones (Bley and Tsien, 1990;

Bernheim *et al.*, 1991). Unitary and whole-cell recordings of currents in neurones from the frog indicated that both L- and N-type channels were enhanced by stimulation of PKC, independent of any effects on G-proteins, such as a removal of tonic inhibition (Yang and Tsien, 1993). Several consensus sequences for PKC phosphorylation exist on the α_1 subunit (Dubel *et al.*, 1992; Williams *et al.*, 1992b), and these subunits are readily phosphorylated by PKC *in vitro* (Ahlijanian *et al.*, 1991).

Phosphorylation by protein kinases is of tremendous functional importance to the control of synaptic transmission since PKC and PKA can modify neurotransmitter release in a number of preparations (Wakade *et al.*, 1985; Malenka *et al.*, 1987). PKC and calmodulin-dependent protein kinase II may lead to a positive feedback mechanism which has the potential to massively enhance small stimulatory signals.

Other second messenger systems also modulate Ca^{2+} channel activity. Activation of the PLC pathway leads to the production of two second messengers, DAG as we have already seen activates PKC, and IP_3 which gives rise to the well characterised mobilisation of Ca^{2+} from intracellular stores. IP_3 and possibly inositol 1,3,4,5-tetrakisphosphate (IP_4) are associated with a sustained later phase of signalling, promoting Ca^{2+} entry into the cell across the cell membrane (see Meldolesi *et al.*, 1991). In cultured cerebellar granule neurones intracellularly applied inositol phosphates increased the amplitude of Ca^{2+} currents by modifying the gating characteristics and the pharmacology of channels (De Waard *et al.*, 1992).

Intracellular Mg^{2+}

Mg^{2+} is the most abundant intracellular divalent cation in mammalian cells (Romani and Scarpa, 1992). Around half of the total body Mg^{2+} is localised to intracellular compartments and only 1% in the extracellular fluid. Of the intracellular Mg^{2+} about 5-10% is free depending on cell type. The remaining Mg^{2+} in various cell compartments is bound to negatively charged ligands such as ATP, citrate, adenosine 5'-diphosphate (ADP), proteins, RNA and DNA. The free and bound Mg^{2+} may be completely or partly exchangeable (Ebel and Gunther, 1980). This Mg^{2+} buffering functions to establish constancy of intracellular free Mg^{2+} ($[Mg^{2+}]_i$). Even though the concentration of Mg^{2+} in the extracellular fluid can be varied widely under experimental conditions the concentration of Mg^{2+} inside the cell is kept within narrow limits. Since Mg^{2+} can only slowly cross membranes and since the Mg^{2+} concentration is maintained below its electrochemical equilibrium this level of control implies the presence of transport systems specialised in the movement of Mg^{2+}. There are two separate mechanisms for Mg^{2+} influx and efflux. When $[Mg^{2+}]_i$ is increased, eg. by Mg^{2+} loading, Mg^{2+} efflux occurs via the Na^+-Mg^{2+} antiport. Conversely, when $[Mg^{2+}]_i$ is depleted, Mg^{2+} is taken up until normal $[Mg^{2+}]_i$ is reached. Efflux and influx systems are coupled to the movement of Na^+ either as Na^+-Mg^{2+} antiport in the case of efflux, or as Na^+, Mg^{2+} cotransport in Mg^{2+} influx (Gunther, 1993).

A regulatory role for $[Mg^{2+}]_i$?

There is a growing body of evidence suggesting a regulatory role for $[Mg^{2+}]_i$ in numerous processes, and it may acquire a regulatory function at constant $[Mg^{2+}]_i$ when other interacting factors such as membrane potential, pH, or $[Ca^{2+}]_i$ are altered. Mg^{2+} plays an important role as a cofactor in many enzymatic reactions (Wacker, 1969) and the movement of ions across the membrane. It plays an essential role in protein synthesis and stabilises the structure of ribosomes and membranes (Wacker, 1980). Additionally, it has also been implicated in the regulation of a wide range of ion channels in excitable membranes. These important roles within the cell have prompted suggestions that Mg^{2+} may be a second messenger co-ordinating cellular responses to environmental influences (Rubin, 1977). Although Mg^{2+} has not been found to have a rapid triggering

function like Ca^{2+}, and this is unlikely to be the case considering its chemistry and relative concentrations of ionised Mg inside and outside of the cell, but small, moderate changes in concentration could be important in the fine tuning of certain aspects of cell activity.

Effects on Na^+ channels

The decrease in conductance of Na^+ channels in *Xenopus* oocytes is caused by a block of the channel pore by Mg^{2+} in a voltage- and dose-dependent manner. Mg^{2+} acts as a fast blocker rather than gradually decreasing current by screening surface charge (Pusch, 1990a,b), but a surface charge screening effect on the intracellular side has been proposed as a blocking mechanism for $[Mg^{2+}]_i$ (Pusch *et al.*, 1989). Lin *et al.* (1991) proposed a model for block in cerebellar granule neurones in which Na^+ and Mg^{2+} compete for a binding site necessary for passage through the channel. Mg^{2+} occupation of this site would occur during depolarisation and due to the selectivity of the pore, Mg^{2+} would not be further permeable and may even be extruded by the small Na^+ influx through the channel. Another possibility is that Mg^{2+} has a strong binding force with this site and that it dissociates very slowly. These two possibilities are likely to coexist leading to the repeated entry of Mg^{2+} into the channel giving high frequency flickering at the single channel level.

K^+ channels of several classes have been reported to be blocked by Mg^{2+}

Inwardly rectifying K^+ channels conduct ions more readily in the inward than the outward direction, a necessary property for normal electrical activity. Although soluble polyamines (spermine, spermidine, putrescine, cadaverine) are required for intrinsic rectification of strong inward rectifiers (Lopatin *et al.*, 1994) the inward rectification of some K^+ channels partly responsible for the resting K^+ conductance is caused by rapid closure of the channel accompanied by the voltage-dependent block by intracellular Mg^{2+} at physiological concentrations (Matsuda *et al.*, 1987). A dual action of intracellular free Mg^{2+} effects the muscarinic K^+ channel. First, Mg^{2+} activates the channel in the presence of guanosine 5'triphosphate (GTP) through G-proteins, then it blocks the outward current by plugging the channel causing its inward rectification (Hille, 1992). Similarly, outward movement of K^+ through the ATP-sensitive K^+ current is blocked by Mg^{2+} (Ashcroft, 1988).

Inhibition of the Ca^{2+}-activated K^+ channel occurs in a concentration-dependent manner. Mg^{2+} appears to compete with K^+ due to the screening of negative surface charge (see below) at the inner surface of the channel protein at physiological concentrations (Ferguson, 1991).

Pumps and transporters are modulated by changes in Mg^{2+} concentration

A number of pumps and transporters are influenced by Mg^{2+} including the Na^+/K^+-adenosine triphosphatase (ATPase), Na^+-K^+-$2Cl^-$ cotransporter, K^+-Cl^- cotransport, Na^+-H^+ antiport, H^+-K^+ pump, Na^+-Ca^{2+} antiporter and the Na^+-Mg^{2+} exchanger (see Bara *et al.*, 1993).

Mg^{2+} alters Ca^{2+} channel function

Voltage-independent Ca^{2+} channels open in response to a specific intracellular or extracellular ligand, although their activators are not known. In invertebrate neurones they are seen to open infrequently in intact cells, but are activated by the formation of cell-free patches. Strong and Scott (1992) observed a regulatory role of $[Mg^{2+}]_i$ in the neurones of *Limnaea stagnalis*, in the control of these channels. Mg^{2+} promoted long closings by a mechanism distinct from open channel block.

Voltage-dependent Ca^{2+} channels are also regulated by $[Mg^{2+}]_i$. In cardiac myocytes, increasing concentrations of Mg^{2+} applied by internal perfusion caused a slight reduction in Ca^{2+} current amplitude. When basal currents were elevated via cAMP-dependent phosphorylation by the application of β-adrenergic agonists the same increases in $[Mg^{2+}]_i$ caused dramatic reductions in the Ca^{2+} current amplitudes (White and Hartzell, 1988). These changes were not due to changes in the velocity of phosphorylation of the channel, or changes in concentration of cAMP but appeared to be a direct effect on the phosphorylated channel, or on channel dephosphorylation. Increasing $[Mg^{2+}]_i$ also caused a shift in the current-voltage relationship and steady-state inactivation curve of -10 mV, decreased 'relief from inactivation' which occurs due to the decrease in the Ca^{2+}-dependent component of inactivation originally described by Lee *et al.*, (1985) and increased the rate of inactivation (Hartzell and White, 1989). Screening of negative surface charges (see later) can explain the shift in current-voltage and inactivation curves. The increase in inactivation was due to an increase in the steady-state level and the

rate of inactivation as shown by two-pulse inactivation protocols. When $[Mg^{2+}]_o$ was comparatively increased, current amplitude was decreased, and the current-voltage and inactivation curves were shifted to more polarised potentials. There was no significant effect on inactivation kinetics, suggesting that Mg^{2+} blocks rapidly from the exterior, but the block from the interior is time and voltage-dependent. The inactivation of the Ca^{2+} channel can occur by either Ca^{2+}-dependent or voltage-dependent mechanisms, but a component of the voltage-dependent inactivation can be modulated by changes in $[Mg^{2+}]_i$ (Hartzell and White, 1989).

The Ca^{2+} release channel of the sarcoplasmic reticulum is also sensitive to the concentration of intracellular Mg^{2+}. Smith *et al.* (1986) demonstrated an effect of Mg^{2+} on the Ca^{2+} release channel in skeletal muscle. Millimolar ATP and Ca^{2+} caused an additive effect in increasing open probability in single channel records. Mg^{2+} was found to permeate the channel and caused a flickering of Ca^{2+} and nucleotide-activated currents. 4 μM Mg^{2+} completely inhibited channel activity in the presence of nanomolar Ca^{2+}. When Ca^{2+} was in the micromolar range the concentration of Mg^{2+} required for complete block was increased, suggesting that Mg^{2+} and Ca^{2+} compete for the activation site.

The actions of Mg^{2+} on a range of channels in the membranes of excitable cells suggests an important role of Mg^{2+} in the regulation of excitability and activity in neurones. This is of particular interest since the influx of Ca^{2+} into the nerve terminal leads directly to the release of neurotransmitter.

Surface potential considerations

An important consideration when investigating the modulatory effects of ions in solution on ion channels are the effects of surface potential. As long ago as 1954, Brink recognised that an increase in Ca^{2+} concentration in the extracellular fluid decreases excitability. Later, in the squid giant axon Frankenhauser and Hodgkin (1957) showed that extracellular Ca^{2+} caused depolarising shifts in the Na^+ current gating curve. Two explanations were given to account for their findings. The divalent gating-particle hypothesis suggested that voltage-dependent block by an extracellular cation, like Ca^{2+}, caused the gating effect. Depolarisation would

remove the blocking particle and increase conductance. This has largely been ruled out because the kinetics of the block by Ca^{2+} are too fast to account for gating. It also could not apply to Ca^{2+} channels which are not blocked but are highly permeable to these ions. Thirdly, the voltage-dependent gating of Na^{+} channels remains in the absence of Ca^{2+} (Hille, 1975) and Ca^{2+} channel gating is present in bilayers bathed in solutions containing Ca^{2+} chelators (Cukierman *et al.*, 1988a,b).

The surface-potential theory has been generally accepted to explain the findings above. It suggests that negative surface charges are present at the outer edge of the membrane which may adsorb divalent cations thus creating an electric field that can influence the resting potential and bias voltage sensors within the membrane. In the presence of a high concentration of external cation, like Ca^{2+}, the charges would be neutralised by bound ions. In the absence of Ca^{2+} the outer membrane surface sets up a local negative charge that an intramembrane voltage sensor would sense as equivalent to a membrane depolarisation opening Na^{+}, K^{+} and Ca^{2+} channels. Actual binding of ions to the surface charge is not necessary, a screening effect caused by cations in the vicinity of the negative surface charge is sufficient to set up electric fields within the membrane.

Charges on the membrane lipid and the channel protein itself contribute to surface potential and manipulation of intracellular and extracellular ion concentrations affect gating although charges on the outer surface exert a stronger influence (Cukierman *et al.*, 1988). Surface charge screening effects become important when interpreting results between studies using different concentrations of ions in solution. For instance when whole-cell Ca^{2+} current recordings are compared to single-channel studies the extracellular concentration of Ca^{2+} or Ba^{2+} may be 1 mM and 90 mM respectively. The charge screening effect of this range of concentrations would undoubtedly have a dramatic effect on the voltage-dependence of Ca^{2+} channel gating.

Cerebellar granule neurones

The role of the cerebellum

The evolution of the cerebellum has left it with the job of controlling the complex mechanisms involved in skilled movements. Its precise role was appreciated in the last century as a result of surgical lesion in animals and clinical lesions in man which showed that badly disordered movements and general clumsiness resulted from damage to the cerebellum and that each cerebellar hemisphere co-ordinates the movements on just one side of the body (Holmes, 1939). Patients also suffered from a disability known as decomposition of movement, which involves being unable to carry out smooth movements involving several joints, each motor performance has to be broken down into simple movements of just one joint at a time, each requiring mental concentration.

The development of the cerebellum with the cerebrum, as a linked evolutionary process is exemplified by mans skill in tool manufacture and usage, and the motor development necessary for speech which gave the human species an immense superiority in survival.

Structure of the cerebellum

The cerebellum is well suited to neurobiological studies. It contains a small number of cell types arranged in a highly stereotyped structure, with geometrical precision. The precise picture of its neuronal arrangement was developed by Ramon y Cajal (1911) who discovered that the majority of these cells develop post-natally, making them easily accessible to cell culture, and they are each morphologically distinct in size and shape allowing their identification *in vitro*. Cerebellar granule neurones are the most abundant neuronal type in the CNS. These small diameter bipolar interneurones (5-8 μm diameter) convey the mossy-fibre input to the Purkinje cells, the sole output neurones from the cerebellar cortex which project to the deep cerebellar nuclei. Granule cells receive inhibitory inputs from Golgi cells where the neurotransmitter is probably GABA (Robello *et al.*, 1989), and give rise to axons that travel to the molecular layer bifurcating to form the parallel fibres. The Purkinje neurones form an extensive dendritic tree at right angles to the parallel fibres so that each parallel fibre makes synaptic contact with many Purkinje cells. The neurotransmitter at the granule cell synapse is

glutamate. The other three types of neurone in the cerebellum are all inhibitory interneurones receiving input from the parallel fibres. Stellate and basket cells project to Purkinje cells, whereas the Golgi cells which also receive an input to their cell bodies via the climbing fibres from the inferior olive project to the dendrites of the granule cells. The sole purpose of the cerebellar circuitry appears to be in the modulation or timing of excitatory output from the deep cerebellar nuclei to the thalamus and brain stem.

Development of granule cells

The electrical properties and the pharmacology of ion channels in these neurones has been investigated in different preparations, made possible by the patch-clamp technique (Hirano *et al.*, 1986; Vicini *et al.*, 1986; Hockberger *et al.*, 1987; Hirano and Hagiwara, 1988; Cull-Candy *et al.*, 1988; Robello *et al.*, 1989; Sciancalepore *et al.*, 1989; Cull-Candy *et al.*, 1989; Marchetti *et al.*, 1991; Slesinger and Lansman 1991a,b,c; De Waard *et al.*, 1992; Forti and Pietrobon, 1993; Bossu *et al.*, 1994; Rossi *et al.*, 1994; Forti *et al.*, 1994; Pearson *et al.*, 1995; Marchetti *et al.*, 1995; Stewart *et al.*, 1995; Randall *et al.*, 1995). Receptor- and voltage-operated ion channels have been studied and found to change according to days in culture (Hockberger *et al.*, 1987; Cull-Candy *et al.*, 1989; Sciancalepore *et al.*, 1989; Rossi *et al.*, 1994; Stewart *et al.*, 1995). Cultured granule cells are usually prepared from immature animals and it is possible that these changes might reflect the natural stages of neuronal development occurring *in vivo*. Four stages of granule cell development have been identified that the cells pass through during differentiation in explant cultures. These were termed neuroblast, immature, intermediate and mature (Hockberger *et al.*, 1987), and correlate well with development *in vitro* (Altman, 1972a,b, 1982). Neuroblasts were defined as small inexcitable cells that displayed only leakage currents under voltage-clamp, representative of cells of the external germinal layer *in vivo*. Development *in vivo* continues as these cells extend processes and the nuclei migrate downwards, settling beneath the Purkinje cell layer giving rise to the internal granule cell layer. This stage of development correlated well with cells of early post-natal cultures after 1 week (immature granule cells), which began to show voltage-dependent conductances. The amplitude of conductances gradually increased during the

second week in culture, during which time they became sufficient to generate action potentials and were designated as being intermediate granule cells. Excitability *in vivo* develops at this time and is based on synaptic transmission between granule cells and Purkinje neurones (Shimono *et al.*, 1976). At later stages in culture after 1 month, only axonal currents remained, indicating channels on the soma to have either translocated or were no longer activatable. These cells were classified as mature granule cells (Hockberger *et al.*, 1987).

Ca^{2+} channels in cerebellar granule neurones

Evidence for the existence of voltage-dependent Ca^{2+} currents in cerebellar granule neurones was provided by the measurements of Ca^{2+} fluxes (Connor *et al.*, 1987). Direct measurements of Ca^{2+} currents began in 1986 when Hirano *et al.* showed monosynaptic connections between granule cells and Purkinje cells. Later experiments have attempted to characterise the Ca^{2+} channel subtypes present in these cells. Several groups have investigated the N and L-type channels in granule cells (Slesinger and Lansman, 1991b; De Waard *et al.*, 1991; Pearson *et al.*, 1993; Pearson and Dolphin, 1993a). De Waard *et al.* (1991) showed that 3 μM ω-CgTx GVIA blocked 63% of the mean current (K_i=10 nM). Nicardipine in this study at a concentration of 10 μM reduced currents by 78% (K_i=0.5 μM) leading to the conclusion that more than half of the channels in cerebellar granule cells had a mixed pharmacology. Pearson *et al.*, (1993) and Randall and Tsien (1995) also demonstrated DHP- and ω-CgTx GVIA-sensitive currents although accounting for less of the total current. These more recent studies also used ω-Aga IVA to demonstrate further diversity. Pearson *et al.* (1995) showed that ~40% of the current was blocked by 100 nM ω-Aga IVA with a K_D=2.7 nM but overlapped completely with current sensitive to 1 μM ω-CgTx GVIA and 1 μM (-)-202-791. Similarly, Randall and Tsien (1995) showed that 46% of the whole-cell current was sensitive to ω-Aga IVA but identified two distinct components, one constituting 11% of the mean total current and half-blocked by 1-3 nM and a second making up 35% and half-blocked by 90 nM both showing no overlap with 10 μM nimodipine and 1 μM ω-CgTx GVIA but both being completely blocked by 5 μM ω-CTx MVIIC. In both these studies a component of current, being 20-

30% of the total was resistant to block by organic compounds but sensitive to Cd^{2+} and Ni^{2+}.

Diversity is also shown by studies of single calcium channels in cerebellar granule neurones. Pietrobon's group have shown distinct DHP-sensitive L-type channels, one displaying sporadic short openings with a low open channel probability which are prolonged in the presence of DHP agonist, have an inactivating profile and showing a high number of nulls. The other showed fast, unresolved openings, which in the presence of DHP agonist were resolved as short 2 ms openings and long closings, non-inactivating, with a lesser proportion of null sweeps (Forti and Pietrobon, 1993). P- and R-type channels were also shown to be functionally diverse. Three distinct channels were identified, each having a characteristic conductance and activation threshold, but similar inactivation having both an inactivating and a non-decaying component (Forti *et al.*, 1994). Later studies (Tottene *et al.*, 1996) showed by pharmacological criteria that one of these channels could be classified as a novel P-type channel, being insensitive to ω-CgTx GVIA and nimodipine, but blocked by ω-Aga IVA (saturating at 50 nM) and ω-CTx MVIIC, yet showing complete voltage-dependent inactivation at potentials having no effect on currents in Purkinje cells. The two remaining channels were both insensitive to all calcium channel blockers and displayed voltage-dependent properties similar to LVA channels. Similarities were apparent to the R-type current described by Randall and Tsien (1995) in that Ni^{2+} could block the residual current in whole-cell recordings with a biphasic concentration-dependence with dissociation constants calculated to be 12 μM and 286 μM

In addition, the channel subtypes involved in the control of neurotransmitter release from these cells in response to depolarisation has been looked into (Huston *et al.*, 1990, 1993, 1995). These studies showed that under physiologically relevant conditions, on the basis of toxin, or DHP-sensitivity, K^+-stimulated [3H]glutamate release from cerebellar granule neurones was dependent on Ca^{2+}-entry through N-, L- and P/Q-type Ca^{2+} channels in addition to an unidentified subtype. With regards to the components that contribute to the whole-cell Ca^{2+} current in granule cells, experiments using novel Ca^{2+} channel blockers have reported differing results and have shown that the different subtypes of Ca^{2+} channels exhibit

overlapping sensitivity to pharmacological agents (De Waard *et al.*, 1991; Pearson *et al.*, 1995).

$[Mg^{2+}]_i$ and $[Mg.ATP]_i$ in cerebellar granule neurones

In cerebellar granule neurones the effect of $[Mg^{2+}]_i$ and intracellularly Mg^{2+}-bound ATP $[Mg.ATP]_i$, has been studied with respect to Ca^{2+} currents in these cells. Increasing $[Mg.ATP]_i$ increased the amplitude of Ca^{2+} channel currents recorded. Conversely, increasing $[Mg^{2+}]_i$ and keeping $[Mg.ATP]_i$ constant caused a reduction in the amplitude of evoked currents. Further to these results, there was a suggestion that increasing $[Mg^{2+}]_i$ caused a selective decrease of the ω-CgTX GVIA sensitive component of the neurones (Pearson and Dolphin, 1993a).

Aims

The following experiments set out to examine whole-cell Ca^{2+} channel currents in cerebellar granule neurones with particular emphasis placed on characterising the various subtypes of Ca^{2+} channel that carry this current. Cerebellar granule neurones have been shown to contain multiple subtypes of Ca^{2+} channel both electrophysiologically and immunologically. They were chosen for use in this study because of the diversity of channel types that have been identified in these cells however, because of varying reports regarding the proportions and properties of these channel types, further establishing the different species of Ca^{2+} channel represents an interesting challenge. A pharmacological approach using a number of natural or synthetic peptides derived from the venom of predator species, and other more established drugs known to act on Ca^{2+} channels was used to characterise the Ca^{2+} channel current in these cells. Some biophysical properties of the Ca^{2+} channel current were also examined with the hope that these too would give clues as to the identity of the component parts of the whole-cell current and possible correlations to cloned Ca^{2+} channels.

A number of membrane conductances are modulated by physiological concentrations of Mg^{2+}. Ca^{2+} channels in cerebellar granule neurones are amongst these as previous studies have shown (Pearson and Dolphin, 1993a,b). A series of studies were carried out to determine if the concentration of intracellular Mg^{2+} affected specific components of Ca^{2+} channel currents characterised in these cells. In addition, if intracellular Mg^{2+} alters channel activity in the majority of cells and since its concentration is carefully regulated within tight limitations it may be possible that environmental stimuli can cause changes in $[Mg^{2+}]i$. Through the use of chemiluminescent probes, intracellular Mg^{2+} levels were measured in cultures of cerebellar granule neurones to determine a resting level. Exposure to the neurotransmitter glutamate was investigated to determine whether it has an effect on the distribution or mobilisation of Mg^{2+} in the cell.

Studies were also designed to investigate the pharmacology of a relatively newly cloned Ca^{2+} channel. The rat α_{1E} channel was expressed in a mammalian cell line with accessory channel subunits to examine the effect of dihydropyridine drugs. Since the pharmacological properties provide a means of classifying Ca^{2+} channels

the aim here was to show that features of expressed α_{1E} channels could be related to an existing subtype of Ca^{2+} channel or described a novel channel. In addition, since a large proportion of current through Ca^{2+} channels in cerebellar granule neurones could be blocked by nicardipine, the possibility that at least some of this current could be attributable to α_{1E} channels was addressed.

Chapter 2

Methods

For electrophysiological studies cultured cells are of particular value. Access to individual cells which are easily identifiable is uncomplicated by the presence of non-neuronal tissue and cell debris that needs to be removed to expose cells for study in slices. Environmental conditions are readily altered by exchanging the extracellular media bathing the cells and the cells can be kept healthy for many days reducing the use of animals.

The use of immortalised cell lines further reduce animal use as cells from a single stock can be used for many passages. Cell lines such as the COS-7 line used here are particularly useful in expression studies because the cells are a homogeneous population.

Culture of neonatal rat cerebellar granule neurones

Preparation of coverslips

Coverslips were incubated in a solution of poly-L-lysine hydrobromide (MW 150-300,000 *Sigma*) prepared at a concentration of 15 mg/l in sterile water for 30 min at 37 ° C. The coverslips were then rinsed once or twice in sterile water and left to dry.

Dissociation of granule neurones

Cells were prepared according to a method similar to that described by White et al. (1979) with several modifications.

The cerebellum from a P6 Sprague-Dawley rat was removed following decapitation and the tissue was rinsed in an enriched phosphate buffered saline (PBS) containing 0.25% glucose and 0.3% bovine serum albumin (BSA). The meningeal layers and connective tissue were dissected away prior to chopping the tissue into 250 μm squares with a McIlwain tissue slicer. The tissue was then dissociated enzymatically at 37 ° C for 20 min in enriched PBS containing 0.025% trypsin (type III from bovine pancreas, *Sigma*). The trypsin solution was then inactivated by the addition of a solution containing additional $MgSO_4.7H_20$ (1.78

mM), 8 μg/ml soybean trypsin inhibitor (SBTI type IIS, *Sigma*), and 10 Kunitz/ml deoxyribose nucleotidase I (DNAase I, type IV from bovine pancreas, *Sigma*). The resulting suspension was then agitated to prevent clumping and centrifuged at 2,500 rpm (300×g) for 60 s. The supernatant was then discarded and the cells resuspended in 5 ml of enriched PBS solution containing 50 μg/ml SBTI, 64 Kunitz DNAase I and 3 mM $MgS0_4.7H_20$. The tissue was then triturated using a fire-polished Pasteur pipette. The resulting suspension was then underlined with 2 ml of 4% BSA in Earle's balanced salt solution (EBSS) (see Table 2.1) and centrifuged for 5 min at 1,200 rpm (300×g) in a Mistral 3000I centrifuge. Treatment with DNAase was necessary to prevent clumping of cells caused by DNA released from ruptured cells.

The cell pellet was then resuspended in 4 ml of Minimum Essential Medium (MEM) containing foetal calf serum (FCS) (see Table 2.2) and diluted to give a final cell count of $5x10^6$ cells ml^{-1}.

100 μl of this suspension was then grown on each coverslip in a 24 well multiculture plate in a humidified environment at 37 ° C, 5% CO_2. After 48 hours *in vitro* 80 μM flurodeoxyuridine (FUDR) supplemented the growth medium to prevent over growth of non-neuronal cells. From day 3 the medium was exchanged for MEM with 10% horse serum (HS) and replaced every 3-5 days. All media were supplemented with chick embryo extract (2.5%), D-glucose (33 mM), glutamine (2 mM), KCl (23 mM) and Penicillin/Streptomycin 50 IU ml^{-1}/50 μg ml^{-1} (see Table 2.2).

Preparation of COS-7 cells

COS-7 cells, an SV40 transformed Monkey kidney fibroblast cell line were obtained from the European Collection of Animal Cell Cultures (ECACC).

Confluent monolayers were split 1:3-1:10 i.e. seeding subcultures at 10-30,000 cells cm^{-2} after treatment with a commercial trypsin/ethylenediaminetetraacetic acid (EDTA) solution containing 0.5 mg/ml trypsin, 0.5 mM EDTA in Puck's Saline (*Gibco BRL*). Cells were grown in a culture medium based on MEM Alpha Medium containing 10% FCS at 37 ° C, 5% CO_2 in a humidified atmosphere.

Constituent			Concentration
Bovine Serum Albumin		(BSA) *Sigma*	40 g l^{-1}
Magnesium Sulphate heptahydrate		($MgSO_4.7H_2O$) *Sigma*	1.24 mM
Earle's Balanced Salt Solution (EBSS)	Sodium Chloride	(NaCl) *Sigma*	116 mM
	Sodium Bicarbonate	($NaHCO_3$) *Sigma*	2.6 mM
	Sodium dihydrogen orthophosphate dihydrate	($NaH_2PO_4.2H_2O$) *Sigma*	1 mM
	Potassium Chloride	(KCl) *Sigma*	5.36 mM
	Glucose	*Sigma*	5.5 mM
	Phenol Red	*Sigma*	0.026 mM

Table 2.1 Composition of BSA in Earle's Salts.

Constituent		Notes	Storage	Final Concentration
Minimum Essential Medium	(MEM)	With Earle's Salts, without glutamine, and bicarbonate *Gibco*	Stored at 4°C	Made up to 1 litre with 2.2 g/l sodium bicarbonate
Foetal Calf Serum OR Horse Serum	(FCS) (HS)	Heat-inactivated, mycoplasma screened *ICN flow*	Stored in aliquots at -20°C	10%
Chicken Embryo Extract	(CEE)	50% in Earle's salts *ICN flow*	Stored in aliquots at -20°C	2.5%
D-glucose		*Sigma*	1.32 M aliquots stored at -20°C	33 mM
Glutamine		*Sigma*	Freshly prepared	2 mM
Potassium Chloride	(KCl)	*BDH chemicals*	2.3 M aliquots stored at -20°C	23 mM
Penicillin/Streptomycin	(Pen/Strep)	*ICN flow*	5000 IU/ 5000 µg ml^{-1} aliquots stored at -20°C	50 IU/50 µg ml^{-1}
Flurodeoxyuridine	(FUDR)	*Sigma*	3.2 mM aliquots stored at -20°C	80 µM

Table 2.2 Composition of modified MEM used in the culture of cerebellar granule neurones.

Transfection by electroporation

For each electroporation a 75 cm^2 flask of COS-7 cells was grown to confluence. After rinsing the cells with sterile PBS 1 ml of pre-warmed trypsin/EDTA was added to the flask ensuring the solution washed over the whole growing surface. The cells were then left for 5-10 min until they no longer adhered to the flask. MEM Alpha Medium was then added to the flask (7 ml) and the cells mixed thoroughly by pipetting to break up clumps. These were then transferred to a 15 ml tube and centrifuged (1,200×g) for 3 min. The supernatant was then discarded and the cells resuspended in 7 ml of PBS. After a second centrifugation the supernatant was removed and the cells resuspended in PBS to a volume of 500 µl. The cell suspension was then transferred to a cooled 1 ml electroporation cuvette containing the plasmid DNA. Cells were gently mixed with the DNA and were incubated on ice for 10 min. The cells were then electroporated at 330 V/500 µF and placed on ice for a further 10 min. The cells were then diluted in 20 ml of MEM Alpha Medium and transferred to 15 cm diameter culture plates.

Replating of COS-7

On the day of study transfected COS-7 cells were replated. Each 15 cm diameter culture dish was washed in sterile PBS twice after removal of media. A non-enzymatic cell dissociation media was used (EDTA, glycerol and sodium citrate prepared in Hank's Balanced Salt Solution without Ca^{2+} or Mg^{2+}, *Sigma*) to gently dislodge adherent cells from the culture dish. 1.5 ml of this solution was added to each dish rocking the vessel to coat the monolayer. The cells were then incubated at 37 °C for 5-10 min. Sharply tapping the vessel dislodged the cells which were then pipetted gently to dissociate clumps and diluted with 10 ml of pre-warmed MEM Alpha Medium. 2 ml of the dissociated cells were then added to 35 mm culture dishes and left to adhere for 30-60 min prior to electrophysiological studies.

Preparation of cDNA was performed by Dr. K. Page and Dr. N. Berrow

The cDNAs used were all from the rat. α_{1E} and β_{1b} subunit cDNAs were supplied in the pMT2 vertebrate expression vector (Genetics Institute, Cambridge, Mass.

U.S.A.) (Soong *et al.* 1993; Stea *et al.* 1994). Full length α_2-δ cDNA (Kim et al. 1992) was excised from the pcDα_2 2-1 plasmid using Kpnl and Notl enzymes. The 3.8 kbase α_2-δ fragment was then ligated into Kpnl/Notl digested pMT2 (Dubel et al. 1992). Green Fluorescent Protein (GFP) cDNA (Marshall et al., 1995) from the bioluminescent jellyfish *Aequorea victoria* containing the S65→T mutation was excised from the Bluescript vector using Kpnl and Notl enzymes. The approximately 1 kbase GFP fragment was ligated into Kpnl/Notl digested pMT2. Multiple restriction digests were used to verify correct insertion of both the GFP and α_2-δ cDNAs into pMT2 before large scale plasmid preparation for expression studies.

Transfection

For transfection 15, 10, 5 and 2 μg of the pMT2 α_{1E}, β_{1b}, α_2-δ and GFP constructs were used respectively. Identification of successfully transfected cells for electrophysiological studies was achieved by the expression of GFP. Cells were illuminated by a super high pressure mercury lamp (Hg100W, LH-M100CB-1 lamphousing, HB-10104AF supply, *Nikon corporation, Instruments Division, Yokohama Plant).* Standard fluorescein optics were employed composed of a 510 nm dichroic mirror and a 520 nm barrier filter.

Electrophysiology

Theory of voltage-clamp

To measure membrane conductances across the cell membrane, albeit indirectly by measuring current, it is necessary to hold the membrane potential constant. By doing so it is assumed that current is linearly proportional to the conductance being studied. The voltage-clamp technique for current measurement has traditionally assigned the roles of potential measurement and current passing to two separate intracellular micropipettes. However, in some situations a single microelectrode is more favourable and it is possible to simulate two electrode voltage clamping by time-division multiplexing using the discontinuous single-electrode voltage clamp technique. Both these methods avoid introduction of

errors in measurement due to unknown voltage drops across the series resistance of the current passing micropipette.

In 'whole-cell patch' recording one micropipette can be used full-time for voltage-recording and current passing. Series resistance compensation attempts to compensate for the aberrations arising when a single electrode is made to perform the tasks of two. For this to work the impedance of the cell must be high in relation to the pipette resistance. The resistance of intracellular micropipettes is very high, so a region of cell membrane is tightly sealed to the tip of a blunt electrode.

In contrast to two-electrode voltage clamps and discontinuous single electrode voltage clamps where the voltage at the tip of the pipette is controlled, in continuous single electrode voltage clamp circuits the voltage at the top of the pipette is controlled. The voltage recorded here is the sum of the membrane potential and the current-induced voltage drop across the pipette. If current through the series resistance is large, significant voltage errors can be introduced. Modern patch-clamp amplifiers provide ways of compensating these errors electronically but they are often not perfect. Care must be taken in the interpretation of residual error.

For cells with small currents discontinuous single electrode voltage-clamp is problematic as it is difficult to set up and noisy. Furthermore, the error for uncompensated series resistance inherent in the continuous single-electrode voltage clamp can be made negligible, making this mode of clamping very attractive for small cells.

In 1976, Neher and Sakman introduced the extracellular patch-clamp technique which allowed single-channel events to be recorded by pressing a heat-polished glass pipette against the membrane of a cell. An electrical seal with a resistance of the order of 50 MΩ could be obtained ensuring that the majority of current arising from the small membrane patch flowed into the pipette and was measured by the electronic circuitry.

Hamill *et al.*, in 1981 refined this technique after observing that unexpectedly tight pipette membrane seals with resistances of 10-100 GΩ and surprising mechanical stability could be achieved when care was taken to keep the pipette surface clean and gentle suction was applied to the interior of the pipette. This development

permitted current recording in four new modes. Single channels could be recorded 'on-cell': the cell-attached mode. The stability of the seal also allowed the patch of membrane to be removed from the cell by withdrawing the pipette after forming a seal: the inside-out or excised-patch configuration. Alternatively, in the whole-cell patch clamp configuration, after a gigaohm seal is obtained, the area of cell membrane within the patch pipette is ruptured by a brief period of suction or the application of a large voltage (1.5 V DC) to the patch for a carefully controlled duration, in the order of 0.1 ms. This can cause dielectric breakdown of the membrane, but too long a period of application may cause deterioration of the seal resistance. Upon rupture of the patch the electrolyte solution in the pipette perfuses into the interior of the cell becoming electrically continuous with it, and replacing the intracellular solution. The fourth recording mode could be obtained by pulling away the pipette from a cell in the whole-cell mode, resulting in an outside-out patch. These new developments were quickly exploited by neurobiologists allowing the study of small cells. Ca^{2+} channels were also easily isolated by using Cs^{+} in the pipette and adding TEA to the extracellular solution to block K^{+} channels and, together with the lower noise levels that were possible, currents could be recorded in spite of the 100-fold lower density of Ca^{2+} channels than the previously recorded Na^{+} and K^{+} currents.

Patch-clamp electronics

The basic electronic design of the patch-clamp amplifier is illustrated in Fig. 2.1. In simple terms it is a current-voltage converter which employs a high resistance feedback resistor (R_f, typically between 500 MΩ and 50 GΩ), across an operational amplifier (A1). The pipette is connected to the inverting input, and the command voltage is fed to the non-inverting input. The operational amplifier has a very high gain (typically 10^5), so the pipette potential is forced to follow the potential at the non-inverting input. Any current that flows in the micropipette also passes through the feedback loop, and output from the differential amplifier (A2) must be proportional to the voltage across R_f. The important stray capacitances in the diagram are shown as broken lines. C_f is the feedback capacitance, normally around 0.1 pF which guarantees stability, but limits the speed of the voltage-

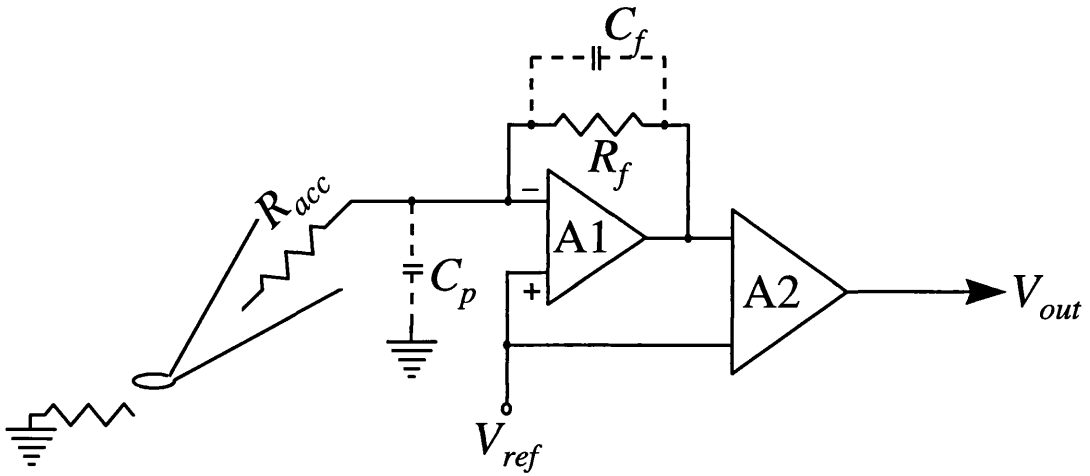

Fig. 2.1. Basic design of the patch-clamp electronics. Operational amplifier A1 is a current-voltage converter with feedback resistor R_f having an associated stray capacitance C_f (shown as a broken line). The patch pipette with resistance R_{acc} and capacitance C_p is connected to the inverting input of A1, (-). Output from A1 is passed to one input of a differentiating amplifier (A2), and output from A2 is proportional to the potential across R_f.

clamp. C_p is the capacitance inherent in the pipette and headstage which is usually around 5 pF.

A number of considerations need to be made in the choice of components. The resistance of R_f needs to be high enough to achieve adequate gain, and to achieve a good signal to noise ratio. Theoretically, noise is lower for larger R_f values. The inherent bandwidth of this resistor is limited by its stray capacitance. A 50 GΩ resistor with 0.1 pF stray capacitance charges with a time constant of 5 ms, with a corresponding bandwidth of 32 Hz. This is inadequate time resolution for the measurement of ionic currents so the high-frequency components of the signal are boosted by an analogue frequency compensation circuit. Other problems associated with high resistance feedback resistors are large voltage coefficients of resistance, leading to non-linearity of responses over the complete voltage range, large temperature coefficients of resistance, and poor stability over time due to ageing. Despite these drawbacks the technology has been successfully used for a number of years.

Pipette capacitance compensation

The stray capacitance mentioned above and shown in Fig. 2.1 must be charged as the potential at the pipette is changed. This charging has a fast component and a smaller, slower tail arising from the capacitance of the pipette glass. It is important to compensate for this so that the potential at the top of the pipette is stepped more rapidly. This reduces the distortion of rapid onset currents and removes the transient from current records. The circuitry is able to compensate for the capacitance by injecting the charging current via a separate pathway to the input, often through a capacitor. Usually patch clamp amplifiers provide fast and slow compensation controls but the compensation is rarely perfect.

Whole-cell capacitance compensation

The cell membrane provides a further source of unwanted capacitance. It is usual to compensate for the charging of this capacitance during whole-cell recording. High access resistance and large whole-cell capacitances lead to time constants of charging of up to several hundred microseconds. Voltage errors can be considerable if ionic currents are large, leading to errors of tens of millivolts in the

membrane potential. For the cells used in this study, average membrane capacitances were 3.6±0.3 (n=71) and 15±2 pF (n=14) for granule cells and COS-7 cells respectively. Average access resistances were 19±0.6 (n=71) and 17±3 (n=14) MΩ leading to voltage-clamp time constants of 68 μs for granule cells and 255 μs for COS-7 cells. Following series resistance compensation (see later) the speed of the voltage-clamp was improved as the effective series resistance was decreased. Assuming 80% series resistance compensation, calculated time constants were 14 μs for granule cells and 51 μs for COS-7 cells. Thus small enough for a disirable time resolution.

The compensation controls on a patch-clamp amplifier allow a transient current to be injected through a capacitor into the pipette, preventing saturation in the feedback resistor. As current being monitored by the patch clamp is proportional to the current through the feedback resistor, the transient current is not seen, though it is still being passed into the cell.

Series resistance compensation

The resistance of the pipette limits the speed of the clamp above the limits imposed by the speed of the electronics. Compensation reduces the departure from ideal electronics by positive feedback or supercharging

Positive feedback or 'correction' boosts the command potential by a proportion of the measured current to partly compensate for the voltage drop across the pipette. Two problems associated with this approach are that the command potential is increased hyperbolically towards high levels of compensation and the circuit approaches saturation. Secondly, the feedback is positive and the system oscillates at high levels of compensation. These problems are partly solved by introducing a variable low-pass filter in the feedback loop. This allows large percentage compensations to be employed but these only apply to the lower frequencies, high-frequency errors remain large.

In supercharging, or 'prediction', brief charging pulses are added to the start and end of the voltage step. As the membrane initially charges to a higher final value than is required it reaches the required voltage faster. Amplitude and duration of this supercharging pulse are set by the operator to prevent overshoot occurring.

Usually a combination of both these techniques are applied to reduce the effects of the pipette resistance.

Voltage error

In the experiments presented in the following chapters R_s was generally 80% compensated. Cells with unusually high R_s (greater than 25 MΩ for either granule cells or COS-7 cells) or when R_s could not be compensated to this level were discarded. From Ohm's Law the voltage error that occurs as a result of the uncompensated R_s is equal to the product of R_s and the membrane current. Maximum estimates of voltage error due to uncompensated R_s for granule cells was 1 mV (assuming R_s=20 MΩ, 80% compensation, and 250 pA current), and 3 mV for COS-7 cells (assuming R_s=17 MΩ, 80% compensation, and 1 nA current). These values were considered to be within tolerable limits.

Junction potential

A potential difference occurs at the boundary between two solutions whose anions and cations have different mobilities. In whole-cell recording, the pipette filling solution is usually not the same as the bath solution so a potential difference exists at the tip of the recording pipette. The magnitude of the liquid junction potential for typical solutions used in electrophysiological experiments is between 2-12 mV. Patch clamp amplifiers provide facilities for applying a separate, variable offset from the holding potential which is used to null the junction potential so that the amplifier reads zero current and zero voltage at the start of an experiment. When the pipette is then sealed against a cell and diffusional equilibrium has been reached between the cell interior and the pipette the amplifier reads zero voltage but the back-off potential used to balance the liquid junction potential remains. All voltage readings of the amplifier have to be corrected by this amount, known as the liquid junction potential correction.

Liquid junction potential was calculated experimentally (Neher, 1992) by filling the recording bath and a pipette with the intracellular solution and zeroing the voltage reading in current-clamp mode by adjusting the variable offset. The bath solution was then exchanged for the normal extracellular solution. The liquid

junction potential could then be read from the amplifier and was reversible on replacing the bath solution with the intracellular solution.

Using this method the liquid junction potential correction for solutions used in recordings from granule cells was -12 mV and -14 mV for solutions used in recordings from COS-7 cells. The potentials given are uncorrected, but for comparative purposes, the corrected data are shown in parentheses.

Problems with space clamp

As the voltage clamp is maintained at the tip of the recording microelectrode any portion of the membrane not separated from the tip by equal access resistance will be unequally clamped. In large cells or those that are not spherical, or have processes such as dendrites and axons running off the cell body, performance of the voltage clamp can be severely limited, a problem that can not be electronically compensated. A voltage drop occurs across the access resistance that can become substantial for distal areas of membrane on processes separated from the cell body by an axial access resistance dependent on the cross section of the process and its distance from the micropipette. Even if the membrane potential at the soma is well controlled, that of the axons or dendrites may alter the time course of synaptic currents biasing measurements.

Space-clamp problems can be overcome by keeping the resistance of the patch pipette as low as possible and also by recording from only those cells that have few processes. It is possible for cells with extensive communications to be replated prior to use, thus destroying axons and dendrites and causing the cells to 'round up'.

Recording

Membrane currents were measured in the whole-cell clamp configuration using an Axopatch 1D, or 200A amplifier (*Axon Instruments, Foster City, California*). Voltage protocols and data acquisition were controlled by a 386 or 486 PC through either a TL-1 or Digidata 1200 interface using the pCLAMP6 software suite, *(Axon Instruments, Foster City, California*). Currents were generally sampled at 5 kHz (200 μs sampling interval), with the exception of experiments designed to examine tail currents or the capacity transient which were sampled at a

faster rate (77 kHz, 12.9 μs interval), and two pulse steady state inactivation protocols were the conditioning step was sampled at 500 Hz (2 ms interval) to save on data storage space and speed analysis. Sampling frequencies and filtering frequencies of the data were chosen to be appropriate for the signal being recorded such that information was not lost to aliasing effects, or insufficient resolution. To this end all recordings were low pass filtered with a corner frequency of 2 kHz using a 4-pole Bessel filter. Capacity transients were minimised by analogue compensation and by subtraction on-line using a P/6 or P/8 subtraction protocol where six or eight hyperpolarising pulses of one sixth or one eighth the amplitude of the test pulse were summed and the resulting leak current subtracted from the actual test pulse. Inspection of the leak pulses showed that no non-linear current components were subtracted from the test pulse, a possible source of inadvertently introducing large artifacts. Depolarising voltage steps were delivered at a maximum frequency of 0.16 Hz to minimise current rundown which was sometimes seen at faster stimulation rates. Recording was begun no less than 2 minutes after rupture of the patch to allow for complete dialysis of the cell interior. 'Run up' of Ca^{2+} channel currents was often seen during the initial period after breaking into the cell.

Patch pipettes were fabricated from borosilicate glass capillary tubing (1.5 mm outer diameter, 1.0 mm bore, 0.1 mm fibre, *Plowden and Thompson, UK*) using a P-87 Flaming/Brown microelectrode puller (*Sutter Instrument Company, Novato, California*). For recordings from granule cells 6-8 MΩ pipettes were used. Recordings from COS-7 cells required lower resistance, 3-4 MΩ pipettes to obtain an adequate voltage-clamp. All pipettes were fire polished to promote the formation of gigaohm seals and to prevent cell penetration, using a *Narishige* microforge. To ensure low noise recordings patch pipettes were coated with Sigmacote (*Sigma*), a hydrophobic material to prevent bathing solution creeping up the wall of the pipette.

For the local application of drugs by low pressure ejection, pipettes were pulled having an internal diameter of 3-5 μm. During periods of drug application the pipette was positioned 100 μm from the cell of interest. Pressure was applied to the pipette until drug was gently ejected around the cell. A second drug pipette

could be used to either apply a second drug or to puff normal extracellular media as a control or to wash away drug following application.

All experiments were carried out at room temperature, ranging from 20-25 °C.

Voltage protocols

For the generation of current-voltage relationships, currents were examined at a range of test potentials between -70 mV and +70 mV from a holding potential of -80 mV, stepping to test potentials for 100 ms with an interepisode time of no less than 6 s.

In experiments investigating the deactivation of tail currents, membrane potential was stepped back to -50 mV for 15 ms before returning to the holding potential after a depolarising step of a duration lasting 15 ms so that the maximum number of channels were deactivating during the tail.

To study steady-state inactivation of currents, cells were held at a potential of -80 mV. A conditioning pulse lasting 10 s was then delivered immediately prior to a step to +10 mV lasting 100 ms. If leak subtraction was being used the scaled subtraction pulses were given before the conditioning step. An interepisode time of 30 s was required to allow the full recovery of inactivated channels before proceeding with the next pulse. Inactivation was examined at potentials ranging from -120 mV to +40 mV.

Current transients were evoked by stepping from -80 mV to -90 mV for a period of 4 ms. At this potential no voltage-dependent currents were activated and only capacity currents and linear leak was recorded.

Data analysis

Analysis was carried out using pCLAMP6 software, (*Axon Instruments, Foster City, California*). Statistical analysis was assisted by the use of Origin (*Microcal Inc.*), Excel (*Microsoft*), and Instat (*Graphpad Instat Software*). Mean values are presented as means±s.e.m., with *n* as the number of neurones in which observations were made. Statistical analysis was performed using the Student's *t-test*, with paired comparisons if relevant. Probabilities are given for 2-tailed *t-tests*. Current-voltage relationships were analysed by measuring the amplitude of the peak current evoked for each test potential. These values were plotted against the

test potential. Where current-voltage relationships have been fitted to a mathematical expression, a Boltzmann function shown in *Equation 1* has been used.

$$I = \frac{\left(g(V - V_{rev})\right)}{\left(1 + \exp\left(\left(V - V_{50(act)}\right)/k\right)\right)} \qquad \textit{Equation 1}$$

where g is the conductance in nS, V_{null} is the reversal potential in mV, $V_{50(act)}$ is the voltage for half activation (mV) and k is the slope factor (mV).

Current-voltage relationships are shown illustrating the average of data from the experimental group. Where fit parameter values are quoted they represent the average values from Boltzmann fits to individual data.

Activation of currents was investigated by fitting a single order exponential to the activating phase of the currents evoked by step depolarisation (see Fig. 2.2). An equation in the form of *Equation 2* was used.

$$I = A_1 . \exp\left(\frac{-(t - t_0)}{\tau_{(act)}}\right) \qquad \textit{Equation 2}$$

where A_1 is the amplitude of current at time t_0 in pA, t is time and t_0 is time at the start of the fit in ms, $\tau_{(act)}$ is the time constant for activation in ms.

Time to peak was defined as the time in ms between the onset of the depolarising voltage step and the time the current amplitude reached its maximum.

Inactivation of currents was fit with a second order exponential, (*Equation 3*, see Fig. 2.2).

$$I = A_1 . \exp\left(\frac{-(t - t_0)}{\tau_{1(inact)}}\right) + A_2 . \exp\left(\frac{-(t - t_0)}{\tau_{2(inact)}}\right) + C \qquad \textit{Equation 3}$$

where A_1 and $A2$ are the amplitudes of the current components inactivating with time constants of $\tau_{1(inact)}$ and $\tau_{2(inact)}$ ms respectively, t is time and t_0 is time at the start of the fit in ms, C is the amplitude of the non-inactivating current component or plateau current in pA.

To analyse tail currents the decaying current tail was best fit by a second order exponential:

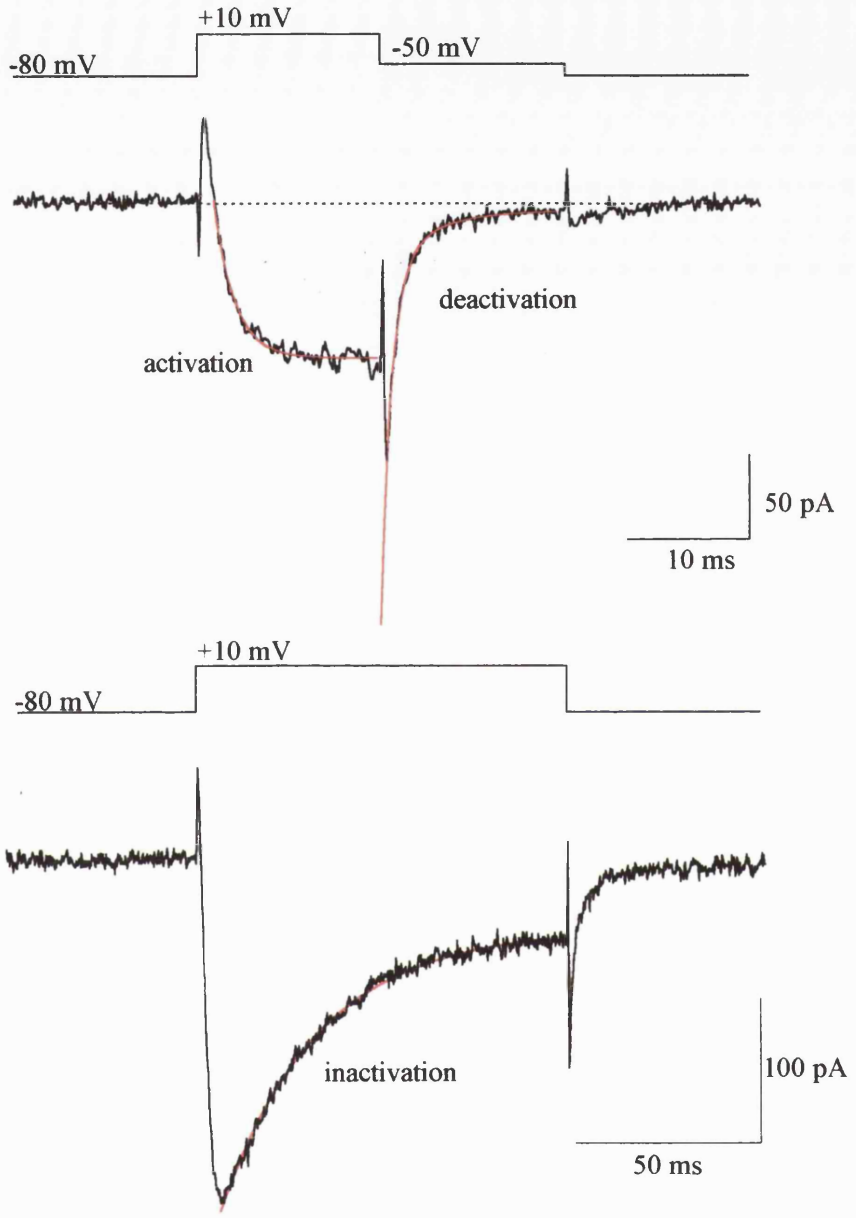

Fig. 2.2. Activation of evoked Ca^{2+} channel currents could be fit with a single exponential function. Inactivation of currents during depolarisation was described by either a single, or double exponential, whilst deactivation of tail currents was fit with a single or double exponential fit function. This could be extrapolated back to the start of repolarisation to provide the instantaneous tail current amplitude. $I_{10\ ms}$ represents the current amplitude 10 ms after repolarisation.

$$I_{tail} = A_1 .\exp\left(\frac{-(t-t_0)}{\tau_{1(deact)}}\right) + A_2 .\exp\left(\frac{-(t-t_0)}{\tau_{2(deact)}}\right) \qquad \textit{Equation 4}$$

where A_1 and A_2 are amplitudes of the two current components in pA that deactivate with time constants of $\tau_{1(deact)}$ and $\tau_{2(deact)}$ ms respectively, t is time and t_0 is time at the start of the fit in ms (see Fig. 2.2).

The exponential fit was extrapolated back to the end of the command voltage step to provide an instantaneous tail current amplitude (I_{inst}), in some experiments the tail current amplitude was also measured 10 ms after repolarisation ($I_{10\,ms}$).

Steady state inactivation protocols were analysed by measuring the peak current amplitude evoked by the test pulse at each of the pre-pulse potentials. Peak current was plotted against the potential during the conditioning step and fitted with a Boltzmann function of the form below, giving the voltage-dependence of gating of the channels and the fraction of available and inactivated channels.

$$\frac{I}{I_{\max}} = \frac{1}{\left(1+\exp\left(V - V_{50(inact)}\right)/s\right)} \qquad \textit{Equation 5}$$

where I/I_{max} is the proportion of available channels, $V_{50(inact)}$ is the voltage at which half the channels are inactivated, and s is the slope factor of the curve in mV.

To investigate the effects of a drug on Ca^{2+} channel currents, repetitive steps to +10 mV were delivered. Peak currents were measured before, and during application of the drug once a steady-state had been reached. Between 3-5 traces were averaged for each value and the percentage change was obtained.

Dose-response curves to calcium channel antagonists were fitted by a power Logistic function of the form:

$$Inhibition = \frac{\left(A_{\min} - A_{\max}\right)}{\left(1+\left(\frac{x}{x_0}\right)^h\right)} + A_{\max} \qquad \textit{Equation 6}$$

where A_{min} and A_{max} are the maximum and minimum inhibitions, x is the concentration of drug, and x_0 is the EC_{50} (see individual figures and text for units)

and h approximates to the Hill coefficient (but see De Lean *et al.*, 1978 for limitations).

Recording solutions

Cerebellar granule neurones

Solutions were designed both for the isolation of Ca^{2+} channel currents using Ba^{2+} as the charge carrier and to maximise the useful recording time of each cell being studied. Table 2.3 shows the intracellular recording solution used in the patch pipette for recording from cerebellar granule neurones. For recording of Ca^{2+} channel currents the major internal cation should be impermeant to the majority of K^+ channels. Cs^+, TEA, Tris and *N*-methyl-D-glucamine (NMDG) are standardly used, here Cs^+ was used. Cs^+ unlike TEA and NMDG has the ability to carry outward current through Ca^{2+} channels allowing a clear definition of the null potential which may be advantageous. The Ca^{2+} channel current and the cells themselves last longer if intracellular Ca^{2+} is buffered. Some studies have been unable to record Ca^{2+} channel currents in granule neurones even with 10 mM Ba^{2+} as a charge carrier (Cull-Candy *et al.*, 1989; Jalonen *et al.*, 1990) and others reported an extremely rapid rundown of currents (Hockberger *et al.*, 1987; Robello *et al.* 1989). A high degree of Ca^{2+} buffering was necessary to obtain stable recordings (Bossu *et al.*, 1989). In this study a relatively high concentration of ethyleneglycol-bis(β-aminoethylether) (EGTA) was required to maintain currents over reasonable recording periods and the intracellular free Ca^{2+} concentration was 10 nM, calculated using the Chelator software for determining total and free ion concentrations (written and provided by Dr. A.D.Hughes, Imperial College). *N*-(2 hydroxyethyl) piperazine-*N*'-(2 ethane sulphonic acid)(HEPES) was used to buffer pH, which was adjusted to 7.2 with CsOH.

A problem often encountered during whole-cell patch recording is irreversible run down of currents due to dialysis of intracellular constituents. Various techniques have been employed to prevent this occurring. Successful amongst these is the inclusion of ATP in the pipette or a complete ATP regenerating system, eg. creatine phosphate and creatine phosphokinase (Forscher, 1985). Rundown seems to occur due to a loss of phosphorylated residues on the channel subunits itself. Activity of Ca^{2+} channels can be restored to inside-out patches of rabbit cardiac cells whose activity has completely disappeared, by exposing the inside face of the patch to Mg.ATP and the catalytic subunit of PKA. Under these conditions the activity of the channel could be even greater than under control, cell-attached

	Concentration (mM)		
Constituent	0.1 mM $[Mg^{2+}]_i$	0.5 mM $[Mg^{2+}]_i$	1 mM $[Mg^{2+}]_i$
HEPES	100	100	100
EGTA	30	30	30
$CaCl_2$	0.57	0.57	0.57
free $[Ca^{2+}]$	10 nM	10 nM	10 nM
$MgCl_2$	2.25	3.23	4.43
free $[Mg^{2+}]$	0.1	0.5	1.0
ATP	3.68	2.34	2.17
[Mg.ATP]	2	2	2
GTP	0.1	0.1	0.1
pH	7.2 (CsOH)	7.2 (CsOH)	7.2 (CsOH)
Osmolarity	320 mOsM (Sucrose)	320 mOsM (Sucrose)	320 mOsM (Sucrose)

Table 2.3 Composition of intracellular solutions for recording from cerebellar granule neurones.

conditions (Ono and Fozzard, 1992). In all recording solutions $MgCl_2$ and ATP were added in the exact proportions necessary to keep the concentration of Mg^{2+} bound ATP constant at 2 mM. The concentration of free Mg^{2+} was also manipulated to precise levels to provide solutions with three different $[Mg^{2+}]_i$ (see Table 2.3). Free $[Mg^{2+}]$ and [Mg.ATP] were calculated using the chelator software.

The composition of the extracellular solution is shown in Table 2.4. External cations impermeable to K^+ and Na^+ channels were used. In addition tetrodotoxin (TTX) was used to block Na^+ channels The charge carrier was Ba^{2+} unless otherwise stated. Ba^{2+} was favoured over Ca^{2+} due to its greater permeability through Ca^{2+} channels leading to larger currents (Fox *et al.*, 1987a,b). Ba^{2+} also does not support Ca^{2+}-dependent inactivation (Chad and Eckert, 1986) and gives more sustained currents which can be recorded over a greater period of time. HEPES buffered the pH, which was adjusted to 7.4 with acetic acid.

Osmolarity of the solutions was adjusted with sucrose to 320 mOsm measured using a Wescor 5500 Vapour Pressure Osmometer.

COS-7 cells

The intracellular solution (Table 2.5) contained Cs^+ as the main cation. Ca^{2+} was buffered with EGTA to nanomolar concentrations. ATP was included in the patch pipette to prevent run down of currents and HEPES buffered pH changes to around 7.2. Osmolarity was adjusted to 310 mOsm.

The extracellular solution (Table 2.5) contained TEA as the principal cation, useful due to its impermeability to K^+ channels. K^+, Mg^{2+} and Na^+ were included within normal physiological limits. HEPES was used to buffer pH to 7.4, and osmolarity was adjusted to 320 mOsm with sucrose. Ba^{2+} was used to carry charge through Ca^{2+} channels. 1 mM was adequate to produce sizeable currents due to the high levels of expression obtained by transfection.

All solutions were stored frozen in aliquots to prevent the hydrolysis of nucleotides.

Supply and preparation of drugs is shown in Table 2.6 unless stated otherwise, all drugs and chemicals were obtained from *Sigma*.

Constituent	Concentration (mM)
TEA-acetate	70
NMDG	70
Potassium hydroxide	3
Magnesium acetate	0.6
Glucose	4
Barium acetate	10
HEPES	10
Tetrodotoxin	0.001
pH	7.4 (acetic acid)
Osmolarity	320 mOsM (sucrose)

Table 2.4 Composition of extracellular recording solution used in recordings of cerebellar granule neurones.

Extracellular solution	
Constituent	Concentration (mM)
TEA-bromide	160
Potassium chloride	3
Sodium bicarbonate	1
Magnesium chloride	1
HEPES	10
Glucose	4
Barium bromide	1
pH	7.4 (Sigma 7-9)
Osmolarity	320 mOsM (sucrose)

Intracellular solution	
Constituent	Concentration (mM)
Ceasium aspartate	140
EGTA	5
Magnesium chloride	2
Calcium chloride	0.1
ATP	2
HEPES	20
pH	7.2 (CsOH)
Osmolarity	310 mOsM (sucrose)

Table 2.5 Composition of extracellular and intracellular recording solutions used to record Ca^{2+} channel currents from COS-7 cells. (Sigma 7-9 contains tris(hydroxymethyl) amino-methone).

Drug	Supplier	Storage
ω-Aga IVA	*Bachem Bioscience Inc.*	96 μM stock in water
ω-CTg GVIA	*Peninsula laboratories*	100 μM stock in water
ω-CTx MVIIC	*Peptide Institute*	100 μM stock in water
Nicardipine	*Sigma*	1 or 10 mM ethanol stock, stored in the dark
s-(-)-BayK8644	*Research Biochemichals Inc.*	10 mM ethanol stock, stored in the dark
r-(+)-BayK8644	*Research Biochemichals Inc.*	10 mM ethanol stock, stored in the dark
TTX	*Sigma*	stored in acetate buffer, pH 4-5

Table 2.6 Storage and Supply of drugs and toxins.

Fluorescence measurements of cell chemistry in intact cells

When certain molecules are exposed to light of appropriate energy, they absorb photons promoting electrons into higher orbitals. As the electrons drop back to their lower energy states, photons are re-emitted, a process known as fluorescence. The spectrum of light that is absorbed and emitted may vary according to the interactions the compound has with other molecules, eg. binding to Ca^{2+}, protons or other ions or the electric field it senses. In recent years this phenomenon has been exploited in the development of fluorescent probes that can transmit information about intracellular events in the living cell. Changes in the concentration of intracellular ions, second messengers and pH which play important roles in cell function are now accessible to direct study without the need to impale cells with microelectrodes.

Fluorescent probes have largely superseded their predecessor chemiluminescent probes such as aequorin. Their advantages over these early indicators which allow the release of only a single photon on each molecular interaction, is that they can undergo millions of transitions before becoming exhausted. Fluorescent signals are usually detected relative to background which has negligible emission keeping the signal to noise ratio high.

The variety of fluorescent probes available is continuously growing. As intracellular Ca^{2+} ($[Ca^{2+}]_i$) is such an important and ubiquitous signal it has been given a lot of attention by experimenters. However, it is now possible to apply fluorescence technology to monitor $[Ca^{2+}]_i$, $[Mg^{2+}]_i$, $[Na^+]_i$, $[Zn^{2+}]_i$, $[Cl^-]_i$, pH_i, potential at the cell and mitocondrial membrane, and secretion.

Fluorescent indicators change the intensity of their emission in response to changes in the concentration of the ion to which they are sensitive. In some cases, the intensity of emitted light is directly proportional to the ions concentration. Other dyes may show an increase in intensity of emission at one wavelength and a decrease in intensity at another. These dyes are known as dual wavelength dyes (Tsien and Poenie, 1986), and their development has greatly aided the measurement of the spatial distribution of ions within the cell. The advantage of these dyes is that since the free form of the indicator has a different excitation spectrum to the ion bound form, a ratio of the two signals provides a direct

measure of the concentration of the ion that is corrected for differences in the cell thickness, non-uniform intracellular dye concentration, and the effects of dye bleaching or leakage of dye from the cell.

The use of fluorescent indicators has been greatly increased by the development of membrane permeant acetoxy-methyl ester derivatives of the dyes. These lipophilic compounds easily cross the cell membrane where they are cleaved by non-specific esterases inside the cell releasing the active, membrane impermeant probe in the cytoplasm and various organelles. Thus the process of loading the dye into cells is far less disruptive than techniques involving microinjection, electroporation or osmotic shock.

Theory

Generally, for the binding of an ion (X) to its ligand (L) an equilibrium expression can be written

$$L + X \leftrightarrow LX \qquad \textit{Equation 7}$$

which has a corresponding dissociation constant:

$$K_D = \frac{[L]\cdot[X]}{[LX]} \qquad \textit{Equation 8}$$

The cytosolic concentration of the ion can be determined from the relation

$$[X] = K_D \frac{[LX]}{[L]} \qquad \textit{Equation 9}$$

For the case of fluorescent indicators where changes in the magnitude of fluorescence at a particular wavelength result from the ligand binding an ion, the ion concentration is determined by the analogous equation

$$[X] = K_D\left(\frac{F - F_{min}}{F_{max} - F}\right) \qquad \textit{Equation 10}$$

where F= fluorescence intensity, F_{min} fluorescence intensity in the absence of ion, F_{max} in the presence of saturating ion concentrations (Grynkiewicz *et al.*, 1985).

A similar equation can be derived to calculate ion concentration of a dual wavelength dye, where the ratio of fluorescence intensities at two wavelengths, one at or close to the maximum for complexed dye, and the second at the maximum for uncomplexed dye are measured.

In the case of MagFURA2 binding Mg^{2+} the concentration of intracellular free Mg^{2+} is given by:

$$[Mg^{2+}]_i = K_D\left(\frac{R - R_{min}}{R_{max} - R} \cdot \frac{Sf_2}{Sb_2}\right) \qquad \textit{Equation 11}$$

where R is the ratio of fluorescence intensities at 340/380 nm, R_{max} and R_{min} are ratios for complexed and uncomplexed dye and $Sf2$ and $Sb2$ are fluorescence intensities at 380 nm with no ion and in saturating ion concentrations respectively.

MagFURA2 despite being reasonably selective for Mg^{2+} over Ca^{2+}, complexes Ca^{2+} with a similar shift in fluorescence spectra. The $K_{D'}$ (Ca^{2+})=53 μM for MagFURA2, much lower than K_D (Mg^{2+})=1.5 mM but far in excess of basal Ca^{2+} for most cells. In situations where Ca^{2+} concentration may rise to levels significantly contributing to the fluorescence, the signal represents an average of $[Mg^{2+}]$ and $[Ca^{2+}]$ weighted by their respective dissociation constants. Assuming both Mg^{2+} and Ca^{2+} are in equilibrium with the dye

$$[Mg^{2+}] = K_D\left(\frac{R - R_{min}}{R_{max} - R} \cdot \frac{Sf_2}{Sb_2}\right) - \left(\frac{K_D}{K_{D'}}\right) \cdot [Ca^{2+}] \qquad \textit{Equation 12}$$

the measured $[Mg^{2+}]_i$ must be corrected for Ca by a term equal to

$$-\left(\frac{K_D}{K_{D'}}\right) \cdot [Ca^{2+}] \qquad \textit{Equation 13}$$

or -28.3 . $[Ca^{2+}]_i$. In situations where $[Ca^{2+}]_i$ maybe expected to rise to concentrations of the order of a few μ molar or higher, error due to a Ca^{2+} signal contaminating the Mg^{2+} signal should be realised.

Two experimental methods were used to make measurements of MagFURA2 fluorescence. Fluorescence microscopy of single cells was employed to measure resting fluorescence in cerebellar granule neurones, and to construct a calibration curve for microscopy measurements. Secondly, fluorescence imaging was used to investigate the responses of granule neurones to glutamate. Each is described below.

Fluorescence microscopy

For fluorescence microscopy measurements of MagFURA2 a 75 W Xenon arc lamp system (*Nikon corporation, Instruments Division, Yokohama Plant*) was used as a light source. Light was focused, and the intensity of the irradiating beam was reduced with neutral density filters to avoid photobleaching. Cells were excited alternately at 340 and 380 nm by means of a rotating block switched by a filter changer. Excitation light was reflected by a 400 nm dichroic mirror and focused onto the cells with a ×40 oil immersion objective (numerical aperture 1.38). A diaphragm placed in the light path allowed optical isolation of single neurones. Emissions at 510 nm were captured by a photomultiplier tube. Output from the photomultiplier was amplified and low-pass filtered with a cut-off frequency of 100 Hz before being digitised and stored on a computer for subsequent analysis. Hardware and software were provided by *Newcastle Photometric Systems, Newcastle upon Tyne, UK.*

Experiments were carried out at 20-23 °C. The fluorescent indicators MagFURA2-AM and the free acid of MagFURA2 were prepared as 1 mM stock solutions in anhydrous dimethyl sulphoxide (DMSO) and stored at -20 °C. 4Br-A23187 was also diluted from a 1 mM DMSO stock. (Fluorescent probes, and 4Br-A23187 were obtained from *Molecular Probes, Eugene, OR, USA*).

Cultured cerebellar granule neurones were rinsed well with Hanks Balanced Salt Solution (HBSS) (Table 2.7) to remove serum and culture medium. MagFURA2 measurements were made in individual neurones by loading cells with 10 μM MagFURA2-AM in HBSS for 15 minutes at room temperature. Loading solutions were mixed vigorously to thoroughly disperse the dye. The cells were then washed to remove excess dye and left for a further 15 mins to allow for full cleavage of the AM-ester by non-specific esterases within the cell, ensuring stable fluorescence, and then given a final wash. Fluorescence was measured from an area approximately 5×5 μm, small enough such that the cell being studied filled the aperture.

Before recording signal from a cell, an area containing no cells or processes was measured at each wavelength to subtract from fluorescence of the emitted light.

Constituent	Concentration (mM)
Sodium chloride	137
Potassium chloride	5
Magnesium sulphate	0.9
Calcium chloride	1.4
Sodium bicarbonate	3
Sodium hydrogen phosphate	0.6
Potassium dihydrogen orthophosphate	0.4
Glucose	5.6
HEPES	20
pH	7.4 (NaOH)
Osmolarity	320 mOsM

Table 2.7 composition of Hank's Balanced Salt Solution

Recordings of resting fluorescence were made by measuring emission for a few minutes and averaging the values obtained.

Calibration was attempted with cells by incubation with HBSS modified to contain 20 mM Mg and 0 Ca, or 0 Mg in addition to 10 μM of the non-fluorescent ionophore 4Br-A23187 to carry Mg^{2+} across the membrane. During 10-12 minutes equilibration time fluorescence did not appreciably change and longer periods of incubation with the ionophore were detrimental to the cells. To make estimates of Mg^{2+} concentration, a calibration curve was constructed using the free acid tetrapotassium salt of MagFURA2. 1 μM MagFURA2 was diluted in a mock intracellular solution composed of 140 mM KCl, 5 mM NaCl, 7.5 mM HEPES and adjusted to pH 7.3 and 320 mOsM with sucrose. Concentrations of Mg from 0 to 10 mM were used to construct a curve and values estimated accordingly.

Magnesium imaging

Fig. 2.3 shows diagrammatically the system used for the fluorimetric monitoring of changes in ion concentration. The excitation light was provided by a xenon arc lamp (Xe100W, LH-M100CB-1 lamphousing, XPS-100 supply, *Nikon corporation, Instruments Division, Yokohama Plant*), and in order to perform ratiometric measurements a filter changer (*Cairn*) was used to rotate a filter block containing 340 and 380 nm bandpass filters which were used to alternate the excitation wavelength. Neutral density filters and a shutter were used to interupt the light path. Light entering the microscope was reflected by a 400 nm dichroic mirror onto the stage of an inverted microscope (*Nikon diaphot*) and focused onto the sample cells using a ×40 UV-F objective (*Nikon*). Emitted light passed through the dichroic mirror and was filtered by a 480 nm barrier filter.

Spatially resolved information on the emitted light was collected using an imaging system consisting of a System2000 cooled charged coupled device (CCD) camera controller coupled to a TE/A Peltier cooled camera head, the CCD sensor output was then converted to a 12-bit signal for processing by a System2000 4/12-bit A/D converter (*Digital Pixel, Brighton, UK*). The captured images were then transferred to a DEC 486/50 PC for on-line monitoring and later analysis. Image data was stored on a magneto-optical storage disk. Acquisition and analysis were controlled by the Kalcium PC acquisition and analysis software (*Kinetic Imaging*).

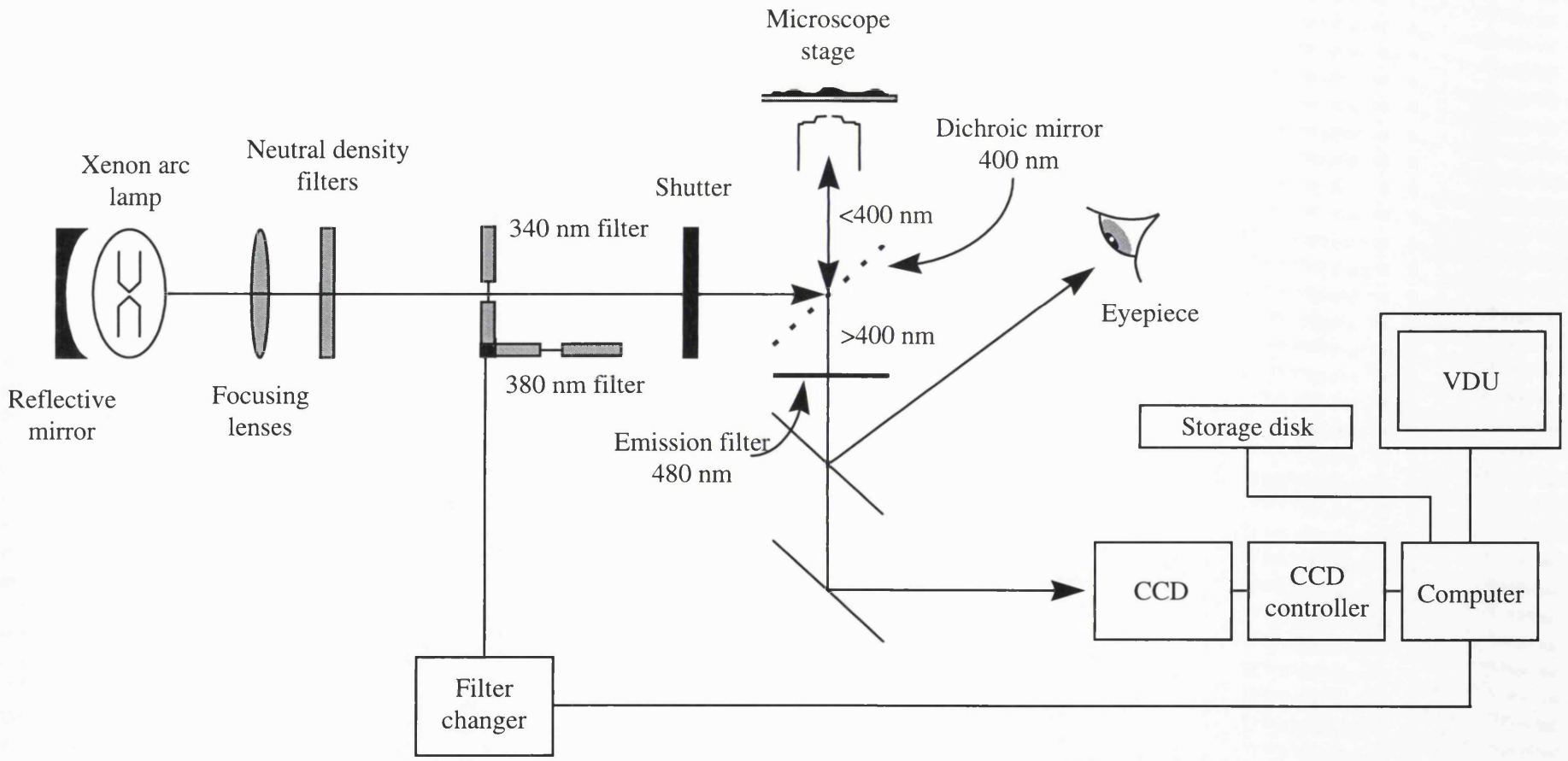

Fig. 2.3 Diagram showing the component parts of the imaging apparatus as it was configured to measure Mg^{2+}. Light from a xenon arc lamp was focused onto a filter changer which could alternate between 340 and 380 nm filters and was controlled by the image acquisition software. A shutter could also be placed in the light path when images were not being acquired. The optics employed a dichroic mirror that reflected light of <400 nm and passed light of >400 nm which then passed through the emission filter (480 nm). The light was then collected by a cooled, charged coupled device camera and individual frames captured by the computer and stored on a magneto optical disk drive for later analysis.

Mg^{2+} imaging studies were all carried out in HBSS at room temperature (20-23 °C) with the exception of experiments conducted in 0Ca-HBSS in which 1.4 mM $CaCl_2$ was replaced by 20 μM EGTA. The method used for loading with MagFURA2-AM was identical to that described above. Cells were held in a chamber of approximately 1 ml volume into which drugs could be added. Washes were carried out by replacing the bathing solution completely once or twice.

A region of the field containing no cells or neurites was sampled and averaged as a measure of background. Average background fluorescence at each wavelength was subtracted from measurements of cellular fluorescence. Background-subtracted data from regions within the somas of individual cells was ratioed to give 340/380 values.

Chapter 3

General properties of Ca^{2+} channel currents in cerebellar granule neurones

Results

The following chapter describes briefly the general properties of Ca^{2+} channel currents in cerebellar granule neurones as an introduction to these cells.

Fig. 3.1 shows a cerebellar culture 14 days after preparation of cells. Cerebellar granule neurones were easily distinguished on morphological criteria as neurones having a small, spherical soma, 5-7 μm in diameter projecting fine neurites. Neurones survived well in culture and could be kept for >28 DIV (days *in vitro*) in medium containing 23 mM K^+. After 7 DIV the majority of cultures contained neurones that formed clumps, interconnected by bundles of fibres. In sister cultures were the K^+ concentration was kept at physiological levels the majority of neurones did not survive for more than 7 days and did not organise into the clusters characteristic of cultures grown under depolarising conditions. The role of depolarisation for the survival of cerebellar granule neurones in culture has been investigated elsewhere (Gallo *et al.*, 1987).

Development of currents

On the day of culture Ca^{2+} channel currents were not present in these cells. Over the course of the next 7 DIV currents increased in amplitude and remained essentially constant over days 7-14 (see Fig. 3.2). For this reason recordings were only made from cells between 7 and 14 DIV. Over the first 7 days there was a coincident small increase in the C_m of cells which stabilised during days 7-14. Since there was a slight increase in C_m over the first week of culture, the increase in peak amplitude was not simply proportional to the increase in current density.

Current transients

Analysis of the capacity transient was carried out in 71 cells from multiple cultures. A recording made from one cell is shown in Fig. 3.3. Hyperpolarising steps to -90 (-102) mV for 4 ms elicited current transients whose decay could only be fit by a second order exponential indicating that the charging of the cell membrane was complicated by the extensive processes formed by granule cells. From the pooled data the fast and slow time constants were averaged and found to

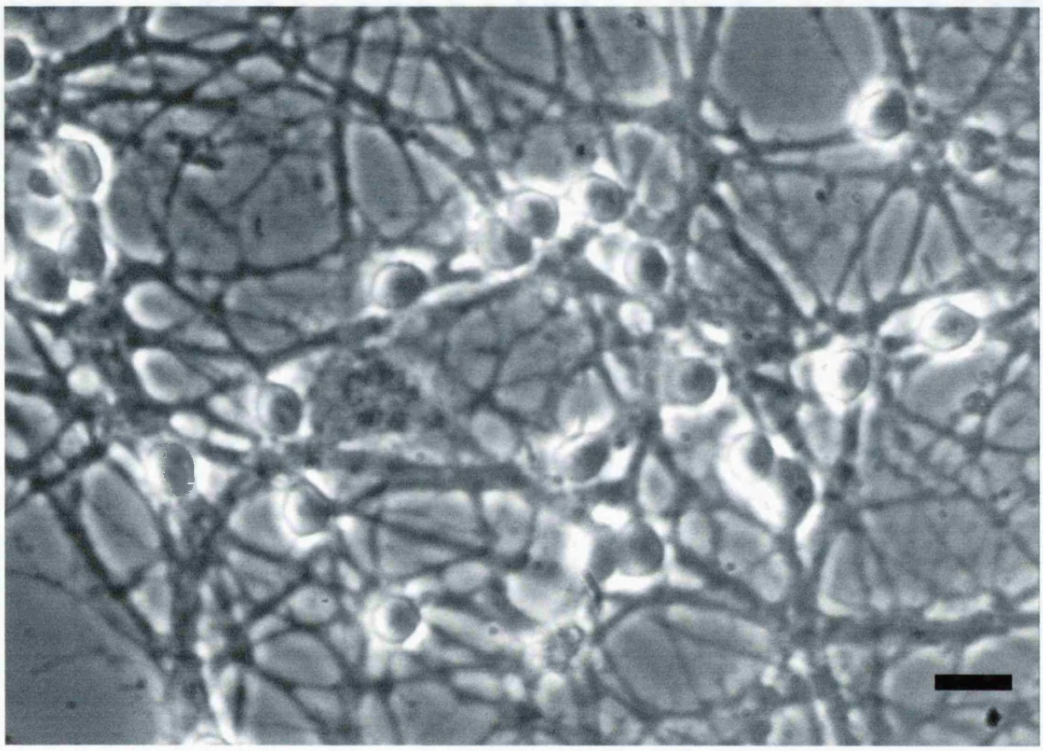

Fig. 3.1 Cerebellar granule neurones grown in culture for 14 days. The picture was taken by a System2000 cooled charged coupled device (CCD) camera controller coupled to a Peltier cooled camera head attached to an inverted microscope employing phase contrast optics and 400× magnification. The image was captured by the Kalcium acquisition software (*Kinetic Imaging*). The scale bar measures 10 μm.

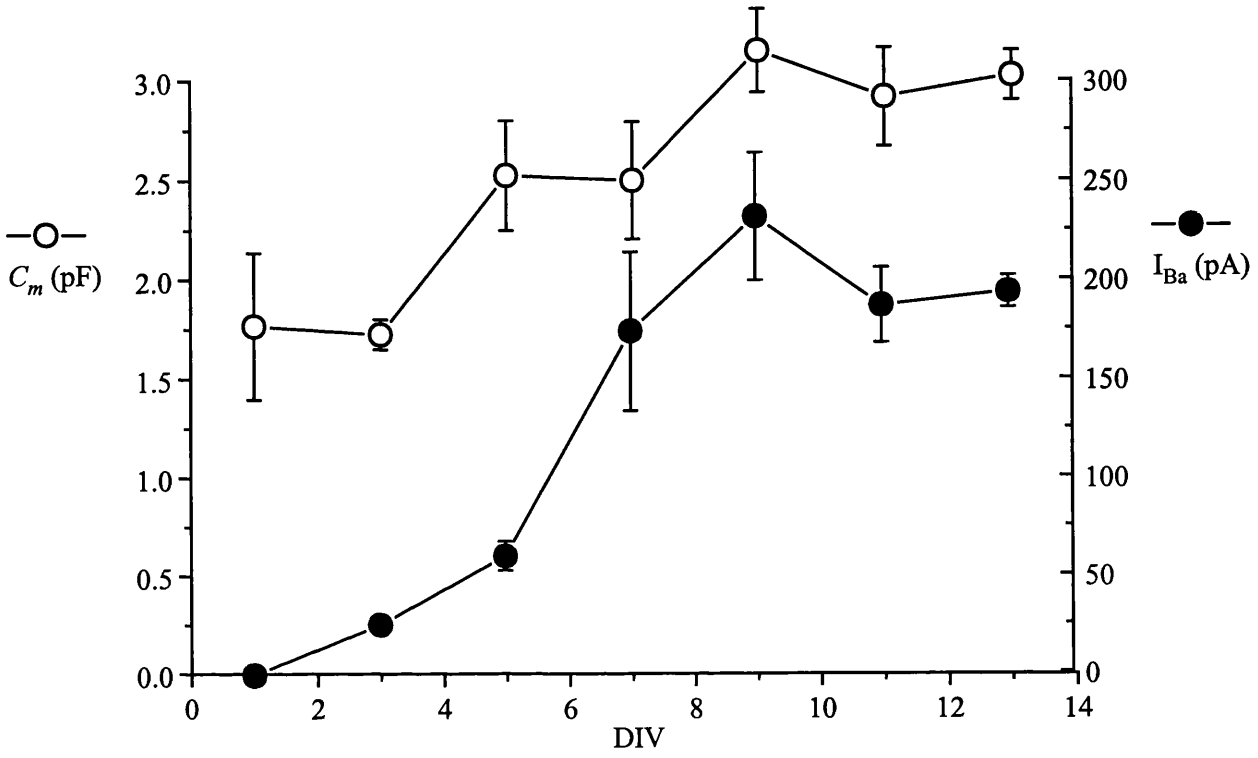

Fig. 3.2 Development of Ca^{2+} channel currents in cerebellar granule neurones over the first 14 days *in vitro*. The open circles show changes in C_m and the filled circles measure the peak inward current at different developmental stages. Each point represents the mean±s.e.m. for a group of 4 cells.

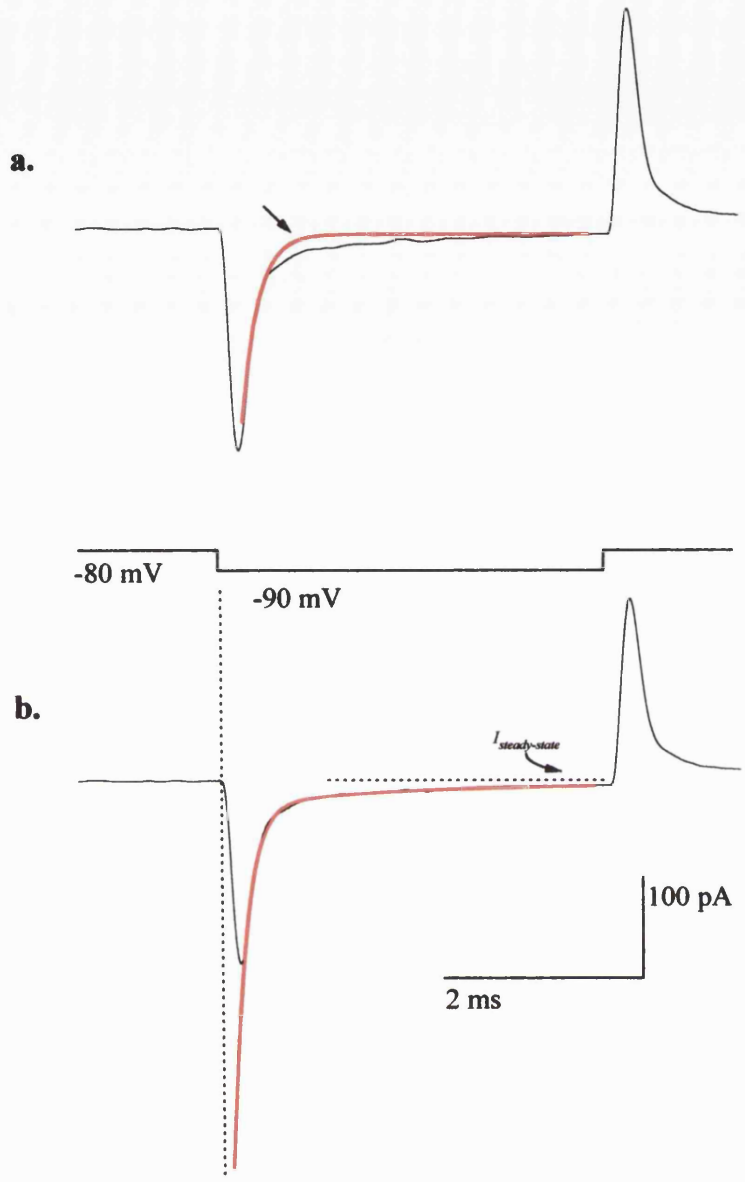

Fig. 3.3 Analysis of the current transient in a single granule neurone. The cell was held at -80 mV and stepped for 4 ms to a potential of -90 mV after achieving the whole-cell configuration and cancellation of pipette capacitance but before neutralisation of whole-cell capacitance and series resistance. **a.** demonstrates a single order exponential fit to the capacity current. The arrow shows regions of the trace not fit by the procedure. **b.** The red line shows a second order exponential fit to the data. The time constants of the exponential gave an indication of the speed of voltage-clamp. The steady-state current ($I_{steady\text{-}state}$) measured at the end of the voltage-step was used to calculate R_m. The current was sampled at a frequency of 77 kHz. (Potentials given are uncorrected for liquid junction potential, which was -12 mV).

be 0.12±0.003 ms and 0.82±0.05 ms respectively, 63±3% of the current decaying with the faster time constant. The average steady-state current was found to be 4.4±0.2 pA, which was used to calculate the input resistance (R_m) by application of Ohm's Law. R_m was found to be 2.6±0.1 GΩ, characteristically high and consistent with previous reports (Rossi *et al*, 1994; Traynelis *et al.*, 1993). Average C_m in these cells was 3.6±0.3 pF. When the cells had reached a mature stage in culture, and assuming a specific C_m of 1 μF/cm^2, Ca^{2+} channel current density attained values of around 50 μA/cm^2 using 10 mM extracellular Ba^{2+}. Average R_s in granule cells was 19±0.6 MΩ.

Ca^{2+} and Ba^{2+} currents

Fig. 3.4a shows families of Ca^{2+} channel currents in individual neurones of similar culture age recorded using either 10 mM Ba^{2+} or 10 mM Ca^{2+} as the charge carrier. Upon inspection of current traces Ba^{2+} currents were seen to be larger in amplitude, activated faster, inactivated more slowly, and had tail currents that deactivated more rapidly. With increasing depolarisation the rate of activation became faster. Inactivation also became slightly more obvious over increasingly positive potentials. The null potential of Ca^{2+} currents was much less positive than the Ba^{2+} current null potential, but both peaked in amplitude at +10 (-2) mV. Both Ba^{2+} and Ca^{2+} currents were sensitive to block by Cd^{2+}. Application of 1 mM Cd^{2+} to cells caused a completely reversible block of 85±6% to currents carried by Ca^{2+} (n=3), and 90±6% to currents carried by Ba^{2+} (n=3), (see Fig. 3.4b).

Activation, inactivation and tail current deactivation of Ca^{2+} channel currents

The activation of Ba^{2+} currents was examined across a range of potentials by delivering short 15 ms depolarising steps to various potentials and fitting an exponential function to the rising phase of the activating current. The time constant of activation showed a voltage-dependence such that larger depolarisations evoked currents which activated faster. Fig. 3.5 shows the average $\tau_{(act)}$ for a group of 8 cells at potentials between -20 (-32) and +50 (+38) mV. Activation was slowest at -10 (-22) mV (3.9±0.8 ms) and fastest at +50 (+38) mV (0.3±0.06 ms).

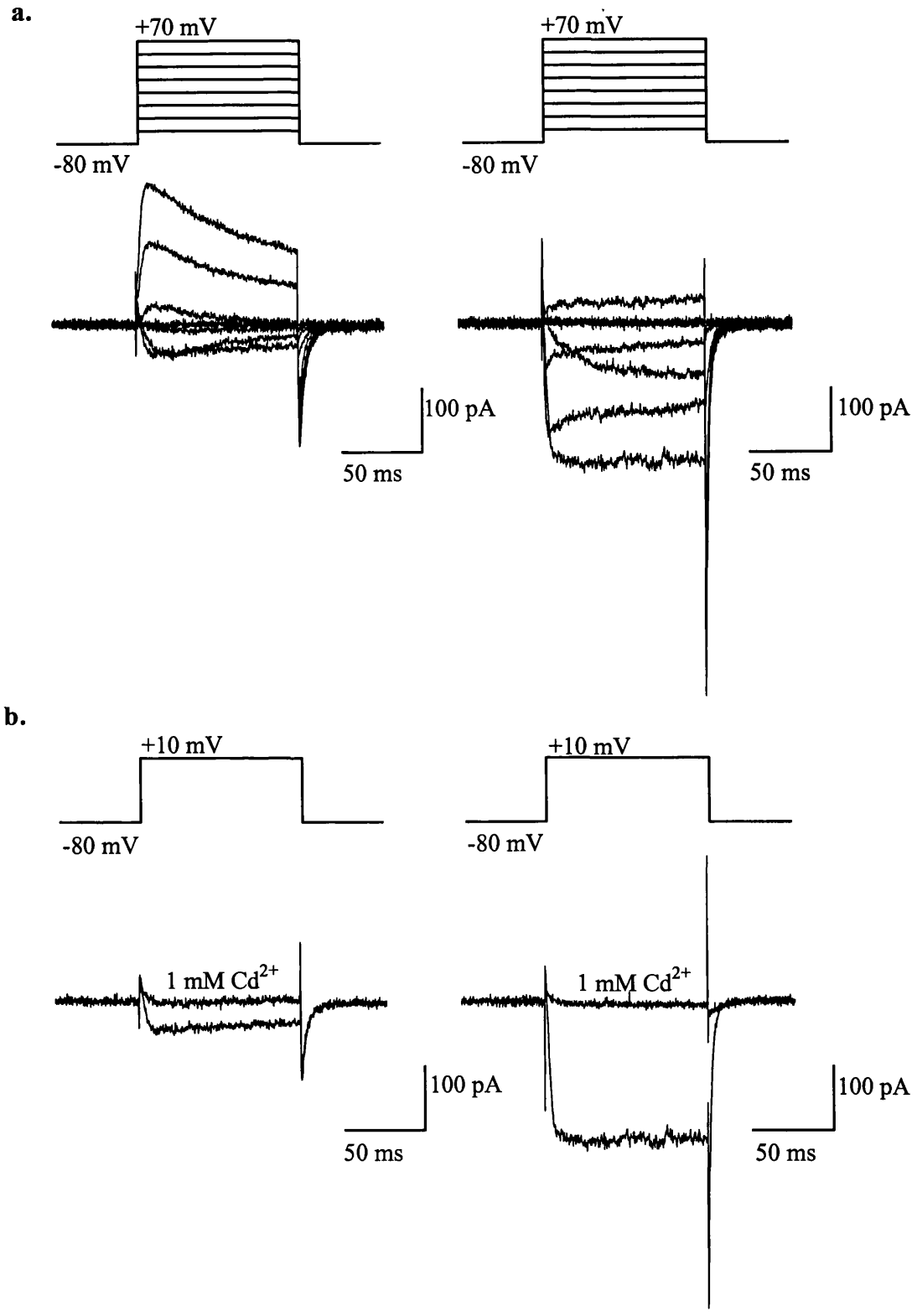

Fig. 3.4 Comparison of Ca^{2+} channel currents carried by 10 mM Ca^{2+} and 10 mM Ba^{2+}. **a.** Families of Ca^{2+} and Ba^{2+} currents in cerebellar granule neurones recorded from a holding potential of -80 mV and stepping to potentials between -70 and +70 mV for 100 ms. **b.** Complete block of Ca^{2+} and Ba^{2+} currents by 1 mM Cd^{2+} , traces shown were recorded before and during application of Cd^{2+}. (Potentials given are uncorrected for liquid junction potential, which was -12 mV).

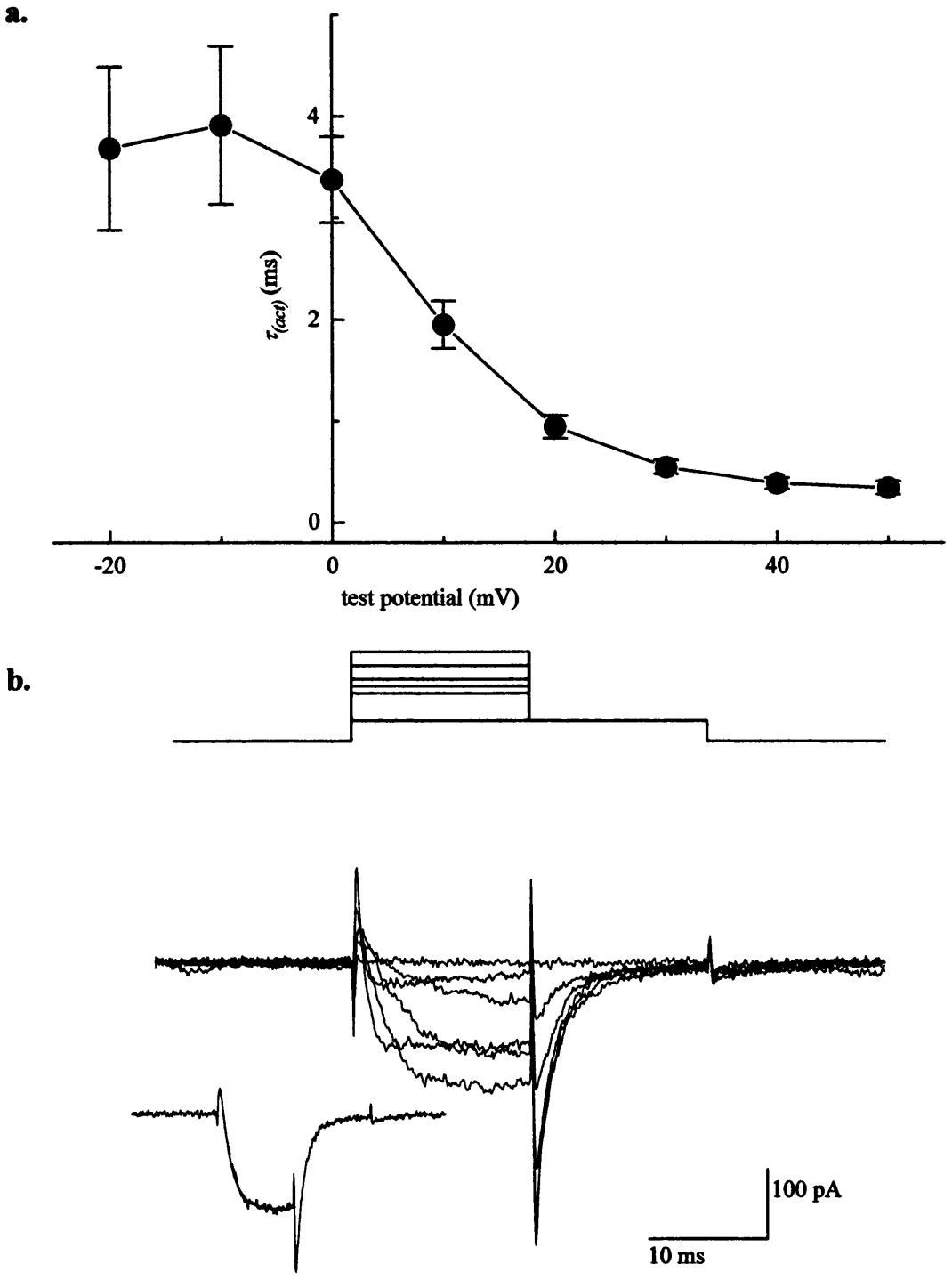

Fig. 3.5 Activation of 10 mM Ba^{2+} currents in cerebellar granule neurones after 10 DIV $\tau_{(act)}$ was measured by fitting a single exponential to the rising phase of the evoked current at potentials between -20 and +50 mV (for protocol see Chapter 2). **a.** Relationship between rate of activation and test potential. The data is the mean±s.e.m. of a group of 8 cells. **b.** Examples of currents evoked for 15 ms to test potentials of -50, -10, 0, +10, +30, +50 mV from a holding potential of -80 mV and stepping back to -50 mV for 15 ms before returning to the holding potential. The inset trace shows a single exponential fit to the current activated at +10 mV. Data was sampled at a frequency of 10 kHz. (Potentials given are uncorrected for liquid junction potential, which was -12 mV).

Closer analysis of the inactivation kinetics of both Ca^{2+} and Ba^{2+} currents is shown in Fig. 3.6a. Currents activated at +10 (-2) mV for 100 ms from a group of 10 cells recorded in either Ba^{2+} or Ca^{2+} were normalised and averaged for comparison. Error bars are shown at several points along the inactivation phase of the current traces. There was little or no inactivation of Ba^{2+} currents over 100 ms. Longer steps were fitted with a second order exponential with 16% of the current inactivating with a $\tau_{(inact)}$ of 645±56 ms and 65% of the current inactivating with a $\tau_{(inact)}$ of 7.4±1 s (n=7; see inset Fig. 3.6a.). A completely non-inactivating component remained that constituted 18% of the total current. In contrast Ca^{2+} currents inactivated much faster and the decay of the current could be described by a single order exponential with $\tau_{(inact)}$=57±9 ms. The rate of decay of the currents carried by Ba^{2+} showed some variation between cultures and between cells of the same culture but rarely displayed substantial inactivation (but compare to the currents illustrated in Fig. 5.2b).

Deactivation of tail currents under these conditions also showed differences. Stepping back from +10 (-2) mV to -80 (-92) mV Ba^{2+} tail currents were smaller than Ca^{2+} current tails and the deactivation was described by a second order exponential with $\tau_{(deact)}$s of 1.8±0.2 ms and 8.5±1.5 ms. Ca^{2+} current tails were larger even though a proportion of the Ca^{2+} current had inactivated after 100 ms and the deactivation was fit well by a single exponential where $\tau_{(deact)}$=4.5±0.3 ms. The time constants of deactivation showed little dependence on pre-repolarisation potential, but Ba^{2+} currents were slowed by less negative holding potentials.

Voltage-dependence of activation and steady-state inactivation

Mean current-voltage relationships for neurones recorded in Ca^{2+} and Ba^{2+} are shown in Fig. 3.6b. The currents were entirely HVA, significant inward current not being activated until the voltage step reached -40 (-52) mV. Maximal inward current was evoked at +10 (-2) mV in both Ca^{2+} and Ba^{2+}. The data was fit with a Boltzmann equation (see *Equation 1*, Chapter 2) which revealed that Ca^{2+} currents activated more positively than Ba^{2+} currents. The $V_{50(act)}$ for currents recorded in Ca^{2+} was +6 (-6)±0.6 mV compared to -0.3 (-12.3)±0.7 mV in Ba^{2+}.

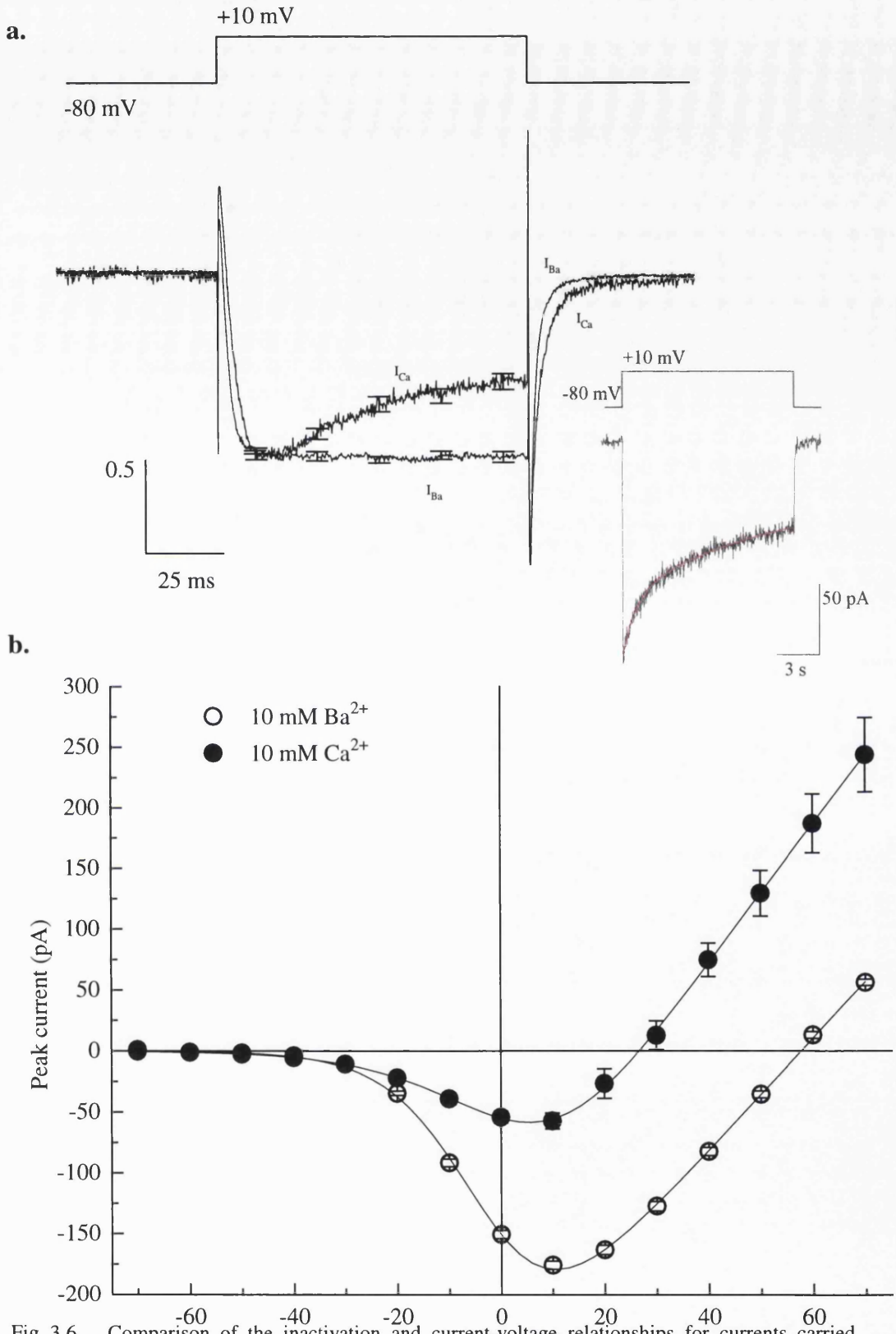

Fig. 3.6 Comparison of the inactivation and current-voltage relationships for currents carried either by 10 mM Ca^{2+} or 10 mM Ba^{2+}. **a.** Inactivation of currents recorded in either Ba^{2+} or Ca^{2+} evoked by stepping the membrane potential to +10 mV for 100 ms. The data are the average of current traces from 10 different cells after normalisation. Error bars are shown at several points. The inset shows an example recording of a longer duration Ba^{2+} current used for determining the time constants of inactivation, the fit shown is a second order exponential. **b.** Current voltage relationships comparing Ba^{2+} and Ca^{2+} currents. The mean data was fitted with a Boltzmann function (see Chapter 2). (Potentials given are uncorrected for liquid junction potential, which was -12 mV).

The current-voltage relationships for Ca^{2+} currents displays a null potential that is much less positive to that of Ba^{2+} currents, and may indicate a contaminating conductance such as a Ca^{2+}-activated conductance for instance a Ca^{2+}-activated K^+ current, or a current that is blocked in the presence of Ba^{2+}.

The voltage-dependence of inactivation of the Ba^{2+} currents is illustrated in Fig. 3.7. The steady-state inactivation was measured for currents recorded during a step depolarisation to +10 (-2) mV following conditioning steps to potentials between -100 mV and +10 (-2) mV for a duration of 10 s. Current traces showed slightly less decay as the potential of the conditioning step became more positive. The data points for each cell could be described by a simple Boltzmann equation. 90% of the current inactivated with average values for $V_{50(inact)}$ and s of -38 (-50)±4 mV and 16±1 mV respectively (n=4).

At the end of the 10 s conditioning step a small proportion of the whole-cell current remained. This non-inactivating component constituted between 10% and 20% of the total current measured at the beginning of the voltage step. Fig. 3.7b shows the 'end current'-voltage relationship. The non-inactivating Ca^{2+} channel current activated more negatively than the whole-cell current (see Fig. 3.6b). Boltzmann fits to the data revealed that the average conductance was 1.3±0.4 nS, and the $V_{50(act)}$ was -16 (-28)±2 mV, nearly 15 mV more negative than the half activation seen for the total activatable current.

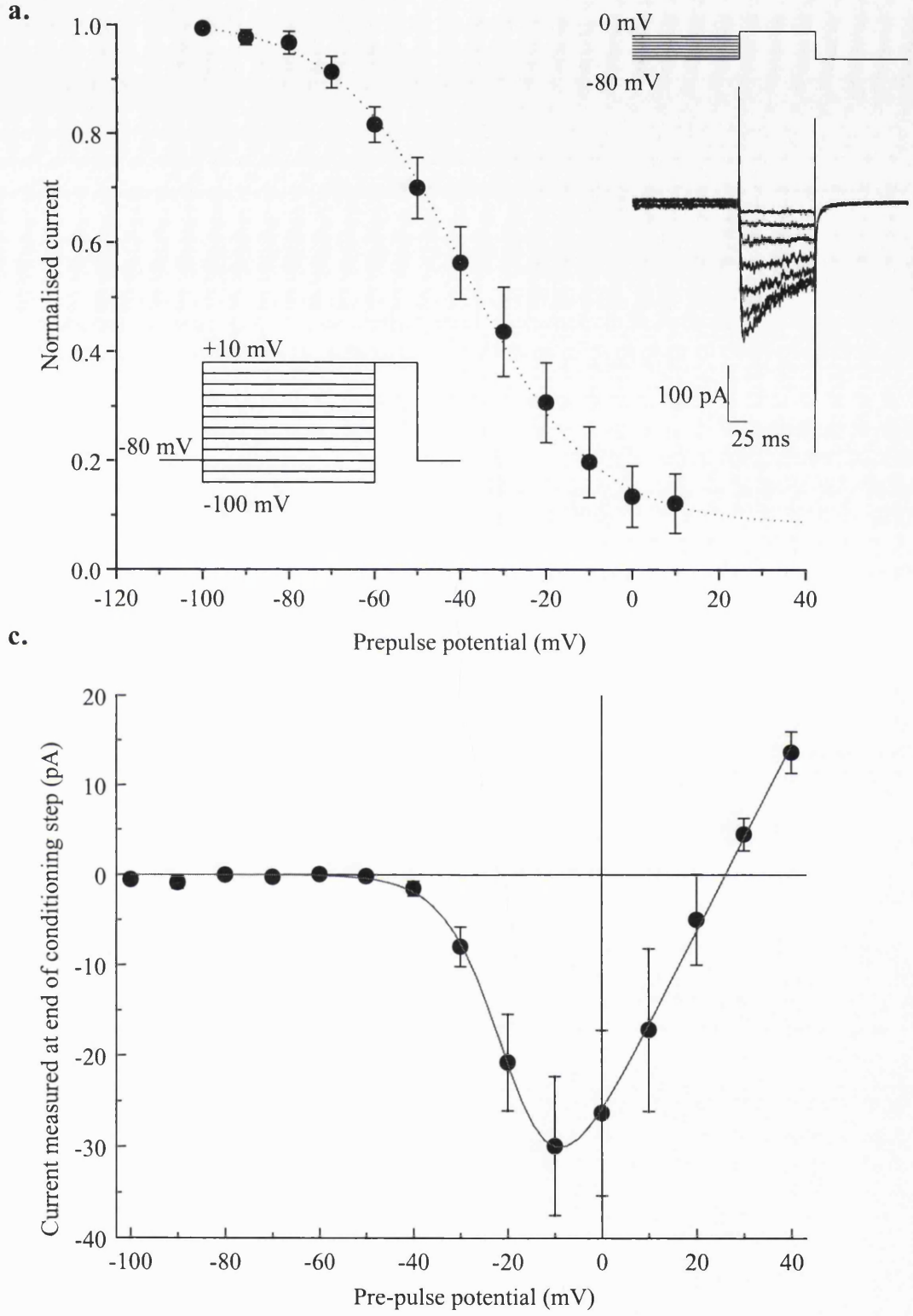

Fig. 3.7 Steady-state inactivation properties of Ba^{2+} currents in cerebellar granule neurones. **a.** Cells were held at potentials ranging from -100 to +10 mV for 10 s prior to a test step to +10 mV for 100 ms. Normalised currents were averaged and their inactivation fitted by a simple Boltzmann relationship (see *Equation 5*, Chapter 2; n=4). **b.** Example test steps showing steady-state inactivation in a single cell where the pre-pulse voltage was between -80 and 0 mV. **c.** Average non-inactivating current remaining at the end of the pre-pulse step plotted as a current-voltage relationship (see text; n=4). (Potentials given are uncorrected for liquid junction potential, which was -12 mV).

Discussion

The time course of HVA current development in cerebellar granule neurones correlated well with other studies. In culture, granule cells show a slightly different age-dependent expression of currents to reports of electrophysiological recordings in slices. Rossi *et al.*, (1994) showed that granule neurones in slices taken from rats from various post-natal stages have Ca^{2+} currents that are only fully expressed by the third post-natal week. The percentage of cells expressing Ca^{2+} currents, and the peak amplitude of these currents was seen to increase steadily throughout the second and third week. C_m during this time showed no change. In the experiments presented here cultured granule cells of an equivalent age to cells recorded from slices reached a fully developed state faster than cells in slices. However, the process of dissociating the cells from cerebellar tissue appears to compromise the Ca^{2+} channels in some way since on the day of culture no currents were recorded whereas slices from animals of the same age expressed currents in just under 40% of cells. It is conceivable that treatment with digestive enzymes during preparation of the cells causes detrimental effects to the channel protein as patch-clamp studies involving the addition of trypsin to the intracellular recording solution showed a loss of functional channels (Hescheler and Trautwein, 1988). Cultures of granule cells may require a period of recovery to replace non-functional channels.

Comparisons of Ca^{2+} channel currents carried by the two divalent ions used here were similar to studies elsewhere in the literature. The higher permeability of HVA Ca^{2+} channels to Ba^{2+} over Ca^{2+} is a characteristic of these channels and was clearly demonstrated for currents in cerebellar granule neurones. In addition, the threshold for activation and the sensitivity to Cd^{2+} show that the current was entirely composed of HVA channels. LVA Ca^{2+} channels do not contribute to the whole-cell Ca^{2+} channel current in cerebellar granule neurones.

The current-voltage relationships comparing Ca^{2+} channel currents carried by Ca^{2+} and Ba^{2+} show large differences in the E_{null}. Theoretically, if the channel being studied is only permeable to one ion then $E_{null}=E_A$ (the Nernst Potential for an ion A) and can be calculated by the formula:

$$E_A = \left(\frac{R'T}{Z_A F}\right) \ln\left(\frac{[A_o]}{[A_i]}\right) \text{ Volts}$$

where R' is the Universal Gas Constant, and equals 8.314 $VCK^{-1}mol^{-1}$, T is absolute temperature, Z_A is the charge on ion A, and F is Faraday's constant, 9.648×10^4 $Cmol^{-1}$, or:

$$= 2.303 \cdot \left(\frac{R'T}{Z_A F}\right) \log_{10}\left(\frac{[A_o]}{[A_i]}\right) \text{ Volts}$$

Calculating the theoretical E_{null} for a divalent cation whose extracellular concentration (10 mM) exceeds its intracellular concentration (~10 nM) by a factor of 1×10^6 produces a value of +174 mV (at 20°C). This potential is far more positive than the E_{null} demonstrated by both Ca^{2+} and Ba^{2+} but because Ca^{2+} channels are also permeable to Cs^+ whose E_A is negative the potential at which currents carried by either 10 mM Ca^{2+} or Ba^{2+} reverse is less positive. A number of factors may contribute to the Ca^{2+} E_{null} occurring at a less positive potential than the Ba^{2+} E_{null}. Ba^{2+} is more effective at screening surface charge because of the smaller size of this cation (Dani, 1986) compared to Ca^{2+}. Also, in the absence of extracellular Ba^{2+} new conductances may be unmasked which were previously blocked such as K^+ currents, and in the presence of Ca^{2+} additional conductances may be activated upon Ca^{2+} entry, such as Ca^{2+}-activated K^+ currents.

Cerebellar granule neurones have been reported to contain multiple Ca^{2+} channel subtypes (Forti and Pietrobon, 1993; Pearson *et al.* 1995; Randall and Tsien, 1995; Tottene *et al.* 1996). This makes it difficult to form conclusions based on the general biophysical properties of the total whole-cell current on the identity of channel subtypes that are contributing to the currents observed. The inactivation kinetics of the currents suggested at least three different channels, one completely non-inactivating that produced a current persisting even after very long depolarising steps. The other two components were distinguishable on the basis of their different rates of inactivation but both inactivated slowly in relation to reports of other native Ca^{2+} channels. The lack of a rapidly inactivating component to the whole-cell current may be a result of differences in culture or recording conditions between this and other studies that have shown rapidly inactivating Ca^{2+} currents in granule cells (Rossi *et al.*, 1994).

Steady-state inactivation of Ca^{2+} channel currents showed little deviation from a simple Boltzmann relationship indicating that the different populations of channels in granule cells inactivate over similar voltage ranges, surprising considering the range of values given for different native HVA channel types from various tissues (Table 1.1). The non-inactivating current remaining after the 10 s conditioning steps during steady-state inactivation experiments represents a current with an extremely slow $\tau_{(inact)}$. P-type channels and L-type channels inactivate most slowly of the channel types so far characterised (Fox *et al.*, 1987b; Usowicz *et al.* 1992;) with $\tau_{(inact)}$ of between 500 and 1000 ms. It is possible that this current is a result of one or more of these subtypes. This should however be viewed with some caution due to the presence of an unidentified conductance causing an unusual E_{null}.

Chapter 4

Pharmacological dissection of the Ca^{2+} channel current in rat cerebellar granule neurones using naturally occurring peptide toxins

Results

This chapter describes work carried out to study the classes of Ca^{2+} channel present in rat cerebellar granule cells. The effects of a number of naturally occurring peptide toxins with potent blocking actions against Ca^{2+} channels were investigated with particular emphasis placed on defining the proportion of whole-cell Ca^{2+} channel current carried by identified or novel subtypes in these cells. The toxin recently identified from a cDNA library prepared from the venom gland of the piscivorous marine snail ω-CTx MVIIC (Hillyard *et al.*, 1992), was used in attempts to further characterise Ca^{2+} currents in these neurones.

Inhibition of Ca^{2+} channel currents by ω-CTx MVIIC

Fig. 4.1 shows the effect on Ca^{2+} channel currents of applying ω-CTx MVIIC to cerebellar granule neurones. Fig. 4.1a shows the concentration-inhibition relationship for a range of concentrations. Maximal inhibition occurred at a concentration of 5 μM. This concentration reduced whole-cell Ca^{2+} channel currents by around 20%. Inhibition by ω-CTx MVIIC was rapid, with maximum block occurring in 10-20 s, and showed partial recovery. From a Logistic fit to the data the EC_{50} was found to be 640 nM and h which approximates to the Hill coefficient was 3 indicating a more complex interaction than one-to-one binding of the toxin to its binding site or sites, and may suggest positive co-operativity.

Fig. 4.1b shows the average current-voltage relationship for 25 different cells across a number of cell cultures before and during application of 5 μM ω-CTx MVIIC. ω-CTx MVIIC reduced the inward current with no effect on the voltage-dependence of activation. From Boltzmann fits to the individual relationships, average control parameter values were calculated under control conditions to be: g=4.4±0.3 nS, E_{null}=+60 (+48)±2 mV, $V_{50(act)}$=-2 (-10)±2 mV and k=8±1 mV. In the presence of ω-CTx MVIIC these changed to g=2.9±0.3 nS (p=0.000002; n=25), E_{null}=+63 (+51)±1 mV, $V_{50(act)}$=-3 (-9)±1 mV and k=7±0.3 mV.

Fig. 4.1c shows example currents evoked by stepping to the peak of inward current (+10 mV) in the absence and presence of ω-CTx MVIIC. The difference current, generated by subtracting the residual ω-CTx MVIIC-resistant current after

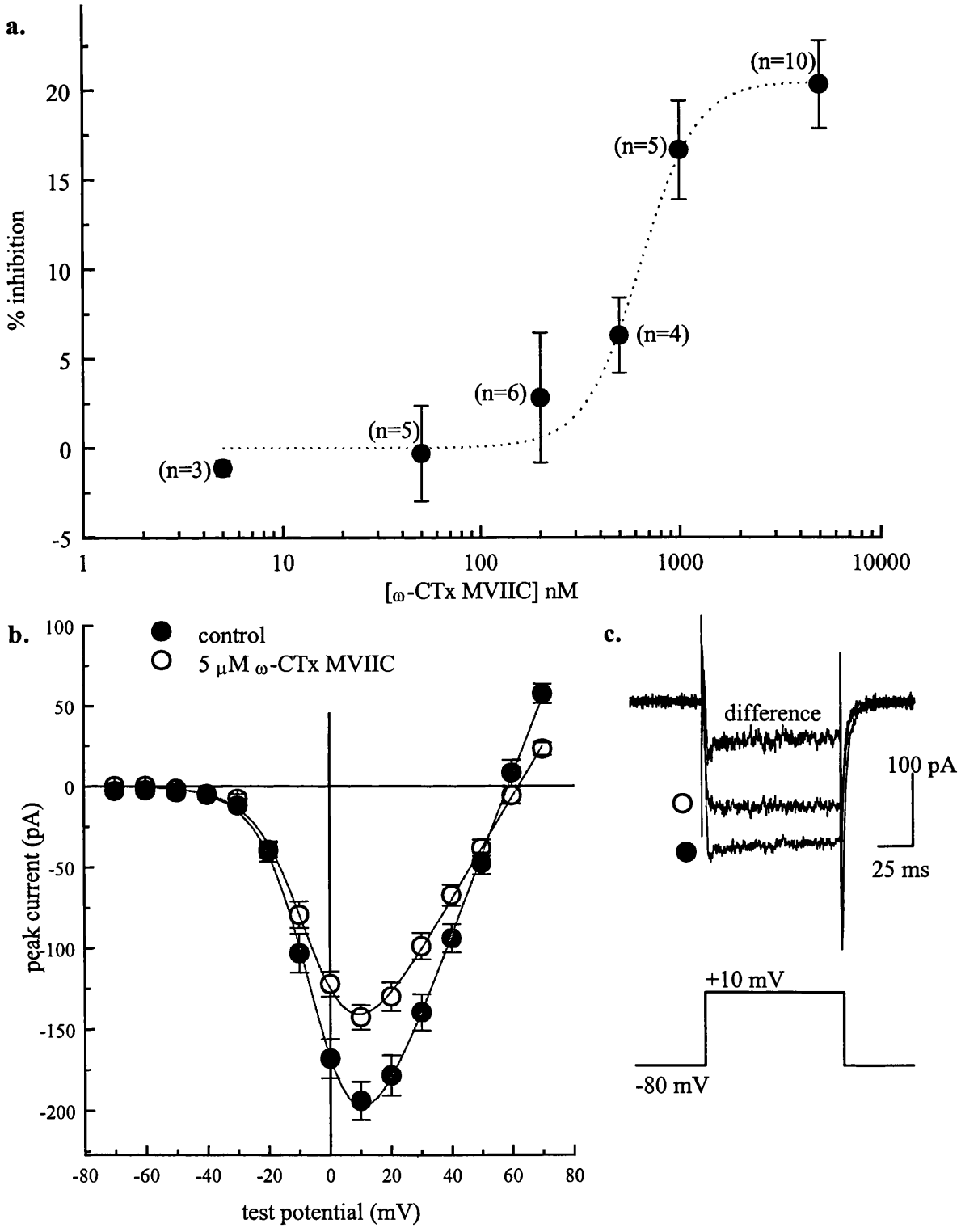

Fig. 4.1 The effect of ω-CTx MVIIC on Ca^{2+} channel currents in cerebellar granule neurones. **a.** Dose-response curve for the effect of increasing concentrations of ω-CTx MVIIC on peak currents. The broken line shows a Logistic fit to the data (see *Equation 6*, Chapter 2) where the EC_{50}=640 nM and h=3. The number of observations for each point are shown in parenthesis. **b.** Current-voltage relationship for currents recorded before and during application of ω-CTx MVIIC. The data is the mean±s.e.m. of 25 cells pooled from several experiments and was fit with a Boltzmann equation (*Equation 1*, Chapter 2; values given in text). **c.** Example current recordings evoked by stepping to a command voltage of +10 mV in a cell before and during application of ω-CTx MVIIC. The difference current was calculated by subtracting the ω-CTx MVIIC-resistant current from the control current. (Potentials given are uncorrected for liquid junction potential, which was -12 mV).

challenge with ω-CTx MVIIC from the control current, is also shown. This represents the ω-CTx MVIIC-sensitive component of the total whole-cell current. The example illustrated shows similar activation and inactivation properties to the control current, but significant variation in the kinetics of the ω-CTx MVIIC-sensitive current was observed (See later discussion, Fig. 4.7)

Inhibition of Ca^{2+} channel currents by ω-Aga IVA

The effect of ω-Aga IVA on Ca^{2+} channel currents is demonstrated in Fig. 4.2. Fig. 4.2a shows the concentration-dependence of inhibition of currents in granule cells. Block by ω-Aga IVA was extremely potent, the EC_{50} for inhibition was 60 pM. Maximal inhibition was seen at a concentration of 1 nM, at which currents were blocked by just over 20%. Although concentrations of up to 500 nM ω-Aga IVA were applied to cells there was not significantly greater block at these concentrations compared to the inhibition at 1 nM. From a Logistic fit h was found to be very close to 1 suggesting a simple one-to-one interaction between the toxin and its binding site. Inhibition was rapid, developing in 10-20 s and usually irreversible within the course of an experiment.

In Fig. 4.2b the current-voltage relationship is shown for cells in the absence and presence of 100 nM ω-Aga IVA. Following application of ω-Aga IVA peak current was reduced by 25±5% and the peak was shifted to a more hyperpolarised potential. These changes are summarised by the average of individual Boltzmann fits to the data. Conductance was decreased from 5.2±0.7 nS to 3.2±0.2 nS (p=0.04; n=5), E_{null} remained the same +59 (+47)±3 mV before and after drug delivery, $V_{50(act)}$ changed from -2 (-14)±2 mV to -7 (-19)±3 mV (p=0.04; n=5), and k was unchanged 8±1 mV compared to 7±1 mV.

An example of the inhibition is shown in Fig. 4.2c which shows currents at the peak of the current-voltage curve in a single neurone before and during application of ω-Aga IVA. The difference trace shows the ω-Aga IVA-sensitive current. In this cell the current sensitive to ω-Aga IVA was completely non-inactivating over a 100 ms voltage step and showed less inactivation compared to control. This was characteristic of the ω-Aga IVA-sensitive current (see Fig. 4.7) After removal of the toxin very little recovery was noted over periods of up to 5 mins.

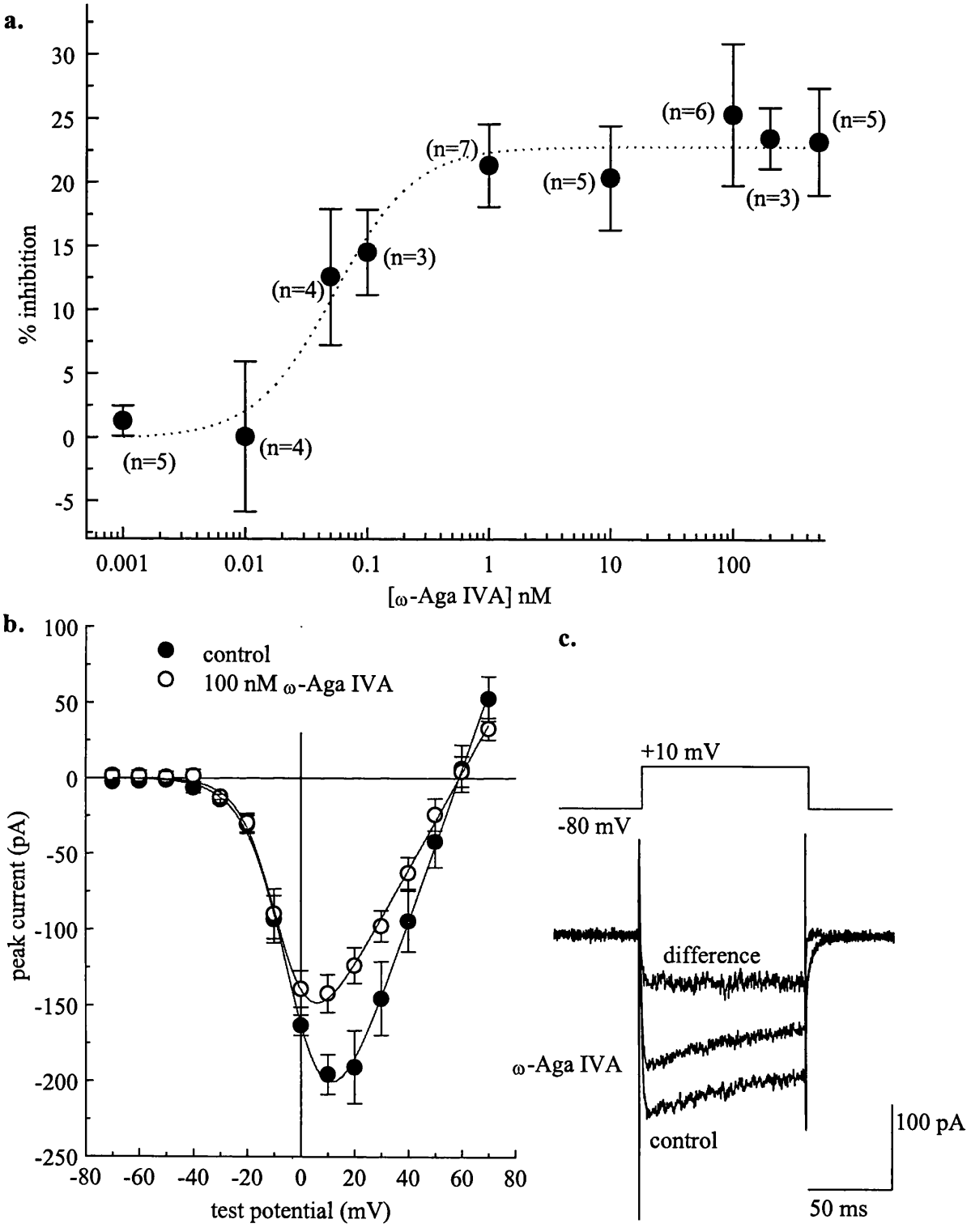

Fig. 4.2 Effect of ω-Aga IVA on whole-cell Ca^{2+} channel currents in cerebellar granule neurones. **a.** Dose-response relationship showing potent block of whole-cell Ca^{2+} channel currents in granule cells by ω-Aga IVA. The data was described by a Logistic fit (broken line). The EC_{50} was estimated to be 60 pM. The number of observations at each concentration is shown in parenthesis. **b.** Average current-voltage data for a group of 5 cells before and during challenge with 100 nM ω-Aga IVA. The data was fit using a Boltzmann equation (described in Chapter 2, *Equation 1*). Averaged values for each parameter are given in the text. **c.** Example current recordings before and during application of 100 nM ω-Aga IVA. The trace labelled difference shows the ω-Aga IVA-sensitive current. (Potentials given are uncorrected for liquid junction potential, which was -12 mV).

Inhibition of Ca^{2+} channel currents by ω-CgTx GVIA

The effect of the *Conus geographus* toxin ω-CgTx GVIA was investigated. Previous studies have shown that 1 μM of this toxin is a saturating concentration for ω-CgTx GVIA binding sites in neuronal preparations (Aosaki and Kasai, 1987; Plummer *et al.*, 1989; Regan *et al.*, 1991; Boland *et al.*, 1994) so this concentration was used in all studies.

Fig. 4.3a demonstrates the effect of 1 μM ω-CgTx GVIA on currents evoked at voltages between -70 (-82) and +70 (+58) mV. The toxin caused an inhibition of current at all voltages with no significant change in the voltage-dependence of activation. For the group of 9 cells shown, Boltzmann relationships were fit to the current-voltage data with average parameter values: g=3.4±0.4 nS, E_{null}=+60 (+48)±3 mV, $V_{50(act)}$=+0.9 (-11.1)±2 mV and k=8±0.7 mV in the absence of toxin, and g=1.9±0.3 nS (p<0.0001; n=9), E_{null}=+63 (+51)±3 mV, $V_{50(act)}$=-1 (-11)±2 mV and k=8±0.5 mV in the presence of ω-CgTx GVIA. The inset to Fig. 4.3a shows inhibition of the peak current after application of ω-CgTx GVIA in a single granule cell. ω-CgTx GVIA caused no discernible change in the kinetics of the current and the ω-CgTx GVIA-sensitive current (trace marked diff.) had similar kinetics to the control trace. In a group of 18 cells from three different experiments the average inhibition of the peak Ca^{2+} channel current was 34±3%.

The inhibition of currents by ω-CgTx GVIA was rapid and completely irreversible with no relief of block even with long periods after removal of the drug. The irreversible nature of the block is illustrated in Fig. 4.3b, which shows cumulative inhibition of ω-CgTx GVIA and ω-CTx MVIIC. In this experiment application of 1 μM ω-CgTx GVIA to a group of 5 cells caused 29±5% inhibition of the whole-cell Ca^{2+} channel current. After ceasing application of ω-CgTx GVIA little recovery of current was seen. After block by ω-CgTx GVIA, 5 μM ω-CTx MVIIC caused a rapid yet reversible block (in 4 out of 5 cells) of 14±3% (as a percentage of the total current before block with ω-CgTx GVIA.). Referring back to Fig. 4.1b, ω-CTx MVIIC at the same concentration produced an inhibition of 28±2% of the current when applied to naive cells. Prior application of ω-CgTx GVIA appears from the data shown in Fig. 4.3b to reduce the proportion of current sensitive to ω-CTx MVIIC, which is in agreement with studies in other systems where ω-CTx

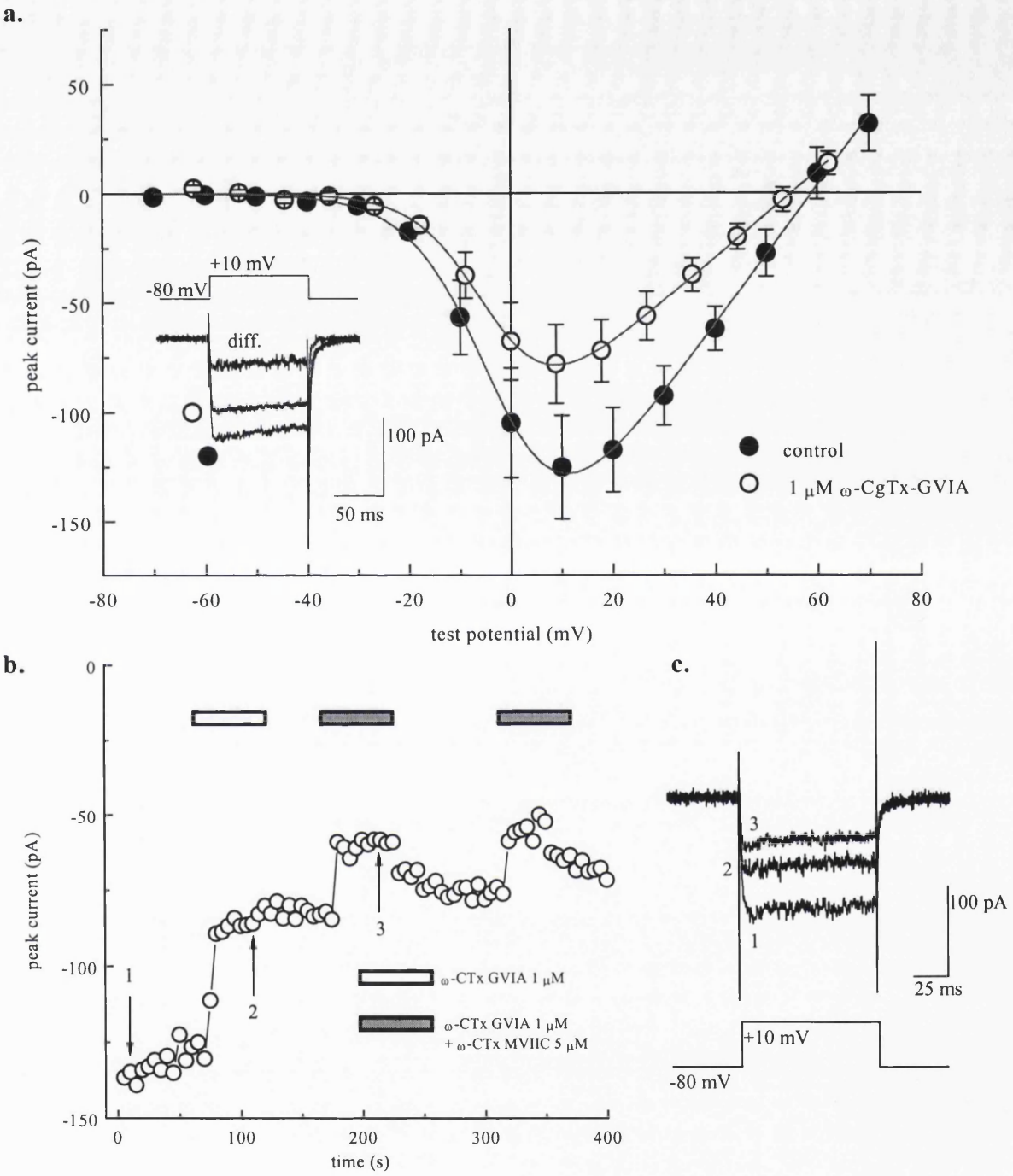

Fig. 4.3 Effect of ω-CgTx GVIA on Ca^{2+} channel currents in granule cells and the co-application of ω-CTx MVIIC. **a.** Current-voltage relation showing inhibition by 1 μM ω-CgTx GVIA in a group of 9 cells. The individual data was fit with Boltzmann equations with the averaged values given in the text. The inset shows currents recorded in a single cell before and during application. The difference current illustrates the typical kinetics of the ω-CgTx GVIA-sensitive current. **b.** Timecourse of application of 1 μM ω-CgTx GVIA and 5 μM ω-CTx MVIIC in a single neurone. Bars show periods of drug delivery. The example current traces show currents at the times indicated by the arrows. (Potentials given are uncorrected for liquid junction potential, which was -12 mV).

MVIIC and ω-CgTx GVIA have been shown to compete for binding sites (Hillyard *et al.*, 1992). Statistical examination of the data showed that the application of ω-CgTx GVIA caused an extremely significant reduction in the ω-CTx MVIIC-sensitive fraction of current (p=0.0002; unpaired *t-test*).

ω-CTx MVIIC exhibits overlapping sensitivity with ω-Aga IVA and ω-CgTx GVIA

The broader selectivity of ω-CTx MVIIC for Ca^{2+} channel subtypes present on neurones is further investigated in Fig. 4.4. This figure determines the proportion of ω-CgTx GVIA-sensitive current and ω-Aga IVA-sensitive current remaining in cells after the application of a maximally blocking dose of ω-CTx MVIIC. In Fig. 4.4a 5 μM ω-CTx MVIIC produced an average inhibition of 32±2% (n=5) which is in line with the inhibition shown previously here. In the continued presence of ω-CTx MVIIC co-application of 1 μM ω-CgTx GVIA caused a further inhibition of Ca^{2+} channel currents which was calculated as a percentage of the total current before challenge with ω-CTx MVIIC to be 10±2%. ω-CTx MVIIC significantly reduced the ω-CgTx GVIA-sensitive fraction of whole-cell current (p<0.0001; unpaired *t-test*; n=5, compared to 9 applications of ω-CgTx GVIA without pre-treatment with ω-CTx MVIIC) occluding 25% of the total current to the blocking effects of ω-CgTx GVIA.

Fig. 4.4b shows a similar experiment in which cells were challenged with 5 μM ω-CTx MVIIC and in its continued presence were subsequently exposed to 100 nM ω-Aga IVA. Here, ω-CTx MVIIC produced a 30±3% inhibition of peak current in a group of 8 cells. ω-Aga IVA further reduced the current by 16±4% in the presence of ω-CTx MVIIC. Comparing this to inhibition by ω-Aga IVA alone (Fig. 4.2, 22±4%), the prior application of ω-CTx MVIIC reduced the ω-Aga IVA-sensitive component of current, but outside significant limits (p=0.32; unpaired *t-test*; n=8 for ω-Aga IVA in the presence of ω-CTx MVIIC and n=5 for ω-Aga IVA alone).

These experiments suggest that in these cells ω-CTx MVIIC blocks a greater proportion of the ω-CgTx GVIA-sensitive current than the ω-Aga IVA-sensitive current.

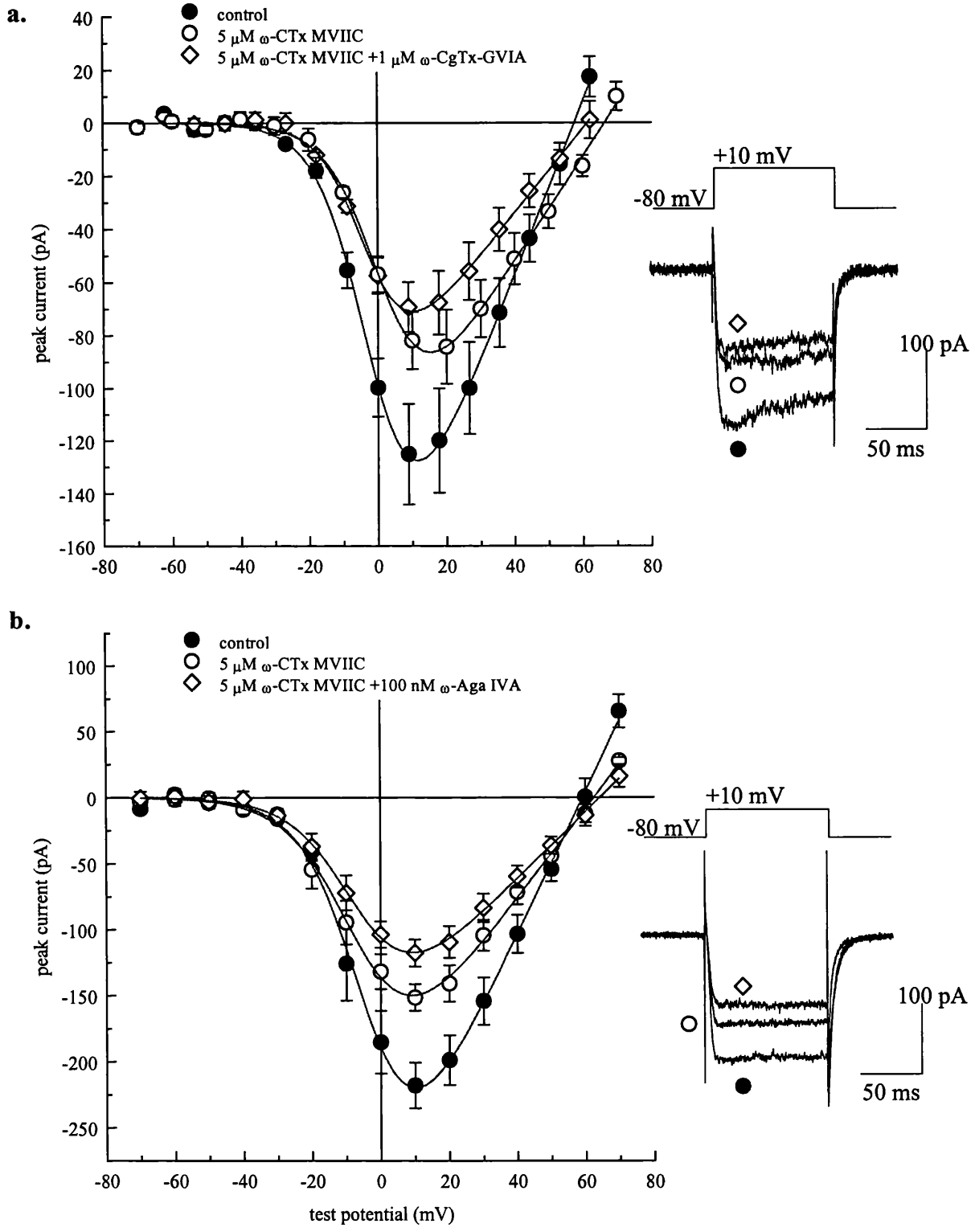

Fig. 4.4 Effect of the coapplication of ω-CTx MVIIC and ω-CgTx GVIA or ω-Aga IVA. **a.** Average current-voltage curves for 5 cells recorded in the absence of toxin, in the presence of 5 μM ω-CTx MVIIC and in the presence of 5 μM ω-CTx MVIIC and 1 μM ω-CgTx GVIA. Example current recordings in each condition are shown to the right of the figure. **b.** Current-voltage data showing the effects of 5 μM ω-CTx MVIIC and 100 nM ω-Aga IVA on peak currents in granule neurones. Each point is the average of 8 cells. Representative traces from a single cell are shown on the right. (Potentials given are uncorrected for liquid junction potential, which was -12 mV).

ω-Aga IVA and ω-CgTx GVIA exhibit overlapping selectivity

The ω-CgTx GVIA- and ω-Aga IVA-sensitive currents were further studied in the experiments shown in Fig. 4.5. To determine whether there was overlap of ω-CgTx GVIA and ω-Aga IVA-sensitive currents these toxins were applied to groups of cells in combination. In a group of 4 cells that were exposed to 1 μM ω-CgTx GVIA 30±5% of the peak current was blocked. In the continued presence of ω-CgTx GVIA application of 100 nM ω-Aga IVA only reduced the currents by 11±3%. However, this was not significantly different from the extent of inhibition by ω-Aga IVA applied alone to a group of 10 cells (p=0.11; unpaired *t-test*).

Fig. 4.5b illustrates the converse situation. 100 nM ω-Aga IVA was first applied to a group of 5 cells and after a steady-state inhibition had been reached 1 μM ω-CgTx GVIA was applied in conjunction with ω-Aga IVA. ω-Aga IVA reduced the evoked currents by an average of 17±2%. Prior application of ω-Aga IVA reduced the ω-CgTx GVIA-sensitive current to 18±3% which was a very significant reduction from the ω-CgTx GVIA-sensitive component in a group of 18 cells where ω-CgTx GVIA was applied alone (p=0.0073; unpaired *t-test*).

No evidence of a Q-type current was found in granule cells under these conditions

Other studies have demonstrated a component of current in granule neurones (Randall and Tsien, 1995) and other neurones (Wheeler *et al.*, 1994) that was less sensitive to ω-Aga IVA than the P-type current but blocked by ω-CTx MVIIC. The dose-response curve to concentrations of ω-Aga IVA did not show a biphasic relationship. To establish whether a component of current remained after block of N- and P-type current a low dose of ω-Aga IVA (1nM) was applied to cells together with 1 μM ω-CgTx GVIA, and then subsequently challenged with ω-CTx MVIIC.

Fig. 4.6 shows an example timecourse of peak Ca^{2+} channel currents measured in a group of 6 cells first exposed to 1 nM ω-Aga IVA and 1 μM ω-CgTx GVIA and then to 5 μM ω-CTx MVIIC together with 1nM ω-Aga IVA and 1 μM ω-CgTx GVIA. The combined effects of ω-Aga IVA and ω-CgTx GVIA decreased the current 42±3%. The subsequent addition of ω-CTx MVIIC did not produce a further significant decrease in the elicited current (3±3%, p=0.16; paired *t-test*;

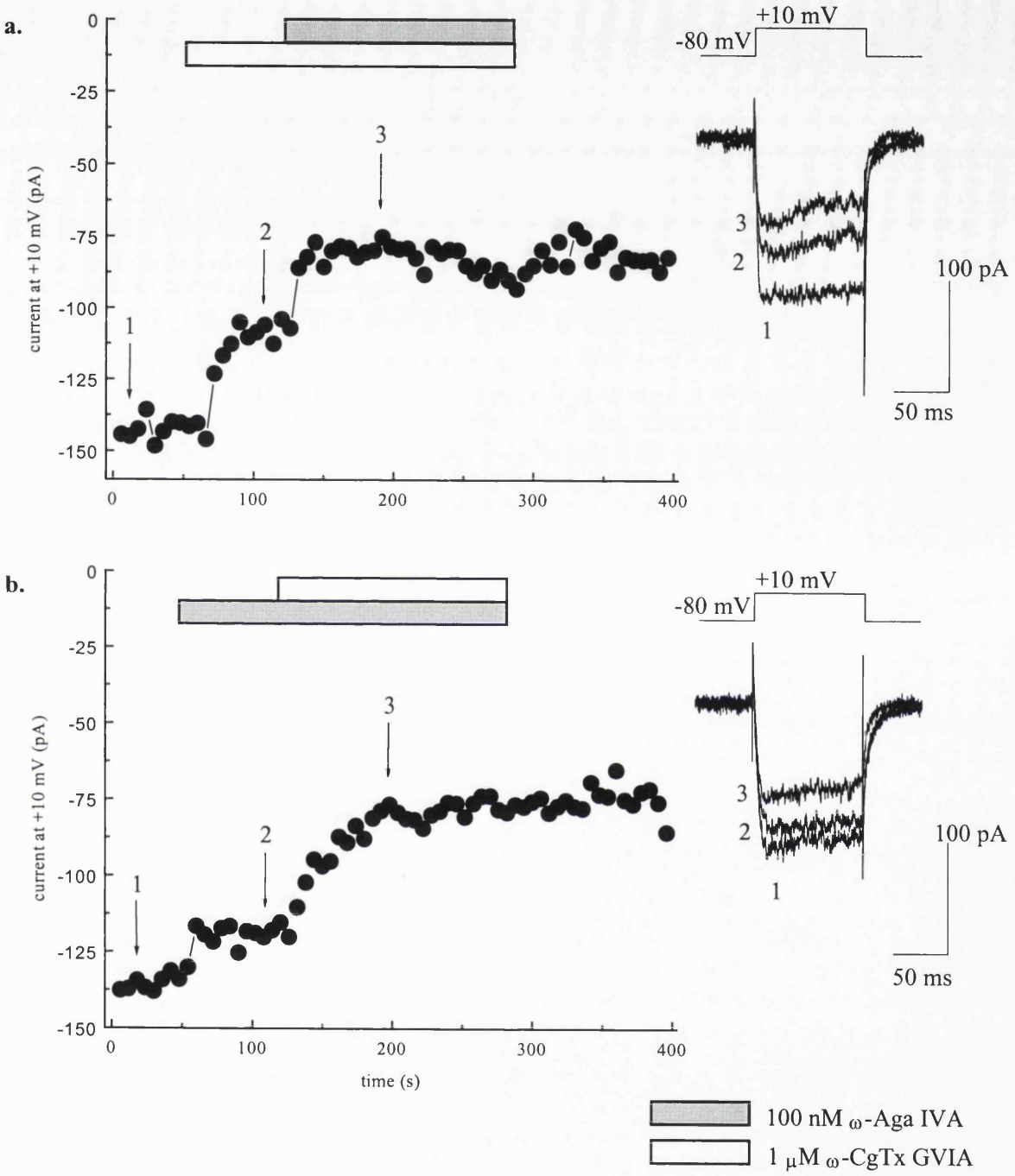

Fig. 4.5 Effects of the application of ω-Aga IVA and ω-CgTx GVIA on Ca^{2+} channel currents measured at +10 mV in cerebellar granule neurones. **a.** Timecourse of application of 1 μM ω-CgTx GVIA and 100 nM ω-Aga IVA. After reaching a steady-state inhibition with ω-CgTx GVIA the drug perfusion was switched to a solution containing concentrations of ω-CgTx GVIA and ω-Aga IVA. Bars show periods of drug delivery. Representative current traces are shown taken from the time points indicated by the arrows. **b.** Similar experiment to **a.** where steady-state inhibition with 100 nM ω-Aga IVA was obtained before application of both toxins. (Potentials given are uncorrected for liquid junction potential, which was -12 mV).

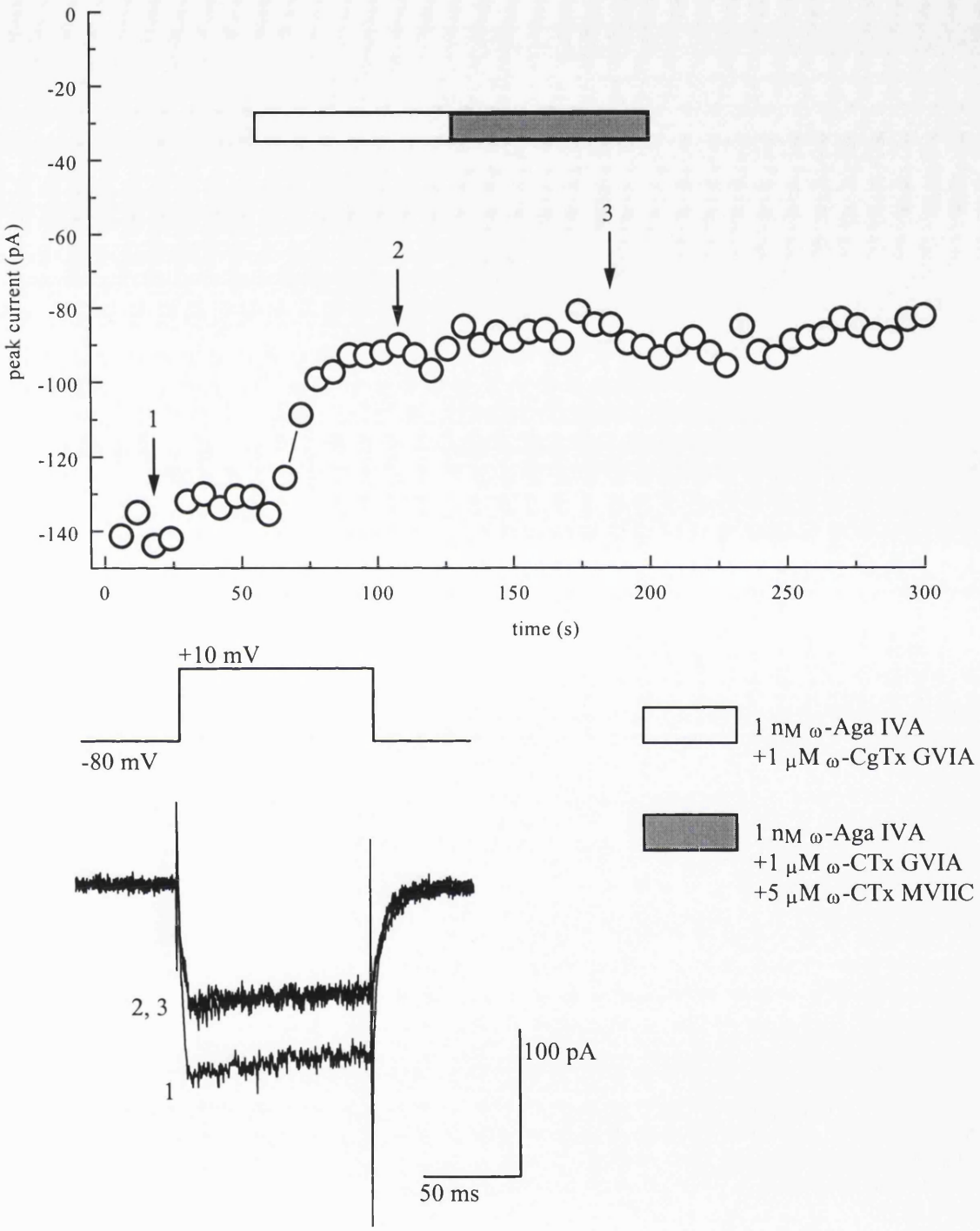

Fig. 4.6 5 μM ω-CTx MVIIC produced no further block in the presence of 1 nM ω-Aga IVA and 5 μM ω-CgTx GVIA. The time course shown was representative of a group of 6 cells. 1 nM ω-Aga IVA and 5 μM ω-CgTx GVIA were applied to cells until a steady-state inhibition had been reached. In the continued presence of ω-Aga IVA and ω-CgTx GVIA the cells were challenged with 5 μM ω-CTx MVIIC. Example current recordings were taken from the times shown by the arrows. (Potentials given are uncorrected for liquid junction potential, which was -12 mV).

n=6). Thus it would appear that under the conditions used here a Q-type current was not present.

Discussion

The utilisation of a pharmacological approach to understanding the diversity of voltage-dependent Ca^{2+} channels within the CNS has been of great value. The availability of pharmacological agents that affect these Ca^{2+} channels has been critical to progress in this area.

The initial classification of HVA Ca^{2+} channels into L-, N-, and P-type channels was largely based on the unique sensitivity of L-type channels to DHP antagonists (Nowycky *et al.*, 1985a,b; Fox *et al.*, 1987a,b), N-type channels to ω-CgTx GVIA (McKlesky *et al.*, 1987), and P-type channels to ω-Aga IVA (Mintz *et al.*, 1992b). However, part of the Ca^{2+} currents in some tissues are insensitive to these agents (Mintz *et al.*, 1992b; Bossu *et al.*, 1994), and together with evidence from molecular cloning techniques there appears to be a much greater diversity of Ca^{2+} channel types in the brain than was previously recognised. Correlating the structurally diverse Ca^{2+} channels identified by molecular cloning with those expressed *in situ* has recently become a highly debated issue.

Several Ca^{2+} channel antagonists with novel selectivities have recently been identified from cone snail venom (Hillyard *et al.*, 1992) and from the funnel web spider (Adams *et al.*, 1990; Venema *et al.*, 1992; Mintz *et al.*, 1992b) and have been used to demonstrate additional Ca^{2+} channels. ω-Aga IVA from the spider venom is a high affinity antagonist of P-type channels in Purkinje neurones and blocks currents that are resistant to DHPs and ω-CgTx GVIA in central and peripheral neurones (Mintz *et al.*, 1992a,b). Another antagonist from this venom, type IIIA targets several HVA Ca^{2+} channels as it appears to recognise a binding domain common to all Ca^{2+} channels. In central neurones ω-Agatoxin IIIA (ω-Aga IIIA) abolished DHP-sensitive currents and substantially inhibited ω-CgTx GVIA and ω-Aga IVA sensitive currents. It also blocked the remaining HVA current in hippocampal CA1 neurones after application of saturating concentrations of nimodipine, ω-CgTx GVIA and ω-Aga IVA (Mintz, 1994). ω-Agatoxin IA (ω-Aga IA) also from the funnel web spider has been shown to inhibit HVA channels in DRG and granule neurones (Scott *et al.*, 1990). ω-Aga IA reduced L- and N-type

current components. Its effects differed from ω-CgTx GVIA in being partly reversible and several orders of magnitude more potent.

The venom from the marine snail *Conus magus* has been shown to contain peptides that block Ca^{2+} channels (reviewed in Olivera *et al.* 1992). One fraction from this venom, ω-Conotoxin MVIIA (ω-CTx MVIIA) shares only 27% of its amino acid sequence with ω-CgTx GVIA yet competes for binding in the brain. ω-CTx MVIIA is a high affinity but reversible blocker of N-type Ca^{2+} channels (Yoshikami *et al.*, 1989). Other toxin fractions from molluscs, whilst retaining significant affinity for the N-type channel also bind to other channel types. SVIIB from *Conus striatus*, ω-CTx MVIIC and ω-Conotoxin MVIID (ω-CTx MVIID) show higher affinity, and preferential block of non-N-type channels (Hillyard *et al.* 1992; Monje *et al.*, 1993; Kristipati *et al.*, 1994). ω-CTx MVIIC has been useful in identifying non-L, non-N-type Ca^{2+} channels. It blocks P-type currents in Purkinje cells but with a much slower development of block and recovery than its actions on N-type channels (McDonough *et al.*, 1996) and also blocks a component of current in hippocampal cells which is insensitive to ω-CgTx GVIA and concentrations of ω-Aga IVA that block P-currents in Purkinje cells (Wheeler *et al.*, 1994). Block of this Q-type current has also been demonstrated by one group in granule cells from the cerebellum (Randall and Tsien, 1995). It was defined as a current insensitive to ω-CgTx GVIA and the L-type blocker nimodipine, and only sensitive to high concentrations of ω-Aga IVA. ω-CTx MVIIC slowly blocked more than 70% of current remaining after treatment with 1 μM ω-CgTx GVIA and 10 μM nimodipine (Randall and Tsien, 1995). To complement these studies suggesting the existence of a Q-type channel, binding experiments have shown that in rat brain ω-CTx MVIIC binds with an affinity ranging from 40 pM to 1 nM (Hillyard *et al.*, 1992; Kristipati *et al.*, 1994; Adams *et al.*, 1993) which is considerably higher than the binding affinities of ω-CTx MVIIC for N-type channels or Q-type channels in cerebellar granule neurones and the potency at which ω-CTx MVIIC blocks P-currents in Purkinje cells. Olivera *et al.* (1994) propose that this high affinity binding site, the O-type channel may be localised to presynaptic termini as it has not been observed by electrophysiological methods, but only in release studies. Furthermore, they suggest that the O-, P-, and

Q-type channels form a subfamily of channel types which are all DHP-, and ω-CgTx GVIA-insensitive but ω-Aga IVA-, and ω-CTx MVIIC-sensitive and may all arise from, or are closely related to the α_{1A} clone. Members of this subfamily only differing in the relative inhibitory potency and kinetics of block: P-type channels thus having slow on and off rates, O-type having the highest affinity and Q-type being inhibited by ω-CTx MVIIC and ω-Aga IVA at equimolar potencies.

The development of new toxins is an ongoing process, with the ω-toxins from the funnel web spider and the cone snails proving most useful in the identification of voltage-sensitive Ca^{2+} channels. With rapid progress in electrophysiological characterisation and molecular definition by cloning, selective antagonists are essential to provide links between cloning and electrophysiology.

Comparisons of electrophysiological characteristics has proved problematic in distinguishing channel subtypes at the molecular level. Certain electrophysiological characteristics expressed by native Ca^{2+} channels in various tissues do not correlate with the classes of Ca^{2+} channel cloned so far. For instance, currents carried by T-type Ca^{2+} channels are not easily fitted into the existing classification. In addition, molecularly homogenous Ca^{2+} channels can show very different inactivation properties from one study to another, and in different expression systems. Recent work has shown that ω-CgTx GVIA can block an inactivating and a non-inactivating HVA Ca^{2+} current (Plummer *et al.*, 1989; Aosaki and Kasai, 1989; Plummer and Hess, 1991; Artalejo *et al.*, 1992; Mynlieff and Beam, 1992) demonstrating that the inactivation properties may not be a reliable factor for relating results from one study to another.

Pharmacological criteria would therefore seem to be more appropriate for defining channel types but problems are also inherent in this approach. The tools presently available do not have complete selectivity and show varied effects in different tissues (Scott *et al.*, 1991). It should also be noted that in the case of a toxin interacting with a native Ca^{2+} channel protein complete block of conductance is often not seen. It is often impossible to say in such situations whether the partial inhibition is the result of a second Ca^{2+} channel subtype being present that is resistant to the toxin or the residual current results from partial toxin block. Analysis of the voltage-dependence and biophysical properties of the current may

not help to decipher this problem since the binding of a toxin to an ion channel may change the basic parameters of conductance. Whether or not the toxin blocks a channel completely must be established. Studies of pure populations of cloned channels at the single-channel level may yield less ambiguous data.

The results presented here demonstrate some of the problems inherent in dissecting the individual Ca^{2+} current components out of cells containing multiple channel subtypes. Overlapping selectivity of toxins to different classes of Ca^{2+} channel prevent definitive conclusions being made to these results. The kinetics of the toxin-sensitive currents give some information to help with characterisation. Fig. 4.7 provides a comparison of the toxin-sensitive components of the whole-cell Ca^{2+} currents investigated. The kinetics of the individual pharmacologically separated currents show some differences, although the error bars show that the toxin-sensitive currents were highly variable in nature. In addition, because control currents showed little inactivation over 100 ms, longer steps showing toxin-sensitive current would give much clearer information. However, certain features are apparent. In comparison to their respective controls the ω-CTx MVIIC- and ω-Aga IVA-sensitive components show a greater current at the end of the voltage-step than at the beginning, and the ω-CgTx GVIA-sensitive current shows little difference in kinetics to its control. The slow development of ω-Aga IVA-sensitive current and to a lesser extent ω-CTx MVIIC-sensitive current may reflect an element of an increase in binding of the toxin to the open channel. It would be expected that this type of pharmacological separation of currents would yield components of current with differing kinetics of activation and inactivation. Thus the ω-CgTx GVIA-sensitive current would be expected to show a more rapidly inactivating profile than the ω-Aga IVA-sensitive component. However, the literature contains a wide degree of variation concerning inactivation of N-type channels in various neuronal cells (Plummer *et al.*, 1989; Nowycky *et al.*, 1985a; Fox *et al.*, 1987a,b; Aosaki and Kasai, 1989; Jones and Marks, 1989a; Kostyuk *et al.*, 1988; Lemos and Nowycky, 1989; Fisher *et al.*, 1990) and individual N-type channels in sympathetic neurones have been shown to give rise to two kinetically distinct current components, one rapidly transient and the other long-lasting and non-inactivating (Plummer and Hess, 1991). It may be that in the conditions used

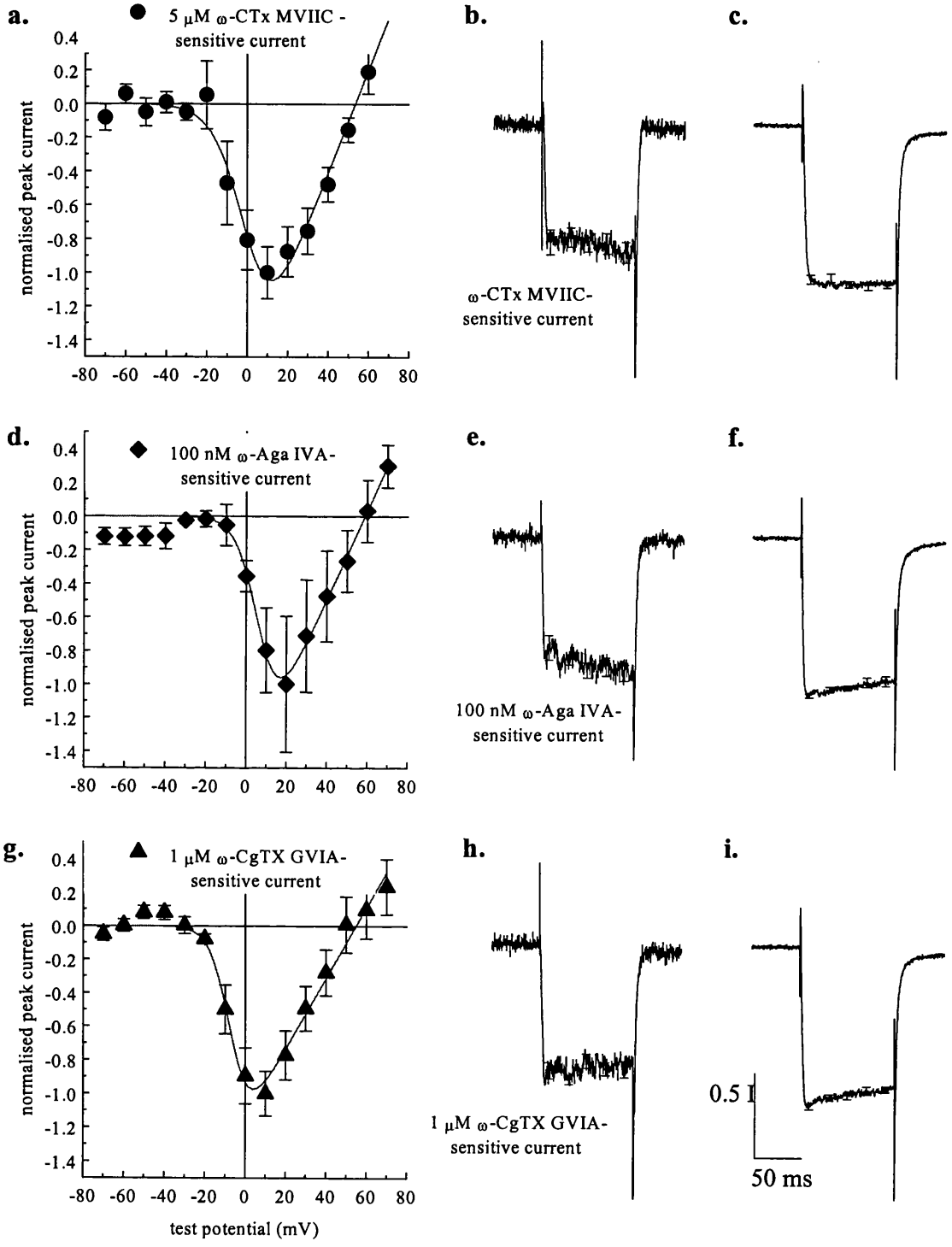

Fig. 4.7 Comparison of toxin-sensitive currents in cerebellar granule neurones. Each component of the whole-cell current is plotted as a current-voltage relationship where the currents in each cell have been normalised. Also shown are normalised, average toxin-sensitive currents measured at the peak of activation compared to total whole-cell currents for the equivalent group. Current traces have error bars plotted at several points. **a.**, **b.** 5 μM ω-CTx MVIIC-sensitive currents, and **c.** average control currents (n=25). **d.**, **e.** 100 nM ω-AgaIVA-sensitive currents, and **f.** their contol traces (n=5). **g.**, **h.** 1 μM ω-CgTX GVIA-sensitive currents, and **i.** control current (n=9). (Potentials given are uncorrected for liquid junction potential, which was -12 mV).

here, the equilibrium between the inactivating and non-inactivating modes is shifted so that the non-inactivating mode of opening is predominant and gives rise to the ω-CgTx GVIA-sensitive currents shown.

Comparison of the toxin-sensitive currents shown as current-voltage relationships show a number of differences. The ω-CgTx GVIA-sensitive component shows a peak in activation at a less positive potential to the ω-Aga IVA-sensitive current and the peak for ω-CTx MVIIC-sensitive current lies in between the two. Similarly, when Boltzmann functions were applied to the average data they gave a $V_{50(act)}$ of -7 (-19) mV for ω-CgTx GVIA-sensitive currents, +7 (-5) mV for ω-Aga IVA-sensitive currents and +1 (-11) mV for ω-CTx MVIIC-sensitive currents. The reports of native ω-CgTx GVIA-sensitive currents in the literature fit reasonably well with the current characterised here. The ω-CgTx GVIA-sensitive currents shown in Fig. 4.7 activate at -20 (-32) mV, and peak at 0 (-12) mV. Close to values given by Fox *et al.*, 1987b (see Table 1.1).

ω-Aga IVA-sensitive currents show more variation. Initial studies on Purkinje cells using low Ba^{2+} extracellular solutions revealed currents sensitive to ω-Aga IVA that activated at -48 mV and peaked at -8 mV (Usowicz *et al.*, 1992), whereas later studies with these cells showed currents that activated at -30 mV and peaked at -10 mV (Biton *et al.*, 1995). The ω-Aga IVA-sensitive current dissected here shows more similarities to a P-subtype recently described at the single channel level in cerebellar granule neurones (Tottene *et al.*, 1996). These channels activated at -10 mV (but using 90 mM Ba^{2+}) and were fully blocked by 50 nM ω-Aga IVA. Steady-state inactivation was complete at -40 mV, quite different from values given for P-type channels in Purkinje cells (V_{50}=-5 mV) and similar to the V_{50} of steady-state inactivation found here (see Fig. 3.7) when the difference in the concentration of external cation is taken into account. In agreement with all studies of native P-type Ca^{2+} channels the kinetics of this current were slow.

The activation threshold and peak of current sensitive to ω-CTx MVIIC fell in between values for ω-CgTx GVIA- and ω-Aga IVA-sensitive currents which may be expected since this toxin appears to block both of these currents to some extent. The current kinetics showed no inactivation over the 100 ms voltage-step used, in contrast to ω-CTx MVIIC-sensitive currents dissected by Randall and Tsien

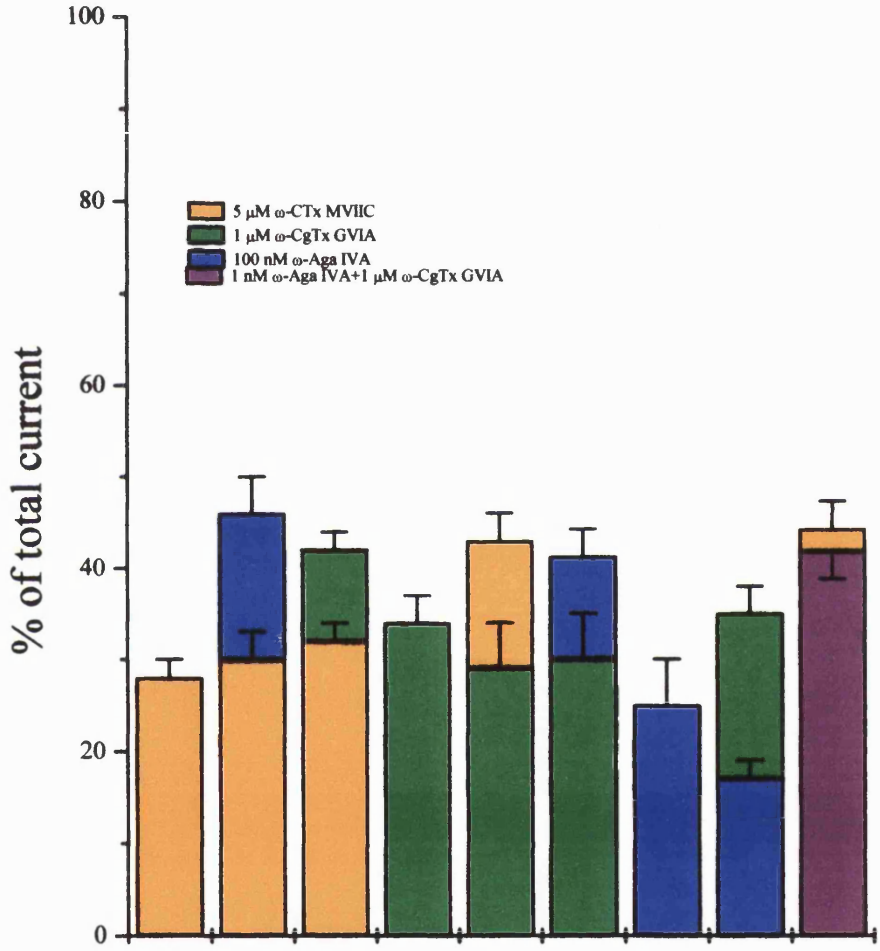

Fig. 4.8 Summary of the effects of ω-CTx MVIIC, ω-CgTx GVIA and ω-Aga IVA applied to granule cells individually or in combination. Bars represent the mean inhibition±s.e.m. where n=5-25. The lowest division represents the toxin(s) applied first in every case.

(1995) which displayed rapid inactivation. Further evidence against a Q-type component of current in granule cells under these conditions.

Fig. 4.8 summarises the effectiveness of the toxins in inhibiting Ca^{2+} channel currents in cerebellar granule neurones. With regard to the proportions of total current carried by identified channel types the data show that 40-45% of the Ca^{2+} channel current in these cells was through N- and P-type channels. It is impossible to establish exact proportions of both N-type and P-type on the basis of these data alone, since a component of ω-CgTx GVIA-sensitive current was blocked by ω-Aga IVA, and a component of ω-Aga IVA-sensitive current was blocked by ω-CgTx GVIA. Also a fraction of both ω-Aga IVA- and ω-CgTx GVIA-sensitive currents remained insensitive to ω-CTx MVIIC. One possible explanation of these results is that a population of channels carrying approximately 10-15% of the total current exists with mixed pharmacology, being sensitive to both ω-Aga IVA and ω-CgTx GVIA, yet insensitive to ω-CTx MVIIC. In this scenario, current components contributing to the total whole-cell current would be 20% ω-CgTx GVIA-sensitive N-type, 10% ω-Aga IVA-sensitive P-type, and 10-15% accounted for by channels with mixed pharmacology, but insensitive to ω-CTx MVIIC. An overlapping pharmacology is not without support. Cells of the bullfrog sympathetic ganglion have been shown to have currents sensitive to ω-Aga IVA and ω-CgTx GVIA (Mintz *et al.*, 1992a).

One point of interest from these experiments agreeing with some studies (Pearson *et al.*, 1995) but not others (Randall and Tsien, 1995) is that under the conditions used here no evidence for the presence of a Q-type current was seen based on the sensitivity of currents to ω-Aga IVA, being fully blocked (25% of the total whole-cell current) by a concentration of 1 nM, and the ω-Aga IVA and ω-CTx MVIIC-sensitive currents remaining non-inactivating. Other studies that demonstrated a Q-type component in cerebellar granule neurones (Randall and Tsien, 1995) showed a subdivision in the current sensitive to ω-Aga IV. In this study only 10% of the total current was blocked by 1-3 nM ω-Aga IVA. A further 35% of total current was however, sensitive to 90 nM ω-Aga IVA. Similar concentrations of ω-CTx MVIIC as used here were found to block both of these ω-Aga IVA-sensitive currents. This difference may result from differences in culture or recording

conditions. In the latter case cells were cultured in media containing 5 mM K^+, which may lead to a different pattern of expression of Ca^{2+} channels. Interestingly, Pearson *et al.* (1995) showed a similar proportion of current blocked by 100 nM ω-Aga IVA (40%) but the toxin appeared to be blocking just one population of channels with a K_D of 2.7 nM.

Between different studies in granule neurones the proportion of current sensitive to ω-CgTx GVIA is largely consistent. Pearson *et al.* (1993, 1995) reported that 25% of the current was blocked by 1 μM ω-CgTx GVIA and Randall and Tsien (1995) reported 20% block at this concentration. Regarding the proportion of L-type/DHP-sensitive currents vary. Nimodipine in Randall's study blocked just 15% of the total current, whereas Pearson showed that (-)-202-791 blocked 35% of total current at 1 μM. In De Waard's study (1991) nicardipine blocked 78% of current with a K_i of 0.5 μM. This suggests that different DHPs may have widely varying potencies and raises the question of their selectivity to L-type channels. DHP-sensitivity is the ubject of the following chapter.

Considering possible correlations between the Ca^{2+} current components so far examined with cloned Ca^{2+} channels it is possible to say with some certainty that the ω-CgTx GVIA-sensitive current is carried by the α_{1B} class of channel. This channel clone has been located to the granular layer of the cerebellum, although at low density (Westenbroek *et al.*, 1992; Fujita *et al.*, 1993) and has been shown to be sensitive to ω-CgTx GVIA in many separate studies since it was first shown in 1985 (Olivera *et al.*, 1985; Nowycky *et al.*, 1985a).

The nature of the channel giving rise to the current blocked by ω-Aga IVA is less clear cut. Although α_{1A} subunits are found at particularly prominent levels in Purkinje cells of the cerebellum (Stea *et al.*, 1994; Westenbroek *et al.*, 1995) and Ca^{2+} channels in Purkinje cells are potently blocked by ω-Aga IVA (Mintz *et al.*, 1992b; Usowicz *et al.*,1992), expression studies have shown several differences between α_{1A} currents and native P-type currents in Purkinje cells as already discussed (see Chapter 1). These differences may result from different accessory subunits coexpressed with the α_{1A} subunit or may result from alternative splice forms of the pore forming subunit. In the granule cell layer of the cerebellum α_{1A} subunits are found, although at lower levels than in the Purkinje cells (Stea *et al.*,

1994; Westenbroek *et al.*, 1995) so α_{1A} subunits may be responsible for the ω-Aga IVA-sensitive current. An alternative from our knowledge of cloned Ca^{2+} channels is that some, or all of the current is carried by the α_{1E} class of channel also shown to be present in the granule layer of the cerebellum (Yokoyama *et al.*, 1995). Currents produced by α_{1E} subunits are, like the α_{1A} channel partially blocked by ω-Aga IVA (Soong *et al.*, 1993; Berrow *et al.*, in press).

Chapter 5

Effect of 1,4-dihydropyridines on Ca^{2+} channel currents in rat cerebellar granule neurones

Results

Over half of the total current remained after block of ω-CgTx GVIA- and ω-Aga IVA-sensitive currents in the cells being studied. To assess the contribution of L-type Ca^{2+} channels to the whole-cell current in cerebellar granule neurones, experiments were conducted using the DHP antagonist nicardipine and other DHP compounds alone, and in combination with neurotoxin Ca^{2+} channel blockers already studied.

Inhibition of Ca^{2+} channel currents by nicardipine

Fig. 5.1a demonstrates the concentration-dependence of the inhibition by nicardipine. Block of current was only seen at relatively high concentrations, and the EC_{50} for block was 4.4 μM. Maximal block was achieved by the application of 100 μM nicardipine and produced a greater than 60% decrease in peak current amplitude. Complete recovery of current was usually seen after removal of the drug, and maximum inhibition occurred in around 60 s, developing more slowly than block with the Ca^{2+} channel toxins. Holding potential in these experiments was -80 mV. The voltage-dependence of DHP activity is well described in these cells (Marchetti *et al.*, 1995), and other systems (Hamilton *et al.*, 1987) and the EC_{50} would be expected to occur at a lower concentration at more depolarised holding potentials. Fig. 5.1b shows the current-voltage data for block with 1 μM nicardipine. At this concentration the peak current was reduced by 16±7% (n=6). A small but significant shift in the voltage-dependence was also noticed on analysis of Boltzmann fits to the curves. $V_{50(act)}$ changed from -10 (-22)±1 mV in control to -12 (-24)±2 mV after application of nicardipine (p=0.03). Whole-cell conductance was reduced from 4.0±0.4 nS to 3.3±0.3 nS (p=0.03). E_{null} and k remained unaltered at +60 (+48)±3 mV and 6±0.4 mV respectively in control, and +61 (+49)±5 mV and 6±0.5 mV in the presence of 1 μM nicardipine. Fig. 5.1c shows example traces from a cell before and during application of 1 μM nicardipine. The difference current, or nicardipine-sensitive current has similar kinetics to the current before block, remaining completely non-inactivating over 100 ms.

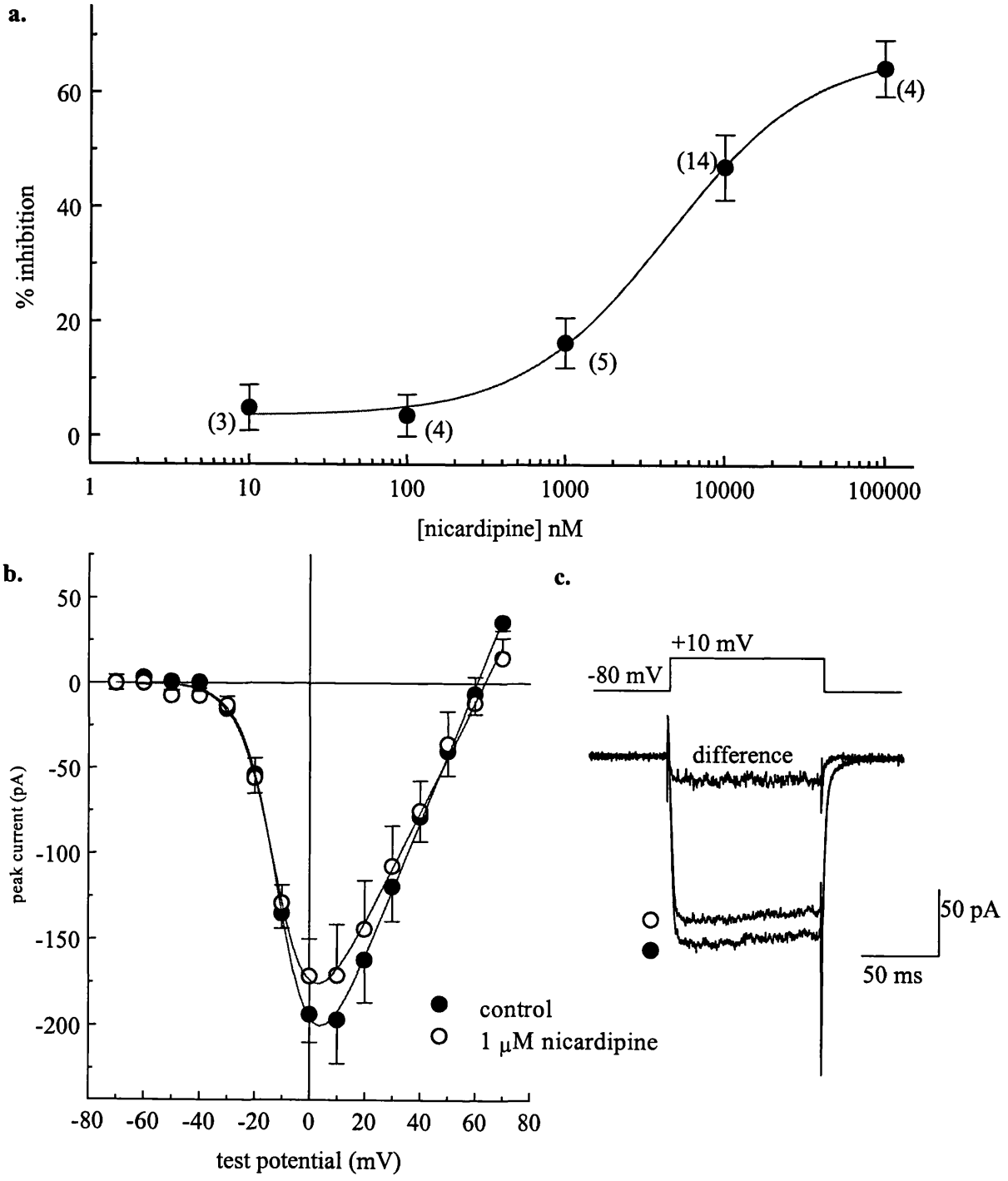

Fig. 5.1 Dose-dependence and effect on voltage-dependence of currents exposed to nicardipine. **a.** Dose-response curve for the effect of nicardipine. Percentage inhibition was plotted against drug concentration. The number of observations is shown in parenthesis. The dotted line is a Logistic fit to the data with EC_{50}=4.4 μM and h=1. **b.** Current-voltage relationship for cells before and during application of 1 μM nicardipine. Points are the mean±s.e.m. of 6 separate applications (error bars are only shown in one direction for clarity). **c.** Example recordings are shown to illustrate the reduction in current amplitude and kinetics of the nicardipine-sensitive current. (Potentials given are uncorrected for liquid junction potential, which was -12 mV).

1 μM nicardipine blocks a component of the current that is insensitive to toxins

To determine how low doses of nicardipine, reported to be selective for L-type Ca^{2+} channels blocked cerebellar Ca^{2+} channel currents in the presence of non-L-type blockers, studies were carried out in which 1 μM nicardipine was applied in the presence of one or more peptide toxins. Fig. 5.2a shows pooled current-voltage data and an example of current recordings from a single cell as part of a group of 9 where 1 μM nicardipine was applied to cells following the application of 5 μM ω-CTx MVIIC. The average inhibition of peak current by nicardipine was 17±4% and was not significantly different to the inhibition seen in Fig. 5.1b (p=0.96; unpaired *t-test*; n=9 cells in which nicardipine was applied after block by ω-CTx MVIIC and n=5 where nicardipine was applied alone) indicating that the 1 μM nicardipine-sensitive current was completely additive to the ω-CTx MVIIC-sensitive current.

In the experiment illustrated in Fig. 5.2b a combination of 100 nM ω-Aga IVA, 1 μM ω-CgTx GVIA and 5 μM ω-CTx MVIIC was applied to cells simultaneously. A decrease in the amplitude of Ca^{2+} channel current of 38±4% (n=7) was seen. In the presence of these toxins 1 μM nicardipine further reduced peak current by 17±3% as a percentage of the control amplitude. Under these conditions the 1 μM nicardipine-sensitive current was equivalent to the nicardipine-sensitive current recorded when applied to a group of 6 cells alone (p=0.94; unpaired *t-test*). This data suggests that 1 μM nicardipine reduces a component of the whole-cell current, presumably L-type current, that is not susceptible to the effects of any of the toxins used here.

As an aside, it is interesting to note that currents in the cell shown and other cells from the same culture were unusual in terms of their inactivation kinetics. This group of cells showed a much more rapidly inactivating current profile in spite of culture and recording conditions being unaltered. Their pharmacological features were similar to other groups of cells showing usual kinetics so were included in the analysis.

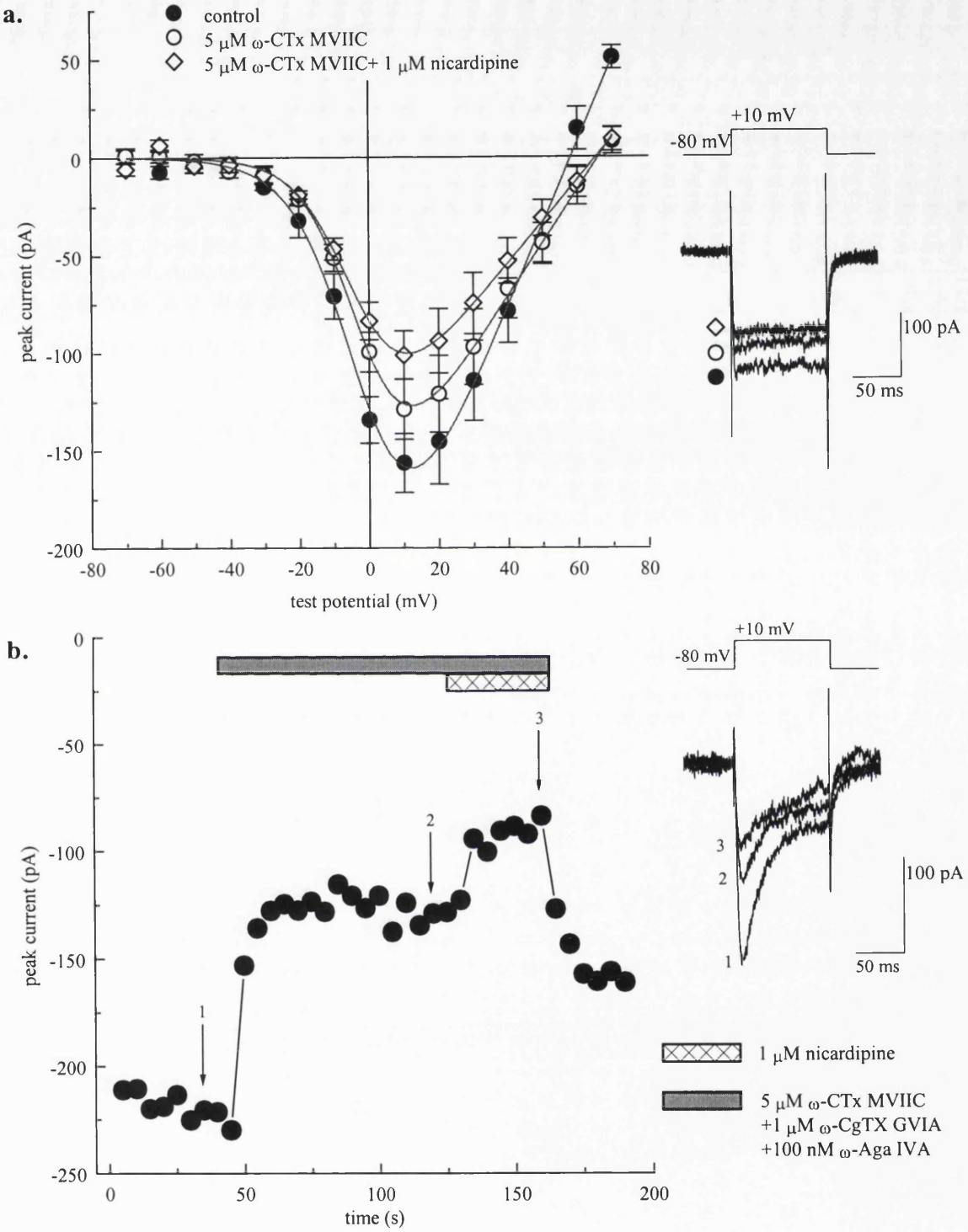

Fig. 5.2 Nicardipine at 1 μM blocks a component of whole-cell Ca^{2+} channel current that is not sensitive to peptide toxins. **a.** 1 μM nicardipine was applied to a group of cells in the presence of 5 μM ω-CTx MVIIC. The current-voltage relationships showing reduction in currents in these 2 conditions are shown. The inset shows recordings taken from the peak of the curve in control, in the presence of ω-CTx MVIIC and in the presence of nicardipine and ω-CTx MVIIC. **b.** Timecourse showing inhibition of 1 μM nicardipine following block with 100 nM ω-Aga IVA, 1 μM ω-CgTx GVIA and 5 μM ω-CTx MVIIC. Representative currents are taken from the timepoints indicated by the arrows. (Potentials given are uncorrected for liquid junction potential, which was -12 mV).

Inhibition of Ca^{2+} channel currents by 10 μM nicardipine

In Fig. 5.3a the results of the application of 10 μM nicardipine are shown. Average reduction in amplitude of currents measured at their peak was 50±7% (n=6). From current-voltage relationships conductance fell from 6.7±1 nS to 1.9±0.2 nS (p=0.0016) and there was an extremely significant hyperpolarising shift in the voltage for half activation (-0.7 (-12.7)±3 mV to -7.6 (-19.6)±3 mV, p=0.0008). The graph in Fig. 5.3b shows the extent of block over a range of test potentials from -20 to +30 mV (same cells as Fig. 5.3a). The inhibition measured increased steadily over this range and was twice as marked at +30 (+28) mV as the reduction in current amplitude at -20 (-32) mV.

The substantial inhibition brought about by applying 10 μM nicardipine to the cells begs the question as to whether it is selective at these concentrations for the L-type Ca^{2+} channel. To test this hypothesis 10 μM nicardipine was applied to a group of cells. After a steady-state of inhibition had been reached 5 μM ω-CTx MVIIC was applied without removal of the nicardipine. In a group of 6 cells 10 μM nicardipine produced 59±7% inhibition. In the presence of 10 μM nicardipine Ca^{2+} channel currents in the same cells were further reduced by 5 μM ω-CTx MVIIC by 21±4% as a percentage of the total current before challenge with nicardipine. Fig. 5.3c demonstrates the cumulative application of ω-CTx MVIIC after block by 10 μM nicardipine. If nicardipine was causing non-specific blockade of Ca^{2+} channels at concentrations above 1 μM the ω-CTx MVIIC-sensitive component of the total whole-cell current would be expected to be reduced. In this case 10 μM nicardipine did not affect the ω-CTx MVIIC-sensitive contribution of the total current. It would appear that the populations of Ca^{2+} channels that are sensitive to nicardipine do not overlap with those sensitive to ω-CTx MVIIC.

The steady-state inactivation properties in the presence of nicardipine were studied to investigate its mechanism of action. Fig. 5.4a,b and c show currents and the resulting steady-state inactivation curves obtained from a cell in the absence or presence of 10 μM nicardipine. The cell was held at holding potentials between -80 mV and +10 (-2) mV for 10 s prior to a voltage-step of 100 ms to +10 (-2) mV. Figs. 5.4a and b compare the normalised and non-normalised currents and Fig.

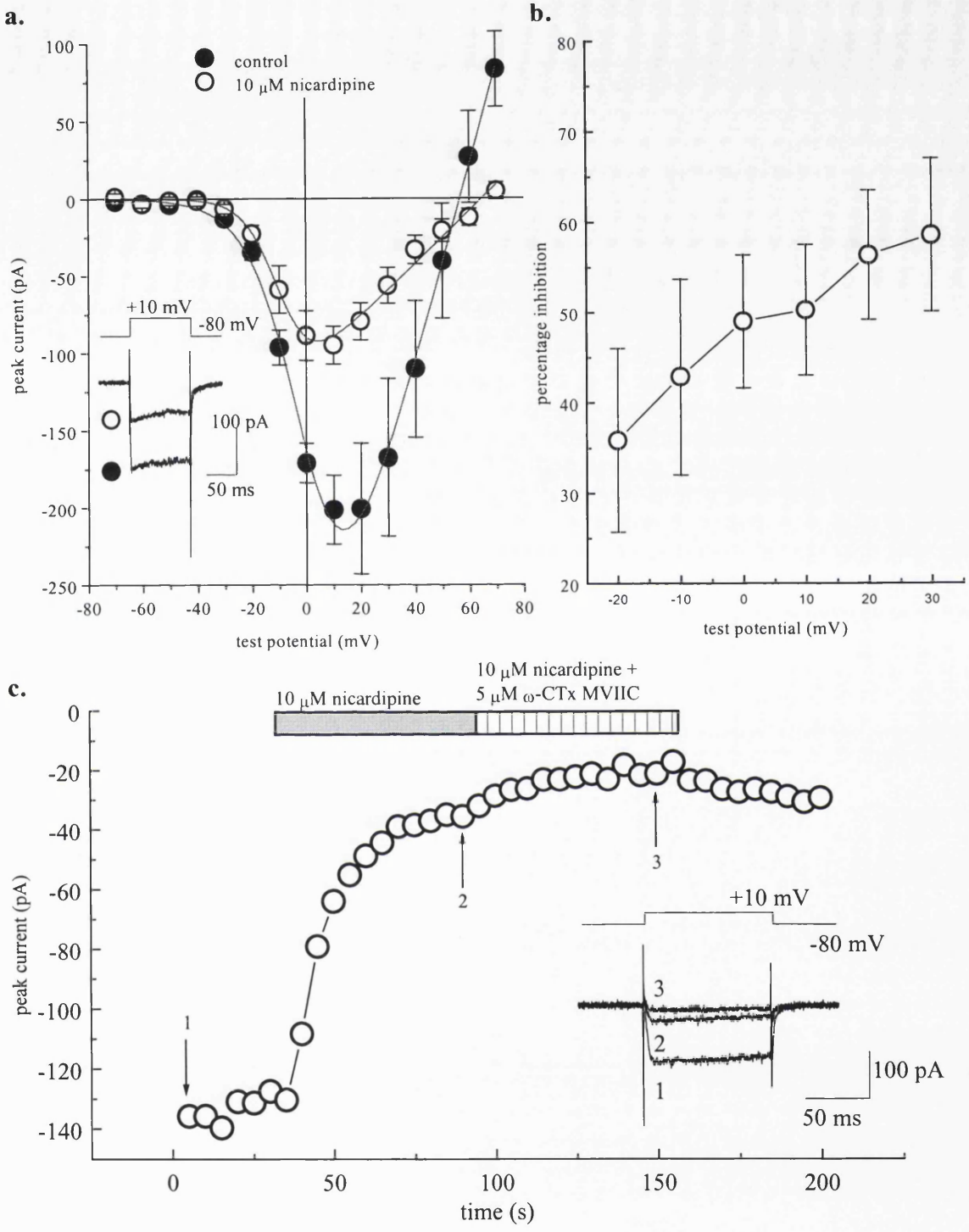

Fig. 5.3 Inhibition by 10 μM nicardipine does not reduce the ω-CTx MVIIC-sensitive component of Ca^{2+} channel current in cerebellar granule cells. **a.** Change in the current-voltage relationship for a group of 6 cells exposed to 10 μM nicardipine. Currents recorded in each condition are shown in the inset. **b.** Inhibition by 10 μM nicardipine over a range of test potentials. Data is shown for the same cells as **a. c.** Timecourse of inhibition by 10 μM nicardipine and the subsequent addition of 5 μM ω-CTx MVIIC to the perfusion solution. In the inset are shown currents recorded in control conditions and at each of the timepoints shown by the arrows. (Potentials given are uncorrected for liquid junction potential, which was -12 mV).

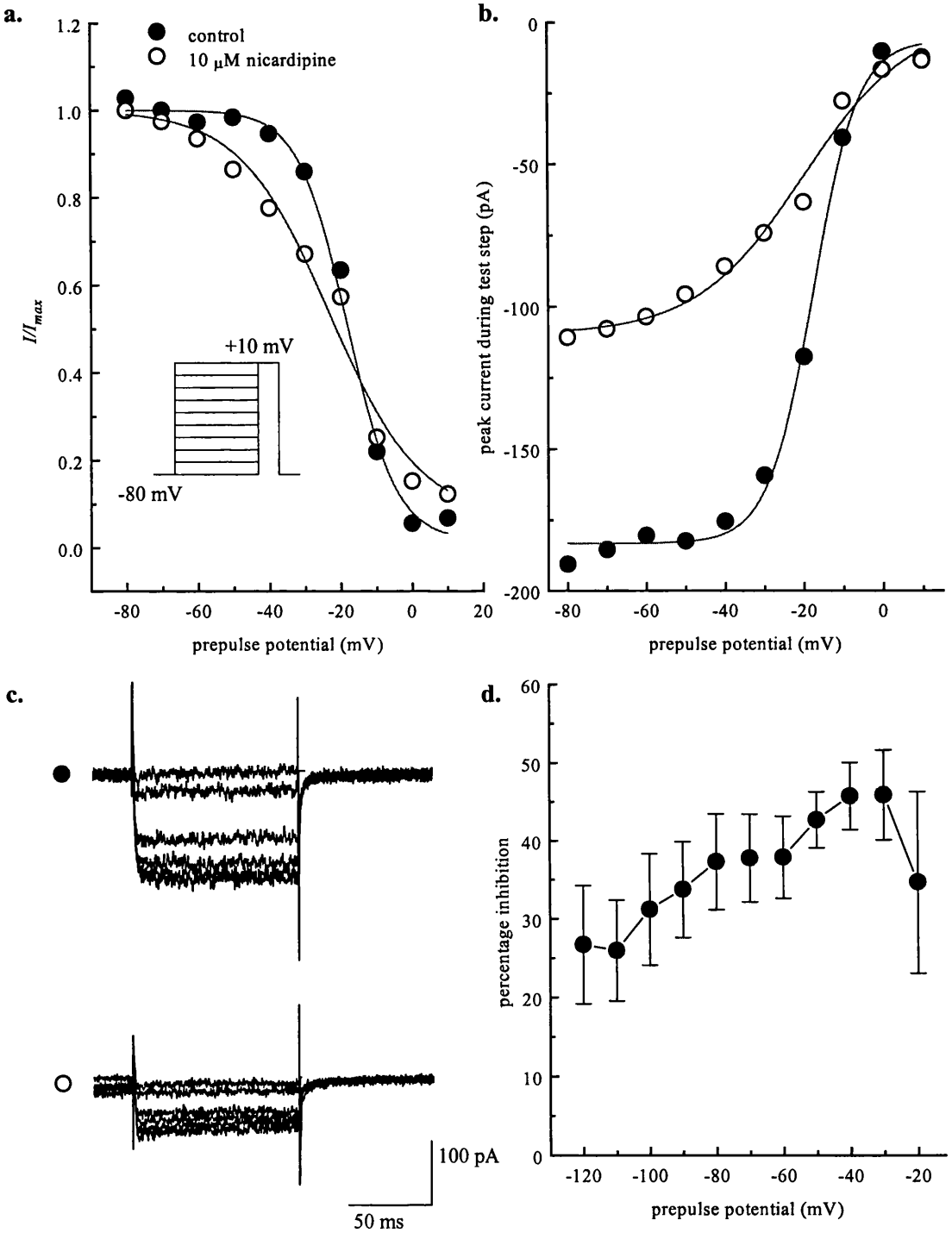

Fig. 5.4 Effect of 10 μM nicardipine on steady-state inactivation **a.** Change in steady-state inactivation for a granule cell in the presence of 10 μM nicardipine. The graph shows the normalised current against the range of prepulse potentials used. The inset shows the voltage protocol. The cell was held at the potentials shown for 1 s prior to the test-pulse to +10 mV for 100 ms. **b.** Non-normalised steady-state inactivation of currents, same cell as **a. c.** Example currents taken from the steepest part of the steady-state inactivation curve in the absence and presence of nicardipine. Currents are shown for currents preceded by prepulses from -50 to 0 mV. **d.** Effect of prepulse potential on inhibition by nicardipine in a group of 5 cells. (Potentials given are uncorrected for liquid junction potential, which was -12 mV).

5.4c shows example current recordings during the test pulse for prepulse potentials from -50 (-62) to 0 (-12) mV. In a group of 7 cells, individual simple Boltzmann fits to the data were averaged. Nicardipine shifted the half-activation to slightly more negative potentials. $V_{50(inact)}$ in the control group was -26 (-38)±2 mV, and became -31 (-43)±3 mV after block with nicardipine. The slope of the fit changed from 8±1 mV in control to 22±2 mV after drug application (p=0.0014) becoming much shallower. Fig. 5.4d demonstrates the effect the prepulse potential had on the percentage inhibition by nicardipine in this group of cells. The extent of inhibition increases towards more depolarised holding potentials.

Effect of BayK8644 on Ca^{2+} currents in cerebellar granule neurones

The DHP BayK8644 exists in two optically isomeric forms due to a chiral centre in the compounds molecular structure. Previously it was only possible to obtain a racemic mixture of the two compounds but now the purified racemates are available. *s*-(-)-BayK8644 potentiates currents carried by L-type Ca^{2+} channels by increasing their open probability. It is also known to produce a shift in activation towards more negative potentials (Kokubun and Reuter, 1984; de Waard *et al.*, 1991). The *r*-(+)- form of BayK8644 is usually reported to be devoid of activity or to show weak antagonism of L-type Ca^{2+} channel currents (see McDonald *et al.*, 1994). In cardiomyocytes *r*-(+)-BayK8644 blocked Ca^{2+} currents at negative potentials but were more potent at depolarised holding potentials showing that the blocking sterioisomers bind preferentially to inactivated or open channels (Hamilton *et al.*, 1987; Hering *et al.*, 1993).

In the following experiments the sensitivity of Ca^{2+} channel currents in cerebellar granule neurones to BayK8644 was tested. Both of the isomers of BayK8644 were studied, with the results shown in Fig. 5.5. Fig. 5.5a and b show the effects of 10 µM *r*-(+)-BayK8644 on Ca^{2+} channel currents. No significant change in amplitude of the current was seen, however a consistent but non-significant shift in the $V_{50(act)}$ of about 7 mV occurred (+4 (-8)±3 mV in control compared to -3 (-15)±3 mV after application of *r*-(+)-BayK8644; p=0.07; n=4). Other parameters averaged from Boltzmann fits were unaltered (g=5.9±0.7 nS, E_{null}=+56 (+44)±3 mV and k=10±0.4 mV in the control group. g=4.8±0.7 nS, E_{null}=+56 (+44)±3 mV

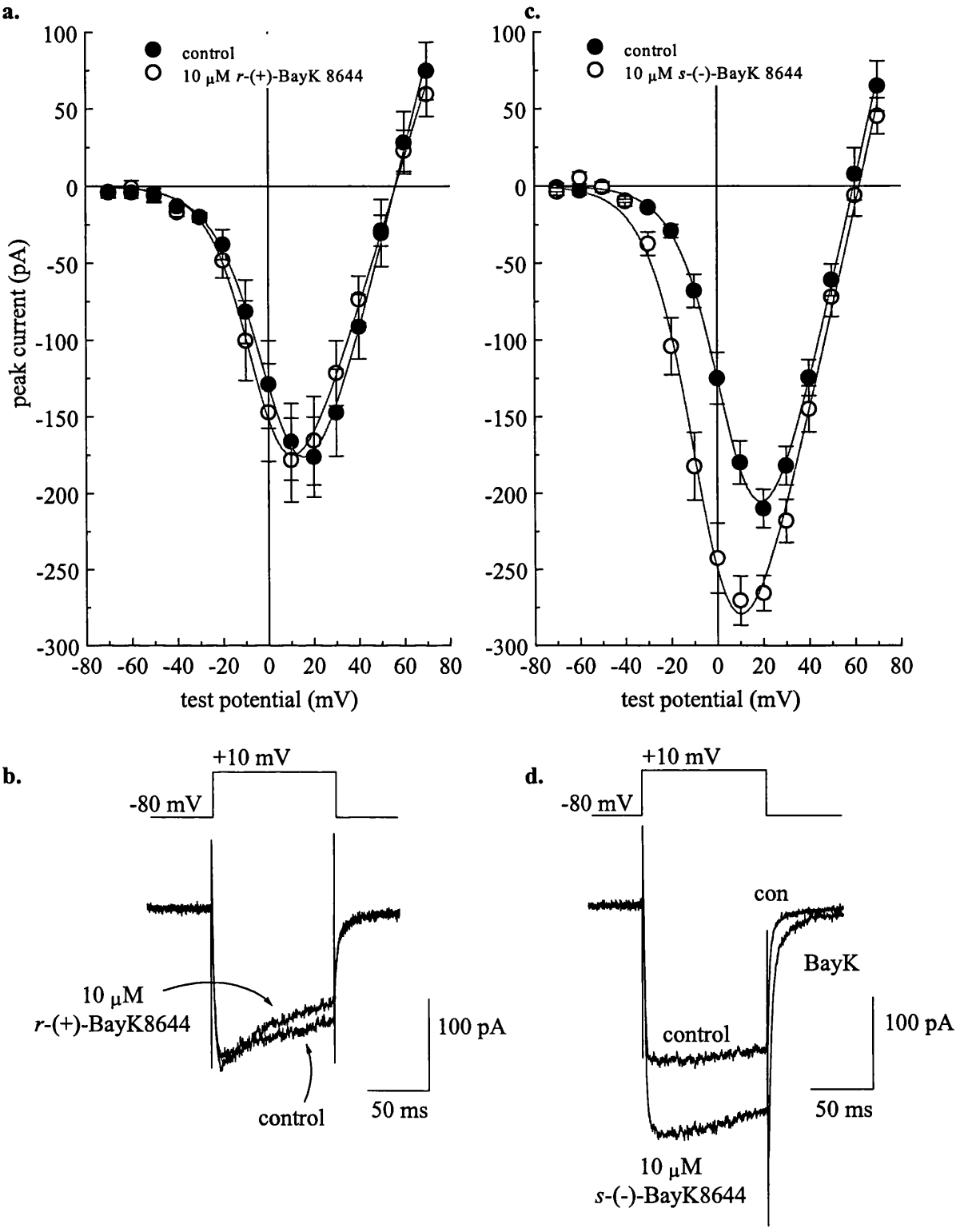

Fig. 5.5 Sensitivity of Ca^{2+} channel currents in cerebellar granule cells to the DHP BayK8644. **a.** Current-voltage relationship before and during application of the agonist *r*-(+)-BayK8644 (10 μM) to a group of 7 cells. **b.** Representative currents recorded in a cell before and during application of *r*-(+)-BayK8644. **c.** Effect of 10 μM *s*-(-)-BayK8644 on the current-voltage relationship in a group of 4 cells. **d.** Currents evoked in the absence and presence of 10 μM *s*-(-)-BayK8644. (Potentials given are uncorrected for liquid junction potential, which was -12 mV).

and k=9±0.3 mV after application of antagonist). Also a small increase in the inactivation kinetics for currents evoked at the same potential was apparent (Fig. 5.5b). No difference in the size or speed of deactivation of tail currents was evident between the control group and treated cells.

The effect of *s*-(-)-BayK8644 is shown in Fig. 5.5c and d. The characteristic increase in amplitude and shift in the voltage-dependence of activation can clearly be seen. The average potentiation of the whole-cell current evoked at +10 mV was 52±6%. $V_{50(act)}$ calculated from Boltzmann fits to the data shifted approximately 11 mV in a hyperpolarising direction (+7 (-5)±2 mV in control to -4 (-16)±3 mV after application of *s*-(-)-BayK8644; p=0.0008; n=7). The other parameters from these fits remained within non-significant limits (g=6.6±0.4 nS, E_{null}=+60 (+48)±2 mV and k=9±0.3 mV in the control group. g=6.9±0.2 nS, E_{null}=+62 (+50)±2 mV and k=10±0.5 mV after application of agonist). Fig. 5.4d shows example currents evoked by stepping the membrane potential from -80 (-92) mV to +10 (-2) mV and demonstrates the large potentiation in current amplitude. The increase in amplitude of currents was greatest when currents were evoked by relatively small depolarisations (more than 100% increases were obtained at potentials less than 0 (-12) mV). The tail current showed both an increase in amplitude and a slowing of deactivation rate. The kinetics of currents evoked in the presence of *s*-(-)-BayK8644 also showed some differences. Fig. 5.6 illustrates some of these changes. Fig. 5.6a shows individual currents evoked in a cell at 4 different potentials in the absence or presence of the DHP agonist. The skew of large increases in current amplitude towards negative potentials can be seen by comparing the upper two traces with the lower traces. In addition, comparing the activation of currents in the absence and presence of *s*-(-)-BayK8644 a slowing was observed being more extreme at negative potentials. The change in activation was examined by measuring the time to peak of the currents evoked at all potentials for this group of cells. Fig. 5.6b shows the results from this analysis. The currents were slower in the presence of *s*-(-)-BayK8644 at all potentials up to the peak of current amplitude. Around the lower negative potentials a wide degree of variation in time to peak was measured resulting in the slowing remaining outside of significant limits. At 0 (-12) mV the effect was most marked. The time

to peak increased significantly from 20±4 ms in control to 52±10 ms during application of 10 μM *s*-(-)-BayK8644 (p=0.033; n=7). The traces in Fig. 5.6a also show an increase in inactivation over 100 ms which is more apparent for larger depolarisations. Fig. 5.6c shows a comparison of the percentage inactivation over 100 ms of currents evoked in the absence or presence of *s*-(-)-BayK8644. Inactivation was faster across this range of potentials in the presence of the agonist, but only reached significant levels at potentials higher than +20 (+8) mV. At a step potential of +30 (+18) mV the percentage inactivation after 100 ms increased from 26±3% in control to 32±3% after application of *s*-(-)-BayK8644 (p=0.019; n=7).

Analysis of the tail currents showed that the instantaneous tail current was significantly larger after application of *s*-(-)-BayK8644. Instantaneous tail currents in control cells had an amplitude of 273±71 pA and increased to 353±50 pA (p=0.024; n=7) during the presence of *s*-(-)-BayK8644.

The time constants of decay of the tail currents were also significantly slowed. The time constant of the fast exponential increased significantly from 1.0±0.1 ms to 1.9±0.4 ms (p=0.022; n=7) and the time constant of the slow exponential increased significantly from 8±0.6 ms to 17±3 ms (p=0.02; n=7).

Recovery from inhibition by 1 μM nicardipine

Experiments already described showed that high concentrations of nicardipine did not reduce the proportion of Ca^{2+} channel current that was sensitive to ω-CTx MVIIC. It was also likely that if nicardipine was only blocking L-type channels that the L-type component could be retrieved by application of *s*-(-)-BayK8644 to a cell in the presence of nicardipine. Any channel activity reduced by non-specific actions of nicardipine against non-L-type channels would not be influenced by exposure to DHP agonist and would not be restored.

Fig. 5.7 shows the effects of combining application of DHP antagonists and agonists and an example of the timecourse of recovery from nicardipine inhibition. In Fig. 5.7a and b, example timecourses are shown for experiments were the wash-on and wash-off rates of nicardipine were measured by fitting a single exponential function to the inhibition of currents or recovery from block. Fig. 5.5a shows

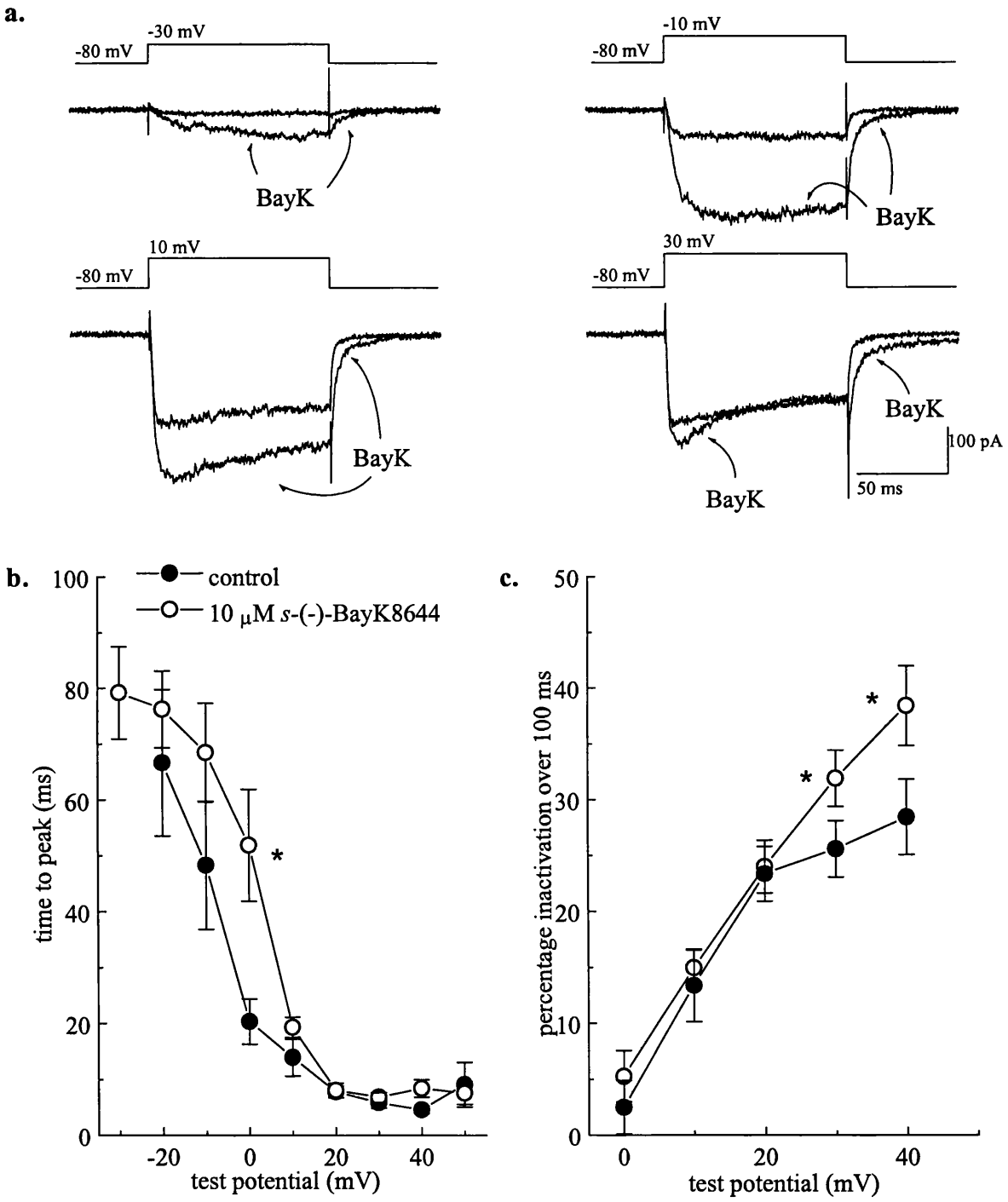

Fig. 5.6 Change in kinetics of currents in cells exposed to *s*-(-)-BayK8644. **a.** Currents recorded in a single granule neurone evoked at the potentials shown in the absence or presence of 10 μM *s*-(-)-BayK8644. The scale bar applies to all traces. **b.** Effect of 10 μM *s*-(-)-BayK8644 on activation of currents. The time to peak is plotted against the test potential in a group of 7 cells. **c.** Effect of 10 μM *s*-(-)-BayK8644 in the same group of cells as **b.** on inactivation of Ca^{2+} channel currents measured as the percentage inactivation of current over a 100 ms voltage step. The asterisks in **b.** and **c.** show significant differences in the data ($p<0.05$). (Potentials given are uncorrected for liquid junction potential, which was -12 mV).

block by 10 μM nicardipine and recovery by perfusing normal extracellular solution across the cell to remove the drug. In Fig. 5.5c currents recorded before and during application of nicardipine, and after wash are shown. Recovery was not complete in this time but occurred rapidly. In 6 similar experiments the rates of wash-on and wash-off were calculated and averaged. The time constant for nicardipine block was 25±5 s, and for rate of recovery with control solution was 60±10 s. Fig. 5.5b shows an example timecourse of currents measured in a cell first challenged with 10 μM nicardipine and subsequently perfused with 10 μM *s*-(-)-BayK8644 to facilitate recovery. Example current traces are shown for a cell in the absence and presence of nicardipine, and after perfusion with *s*-(-)-BayK8644. In a group of 7 cells the time constant for block by nicardipine was 19±2 ms. During application of *s*-(-)-BayK8644 currents returned to amplitudes in excess of control values with a time constant of 44±7 s. Although recovery during application of *s*-(-)-BayK8644 was faster, the differences between the two conditions were not significant (p=0.21; n=6).

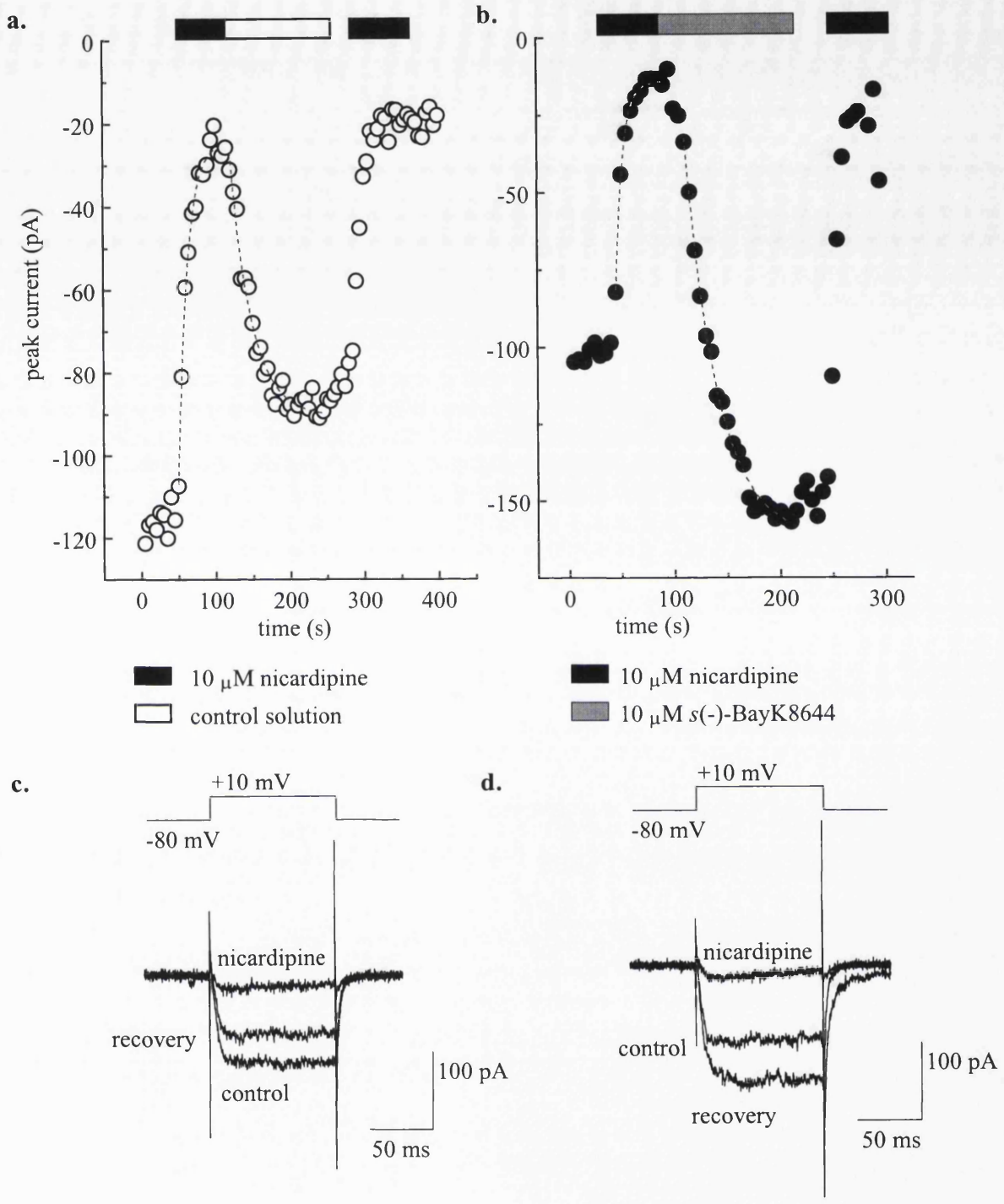

Fig. 5.7 Analysis of the time constants of block by 10 μM nicardipine and recovery facilitated by perfusion of normal extracellular solution or 10 μM *s*-(-)-BayK8644. **a.** Timecourse of block by 10 μM nicardipine and wash off by perfusing normal extracellular recording media over the cell. The broken lines show exponential functions fit to the decay or recovery of peak current. **c.** Example currents recorded before, during and after recovery from block by nicardipine. **b.** Similar experiment to that of **a.** but here the recovery from nicardipine block is facilitated by the application of 10 μM *s*-(-)-BayK8644. **d.** Example of currents recorded before and during block by 10 μM nicardipine and after recovery in the presence of *s*-(-)-BayK8644. (Potentials given are uncorrected for liquid junction potential, which was -12 mV).

Discussion

The L-type family of Ca^{2+} channels exist as multiple subtypes throughout the brain and have been characterised on the basis of their sensitivity to DHP compounds in many tissues (Ahlijanian *et al.*, 1990; Snutch *et al.*, 1991; Williams *et al.*, 1992b; Chin *et al.*, 1992). The ability of these drugs to antagonise Ca^{2+} influx has led to their use in the treatment of conditions such as angina and hypertension. Their blocking actions on the Ca^{2+} channel have attracted the attention of workers in the field of neurodegenerative diseases because they may exert a neuroprotective role to prevent the intracellular Ca^{2+} overload that occurs during these processes (Weiss *et al.*, 1990; Regan and Choi, 1994). However, their main mode of action against brain damage has been attributed to a direct action on smooth muscle in the cerebral vasculature (McCarthy and Cohen, 1989). For the successful treatment of brain disorders a drug must be able to cross the blood brain barrier. One highly lipophilic DHP antagonist, nimodipine has been shown to be beneficial in models of age-induced loss of learning and memory functions (Deyo *et al.*, 1989; Schuurman, 1993).

Within the CNS different α_1 subunits of the Ca^{2+} channel exist that are sensitive to DHPs. At least 2 different genes encode L-type Ca^{2+} channels in the brain and alternative splicing creates further diversity. Single-channel studies have shown that L-type Ca^{2+} channels with dramatically different voltage-dependent properties co-exist in cerebellar granule neurones (Forti and Pietrobon, 1993). The functional consequences of this molecular diversity are not understood but some evidence suggests that the L-type Ca^{2+} channel has a post-synaptic function to initiate Ca^{2+}-dependent events in response to dendritic activity (Ahlijanian *et al.*, 1990). L-type channels are seen to cluster around the proximal regions of major dendrites in many central neurones and may couple strong synaptic input to regulation of gene expression in cortical neurones (Murphy, T. H. *et al.*, 1991) and to induction of NMDA receptor-independent long-term potentiation (Grover and Teyler, 1990; Aniksztejn and Ben-Ari, 1991) and long-term depression (Wickens and Abraham, 1991). In preparations of peripheral neurones, under normal conditions N-type Ca^{2+} channels have been suggested to mediate neurotransmitter release (Miller,

1987), but during prolonged depolarisation, or repetitive stimulation the L-type channel plays a more significant role (Ceccarelli *et al.*, 1988). In neurotransmitter release studies measuring the release of newly synthesised [^{3}H]-glutamate from cultured cerebellar granule neurones after depolarisation with 50 mM K^+ the Ca^{2+}-dependent release was partially inhibited by DHP antagonists in addition to ω-CgTx GVIA and increased by DHP agonists showing that both L and N-type channels have the potential to be involved in the release process (Huston *et al.*, 1990; Huston *et al.*, 1993; Huston *et al.*, 1995).

The single channel kinetics and voltage-dependent properties of brain L-type Ca^{2+} channels have been difficult to compare to the well characterised cardiac L-type channel (Cavalie *et al.*, 1986) primarily because of the mixed populations of channel types that are present in any one neuronal cell. Single channel studies have however revealed DHP-sensitive channels with different gating properties. Forti and Pietrobon (1993) showed 2 L-type channels with single channel conductance and voltage-dependent properties similar to the cardiac channel distinguished on the basis of their gating patterns, one showing bursts of brief openings interrupted by rare periods of activity with long open durations, the other characterised by sporadic short openings interrupted by rare longer openings and a very low overall open probability. A third L-type channel in this study had completely different voltage-dependent properties. It opened only rarely and briefly at high positive voltages, but showed remarkably long open times at negative voltages after a positive prepulse with some delay after repolarisation. They presumed that since this type of channel did not inactivate during the predepolarising voltage step, and after depolarisation entered a completely different set of open and closed states this gating could not be described as reopening of channels. Reopening has been studied by Slesinger and Lansman (1991c, 1996) and is a pathway for Ca^{2+} entry through L-type channels that reopen after repolarisation. Reopenings appear as large single channel events following a positive voltage step with a few millisecond delay which is thought to be due to the release of a positively charged cytoplasmic blocking particle at negative potentials (Slesinger and Lansman, 1996) and has been observed in various preparations (Fisher *et al.*, 1990; Thibault, 1993). Slesinger and Lansman (1996) argued that the anomalous gating pattern seen by Forti and Pietrobon (1993) could

be explained by the relatively depolarised holding potential used in their experiments causing delayed openings. Averaging of this channel activity with rapidly activating channels that then become blocked would then not give a true representation of the timecourse of block.

The results of this chapter have demonstrated a component of the Ca^{2+} channel current in cerebellar granule neurones that is sensitive to the DHP antagonist nicardipine. At least some of this current is carried by the L-type Ca^{2+} channel. When concentrations in the range 1-10 μM were applied to cells the current sensitive to nicardipine was completely additive with the components of the whole-cell current sensitive to ω-CTx MVIIC or a combination of ω-CTx MVIIC, ω-Aga IVA and ω-CgTx GVIA. This can be taken to suggest that nicardipine blocks a population of channels at these concentrations that is separate to those blocked by ω-CTx MVIIC, ω-Aga IVA and ω-CgTx GVIA. At higher concentrations nicardipine inhibited currents in these cells by a proportion which could not be solely attributed to non-N/non-P-type channels as it reduced currents by a larger percentage than the currents which make up the ω-CTx MVIIC/ω-CgTx GVIA/ω-Aga IVA-insensitive component. At 100 μM, currents were blocked by 64±5% following application of nicardipine. In previous studies in granule neurones a similarly large reduction in Ca^{2+} channel currents has been observed after exposure to nicardipine (DeWaard *et al.*, 1991). The conclusions of this study which also examined the effect of ω-CgTx GVIA were that a population of channels was present with a mixed pharmacology being sensitive to nicardipine and ω-CgTx GVIA. More recently, again fitting in with the results here, Diochot *et al.* (1995) showed that DHPs and other Ca^{2+} antagonists have a substantial inhibitory effect on neuronal non-L type Ca^{2+} channels. Nicardipine in the latter study blocked HVA currents in DRG neurones completely at a concentration of 200 μM.

It seems reasonable to conclude from the data here that nicardipine at high concentrations has non-selective blocking effects on various Ca^{2+} channel currents including ω-Aga IVA-sensitive and ω-CgTx GVIA-sensitive currents. However, at lower doses up to 10 μM it appears not to have a significant interaction with channels carrying these toxin-sensitive currents, although some individual cases

show exception to this. A proportion of the nicardipine-sensitive current must be carried by L-type channels of either the C or D class since characteristic effects of both DHP agonists and antagonists have been shown, and both these Ca^{2+} channel subunits are known to be expressed at high levels in the granule cells of the cerebellum (Hell *et al.*, 1993). Some of the inhibition may also be accounted for by the effect of nicardipine against the α_{1E} Ca^{2+} channel which has been shown to be sensitive to nicardipine (see Chapter 6) and is also present in the cerebellum (Yokoyama *et al.*, 1995). It is also possible that nicardipine blocks novel as yet unidentified Ca^{2+} channels present in cerebellar granule cells.

The actions of Ca^{2+} antagonists have been extensively studied and are explainable in terms of the modulated receptor model adapted from work on the interactions between local anaesthetics and the Na^{+} channel (Hille, 1977; Hondegham and Katzung, 1977). In general terms a charged drug molecule may gain access to its channel binding site from the aqueous environment and an uncharged drug may interact via the lipid environment of the membrane and preferentially binds to the channel in a particular state. The state-dependence of DHP binding is such that at more positive membrane potentials greater binding of DHP is likely and greater block of the channel results because binding to the inactivated state is favoured. Similarly, strong hyperpolarisations permit the release of drug binding weakly to the closed state. A positive shift in holding potential increases DHP block (Kass and Arena, 1989; Okabe *et al.* 1987) and the calculated K_D for inactivated channels has been shown to be several orders lower than for the resting channels (Bean *et al.*, 1986). Furthermore, shifting the holding potential to favour the resting state has been shown to effectively remove the nimodipine inhibition in rabbit smooth muscle (Worly *et al.*, 1991). The state-dependent binding has been clearly demonstrated in single channel studies in cerebellar granule neurones where DHPs increased the number of blank sweeps and restricted channel openings during active sweeps to brief initial bursts and this change manifests in whole-cell recordings as a blocker induced negative shift in the steady-state inactivation (see McDonald *et al.*, 1994). The results here (see Fig. 5.4) demonstrate the shift in steady-state inactivation characteristic of DHP action and also a dependence of the extent of block on membrane potential was seen.

Dihydropyridine activators produce an enhancement of L-type channel current amplitude, but have no potentiating effect on currents carried by other channels (Stea *et al.*. 1994; Sather *et al.*. 1993; Stea *et al.*, 1993; also Chapter 6 this study) although a small inhibition of α_{1A} currents has been seen (Mori *et al.*, 1991). At the single channel level the stimulation results from a large increase in the probability of channel opening together with the induction of long openings (Hess *et al.* 1984). A decrease in the number of blank sweeps has been attributed to the effects of DHP activators (Hess *et al.* 1984; Isenberg and Klockner, 1985) and some studies have shown an increase in unitary current amplitude (Caffrey *et al.* 1986; Kokubun and Reuter, 1984).

Fig. 5.5 shows the effects of both isomers of BayK8644. The agonist produced effects that fit in well with existing reports for the effects of DHP activators on L-type currents. Namely, an increase in current amplitude that is more pronounced for small depolarisations, a shift in peak of activation to a more negative potential and an altered current timecourse involving a deceleration of activation and an increase in the rate of inactivation. In addition a pronounced increase in amplitude and slowing of deactivating tail currents was seen. These effects have been well documented (see McDonald *et al.*, 1994) with one exception, being the slowing of activation. Reports of both acceleration of whole-cell (Josephson and Sperielakis, 1990; Lacerda and Brown, 1989) and single channel (Hess *et al.* 1984) currents, and a slowing has been reported (Marks and Jones, 1992). Although this was seen in cells expressing solely L-type current.

The mode of action of DHP activators is presently unclear. Reports have shown that these drugs are only effective if applied externally to skeletal muscle channels incorporated in lipid bilayers (Valdivia and Coronado, 1990) and internal BayK8644 was ineffective in frog ventricular myocytes (Fischmeister and Hartzell, 1990), but in bovine adrenal chromaffin cells BayK8644 was just as effective if applied internally or externally (Cena, 1989). Two theories of the mechanism of action have been proposed, one based on the promotion of a long-opening mode of gating (Hess *et al.* 1984), the other based on the modification of normal gating (Lacerda and Brown, 1989; Bechem *et al.*, 1989), however neither explains the behaviour of DHPs in all situations.

Evidence suggests that the binding site for DHP antagonist drugs is accessible only from the external face. Charged and uncharged DHP blockers are relatively ineffective when applied internally to cells (Okabe *et al.* 1987; Valdivia and Coronado, 1990, 1990; Kass and Arena, 1989). Permanently charged DHP blockers are ineffective from the external side (Cohen *et al.* 1987; Hescheler *et al.* 1982; Pelzer *et al.* 1982) with notable exceptions including amlodipine, a charged DHP with an extended lipophilic side chain allowing entry into the membrane from the extracellular side and diffusion to its binding site (Kass and Arena, 1989). These studies and other findings that showed the blocking potency of DHPs was enhanced when the proportion of uncharged external molecules was increased, suggest that uncharged molecules reach their binding site from the lipid phase and that charged intracellular molecules reach the binding site following diffusion of neutral molecules across the membrane (Kass and Arena, 1989; Triggle and Swamy, 1983).

The initial studies conducted to locate the DHP binding site on the L-type channel started with a biochemical approach and narrowed the binding domain down to being situated between amino acids 1390 and 1437 (Regulla *et al.*, 1991). With further contributions from several groups (Nakayama *et al.*, 1991; Striessnig *et al.*, 1991; Tang *et al.* 1993a,b) Grabner *et al.* (1996) arrived at the minimum sequences already discussed (Chapter 1). These studies point towards an interfacial location of the receptor between domains III and IV. The binding regions for DHP agonists and antagonists are similar although not identical, agonist effects require additional residues. It is likely that DHP agonists and antagonists compete for the same binding site. The results shown in Fig. 5.7 showed that *s*-(-)-BayK8644 speeded recovery from nicardipine block but not to significant levels. The example cells shown demonstrate that although earlier experiments showed no overlap of toxin-sensitive currents at lower doses of nicardipine, in some cases the inhibition by 10 μM nicardipine was extensive.

To summarise, Fig. 5.8 shows graphically how nicardipine inhibited Ca^{2+} channel currents in cerebellar granule neurones in combination with other blockers used in these experiments. At a concentration usually referred to as being selective for L-type Ca^{2+} channels (1 μM), nicardipine blocked just less than 20% of the total whole-cell current. At this concentration the nicardipine-sensitive current did not

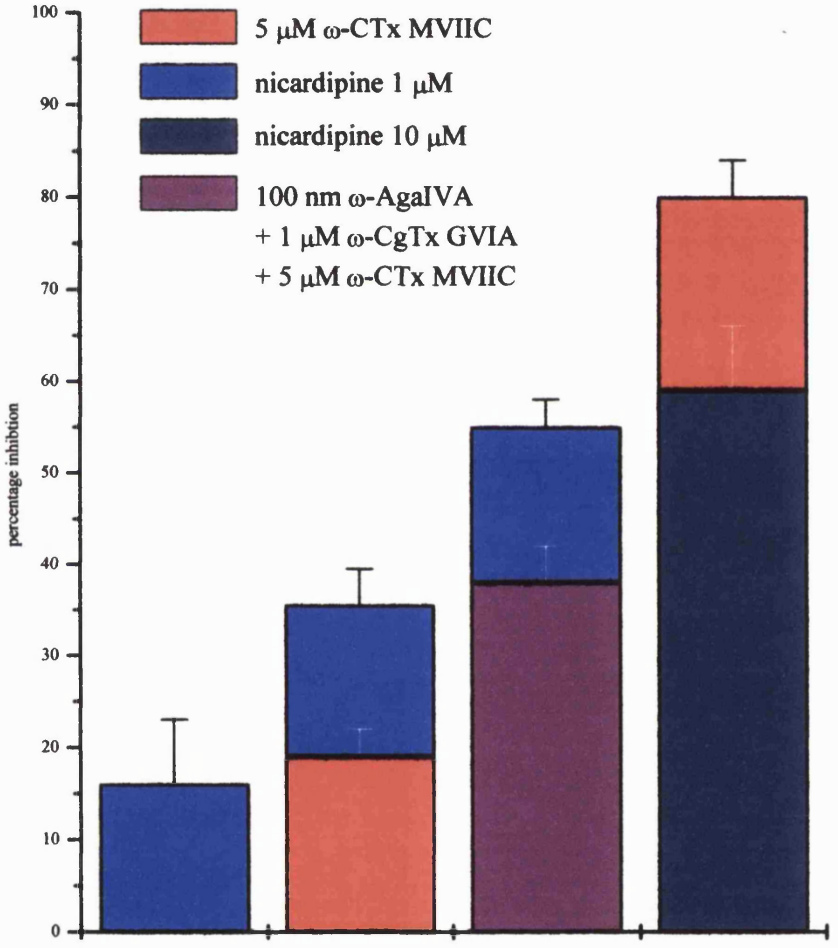

Fig. 5.8 Summary of the effects of nicardipine applied to granule cells individually or in combination with various toxins. Bars represent the mean inhibition±s.e.m. where n=5-9. The lowest division represents the drug(s) applied first in every case.

overlap with currents carried by toxin-sensitive Ca^{2+} channels. Higher concentrations of nicardipine (10 μM) however, blocked more of the total current than could be attributed to L-type channels alone but interestingly did not reduce the ω-CTx MVIIC-sensitive component.

Chapter 6

Functional expression of a rat brain cloned α_{1E} Ca^{2+} channel in COS-7 cells

Results

The α_{1E} Ca^{2+} channel clone is a relatively newly identified subunit that encodes a Ca^{2+} channel with unusual properties in that it appears not to account for any of the more established Ca^{2+} current types and has properties that fall between the HVA and LVA Ca^{2+} channel groups (Soong *et al.* 1993; Williams *et al.*, 1994; Schneider *et al.*, 1994; Yokoyama *et al.*, 1995; Stephens *et al.*, 1997). Investigations of the distribution of this class of channel have shown high density of expression in the Purkinje cells and granule cells of the cerebellum (Soong *et al.* 1993; Yokoyama *et al.*, 1995) and prompted investigations of this channel clone as a candidate for a proportion of the DHP-sensitive current in granule cells.

COS-7 cells are an effective expression system

Previous studies using COS-7 cells have shown that they are a suitable system in which to examine the expression of Ca^{2+} channel subunits. Electrophysiological experiments have shown that in untransfected COS-7 cells no Ca^{2+} channel currents are present (Stephens *et al.*, 1997; Brice *et al.*, in press; Berrow *et al.*, in press). In addition, following transfection with either $\alpha_2\delta/\beta_{1b}$ or β_{1b} alone no Ca^{2+} channel currents could be evoked. Immunocytochemical studies have confirmed that untransfected COS-7 cells lack Ca^{2+} channel proteins. A pan-specific antibody directed against β_{1-4} subunits showed that no endogenous β subunits were present (Brice *et al.* in press). This study also failed to detect the $\alpha_2\delta$ subunit using specific antibodies raised against this protein.

Transfected and untransfected COS-7 cells have also been subjected to reverse transcription (RT)-PCR to confirm the presence or absence of Ca^{2+} channel α_{1E} subunit mRNA. PCR primers for regions of sequences conserved throughout all mammalian $\alpha 1_E$ cDNAs so far cloned (rat, mouse, human, rabbit) generated no PCR products in untransfected cells or in transfected cells in the absence of the RT step, but were produced in cells transfected with α_{1E} cDNA (Stephens *et al.* 1997; Berrow *et al.*, in press).

Expression of $\alpha_{1E}/\beta_{1b}/\alpha_2\delta$

In the following experiments transfection of $\alpha_{1E}/\beta_{1b}/\alpha_2\delta$/GFP resulted in the appearance of Ca^{2+} channel currents in >80% of cells positive for GFP. Expression levels peaked between 48-72 hours after transfection. Robust currents could be evoked using 10 mM Ba^{2+} as a charge carrier but problems were experienced with regards to clamping the currents. 1 mM Ba^{2+} was adequate in producing sizeable currents and was used in all recordings in COS-7 cells. Average current amplitude was -685±129 pA and showed considerable variation from cell to cell. The whole-cell capacitance of these cells also varied in spite of efforts to select cells of a similar appearance and size. Average C_m was 15±2 pF. Assuming a specific C_m of 1 μF/cm2, Ca^{2+} channel current density in these cells was 43 $\mu A/cm^2$ with 1 mM Ba^{2+}. Currents in this chapter are presented as current densities to allow for differences in cell size. Average R_s was 17±3 MΩ.

Fig. 6.1a shows example current recordings in a typical cell held at -80 (-95) mV and stepped to the potentials shown. Currents activated fairly rapidly. Time to peak was calculated to be 19±2 ms in a group of 14 cells for currents evoked at +10 (-5) mV. The rising phase of the current was fitted with a single exponential producing $\tau_{(act)}$ as a measure of the activation rate. In the same 14 cells $\tau_{(act)}$ was 3.7±0.4 ms measured at +10 (-5)mV. $\tau_{(act)}$ showed a clear decrease as the depolarising step was increased (see filled circles Fig. 6.4b). The decay of the current was also relatively rapid and well described by a single exponential. The average time constant for inactivation was 277±45 ms (n=14) measured at +10 (-5) mV. Fig. 6.1b shows the average normalised decay of the peak current over 100 ms. At the end of this 100 ms voltage step approximately 35% of the total current had decayed.

In most cells the current began to activate at -30 (-45) mV and showed a variable peak between -10 (-25) mV and +10 (-5) mV. All relationships were fitted with Boltzmann equations to examine the voltage-dependence of activation. The averaged parameter values revealed that the whole-cell conductance was 2±0.5 nS/pF and the $V_{50(act)}$ was -7 (-22)±4 mV. (In Fig. 6.2c the filled circles show an example of a current-voltage relationship in a typical cell.)

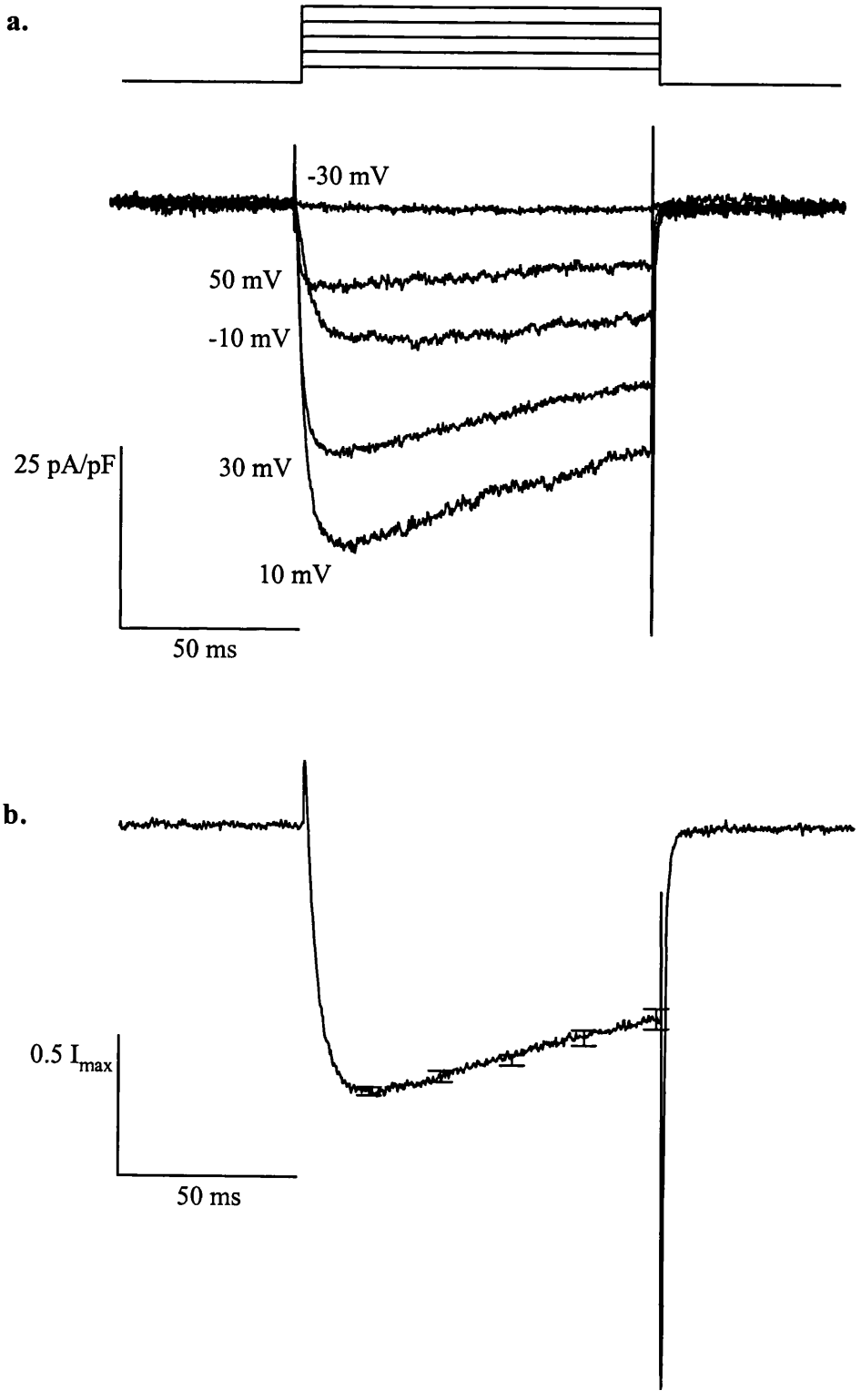

Fig. 6.1 Ca^{2+} channel currents on COS-7 cells. **a.** Family of currents recorded in a single COS-7 cell evoked at the potentials shown from a holding potential of -80 mV for 100 ms. **b.** Average inactivation for a group of 14 cells. Currents evoked at +10 mV were normalised and averaged. Error bars representing the s.e.m. are shown at several time points. (Potentials given are uncorrected for liquid junction potential, which was -15 mV).

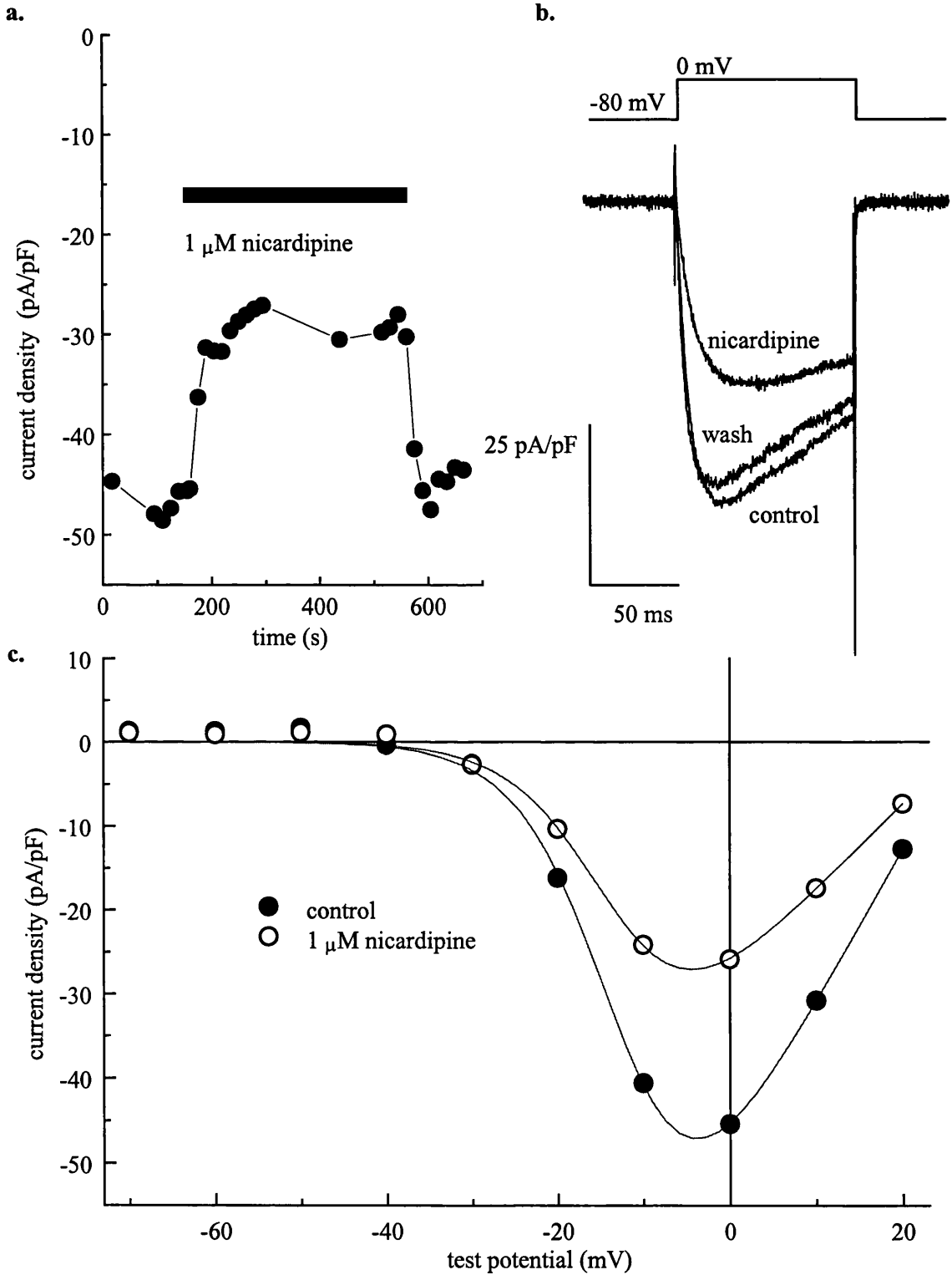

Fig. 6.2 Sensitivity of Ca^{2+} channel currents in COS-7 cells to 1 μM nicardipine. **a.** Time course of inhibition of currents by nicardipine. The figure shows the inhibition of peak current density in a cell during application of 1 μM nicardipine and recovery after removal of the drug. Periods where no data points are shown correspond to acquisition of current-voltage data and only the appropriate point is shown. **b.** Example currents from the same cell as in **a.** showing traces recorded before, during and after application of nicardipine. **c.** Current-voltage relationship for the same cell as **a.** showing the effect of 1 μM nicardipine. The data was fit with a Boltzmann equation (see *Equation 1*, Chapter 2). (Potentials given are uncorrected for liquid junction potential, which was -15 mV).

Pharmacology of $\alpha_{1E}/\beta_{1b}/\alpha_2\delta$ currents

The effect of DHP drugs on COS-7 cells expressing the α_{1E} Ca^{2+} channel was studied. Fig. 6.2a shows the effect of 1 μM nicardipine on currents. Block was rapid and the example shown demonstrates the reversible nature of the inhibition, most cells recovered fully after removing the drug. The peak current was inhibited by 51±7% (p=0.0067; n=8) with no effect on the voltage-dependence of activation. $V_{50(act)}$ calculated from current-voltage relationships before and after addition of the drug remained unchanged (-7 (-22)±4 mV, -9 (-24)±4 mV respectively; p=0.52, n=5, see Fig. 6.2c). The voltage-dependence of inhibition by nicardipine is illustrated in Fig. 6.3 which shows current-voltage relationships in the absence and presence of 1 μM nicardipine at two different holding potentials. To the left of the figure (6.3a) the cell was held at -80 (-95) mV and stepped to potentials ranging from -70 (-85) mV to +70 (+55) mV. Inhibition at -80 (-95) mV measured at the peak of inward current in a pair of cells was 42±2 %. Fig. 6.3b shows the same cell held at a more depolarised potential (-50 (-65) mV) before and after application of nicardipine. At this holding potential more than half of the current was inactivated and the inhibition was 63±7 %. This data agrees with the well documented voltage-dependence of inhibition by DHPs (Hamilton *et al.*, 1986).

The extent of nicardipine block seen over all test potentials stepping from a holding potential of -80 (-95) mV is shown in Fig. 6.4a. Percentage inhibition remained constant across the whole voltage range. The voltage-dependence of block seen here is a feature of the holding potential, 100 ms depolarising voltage steps being too brief to cause greater development of block. Another feature of the block by nicardipine is shown in Fig. 6.4b. After application of the drug the speed of activation of currents evoked at all potentials was slightly but consistently slowed. $\tau_{(act)}$ was decreased to a greater extent at more positive potentials.

Fig. 6.4c shows the effect of application of the DHP agonist *s*-(-) BayK8644. The drug was applied at 10 μM to a group of 2 cells causing no change in the amplitude of evoked currents and no change in the voltage-dependence or kinetics of currents. This result was confirmed in another study under identical conditions (Stephens *et al.*, 1997).

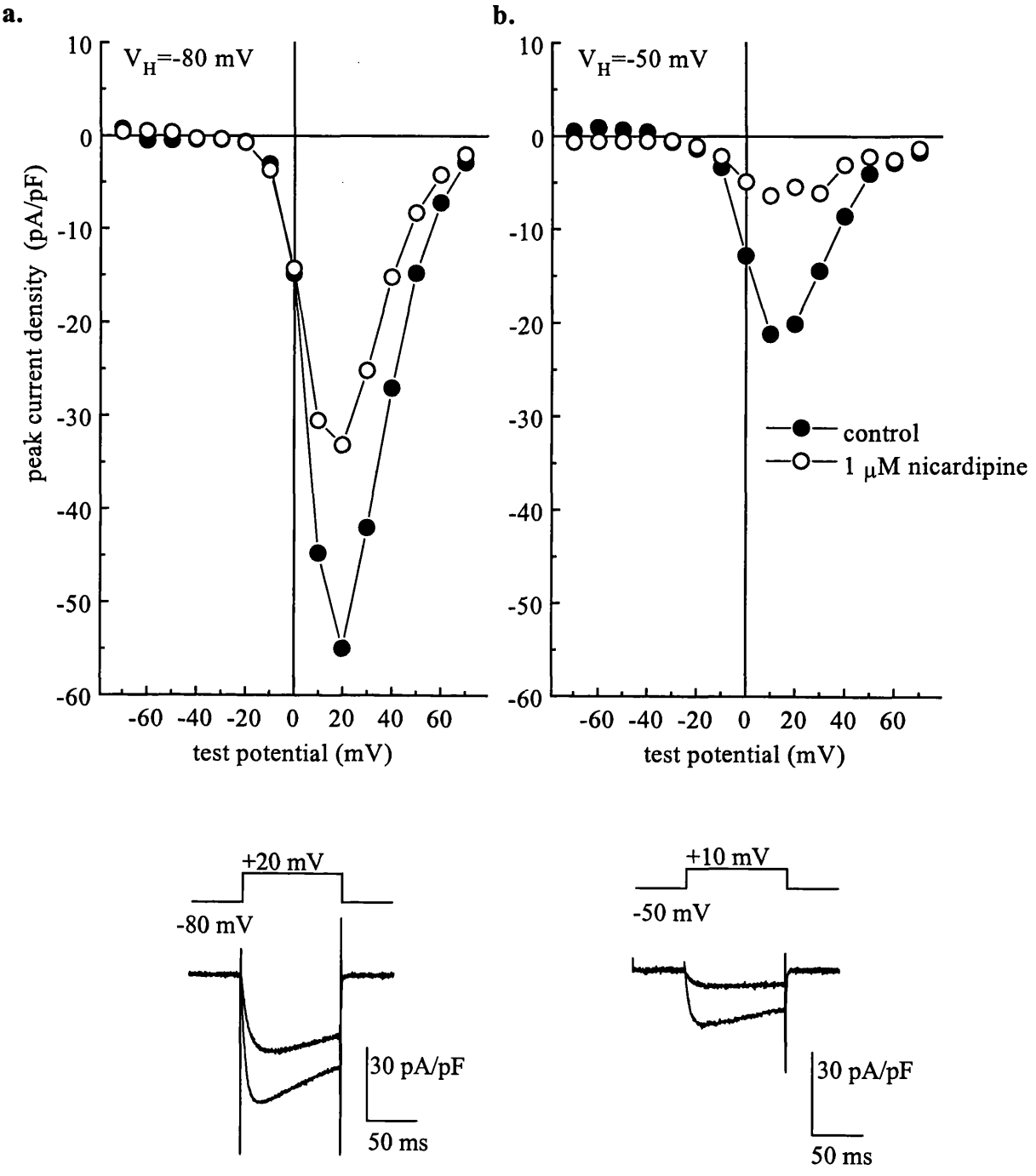

Fig. 6.3 Voltage-dependence of nicardipine block. **a.** Current-voltage relationships showing inhibition of evoked Ca^{2+} channel currents in a single COS-7 cell recorded from a holding potential of -80 mV. The illustrations below show example current traces recorded at the peak of current before and during application of 1 μM nicardipine. **b.** Current-voltage relationships for the same cell as **a.**, but currents were evoked from a holding potential of -50 mV. The traces below show the current recorded during a step to +10 mV before and during exposure to nicardipine. (Potentials given are uncorrected for liquid junction potential, which was -15 mV).

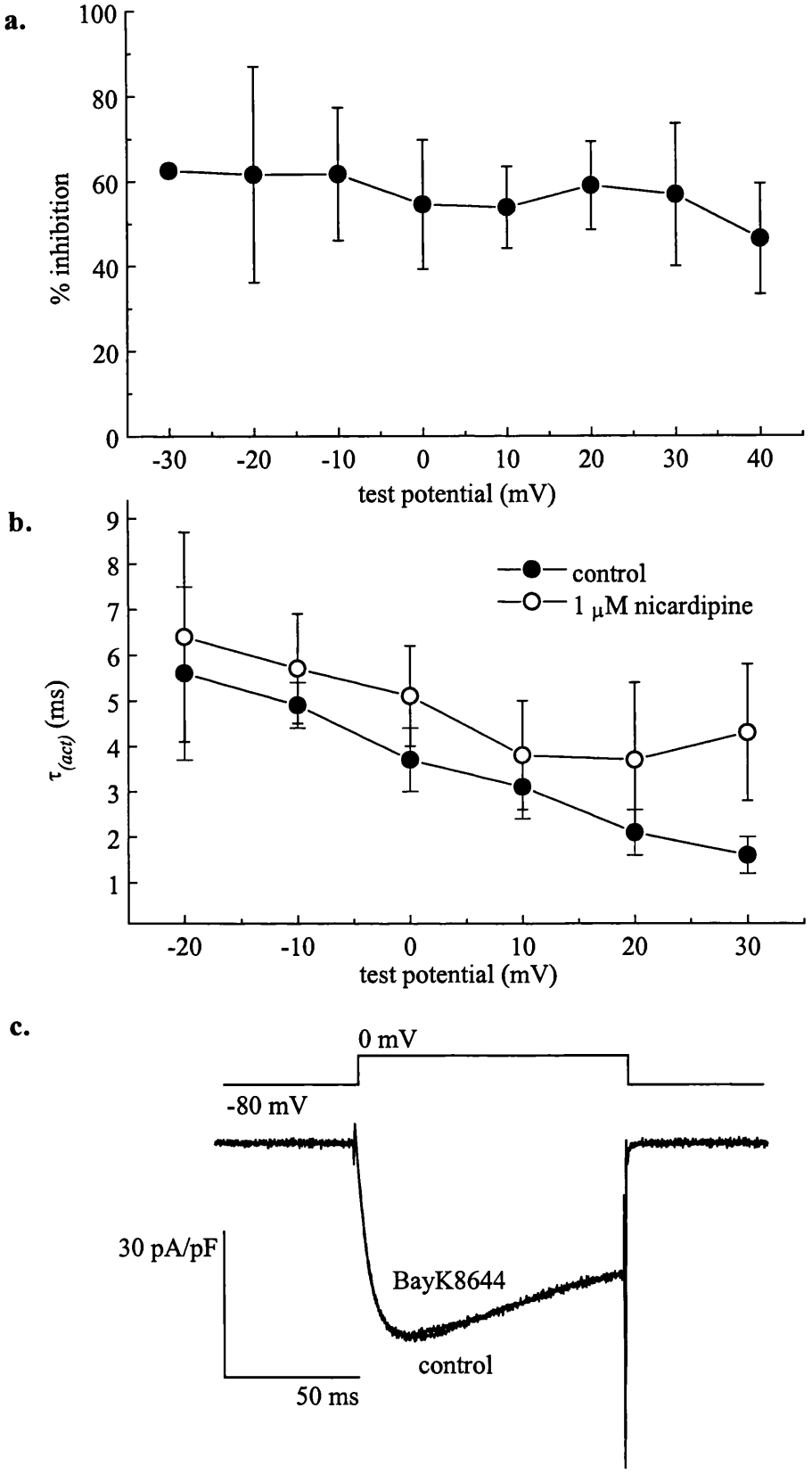

Fig 6.4 Some characteristics of DHP activity on Ca^{2+} channel currents in COS-7 cells. **a.** Percentage inhibition by 1 μM nicardipine measured over a range of potentials from -30 to +40 mV. Holding potential was -80 mV (n=8). **b.** Time constant of activation for currents evoked at potentials from -20 to +30 mV either in the absence, or presence of 1 μM nicardipine (n=8). **c.** Effect of the DHP agonist *s*-(-)-BayK8644 on Ca^{2+} channel currents in COS-7 cells. Example currents recorded in a single cell before and during application of *s*-(-)-BayK8644 were evoked at a potential of 0 mV. (Potentials given are uncorrected for liquid junction potential, which was -15 mV).

Discussion

Species differences between α_{1E} clones and differences in expression systems together with the coexpression of different accessory subunits from one study to another have complicated the interpretation of data from studies designed to identify a possible neuronal correlate of the α_{1E} channel. Experimental conditions also vary between studies. Voltage-dependent properties of membrane conductances are altered significantly by screening of surface charges, particularly by divalent cations, as shown earlier for currents in cerebellar granule neurones. It is important to bear this in mind when making comparisons. Some groups suggest a correlation to the HVA R-type current (Randall and Tsien, 1995; Zhang *et al.*, 1993), whilst others identify it as a LVA T-type Ca^{2+} current (Soong *et al.*, 1993). One possible explanation for differing results between studies is the interference of endogenous Ca^{2+} channel subunits. When a rat brain α_{1E} channel was coexpressed in *Xenopus* oocytes with the β_{1b} subunit no increase in peak current was observed (Soong *et al.*, 1993). However, in COS-7 cells the combination of α_{1E}/β_{1b} resulted in a nine-fold increase in current density (Stephens *et al.*, 1997). One possible explanation of these findings is that the oocyte expresses an endogenous β subunit which is assembled with the injected α_1 subunit, masking any increase in current density. (Roux *et al.*, 1996). In support of this line of reasoning a β subunit has been cloned from *Xenopus* oocytes resembling the type 3 β subunit. It appears obvious that the choice of expression system is important in avoiding ambiguous results and that COS-7 cells are particularly suitable to this task. COS-7 cells have no endogenous Ca^{2+} channel subunits unlike other mammalian expression systems such as CHO cells (Skryma *et al.*, 1994) and HEK293 cells (Berjukow *et al.* 1996) which do have endogenous Ca^{2+} currents, and *Xenopus* oocytes which have endogenous Ca^{2+} channel α_1 subunits (Bourinet *et al.*, 1992), and endogenous β subunits (Roux *et al.*, 1996).

Stephens *et al.* (1997) showed that the voltage-dependent inactivation properties of these channels in COS-7 cells lay between those given for LVA and HVA Ca^{2+} channels ($V_{50(inact)}$ was shown to be -59 (-74) mV). The activation and inactivation kinetics and voltage-dependence of activation of α_{1E} channels shown here also

indicate characteristics that fit between traditional LVA and HVA channels. Reports of T-type Ca^{2+} channels in neuronal tissues show a more negative voltage-dependence of activation (-20 mV to -60 mV) and inactivation (-50 mV to -95 mV) (reviewed in Huguenard 1996), however it is possible that α_{1E} represents a channel with properties at the depolarised extreme of these ranges. Another feature of LVA channels that distinguishes them from HVA channels is the relative permeabilities of the channels to Ba^{2+} and Ca^{2+}. LVA channels are found to be equally permeable to Ca^{2+} and Ba^{2+} (Huguenard 1996) whereas HVA channels are more permeable to Ba^{2+} (see Fig 3.4, this study). Current densities in COS-7 cells expressing $\alpha_{1E}/\alpha_2\delta/\beta_{1b}$ were not significantly different when recording in either 2 mM Ca^{2+} or 10 mM Ba^{2+} (Stephens *et al.*, 1997). Oocyte studies also showed a similar relative permeation by Ba^{2+} and Ca^{2+} of rat brain α_{1E} channels (Bourinet *et al.*, 1994) and human α_{1E} channels (Schneider *et al.*, 1994). Conversely, the α_{1E} clone could represent a HVA channel at the hyperpolarised extreme of voltage-dependent properties for this class of channel. The R-type current proposed as a component of whole-cell Ca^{2+} channel currents in cerebellar granule neurones (Randall and Tsien, 1995) has some similar biophysical characteristics to α_{1E} currents including rapid inactivation, activation threshold, and steady-state inactivation. In addition single channel studies in granule cells identified a 15 pS Ca^{2+} current termed G2 which shared some of these properties (Forti *et al.*, 1994). Single channels recorded in oocytes expressing α_{1E} were calculated to have a 14 pS conductance (Schneider *et al.*, 1994), far greater than conductance values given for T-type channels which range from 5-9 pS (Huguenard, 1996).

With regards to the pharmacology of α_{1E} Ca^{2+} channels the literature remains equivocal. No specific antagonists are available and some reports give conflicting results, but differences in the species from which the clone was taken may account for some of the discrepancies. There seems to be agreement concerning the effects of inorganic Ca^{2+} channel blockers. Ni^{2+} has been repeatedly shown to block α_{1E} currents expressed in oocytes (Soong *et al.*, 1993; Wakamori *et al.*, 1994; Schneider *et al.*, 1994) and HEK293 cells (Williams *et al*, 1994) with an EC_{50} in the low micromolar range. Cd^{2+} also potently blocks these currents in all studies

with a submicromolar EC_{50} (Williams *et al*, 1994; Soong *et al.*, 1993; Wakamori *et al.*, 1994). A similar sensitivity to both Ni^{2+} and Cd^{2+} is sometimes reported for LVA channels although findings vary widely but is not seen for HVA channels with the exception of the R-type current which was found to be sensitive to Ni^{2+} at similar concentrations to those effective in inhibiting LVA channels (Randall and Tsien, 1995). R-type currents were very sensitive to Cd^{2+} like all other HVA channels (Randall and Tsien, 1995).

Reports of block by peptide toxins are less unanimous. Some studies have shown an effect of ω-Aga IVA on human or rat α_{1E} currents at concentrations reported to block P- and Q-type currents (Williams *et al*, 1994; Soong *et al.*, 1993), whereas others have seen no effect (Wakamori *et al.*, 1994; Schneider *et al.*, 1994). Williams *et al.* (1994) also report slight inhibition by ω-CgTx GVIA and ω-CTx MVIIC whist other studies have not been able to produce block with ω-CgTx GVIA (Soong *et al.*, 1993; Wakamori *et al.*, 1994; Schneider *et al.*, 1994). Interestingly the doe-1 Ca^{2+} channel from *Discopyge ommata* which could be described as α_{1E}-like was sensitive to ω-CgTx GVIA and in contrast to α_{1B}/N-type channels where block is rapid and irreversible block of doe-1 developed slowly and was slowly but completely reversible (Ellinor *et al.*, 1993).

In studies using COS-7 cells the neurotoxin ω-Aga IVA caused inhibition of rat α_{1E} currents with a K_D of 51 nM (Stephens *et al.* 1997). However, the block was incomplete, reaching 80% at 1 μM. The affinity of ω-Aga IVA for α_{1E} channels in this study is far lower than reports of block by ω-Aga IVA on P-type currents in central neurones where it ranged from 1-3 nM (Mintz and Bean, 1993a; Pearson *et al.*, 1995; Randall and Tsien, 1995) and is closer to the reported affinity of ω-Aga IVA on the current component termed Q-type in cerebellar granule neurones (Randall and Tsien, 1995). The Q-type current was characterised in granule neurones as an inactivating current blocked by high concentrations of ω-Aga IVA and also by ω-CTx MVIIC. The inactivation properties of α_{1E} show similarities to Q-type currents but α_{1E} currents are not sensitive to ω-CTx MVIIC (Stephens *et al.*, 1997; Wakamori *et al.*, 1994; Schneider *et al.*, 1994). Interestingly, a T-type current in the DRG cell line ND7-23 was inhibited by ω-Aga IVA (Pearson *et al.*, 1995).

Experiments using L-type Ca^{2+} channel blockers are also equivocal. Methoxyverapamil and diltiazem have been shown to inhibit human α_{1E} currents at high concentrations (Schneider *et al.*, 1994), but the DHP antagonists nifedipine and (+)PN200-110 produced no effect in the rat and rabbit clones (Soong *et al.*, 1993; Wakamori *et al.*, 1994). The DHP agonist BayK8644 has also been shown to cause no potentiation of these currents by rat, rabbit or human clones (Soong *et al.*, 1993; Wakamori *et al.*, 1994; Schneider *et al.*, 1994), but one group report a small inhibition expressing the human clone (Williams *et al*, 1994).

Antagonists of T-type currents are often found to be rather non-specific. For example amiloride has relatively specific blocking actions on the T-currents in neuroblastoma cells (Tang *et al.*, 1988), but centrally at higher concentrations it has been shown to reduce components of HVA currents (Takahashi and Akaike, 1991). Octanol has been found to be a specific antagonist of T-currents in rat sensory neurones without reducing HVA currents (Sinton *et al.*, 1989) but in the hippocampus higher concentrations reduced all components of the Ca^{2+} current (Takahashi *et al.*, 1991). In experiments with α_{1E} expressed in *Xenopus* oocytes Soong *et al.* (1993) could produce no inhibition of current using octanol, but amiloride at high concentrations (1 mM) reduced currents to a small extent. Schneider *et al.* (1994) was also able to block α_{1E} channels using amiloride at similarly high concentrations producing 60% inhibition. These data go some way towards showing a link between LVA T-type channels and the α_{1E} clone, but at the concentrations used here non-specific effects of T-type Ca^{2+} channel antagonists have been demonstrated.

Previous studies have demonstrated a lack of sensitivity to nifedipine (Soong *et al.*, 1993; Wakamori *et al.*, 1994) and have used the lack of sensitivity to the agonist BayK8644 as indicative of DHP insensitivity (Williams *et al.*, 1994). *s*-(-) BayK8644 had no effect on α_{1E} currents in COS-7 cells but Fig 6.2 shows that α_{1E} currents are substantially blocked by the DHP antagonist nicardipine. There is an increasing body of evidence that suggests certain LVA channels are inhibited by DHP antagonists but not enhanced by agonists such as BayK8644. LVA channels found in cultured smooth muscle cells from rat aorta have been shown to be inhibited by nicardipine (Neveu *et al.*, 1993) and in other tissues LVA currents are

inhibited by other DHP compounds (Akaike *et al.*, 1989; Kuga *et al.*, 1990; McCarthy and Cohen 1989). Embryonic DRG neurones from the mouse have T-currents that are inhibited by DHPs (Richard *et al.*, 1991). More recently an endogenous LVA current characterised in HEK293 cells has been suggested to correspond to the α_{1E} clone on the basis of its biophysical properties and was shown to be sensitive to isradipine and nimodipine but insensitive to BayK8644. Antagonists reduced T-currents in rat basal forebrain with potencies in the order nicardipine>nimodipine=nitrendipine>nifedipine with nicardipine being more than 100 times more potent than nifedipine (Allen *et al.*, 1993). It is possible that this order of potency translates to other systems studied and is the reason why effects have not been seen using nifedipine but have with nicardipine.

The pharmacological features of some T-type channels are remarkably similar to the findings of α_{1E} expressed in COS-7 cells and other studies already discussed. The biophysical properties overlap to some extent with LVA channels but also with the HVA R-type current. The R-type current however was isolated after the application of 200 nM ω-Aga IVA, and 10 μM nimodipine. The results here show that under these conditions a substantial part of the current carried by α_{1E} channels would be blocked, therefore the R-type current cannot be a direct correlate of the α_{1E} Ca^{2+} channel clone. In cerebellar granule cells the residual current inactivated faster than α_{1E} currents and inactivated faster when Ca^{2+} was used as a charge carrier in place of Ba^{2+} (Randall and Tsien, 1995). The opposite is true for the α_{1E} current (Stephens *et al.*, 1997).

It is possible that the α_{1E} channel is a subtype of T-type current as suggested previously (Soong *et al.*, 1993). The differences in inactivation properties may in fact be a result of the β subunit it is expressed with. On the other hand α_{1E} may encode a novel slowly inactivating T-type current. The rat thalamic reticular nucleus, an area showing immunostaining for α_{1E} has been found to express a relatively slowly inactivating T-type current (Huguenard and Prince, 1992).

The results here provide evidence that the α_{1E} Ca^{2+} channel clone represents a novel Ca^{2+} channel with some LVA-like pharmacological properties and some

properties, such as voltage-dependence and kinetics that fall in the middle of the existing classification separating LVA from HVA channels.

The susceptibility of α_{1E} currents to nicardipine make this channel a possible contender for a component of the large DHP-sensitive current identified in cerebellar granule cells. The inactivation properties of currents in COS-7 cells were faster than any component of granule cells. However, currents in granule cells displayed unusually slow inactivation rates and no evidence of a current component inactivating with a time course similar to N-type channels in the literature in spite of pharmacological criteria showing these channels to be present. The nicardipine -sensitive current expressed in COS-7 cells displayed an activation threshold and peak whole-cell conductance at more negative potentials than nicardipine-sensitive currents in cerebellar granule neurones. α_{1E} currents activated at -30 (-45) mV and peaked at 0 (-15) mV, 15-20 mV more negative to 1 μM nicardipine-sensitive currents, which activated at -10 (-22) mV and peaked at +10 (-2) mV and 10 μM nicardipine-sensitive currents which activated at -20 (-32) mV and peaked at +20 (+8) mV (difference currents not shown). The voltage-dependent inactivation of currents in granule neurones by no means occurred over similar voltage ranges. $\alpha_{1E}/\beta_{1b}/\alpha_2\delta$ currents in COS-7 cells have been shown to half-inactivate at -59 (-74) mV, again 20 mV more negative to currents in granule cells ($V_{50(inact)}$=-38 (-50) mV).

Presuming currents studied in COS-7 cells are not partially blocked by nicardipine, the EC_{50} would be close to 1 μM, since this concentration produced 51% block. The EC_{50} calculated from block by nicardipine in granule neurones was 4.4 μM, demonstrating a less potent block of currents in cerebellar granule neurones. In addition DHP agonists produced large potentiations of current in granule neurones at 10 μM, but 1 μM *s*-(-)-BayK8644 had no effect on α_{1E} currents. In conclusion, currents recorded in COS-7 cells carried by α_{1E} channels, although being sensitive to nicardipine showed little similarity to nicardipine-sensitive currents in cerebellar granule neurones in terms of their kinetics, voltage-dependent properties, and sensitivity to DHP agonist.

Chapter 7

Measurements of intracellular free Mg^{2+} and the effect of this ion on Ca^{2+} channel currents and their pharmacology in rat cerebellar granule neurones

Results

The effects of changing the intracellular free concentration of Mg^{2+} on Ca^{2+} channel currents was assessed in cerebellar granule neurones by manipulating the free Mg^{2+} contained within the whole-cell patch pipette. Solutions containing intracellular free Mg^{2+} of 0.1 and 0.5 mM were compared, in addition to a more limited group of cells recorded with 1.0 mM free Mg^{2+} in the pipette. The concentration of Mg^{2+}-bound ATP was 2 mM in each group.

Characteristics of currents recorded with 0.1, 0.5 or 1.0 mM $[Mg^{2+}]_i$

Fig. 7.1a shows the effects of altering $[Mg^{2+}]_i$ on the Ca^{2+} channel current. Mean current-voltage relationships are shown for all cells recorded. The peak amplitude of currents decreased as $[Mg^{2+}]_i$ increased and the peak of the current-voltage relationship was shifted to a less positive potential in the higher $[Mg^{2+}]_i$ groups. To quantify these differences, current-voltage curves from individual cells were fitted with a Boltzmann equation (*Equation 1*) and the parameter values describing the curves were averaged for each group. The results are summarised in Table 7.1a. Maximum cell conductance in the 1.0 mM $[Mg^{2+}]_i$ group was reduced to less than half of the conductance measured in 0.1 mM $[Mg^{2+}]_i$. A significant change in $V_{50(act)}$ was not seen between the 0.1 and 0.5 mM $[Mg^{2+}]_i$ groups, however raising $[Mg^{2+}]_i$ to 1.0 mM caused a -10 mV shift in the $V_{50(act)}$. With increasing $[Mg^{2+}]_i$ a small but consistent reduction in E_{null} was observed. Over the range of concentrations used E_{null} was shifted by approximately 10 mV. No statistically significant changes in the slope factor for activation of Ca^{2+} channel currents was observed.

The rate of inactivation over 100 ms is illustrated in Fig. 7.1b which shows averaged currents recorded at +10 (-2) mV from each group of data. The decay of the averaged currents during the course of the depolarising voltage-step was not sufficient to enable fitting of an exponential, and over this time-course no inactivation was apparent in either of the three groups of data. No observable difference in the activation kinetics or time to peak of the currents recorded under these conditions was evident.

	0.1 mM $[Mg^{2+}]_i$	0.5 mM $[Mg^{2+}]_i$	1.0 mM $[Mg^{2+}]_i$
a.			
g (nS)	4.6±0.2	3.7±0.1 ***	2.0±0.3 ***
E_{null} (mV)	59±0.7	54±0.7 ***	51±3 *
$V_{50\ (act)}$ (mV)	-0.3±0.7	-2±0.6 *	-12±2 ***
k (mV)	8±0.2	7±0.2	6±0.5
n	310	120	5
b.			
% inactivation	91±1	79±1 ***	
$V_{50\ (inact)}$ (mV)	-41±0.3	-33±2	
s (mV)	13±1	11±1 *	
n	3	4	

Table 7.1 Summary of parameter values describing the current-voltage relationships in cells with 0.1, 0.5, or 1.0 mM $[Mg^{2+}]_i$ (**a.**), and steady-state inactivation in cells with 0.1 or 0.5 mM $[Mg^{2+}]_i$ (**b.**). Statistical significance is shown for comparison of the average data between 0.1 and 0.5 mM $[Mg^{2+}]_i$, and 0.5 and 1.0 mM $[Mg^{2+}]_i$, and was calculated using unpaired *t-tests*. Significance is shown where appropriate by asterisks (*p<0.05; **p<0.01; ***p<0.005). (Potentials given are uncorrected for liquid junction potential, which was -15 mV.)

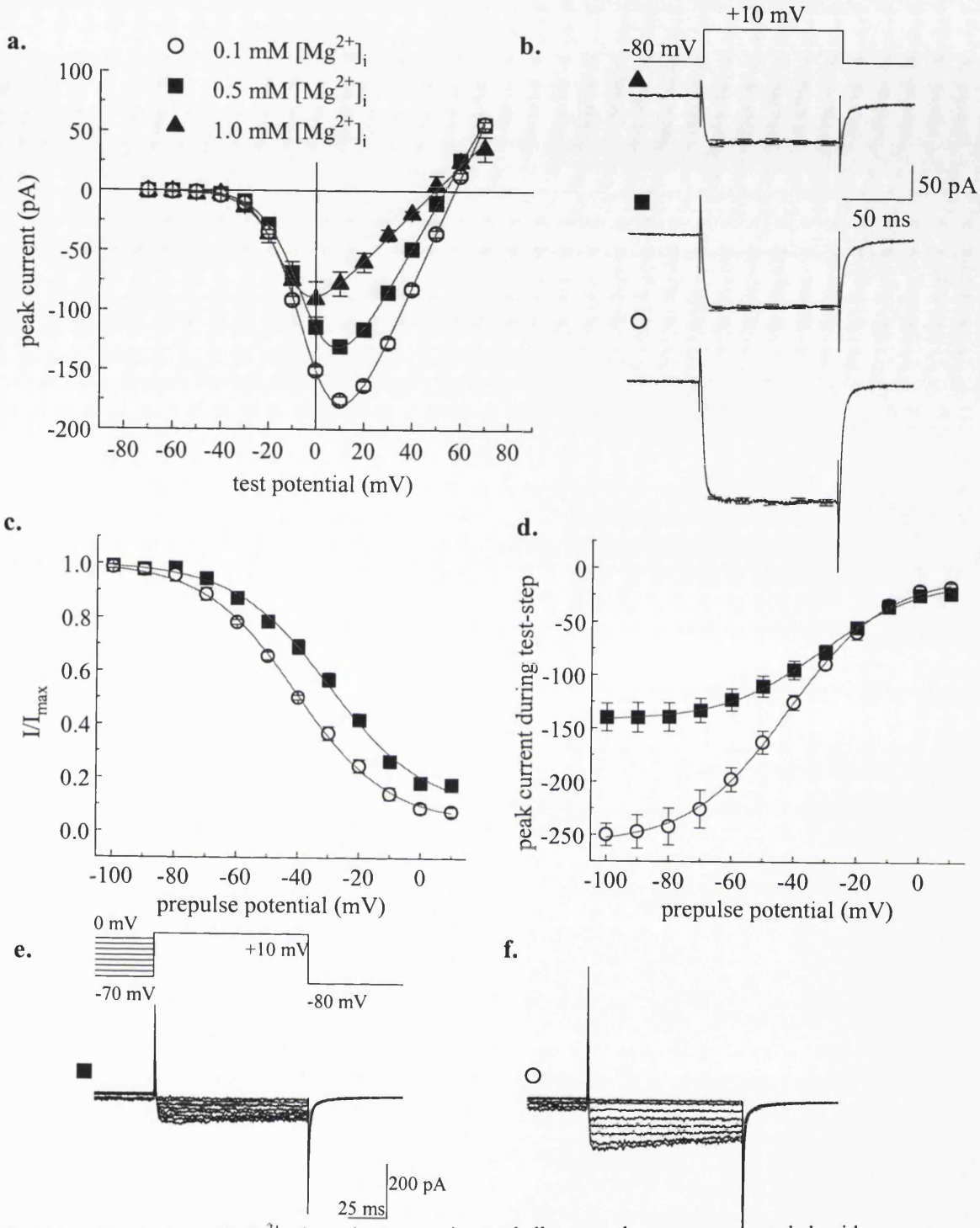

Fig. 7.1 Comparison of Ca^{2+} channel currents in cerebellar granule neurones recorded with different $[Mg^{2+}]_i$. **a.** Average current-voltage relationships for currents recorded in the presence of 0.1, 0.5 or 1.0 mM $[Mg^{2+}]_i$. The number of cells averaged for each condition were 310, 120 and 5 respectively. **b.** Averaged currents evoked at +10 mV for cells under each of the conditions in **a.** Currents were averaged from groups of 50, 50 and 10 cells respectively. Error bars showing the s.e.m. are shown at various time points. **c.** Steady-state inactivation of Ca^{2+} channel currents in cells containing 0.1 or 0.5 mM $[Mg^{2+}]_i$. The averaged data was fit with a Boltzmann equation (*Equation 5*, Chapter 2) after currents evoked following each conditioning step were normalised. **d.** Data are the same as cells in **c.** averaged without normalisation. **e.** and **f.** Example families of currents from individual cells showing steady-state inactivation. The currents shown were activated for 100 ms to +10 mV from conditioning potentials of 10 s duration between -70 and 0 mV. The symbols shown in **a.** are the same throughout. (Potentials given are uncorrected for liquid junction potential, which was -12 mV)

The decay of tail currents under each condition was also examined. Increases in $[Mg^{2+}]_i$ caused a slight slowing in the speed of deactivation. To quantify any changes, tail current deactivation was described by a second order exponential (see Methods). For groups of 10 cells, the fast and slow time constants of deactivation and their relative proportions were: 1.7±0.2 ms and 7.5±0.6 ms 68:32, 0.1 mM $[Mg^{2+}]_i$; 1.3±0.3 ms and 8.4±0.5 ms 66:34, 0.5 mM $[Mg^{2+}]_i$; and 1.9±0.5 ms and 10.3±1 ms 80:20, 1.0 mM $[Mg^{2+}]_i$.

To test for possible Mg^{2+}-induced shifts in steady-state inactivation of Ca^{2+} channel currents the voltage-dependence of steady-state inactivation was measured using a 10 s conditioning step. Steady-state inactivation was compared between cells recorded in 0.1 and 0.5 mM $[Mg^{2+}]_i$. Less Ca^{2+} channels were available as $[Mg^{2+}]_i$ was increased, i.e. the current was reduced, and a shift in the voltage-dependence of inactivation of the remaining channels occurred. Fig. 7.1c shows the obtained data fit by a single Boltzmann function in each case. The average parameter values from fits to individual curves are summarised in Table 7.1b. The voltage for half inactivation in 0.1 mM $[Mg^{2+}]_i$ was shifted nearly -10 mV relative to 0.5 mM $[Mg^{2+}]_i$. This change was found to be statistically significant (p=0.013, unpaired *t-test*). The only other difference to note was that in these cells inactivation was greater in 0.1 mM $[Mg^{2+}]_i$. In 0.1 mM $[Mg^{2+}]_i$ average percentage inactivation was 91±1%. In 0.5 mM $[Mg^{2+}]_i$ only 79±9% of the current was inactivated, an extremely significant reduction (p=0.0002; unpaired *t-test*). The reason for this change could be seen when averaged non-normalised currents were compared against each other. The proportion of non-inactivating current remaining in both 0.1 and 0.5 mM $[Mg^{2+}]_i$ was similar in amplitude (approximately 20 pA). Thus, increasing $[Mg^{2+}]_i$ has no effect on the population of channels that carry this non-inactivating current component, and it constitutes a greater proportion of current in cells where the $[Mg^{2+}]_i$ is increased. Examples of currents during the test-step in individual cells recorded in either 0.1 or 0.5 mM $[Mg^{2+}]_i$ are shown for comparison (Fig. 7.1d).

Effects of $[Mg^{2+}]_i$ on ω-CgTx GVIA-sensitive components of the Ca^{2+} channel current

To establish whether the reduction in current amplitude brought about by increasing $[Mg^{2+}]_i$ was caused by a selective loss of a particular subtype of Ca^{2+} channel current the pharmacology was compared between cells in the presence of 0.1 mM $[Mg^{2+}]_i$ and 0.5 mM $[Mg^{2+}]_i$.

In Fig. 7.2 the effect of ω-CgTx GVIA is shown. A difference in the extent of inhibition was observed between 0.1 and 0.5 mM $[Mg^{2+}]_i$. In the presence of the higher $[Mg^{2+}]_i$ 1 μM ω-CgTx GVIA produced less inhibition. Fig. 7.2a and b compare the average current-voltage data from cells under these two conditions. No significant differences were measured in $V_{50(act)}$, E_{null}, or k in each group. Conductance decreased due to ω-CgTx GVIA block from 3.4±4 to 1.9±0.3 nS in 0.1 mM $[Mg^{2+}]_i$ (p=0.0001, paired *t-test*, n=9) and from 2.2±0.3 to 1.5±0.2 nS in 0.5 mM $[Mg^{2+}]_i$ (p=0.038, paired *t-test*, n=5). To determine whether this trend continued if the $[Mg^{2+}]_i$ was further increased ω-CgTx GVIA was applied to cells with 1.0 mM $[Mg^{2+}]_i$ (Fig. 7.2c). The group of cells in Fig. 7.2c were from a different culture of cells to those of 6.2a and b which showed unusually small currents in comparison. The extent of inhibition was further reduced in this group of cells. Whole-cell conductance decreased from 2.0±0.3 to 1.5±0.2 nS (p=0.017, paired *t-test*, n=5). The average inhibition resulting from all cells exposed to 1 μM ω-CgTx GVIA is summarised as a bar chart in Fig. 7.2d. Peak currents averaged from all experiments in each condition decreased by 34±3% in 0.1 mM $[Mg^{2+}]_i$ (n=18), to 28±3% in 0.5 mM $[Mg^{2+}]_i$ (not significantly different, p=0.16, unpaired *t-test*) to 19±3% in 1.0 mM $[Mg^{2+}]_i$ (p=0.0066, unpaired *t-test*).

The effect of ω-Aga IVA and ω-CTx MVIIC was not affected by $[Mg^{2+}]_i$

Inhibition by ω-CTx MVIIC and ω-Aga IVA between cells with 0.1 and 0.5 mM $[Mg^{2+}]_i$ was not significantly different. Fig. 7.3 demonstrates block by these two toxins. 5 μM ω-CTx MVIIC produced a 30±3% reduction in Ca^{2+} channel currents recorded with 0.1 mM $[Mg^{2+}]_i$ whereas with 0.5 mM $[Mg^{2+}]_i$ in the patch pipette a 25±4% decrease was seen (Fig. 7.3 a and b). The ω-CTx MVIIC-sensitive current component was smaller in the latter group, in line with there being a smaller ω-

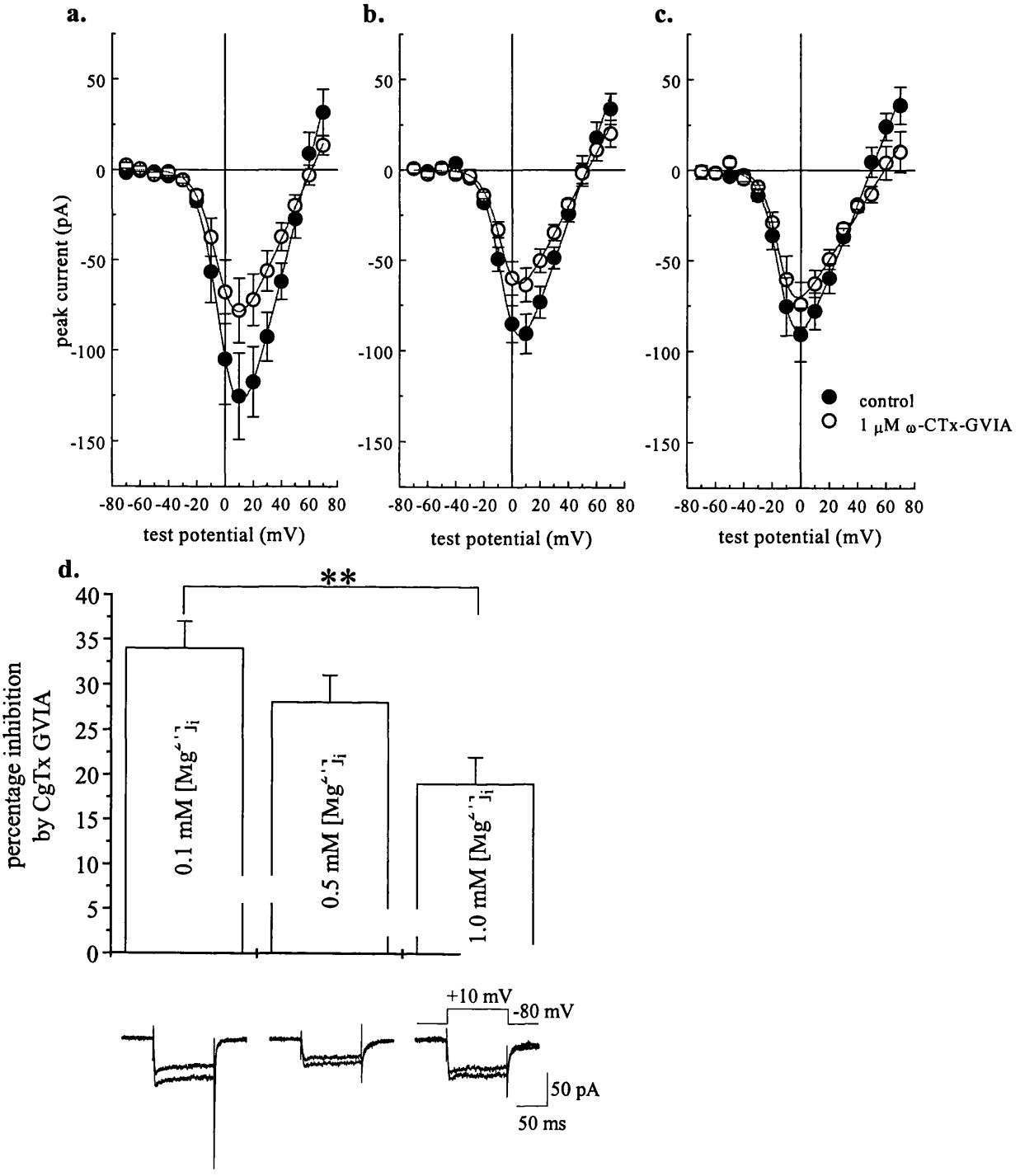

Fig. 7.2 Effect of increasing $[Mg^{2+}]_i$ on the inhibition of Ca^{2+} channel currents by ω-CgTx GVIA in cerebellar granule neurones. **a.-c.** Current-voltage relationships showing inhibition by 1 μM ω-CgTx GVIA on cells with 0.1 mM (**a.**, *n*=9), 0.5 mM (**b.**, *n*=5), and 1.0 mM $[Mg^{2+}]_i$ (**c.**, *n*=5). The symbols representing control and treated groups are the same in each figure. **d.** Comparison of the average inhibition by ω-CgTx GVIA in cells with different $[Mg^{2+}]_i$. The number of cells in each group were 18, 10, and 5 at 0.1, 0.5 and 1.0 mM $[Mg^{2+}]_i$ respectively. The asterisks denote a very significant difference in inhibition in cells of the 1.0 mM $[Mg^{2+}]_i$ group (p=0.0066, unpaired *t-test*). Example currents showing inhibition in each of the three conditions are shown beneath their respective column. The currents were evoked at +10 mV for 100 ms. (Potentials given are uncorrected for liquid junction potential, which was -12 mV)

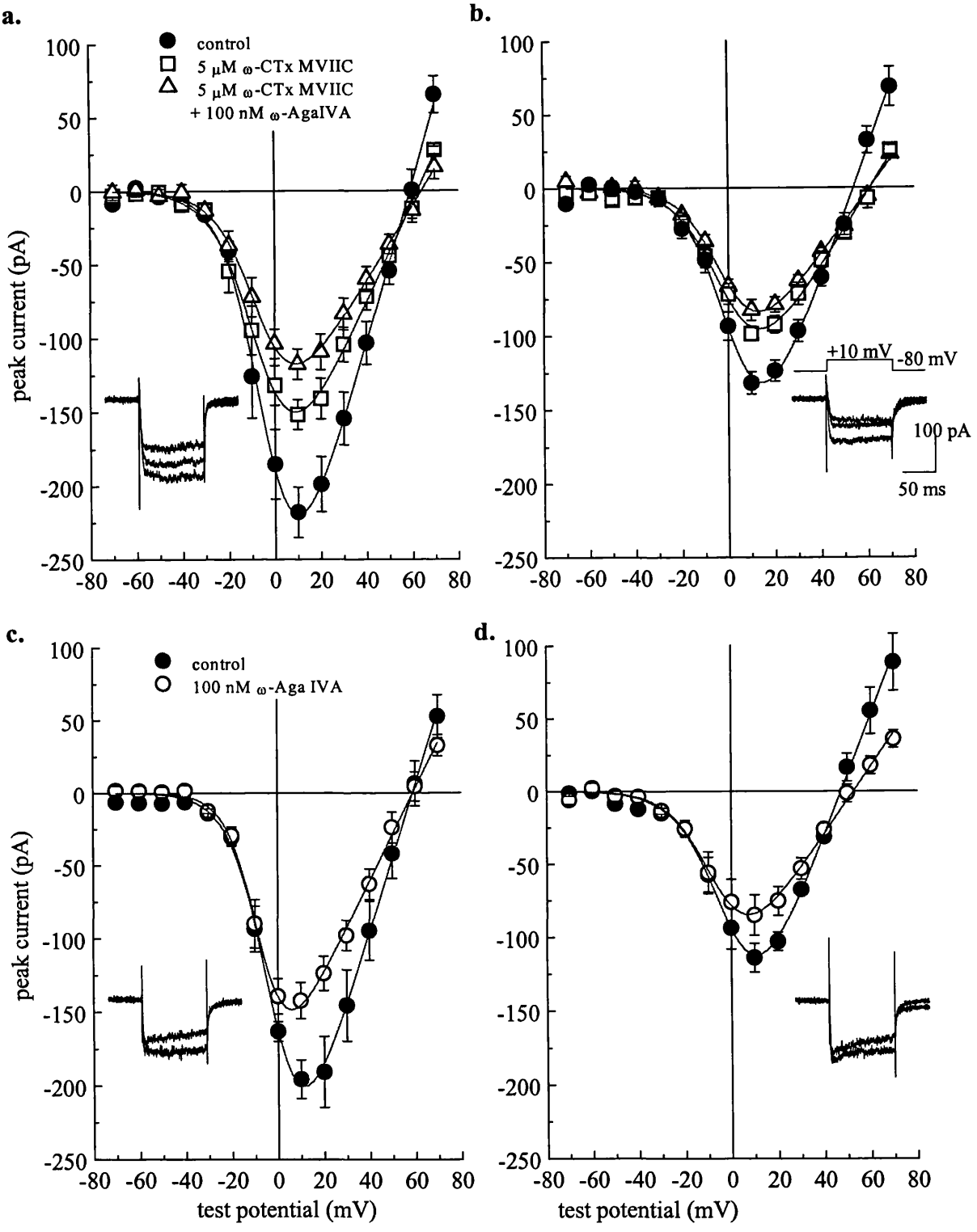

Fig. 7.3 Comparison of the effect of the toxins ω-CTx MVIIC and ω-Aga IVA on Ca^{2+} channel currents on cells with 0.1 and 0.5 mM $[Mg^{2+}]_i$. **a.** and **b.** show the cumulative application of 5 μM ω-CTx MVIIC and 100 nM ω-Aga IVA on current-voltage relationships in cells with 0.1 (**a.**, n=8) and 0.5 mM $[Mg^{2+}]_i$ (**b.**, n=8). The insets show example recordings made in the absence of toxins, in the presence of 5 μM ω-CTx MVIIC and in the presence of 5 μM ω-CTx MVIIC and 100 nM ω-Aga IVA. The scale and voltage-step shown in the inset in **b.** applies to all examples. **c.** and **d.** Average current-voltage relationships illustrating the inhibition by 100 nM ω-Aga IVA in 0.1 mM $[Mg^{2+}]_i$ (**c.**, n=5) and 0.5 mM $[Mg^{2+}]_i$ (**d.**, n=6). Insets show currents recorded in the absence and presence of ω-Aga IVA. (Potentials given are uncorrected for liquid junction potential, which was -12 mV)

CgTx GVIA-sensitive component but the difference between groups was not statistically significant. (p=0.28, unpaired *t-test*). Fig. 7.3c and d compares the effects of 100 nM ω-Aga IVA on the two groups of cells. In the presence of 0.1 mM $[Mg^{2+}]_i$ ω-Aga IVA produced 25±5% inhibition as shown previously (Fig. 4.2) and from current-voltage relationships a shift in the $V_{50(act)}$ of 5 mV in the hyperpolarising direction (Fig. 4.2c). In 0.5 mM $[Mg^{2+}]_i$ (Fig. 7.3d), ω-Aga IVA caused a 27±8% decrease in current amplitude at +10 (-2) mV. From current-voltage relationships the average $V_{50(act)}$ shifted from +1 (-11)±2 mV to -3 (-15)±3 mV, similar in magnitude and direction to the effect in cells with 0.1 mM $[Mg^{2+}]_i$ but outside the limits of statistical significance (p=0.2; paired *t-test*; n=6).

Following block by 5 μM ω-CTx MVIIC in the cells shown in Fig. 7.3a and b ω-Aga IVA was subsequently applied. The percentage block of Ca^{2+} channel current by ω-Aga IVA after application of ω-CTx MVIIC was 16±4% and 13±4% in 0.1 and 0.5 mM $[Mg^{2+}]_i$ respectively (not significantly different, p=0.62, unpaired *t-test*). No apparent difference was noticed in the ω-Aga IVA-sensitive component in cerebellar granule neurones at different $[Mg^{2+}]_i$.

$[Mg^{2+}]_i$ and DHP activity

The effect of dihydropyridine agonists and antagonists was tested in cells with 0.1 and 0.5 mM $[Mg^{2+}]_i$. Inhibition by 10 μM nicardipine is shown in Fig. 7.4a and b. The results showing the application of 10 μM nicardipine in cells with 0.1 mM $[Mg^{2+}]_i$ has already been discussed (see Fig. 5.3). When $[Mg^{2+}]_i$ was increased to 0.5 mM a similar degree of inhibition and change in the voltage-dependence of activation was seen. Average inhibition was 54±7% in cells with 0.5 mM $[Mg^{2+}]_i$ compared to 50±7% in cells with 0.1 mM $[Mg^{2+}]_i$. The shift in $V_{50(act)}$ of 7 mV seen to occur in cells with 0.1 mM $[Mg^{2+}]_i$ was also present in cells with 0.5 mM $[Mg^{2+}]_i$. In control cells average V_{50} was calculated to be +3 (-9)±4 mV and shifted significantly to -6 (-18)±2 mV after application of 10 μM nicardipine (p=0.014, paired *t-test*; n=8). From the current-voltage data the peak conductance decreased from 4.7±0.6 nS to 1.3±0.2 nS during application of nicardipine (p=0.003; paired *t-test*; n=8). Between the two groups no significant differences were noticed during exposure to nicardipine due to the concentration of free Mg^{2+}.

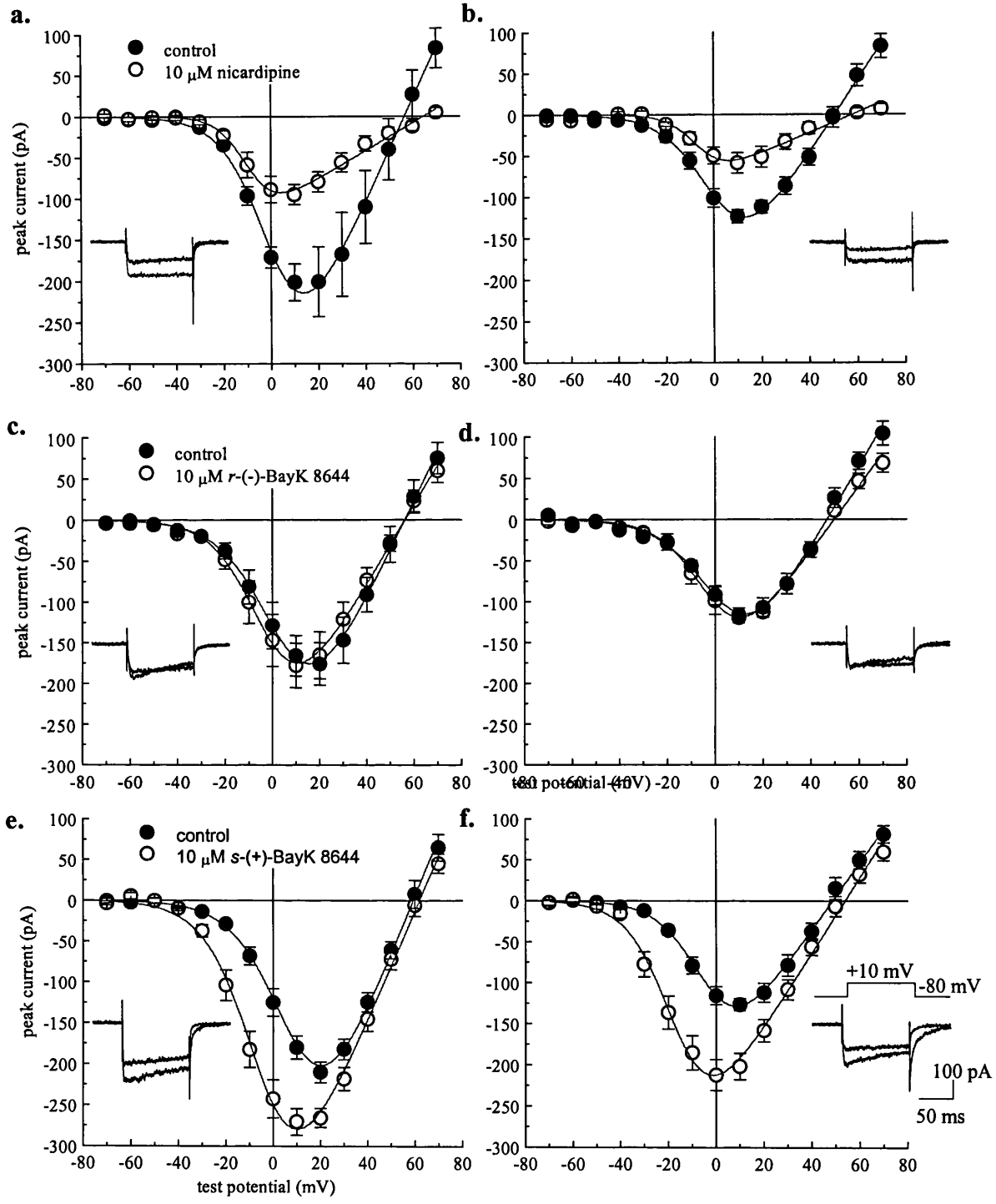

Fig. 7.4 Comparison of the effects of dihydropyridines on Ca^{2+} channel currents in cerebellar granule neurones in cells with 0.1 or 0.5 mM $[Mg^{2+}]_i$. **a.** and **b.** show current-voltage relationships in two groups of cells before and after application of 10 μM nicardipine. **a.** shows cells with 0.1 mM $[Mg^{2+}]_i$ (n=8) and **b.** shows cells with 0.5 mM $[Mg^{2+}]_i$ (n=8). The insets show example current recordings made before and during application of nicardipine. **c.** and **d.** show the effects of the application of 10 μM r-(+)-BayK8644 on cells in 0.1 mM $[Mg^{2+}]_i$ (n=4), and 0.5 mM $[Mg^{2+}]_i$ (n=5). **e.** and **f.** Current-voltage relationships and example currents showing the effect of 10 μM s-(-)-BayK8644 on cells with 0.1 mM $[Mg^{2+}]_i$ (n=7) and 0.5 mM $[Mg^{2+}]_i$ (n=8). The insets show currents evoked for 100 ms at +10 mV and the scale bar shown in **f.** applies to all figures. (Potentials given are uncorrected for liquid junction potential, which was -12 mV)

Fig. 7.4c and d compare the effects of application of 10 μM *r*-(+)-BayK8644 on cells with 0.1 or 0.5 mM $[Mg^{2+}]_i$. Similar to the effect of application of the *r*-(+)-isomer on cells with 0.1 mM $[Mg^{2+}]_i$ (Fig. 5.5a), no inhibition of current was seen at 0.5 mM Mg^{2+} (Fig. 7.4d). Also like the low $[Mg^{2+}]_i$ group a similar shift in $V_{50(act)}$ was noticed when current-voltage relationships were analysed. The average $V_{50(act)}$ was +3 (-9)±2 mV before and -1 (-13) mV during application of *r*-(+)-BayK8644. This shift was found to be significant (p=0.014; paired *t-test*; n=5).

With application of 10 μM *s*-(-)-BayK8644 a comparable increase in current was seen between cells with 0.1 and 0.5 mM $[Mg^{2+}]_i$ (Fig. 7.4e and f). The current-voltage relationship was shifted to the left to an equivalent degree in both cases. $V_{50(act)}$ shifted from +7 (-5)±2 to -4 (-16)±3 mV in 0.1 mM $[Mg^{2+}]_i$, and from -3 (-15)±2 to -15 (-27)±3 mV in 0.5 mM $[Mg^{2+}]_i$.(p=0.0008; paired *t-test*; n=7, and p<0.0001; paired *t-test*; n=8, respectively). Although comparison of the peak currents before and during application of *s*-(-) BayK8644 showed a significantly higher increase in currents recorded with 0.5 mM $[Mg^{2+}]_i$ in the patch pipette when increases were compared at each test-potential the average increase was very similar with no statistically significant difference between the two groups (Fig. 7.5a, circles).

Analysis of the tail currents showed some differences to note. On first inspection of the tail currents (Fig. 7.5b) it would appear that the increase in tail current amplitude caused by *s*-(-)-BayK8644 was greater in cells with 0.5 mM $[Mg^{2+}]_i$. However, the tail current amplitudes in control cells with 0.5 mM $[Mg^{2+}]_i$ were larger and the tail currents decayed slightly less rapidly than in control cells with 0.1 mM $[Mg^{2+}]_i$. The speed of deactivation was measured by fitting a biexponential function to the current tails generated by repolarisation from +10 (-2) mV to -80 (-92) mV. Recordings made in 0.1 mM $[Mg^{2+}]_i$ produced currents that decayed with time constants of 1.0±0.1 ms and 8±0.8 ms Addition of *s*-(-)-BayK8644 slowed both the time constants. In the presence of the agonist the decay was fit by constants of 2±0.4 ms and 18±3 ms. Average potentiation of the fast and slow components was 100±22% and 149±39% respectively (n=7). In experiments with 0.5 mM $[Mg^{2+}]_i$ control currents decayed with time constants of 1.5±0.3 ms and 13±3 ms. During the presence of *s*-(-)-BayK8644 the tails decayed

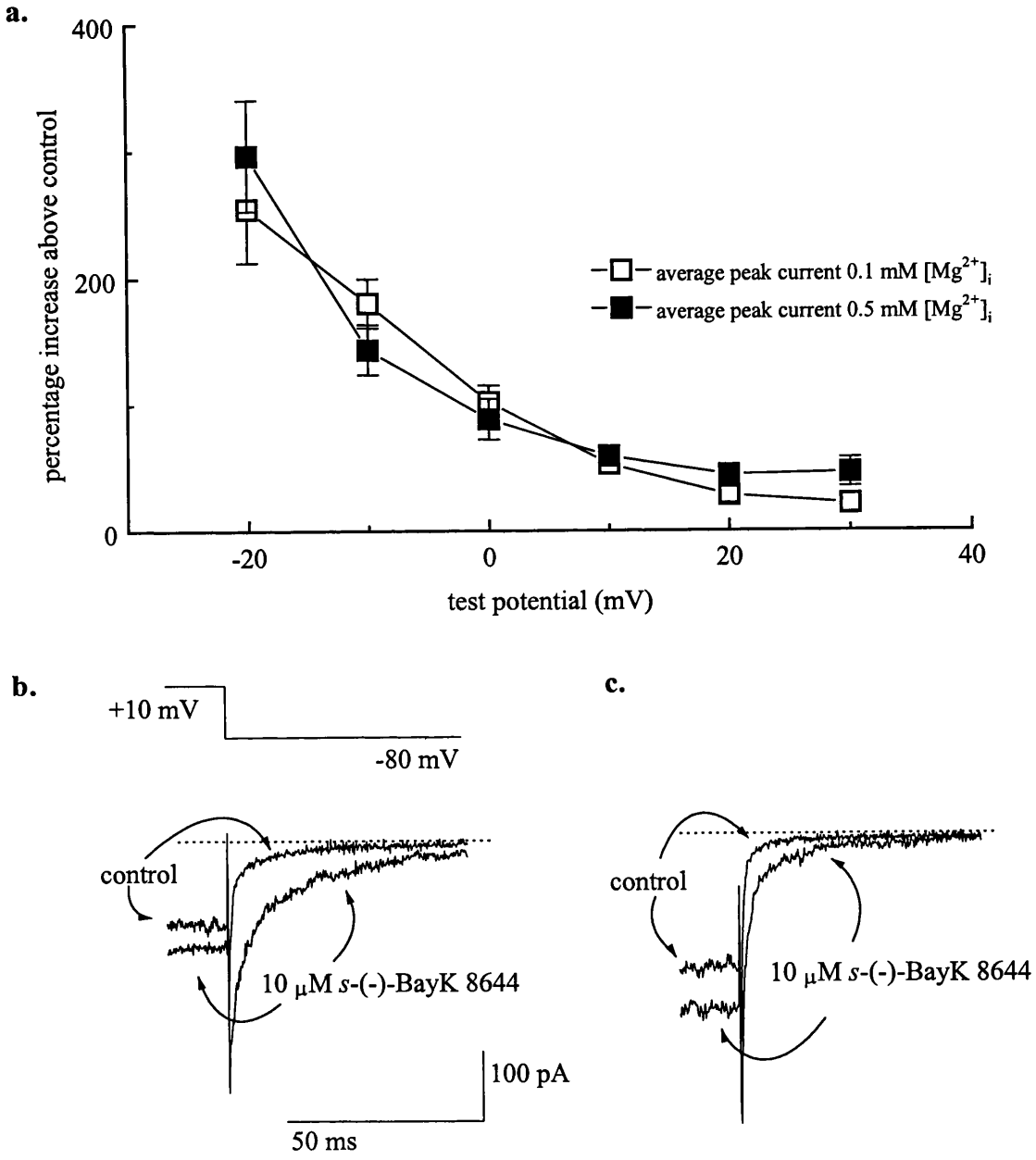

Fig. 7.5 Features of *s*-(-)-BayK8644 potentiated currents in cells with 0.1 and 0.5 mM $[Mg^{2+}]_i$ **a.** Graph comparing the average potentiation due to application of 10 μM *s*-(-)-BayK8644 on peak current from the range of potentials shown. Average values are shown for a group of 7 cells with 0.1 mM $[Mg^{2+}]_i$ (open symbols), and 8 cells with 0.5 mM $[Mg^{2+}]_i$ (filled symbols). **b.** and **c.** Examples of recordings showing the control and *s*-(-)-BayK8644 potentiated tail currents in individual cells with 0.5 and 0.1 mM $[Mg^{2+}]_i$ respectively. (Potentials given are uncorrected for liquid junction potential, which was -12 mV).

with time constants of 2.5±0.6 ms and 24±4 ms. Average increases in this group were 67±41% and 85±32% for the fast and slow time constants respectively.

Use of fluorescent probes to measure $[Mg^{2+}]_i$

The majority of studies investigating the mechanisms of Mg^{2+} homeostasis have involved erythrocytes (Gunther and Vormann, 1989) and cardiac myocytes (Murphy, E. *et al.*, 1991), and most studies of neuronal tissue have been limited to the squid giant axon (Baker and Crawford, 1972; De Weer, 1976; Brinley and Scarpa, 1975; Caldwell-Violoch and Requena, 1979). As previously discussed, many studies have demonstrated modulation by Mg^{2+} on ion channel activity and cellular enzymes but relatively little is known concerning the role of internal free Mg^{2+} in vertebrate neurones in comparison to other cations. These and other studies (Flatman, 1991; Murphy, E. *et al.*, 1991; Gunther, 1993) have determined that the majority of cells have a large buffering capacity for Mg^{2+} and that $[Mg^{2+}]_i$ does not generally vary under normal conditions. Estimates of resting $[Mg^{2+}]_i$ in mammalian cells have been in the range 0.5-1.0 mM (London, 1991; White and Hartzell, 1989; Romani and Scarpa, 1992) lower values than those first reported in the squid axon which were measured to be 3 mM (Brinley and Scarpa, 1975).

Since changes in $[Mg^{2+}]_i$ have the consequence of modulating Ca^{2+} channel currents in cerebellar granule neurones and possibly modulating currents carried by different Ca^{2+} channel subtypes over different concentration ranges the question of what the normal resting concentration of Mg^{2+} in these cells was addressed.

Recently several interesting studies have used peripheral cells to demonstrate that certain stimuli can induce moderate increases of $[Mg^{2+}]_i$ (Murphy *et al.*, 1989; Harman *et al.*, 1990; Ishijima *et al.*, 1991). In another study Brocard *et al.* (1993) have shown in rat forebrain neurones that applications of glutamate can produce large increases in $[Mg^{2+}]_i$ via activation of NMDA receptors. A glutamate-induced increase in $[Mg^{2+}]_i$ was investigated in cerebellar granule neurones.

Determination of the resting $[Mg^{2+}]_i$ in cerebellar granule neurones by fluorescence microscopy

Although loading of granule cells with Mag-FURA2 AM was very efficient, measurements of R_{min} and R_{max} were unsuccessful. Use of 10 μM 4Br-A23187 in combination with 0 or 20 mM Mg produced only small changes in the fluorescence ratio after 10-15 minutes equilibration. Resting $[Mg^{2+}]_i$ was

determined by comparing ratio values to a calibration curve constructed with Mg^{2+} concentrations between 0 and 10 mM (shown in Fig. 7.6) and was found to be 0.49±0.05 mM (n=14)

Magnesium imaging: stimulation of cerebellar granule neurones with glutamate

Stimulation with 100 μM glutamate plus 1 μM glycine to potentiate responses via NMDA receptors caused an increase in the ratio of fluorescence at the two wavelengths with two phases. Immediately upon addition of glutamate to the bath an linear increase in 340/380 ratio was observed. In approximately half of the cells examined, in addition to the gradual increase seen over the course of an experiment a rapid and transient spike was seen, followed by an elevated plateau. The transient spike occurred with a variable delay after challenge with glutamate, occurring 1-5 minutes after addition of drug. Fig. 7.7 shows fluorescence ratio for two cells, one showing a typical spiking cell (cell 1) and the other showing a linear increase (cell 2, fitted by a straight line).

In three separate experiments in which glutamate was applied to granule cells, ratios in a total of 72 cells were analysed. Of these, 43 showed responses similar to cell 1, the remaining 29 all demonstrated a small steady increase in $[Mg^{2+}]_i$ in the presence of glutamate. After removal of the drug and washing, ratio values returned to resting levels.

The mean ratio of resting fluorescence in 69 cells from three experiments was 0.33±0.004. After 300 s exposure to glutamate the average increased to 0.37±0.005. After washing, the ratio returned to 0.34±0.005. Fig. 7.8 shows a sequence of images from an experiment in which glutamate was applied to cells. The large asynchronous increase of $[Mg^{2+}]_i$ can be seen in approximately half of the cells with no apparent relationship to their spatial arrangement in the field.

To determine the mechanism of this increase experiments were conducted in which glutamate was applied to cells in the presence and absence of extracellular Ca^{2+}. Normal HBSS was modified by replacing $CaCl_2$ with 20 μM EGTA. The same group of cells was challenged with glutamate first in the presence of normal HBSS, secondly in the presence of 0 Ca-HBSS and a third time in normal HBSS. The initial 5 measurements before challenge with glutamate were averaged as a

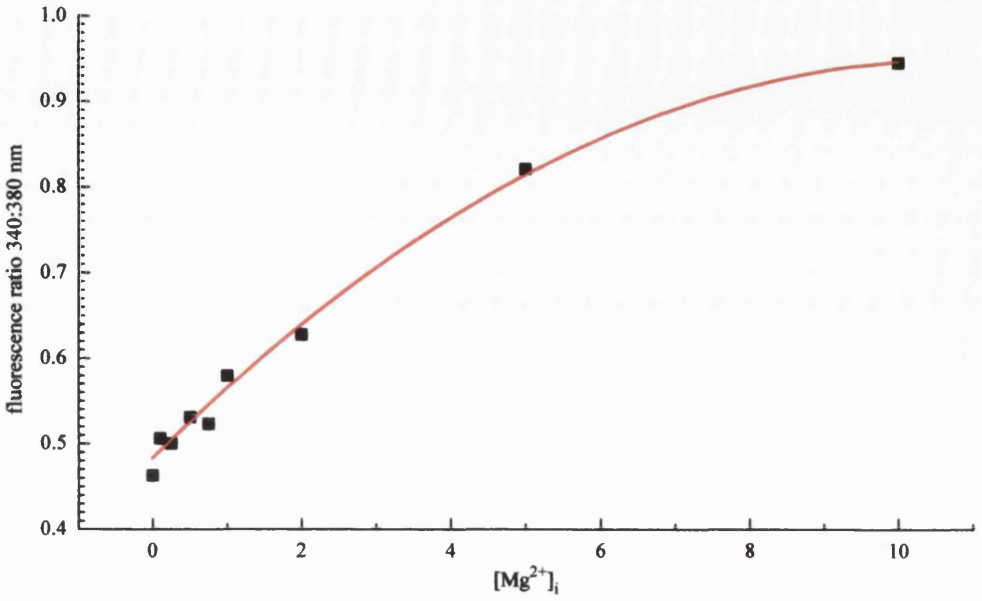

Fig. 7.6 Calibration curve showing background subtracted *in vitro* measurements of MagFURA2 fluorescence ratio (340:380 nm) in a mock intracellular solution containing 0 to 10 mM Mg.

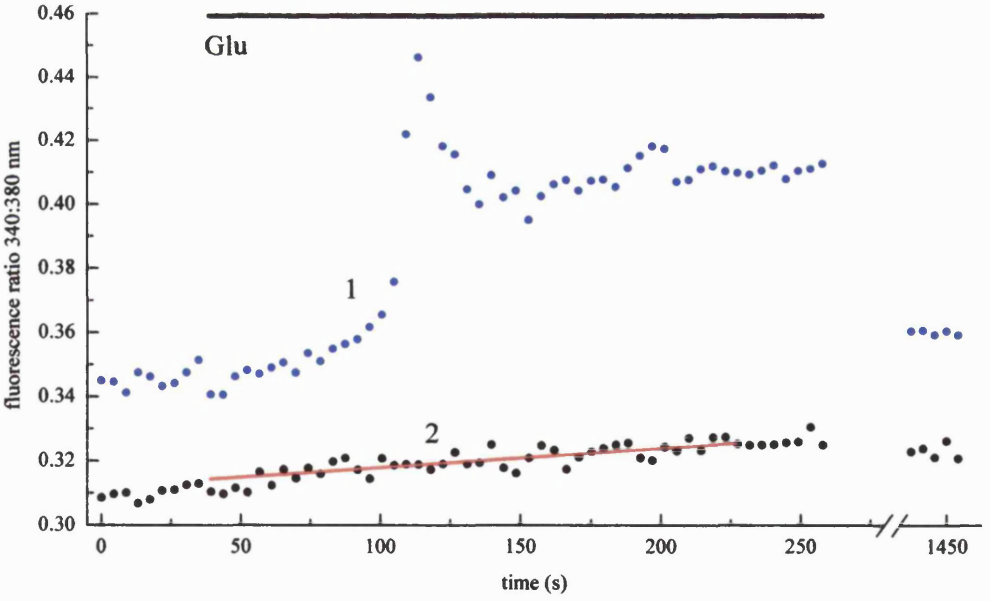

Fig. 7.7 Change in fluorescence ratio (340:380 nm) in granule cells loaded with MagFURA2 after challenge with 100 µM glutamate (+1 µM glycine; solid bar). Cells showing the two different responses (marked 1 and 2, refer to text). The responses in cell 2 have been fit by a straight line (red). The axis break represents a period of 20 minutes during which, glutamate was washed out of the chamber. Measurements after this recovery time are shown after the break.

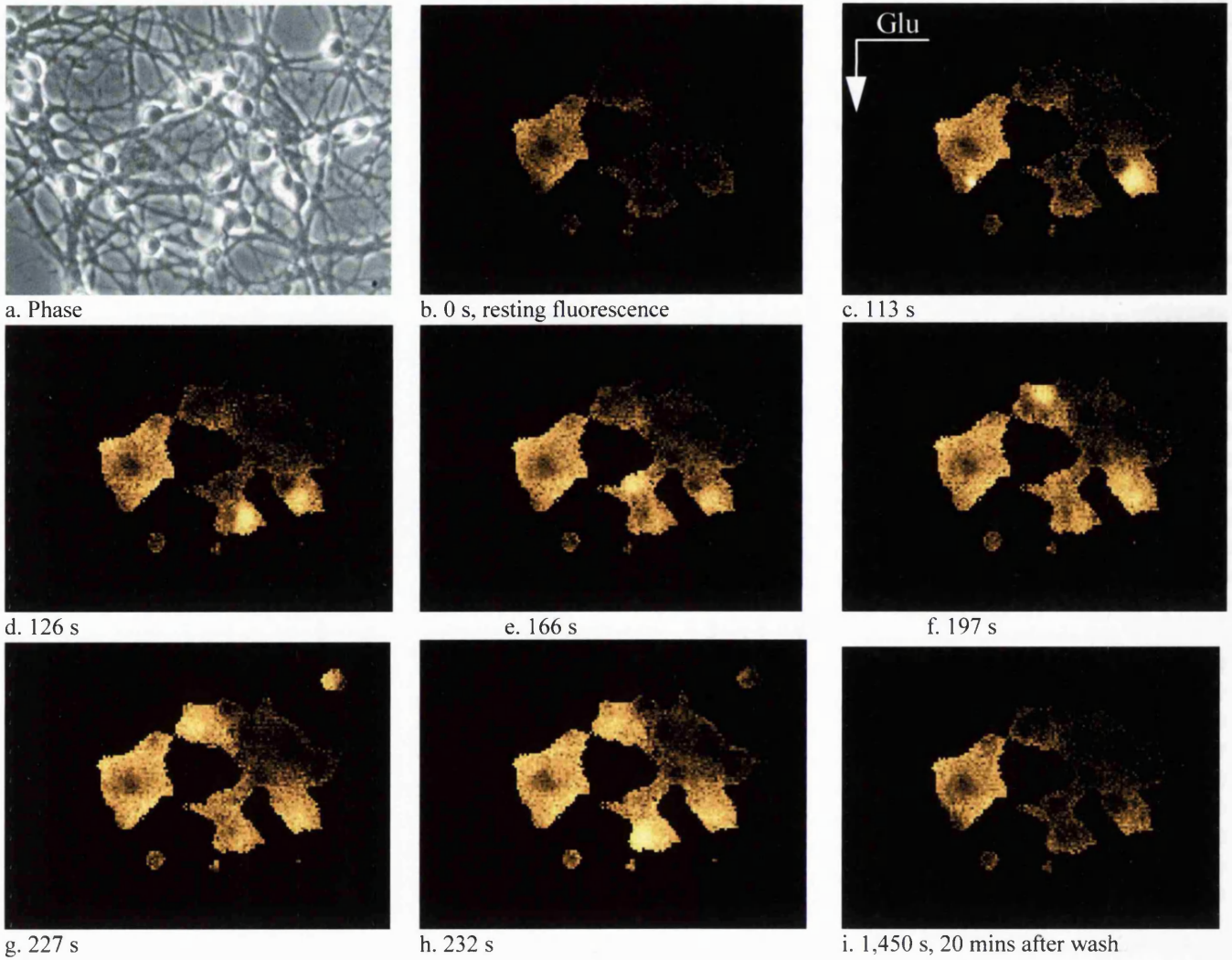

Fig. 7.8 Phase contrast picture (a.) and sequence of pseudocolour images (b-i) showing the change in 340/380 nm ratio of fluorescence after application of 100 μM glutamate +1 μM glycine to a group of cerebellar granule neurones. Time is indicated under each panel. Glutamate was applied after 40 s and is present in panels c-h. Panel i shows fluorescence 20 mins after wash.

baseline value, and 5 measurements taken 20 minutes following the removal of glutamate were averaged as a recovery value. Fig. 7.9 shows responses in a number of representative cells from this experiment. In the presence of Ca^{2+}, increases are seen and 13 out of 26 cells in this population showed the spike and elevated plateau seen previously (Fig. 7.9a). On removal of extracellular Ca^{2+} the responses changed (Fig. 7.9b). A gradual increase was seen in all cells which was more pronounced than in the normal HBSS. In addition, none of the cells examined produced the massive spiking response seen in the presence of Ca^{2+}. Once Ca^{2+}-containing HBSS was restored and the cells challenged again, the spike and plateau response returned in 21 out of 26 cells, a greater proportion of cells than initially showed the response (Fig 7.9c).

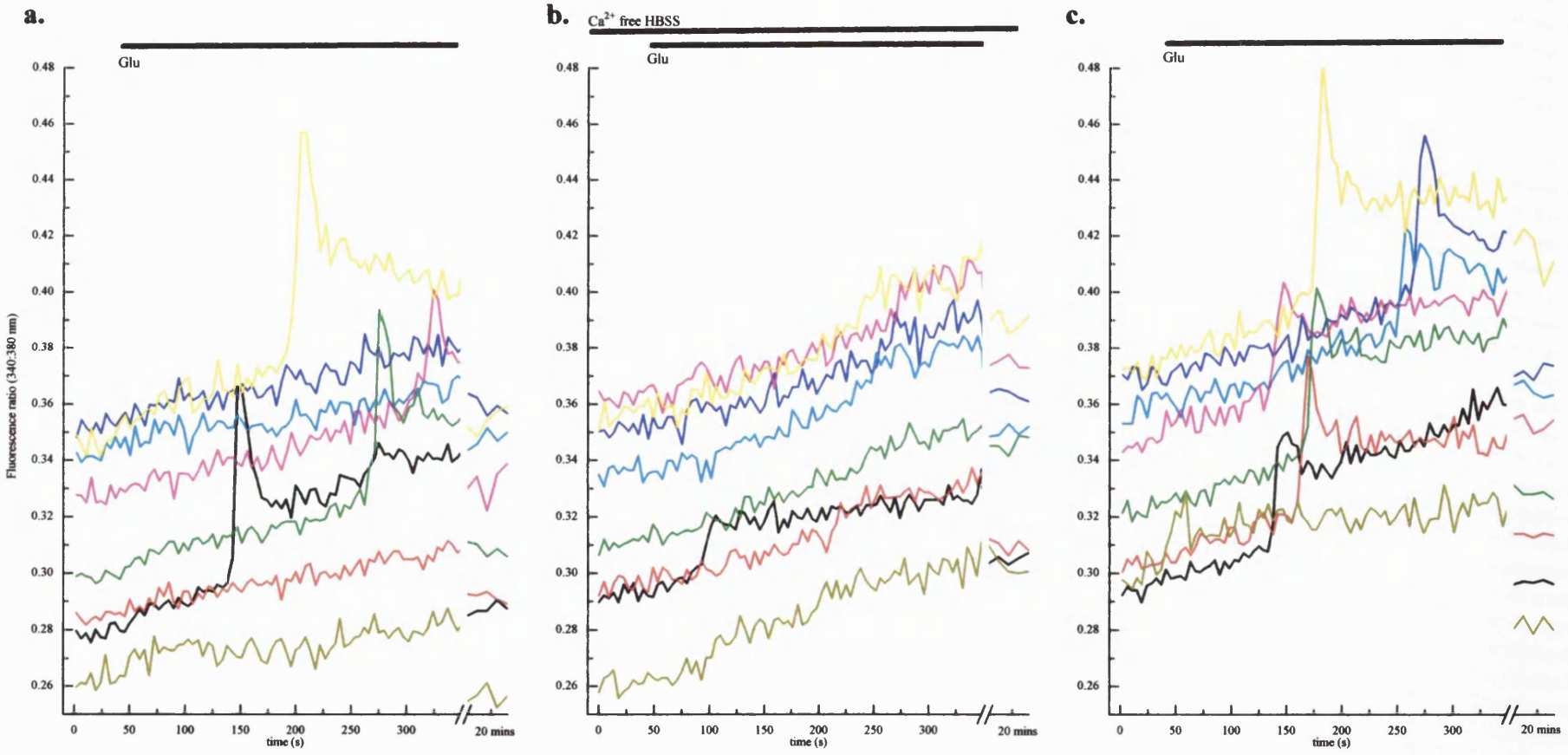

Fig. 7.9 Effect of the removal of extracellular Ca^{2+} on MagFURA2 responses in cerebellar granule neurones. Fluorescence ratio is plotted against time. 100 μM glutamate (+1 μM glycine) application is indicated by the bar. Responses to glutamate are shown in 8 cells out of a field containing 26 **a.** before removal of extracellular Ca^{2+}, **b.** after removal, and **c.** after replacing extracllular Ca^{2+}. The axis break represents a period of 20 minutes recovery after glutamate was removed.

Discussion

Intracellular free Mg^{2+}

Over recent years the advancement of techniques to measure the activity of Mg^{2+} in the intracellular compartment have produced an increase in interest in the effects of this ion on channel function. Because $[Mg^{2+}]_i$ has been implicated in the occurrence of arrhythmias and ischaemic heart disease (Abraham *et al.*, 1987; Borchgrevink *et al.*, 1987) the effect of $[Mg^{2+}]_i$ on mammalian cardiac ion channels has received special attention (see Agus and Morad, 1991). Mg^{2+} in the extracellular compartment may alter ion channel currents by either entering the channel and causing a reduction in the amplitude of currents (Hess *et al.*, 1986), or by screening the membrane surface charge to produce a shift in the voltage dependence of the gating parameters of the channel (Kass and Krafte, 1987). Intracellular Mg^{2+} contributes to the inward rectification of several K^+ channels by plugging the open channel during outward currents (Matsuda *et al.*, 1987; Ashcroft, 1988). Its modulatory effect on Ca^{2+} channels however is unclear. Ca^{2+} channels are blocked by a variety of multivalent cations including Mg^{2+} (Hagiwara and Byerly, 1981), and in the total absence of divalent cations the channels become permeable to non-specific monovalent cations. In this situation Ca^{2+} channel currents carried by Na^+ would be more than half blocked by just 1.3 μM Ca^{2+} (Hess and Tsien, 1984). This suggests the existence of a high-affinity binding site for Ca^{2+} which has a micromolar dissociation constant which governs the permeation process and ion selectivity. However, in single channel studies, Ca^{2+} channel currents saturate with an apparent dissociation constant of 14 mM (Hess *et al.*, 1986) suggesting a second much lower affinity site.

Various models based on these experimental findings have been suggested to explain the ion permeation process and blockade by divalent cations. Kostyuk *et al.* (1983) found that in the absence of divalent cations, Ca^{2+} channel currents carried by 30 mM Na^+ in snail neurones could be blocked by Ca^{2+} at concentrations of 0.03-1.2 μM. The proportion of current blocked by Ca^{2+} was unchanged between -20 and -60 mV. Their conclusion was that the high affinity Ca^{2+}-binding site was not located in the permeation pathway but located

externally, allosterically modulating the channel by controlling pore conformations. With this site occupied by Ca^{2+}, the pore was proposed to conform in such a way that it allows Ca^{2+} to pass. In this scenario, in the absence of Ca^{2+} at the regulatory site the pore assumes a conformation allowing the passage of monovalent ions.

An alternative hypothesis was shared by other groups (Almers and McCleskey, 1984; Hess and Tsien, 1984; Tsien *et al.*, 1987) postulating two high-affinity binding sites within the permeation pathway. In this model the pore would be permeable to monovalent ions which could bind weakly to the two binding sites and could carry large currents. In the presence of micromolar Ca^{2+} one of the high-affinity sites would be occupied thus blocking the channel to monovalent ions due to its high binding affinity and slow off-rate from this site. In higher Ca^{2+} concentrations a second Ca^{2+} ion would be likely to enter the pore. The doubly occupied channel would elevate the free energy of Ca^{2+} ions occupying the pore and thus change the apparent dissociation constant to millimolar range, comparable to the saturation of single Ca^{2+} channels.

In support of the two-site model divalent ion block of monovalent currents through Ca^{2+} channels has been shown to be voltage-dependent (Fukushima and Hagiwara, 1985; Lansman *et al.* 1986). This suggests that the high-affinity binding sites are within the electric field of the membrane and maybe within the pore itself. In the case of block of Ba^{2+} currents by Mg^{2+} and Cd^{2+}, increasing the extracellular Ba^{2+} concentration increased the off-rate of the blocking ion suggesting an interaction between the blocking ion and the permeant ion (Lansman *et al.*, 1986). In addition, intracellular divalent ions can block monovalent ion currents probably via a blocking site in the pore (Hess *et al.*, 1989). Although these studies give substance to the two-site model they may also be explained by modifying the allosteric model to additionally include an internal regulatory binding site at which divalent ions bind blocking the passage of monovalent ions and secondly to suppose that there is a voltage-dependence to the rate constants in monovalent-permeable and -impermeable conformations.

Considering the blockade of Ca^{2+} channel currents by multivalent cations the two hypotheses above explain block by either competition inside the pore for binding or interaction with an external regulatory site. Another factor may also explain

block or contribute to the blocking actions of a multivalent ion first proposed by Muller and Finkelstein (1974), and states that the local concentration of Ca^{2+} around the channel entrance could be reduced by the screening of negative surface charge.

Single channel studies in cell-attached patch recordings from guinea pig ventricular cells tested these hypotheses (Lansman *et al.*, 1986) and suggested that the mechanism of block was best described in terms of the two-site model.

Against this background of theory and experimental evidence the present data can be partly explained. The main features of raising $[Mg^{2+}]_i$ on Ca^{2+} channel currents in cerebellar granule neurones were a decrease in whole-cell current amplitude and a shift in the voltage-dependence of activation. The negative shift in the current-voltage relationship which was accompanied by an equivalent shift in the null potential upon increasing $[Mg^{2+}]_i$ is characteristic of screening of fixed negative charges close to the channel opening on the internal surface of the membrane. Although this was not a mechanistic study and the data here are not thorough enough to suggest a blocking mechanism for internal Mg^{2+} a number of observations were made. The studies already discussed (Matsuda *et al.*, 1987; Ono and Fozzard, 1992; Strong and Scott, 1992) suggest Mg^{2+} blocks the open channel to reduce current amplitude. In this study increasing $[Mg^{2+}]_i$ did not produce an increase in the rate of inactivation of Ca^{2+} channel currents. This could be taken as evidence against a high-affinity, slowly dissociating block, but does not rule out a low-affinity, rapidly dissociating block of the open channel. Inhibition by $[Mg^{2+}]_i$ has been reported to show a dependence on voltage in snail neurones (Strong and Scott, 1992) which would appear in agreement with block of the open channel. Comparison of the currents recorded here showed that the percentage reduction in current over all voltages was similar when the shift in the voltage-dependence of activation and reversal potential were taken into account.

Another rather unusual result was the shift in voltage-dependence of inactivation seen when cells with 0.1 mM $[Mg^{2+}]_i$ were compared to 0.5 mM $[Mg^{2+}]_i$. Since there was an obvious effect on the voltage-dependence of activation caused by Mg^{2+} screening surface charge, an equivalent change was expected in the voltage-dependence of inactivation and steady-state inactivation would be expected to proceed more rapidly due to the decrease in intramembrane potential caused by

intracellular Mg^{2+}. Surprisingly an opposite shift was seen. A possible explanation is that Mg^{2+} selectively blocks a subpopulation of Ca^{2+} channels that inactivate at more negative potentials than the current remaining in the presence of 0.5 mM $[Mg^{2+}]_i$. However, no evidence of subpopulations of channels with different steady-state inactivation properties was apparent considering that a single Boltzmann function could adequately describe the data. From the steady-state inactivation data it does appear that a subpopulation of Ca^{2+} channels are present that are both non-inactivating and not modulated by intracellular Mg^{2+} within the range of concentrations used. This population of channels may be L-type considering that $[Mg^{2+}]_i$ also had no effect on tail currents.

The pharmacological features of currents recorded in the presence of different $[Mg^{2+}]_i$ showed one or two notable differences. Increases in the $[Mg^{2+}]_i$ caused a significant reduction in the ω-CgTx GVIA-sensitive current in these cells as indicated previously (Pearson *et al.*, 1993a). The reduction of this component of the current was however too small to account for the large reduction in total current caused by the increased concentration of $[Mg^{2+}]_i$. The reduction in other current components, (ω-Aga IVA-sensitive and nicardipine-sensitive currents) were in proportion to the reduction of the total current. ω-CTx MVIIC-sensitive currents were moderately reduced at the higher $[Mg^{2+}]_i$ and the loss of ω-CTx MVIIC-sensitive current was equal in amplitude to the ω-CgTx GVIA-sensitive current reduced when $[Mg^{2+}]_i$ was raised from 0.1 to 0.5 mM, additional evidence that ω-CTx MVIIC blocks the N-type current in granule cells.

The modulatory effect of $[Mg^{2+}]_i$ on the L-type Ca^{2+} channel expressed in guinea-pig cardiac myocytes occurred at concentrations of 1-3 mM, causing 50% inhibition of the current (White and Hartzell, 1988). In granule cells half of the total whole-cell current was blocked in cells with 0.5 mM $[Mg^{2+}]_i$. This may suggest a differential sensitivity of cardiac L-type channels and the channels expressed by cerebellar granule neurones to modulation by intracellular Mg^{2+}. The sensitivity of ω-CgTx GVIA-sensitive channels in granule cells appears to be greater than other channel types in these cells, and L-type channels in myocytes leading to possible explanations of the discrepancies between differences in the

reported effects of intracellular Mg^{2+} on currents in vertebrate neurones (Robbins *et al.*, 1992) and cardiac cells (Romani and Scarpa, 1992).

Thus it appears that Mg^{2+} can modulate the currents carried by multiple channel species in cerebellar granule cells, but preferentially reduces the ω-CgTx GVIA-sensitive N-type current over this concentration range and spares a sub-population of Ca^{2+} channels that are non-inactivating.

Measurements of intracellular Mg^{2+} using MagFURA2

Since the development of the pH-insensitive intracellular fluorescent Mg^{2+} indicator MagFURA2 (Raju *et al.*, 1989), the role of $[Mg^{2+}]_i$ in many cellular processes has been investigated. MagFURA2 allows simple measurements to be made showing changes in $[Mg^{2+}]_i$. The accuracy of estimations of actual $[Mg^{2+}]_i$ depend largely on whether or not good estimations of R_{max} and R_{min} are possible in the tissue or cell culture being used. Unfortunately, the available ionophores when used alone are often ineffective in carrying Mg^{2+} across the cell membrane to obtain measurements of fluorescence in intact cells in the presence of zero and saturating concentrations of Mg^{2+} whilst retaining the dye in cells. *In vitro* calibration attempts may also prove problematic since intracellular conditions may not be perfectly reproducible *in vitro*. Intracellular viscosity alters the dye spectra and would be difficult to simulate. Similarly, the excitation maximum of the dye is shifted to a longer wavelength by serum proteins (Ishijima *et al.*, 1991).

The method of background subtraction used here involved acquiring images from regions of the coverslip containing no cells. This method corrects for the incomplete blockade of excitation light and fluorescence of the various optical components used (glass coverslip and extracellular medium), but not for cell autofluorescence which can occur at these wavelengths. A technique for subtracting background signal that compensates for autofluorescence can be carried out by acquiring background images of the cells at each wavelength before introduction of the dye. Alternatively, images of detergent treated cells can be taken at the end of an experiment for subtraction.

Fluorescence microscopy measurements of $[Mg^{2+}]_i$ in cerebellar granule neurones estimated from a calibration curve of known Mg^{2+} containing solutions (0.49±0.05 mM) were similar to other estimates of $[Mg^{2+}]_i$ in the literature. Cortical neurones

were reported to have $[Mg^{2+}]i$ of 0.6 mM, (Brocard *et al.*, 1993), whilst some non-neuronal cells, such as cardiac cells were found to have 0.48 mM (Murphy *et al.*, 1989), and Swiss 3T3 cells 0.2 mM $[Mg^{2+}]_i$ (Ishijima *et al.*, 1991). However, a substantial range exists even amongst studies limited to mammalian cells. A value of 0.1 mM was reported for NG108-15 cells (Robbins *et al.*, 1992) and hepatocytes were shown to contain 1.1 mM free Mg^{2+} (Harman *et al.*, 1990).

The value obtained suggests that under normal physiological conditions, intracellular Mg^{2+} may be providing a tonic inhibition of Ca^{2+} channels, especially of the N-type Ca^{2+} channel. Relatively small increases in $[Mg^{2+}]_i$ from the resting level would be expected to lead to further inhibition of these channel species. Abnormal conditions such as during hypoxia (Harman *et al.*, 1990) or when glucose is depleted cause increases in $[Mg^{2+}]_i$ as ATP levels and pH falls (Murphy, E. *et al.*, 1991). Other physiological stimuli have also been shown to bring about changes in $[Mg^{2+}]_i$. Ishijima *et al.*, (1991) caused increases in $[Mg^{2+}]_i$ as an early cellular response to growth factors. Epidermal growth factor, insulin and bombesin caused moderate $[Mg^{2+}]_o$-dependent increases in $[Mg^{2+}]_i$ within 30-60 minutes of application.

The studies cited above show that a stimulus-induced increase in $[Mg^{2+}]_i$ is not without precedent. Granule cell $Mg^{2+}{}_i$ responses to glutamate have been demonstrated. However, these studies did not determine the mechanism of the observed effect, and did not fully establish from where the increase in cytosolic Mg^{2+} originated. It is possible that a similar mechanism to the proposal of Brocard *et al.* (1993) occurs here; namely, that glutamate activates NMDA receptors allowing Ca^{2+} to flood into the cell where it binds to intracellular binding sites normally occupied by Mg^{2+}. The displacement of Mg^{2+} from these sites thus produces the increase in $[Mg^{2+}]_i$ observed. One criticism of this proposal is that the influx of Ca^{2+} that is responsible for the increase in measured fluorescence is a result of the Ca^{2+} itself binding to the dye. The relative K_Ds of Ca^{2+} and Mg^{2+} for MagFURA2 modify measurements of $[Mg^{2+}]_i$ by ratiometric methods as shown in *Equation 13*. Glutamate-induced increases in $[Ca^{2+}]_i$ have been shown to average 600 nM in cortical neurones (Rajdev *et al.*, 1991). This magnitude of Ca^{2+} increase would only contribute a 0.03 mM error to $[Mg^{2+}]_i$ measurements lending support to the increase being attributed primarily to Mg^{2+}. Similar measurements

of Ca^{2+} increases with FURA2 in granule cells under the same conditions as the MagFURA2 experiments would be necessary to show without doubt that the fluorescence change was due exclusively to an increase in $[Mg^{2+}]_i$. Further pharmacological studies are also required to determine which receptors are involved, by mimicking and blockade of the response

The responses in granule cells differed in two respects to glutamate-induced accumulation of $[Mg^{2+}]_i$ in forebrain neurones (Brocard *et al.*, 1993). Average increases in $[Mg^{2+}]_i$ were not reduced on the removal of Ca^{2+} from the extracellular medium in spite of the loss of the transient spike. Secondly, the large rapid increases in $[Mg^{2+}]_i$ occurred after a variable delay, which may suggest that a threshold features in this part of the response. Influx of Ca^{2+} and efflux of K^+ through NMDA receptor channels may be responsible for these changes. Increased $[Ca^{2+}]_i$ may cause displacement of $Mg^{2+}{}_i$ from intracellular binding sites. It may also bring about an explosive release of Ca^{2+} from intracellular stores if it reaches a threshold to stimulate Ca^{2+}-induced Ca^{2+} release. This in turn would generate a further massive increase in $[Mg^{2+}]_i$ which would be abolished in the absence of extracellular Ca^{2+}.

The efflux of intracellular K^+ may in addition generate a hyperpolarisation of the cell membrane sufficient to cause a reversal of the Na^+-Mg^{2+} exchange which has been shown in squid axon and mammalian myocytes (Flatman, 1991; Murphy, E. *et al.*, 1991) thus accounting for the steady rise in $[Mg^{2+}]_i$ that persists in the absence of extracellular Ca^{2+}.

Concluding remarks

The past few years have seen major advances in our understanding of the structural and functional properties of neuronal voltage-dependent Ca^{2+} channels. A major factor contributing to the wealth of literature that has been published in the last few decades investigating the role of ion channels in excitable cells is the rapid development of new techniques in the areas of biochemistry, membrane biophysics, and pharmacology. Principal amongst these are the successful advancement of molecular cloning techniques and the refinement of the patch clamp technique. Cloning and protein purification studies have allowed the structural detail to be identified, whereas expression studies have defined the biophysical and some of the pharmacological properties of a number of cloned channels. Nucleic acid sequences have been elucidated allowing the study of the role of individual regions, or single amino acids in the membrane protein by site-directed mutagenesis and injection of mRNA and cDNA into expression systems for analysis of the altered channel. These experimental methods are being combined with theoretical analyses to develop elaborate structural models of channel proteins suggesting ideas for further, more informative experimental studies. Difficulties in the development of precise models of large proteins that include factors such as aqueous and lipid environment, membrane potential and free energy are being overcome by advances in the technology and methodology of energy calculations.

There are now six recognisably distinct Ca^{2+} channel α_1 clones, the SCD clones which fall into a DHP-sensitive L-type channel subfamily, and the ABE clones which constitute a non-L-type channel subfamily. The majority of the subunit diversity of the α_1 and auxiliary subunits has probably been uncovered, although gaps occur in the existing classification. For instance, the T-type channel does not closely correlate to any of the recognised clones. It may prove either to have an α_1 subunit closely related to the α_{1E} or may be completely unrelated. The physiological expression of Ca^{2+} channel subunits has yet to be established. The subunit diversity of the pore-forming and the auxiliary subunits and the multiple splice variation that is present throughout (Perez-Reyes and Schneider, 1994) reveal a remarkable potential for molecular heterogeneity, although the full extent of this is probably not exploited. The significance of such a diversity and the spatial regulation of the expression of some subunit isoforms results in qualitative

differences in Ca^{2+} currents in different cell types and different cell regions. As well as region specific differences in the localisation of Ca^{2+} channel α_1 subunits, region specific differences in auxiliary subunit expression could also change the properties of the Ca^{2+} current in a specific location since different combinations of a given α_1 subunit with different auxiliary subunits gives rise to Ca^{2+} currents with different properties (Sather *et al.*, 1993; Olcese *et al.*, 1994; Stea *et al.*, 1994; De Waard and Campbell, 1995). Different Ca^{2+} channel subunits also possess alternative sites susceptible to phosphorylation by second messengers and binding of activated G-protein subunits. The possibility of differential modulation of Ca^{2+} channels has often been discussed but few examples have been clearly demonstrated in neurosecretory systems (Artalejo *et al.*, 1990). This creates a further level of control, specific to cell type and cell region. Examples of spatial localisation within the CNS can be found for L-type Ca^{2+} channels which occur predominantly in cell bodies and in some cases, proximal dendrites where they may serve functional roles in excitation-transcription coupling (Murphy *et al.* 1991). Conversely, non-L-type channels are expressed prominently in the terminals of nerves, often co-existing at individual synaptic boutons where they share the task of producing the rapid Ca^{2+} influx necessary to trigger neurotransmitter release (Huston *et al.*, 1995). A rich diversity of Ca^{2+} channels provides the cell with the means to control the intracellular Ca^{2+} concentration more precisely.

The Ca^{2+} channel species occurring in the cerebellar granule neurone have been shown to be diverse. This study demonstrated the presence of L-type, N-type and P-type Ca^{2+} channels. Using neurotoxin channel blockers N- and P-type Ca^{2+} channels were found to account for 40-45% of the total whole-cell Ca^{2+} channel current and L-type channels accounted for up to 55% of the remaining current with the possibility that part of the DHP-sensitive component was produced by a non-L-type channel. One feasible explanation is that part of this current could be carried by a channel encoded by the α_{1E} clone, since it was also shown that channels of this class are susceptible to block by nicardipine. Although whole tissue studies have shown expression of the α_{1E} in the granule cells of the cerebellum (Yokoyama *et al.*, 1995), immunocytochemistry using anti-α_{1E}

antibodies and/or RT-PCR techniques to establish the presence of the α_{1E} subunit in preparations of granule cells would be very interesting.

Other studies have shown that further diversity occurs in the cerebellar granule cell. At the single-channel level functional diversity of L-type channels (Forti and Pietrobon, 1993), and diversity amongst channels reported to be P- and R-type on the basis of pharmacological criteria has also been shown (Tottene *et al.*, 1996). Thus cerebellar granule cells appear to show the greatest diversity of Ca^{2+} channel subtypes than any other mammalian neurone studied so far. This diversity may provide a significant flexibility in the precise control of cellular functions dependent on Ca^{2+} and may be the basis for selective modulation of local Ca^{2+}-dependent events during specific patterns of neuronal activity. Also interesting is the notion that all of these channel subtypes maybe involved in neurotransmitter release. If so, do different pre-synaptic Ca^{2+} channel subtypes at the terminus correspond to different post-synaptic neurotransmitter receptors?

A favourable consequence of greater molecular diversity of Ca^{2+} channels is a greater potential for therapeutic applications of selective Ca^{2+} channel blockers. L-type Ca^{2+} channel antagonists such as the DHPs have been successfully applied to the treatment of hypertension and cardiovascular disorders (see Kanneganti and Halpern, 1996) and tested in models of neurodegeneration (Weiss *et al.*, 1990; Regan and Choi, 1994) and memory loss (Deyo *et al.*, 1989; Schuurman *et al.*, 1993). The implications of DHP-sensitivity of α_{1E} channels at concentrations that block L-type channels is that any therapeutic effect of a DHP or other Ca^{2+} channel antagonists on neuronal disease models may be causing its effect via an effect on this non-L-type channel.

The availability of synthetic conopeptides has provided the opportunity for the evaluation of the possible therapeutic effects of selectively blocking neuronal Ca^{2+} channels in pathological conditions. SNX-230 (synthetic ω-CTx MVIIC) blocks non-L, non-N-type channels more readily than N-type channels. In rat models of global ischaemia it did not have appreciable neuroprotective effects (Valentino *et al.*, 1993). Synthetic ω-CTx MVIIA (SNX-111) however, protected CA1 pyramidal neurones of the hippocampus from damage caused by transient global ischaemia in the rat (Valentino *et al.*, 1993). A single dose of SNX-111 was able to provide a neuroprotective effect even when administered 24 hours after the

ischaemic insult. Other studies have also seen a neuroprotective effect in rat models of neocortical infarction and traumatic brain injury (Hovda *et al.*, 1994) pointing to the potential use of conopeptides and their derivatives in the prevention of neuronal damage.

There is potentially a vast unexplored wealth of similar peptides to be discovered in the venom of the many related predatory snails and spiders. It is estimated that of the 500 *Conus* species around 10-20% of these are primarily fish-hunters. Of these, ω-conotoxins have been purified from only 6 (see Olivera *et al.*, 1994). It is not known whether ω-conotoxins are only found in the fish-hunting species of snail, and it is likely that other *Conus* species, preying on molluscs and other marine invertebrates possess venom containing paralytic peptides with novel modes of action. Similarly, of the many thousands of spider species described, only a small number of venoms have been examined. Given the similarity of sequence identity between the membrane proteins of insects and vertebrates, it would not be surprising to find in this huge pool of toxins, some which aid the discrimination of ion channels in the mammalian brain.

The aim of the work presented in the final chapter was to further explore initial studies (Pearson and Dolphin, 1993a) that had shown a selective inhibition of ω-CgTx GVIA-sensitive Ca^{2+} channel current in cerebellar granule cells and attempt to demonstrate stimulus-induced changes in $[Mg^{2+}]_i$ which may occur in physiological conditions as a mechanism for controlling ion channel function and thereby alter neurotransmitter release. A role of $Mg^{2+}{}_i$ in the regulation of ion channels is not surprising in view of its role as a regulator of other membrane channels and transporters (see Chapter 1) in both non-neuronal and neuronal cells. In neuronal cells, inhibition of ion channels by an intracellular ion is particularly interesting due to the role of Ca^{2+} channels in neurotransmission. Selective inhibition of a particular subtype over a particular range of concentrations is of added importance since there is a possibility that specific subtypes of Ca^{2+} channel may be located in 'hot spots' and even linked to the release of a certain transmitter.

Monitoring intracellular ion concentration by the use of fluorescent indicators was made possible 10 years ago with the development of an indicator for Ca^{2+} which could be loaded into small mammalian cells (Tsien *et al.*, 1982). Since then, rapid

improvements in fluorescence and binding properties of indicators have paved the way for measurements of cytosolic ion concentration, forming an essential bridge between our understanding of the molecular mechanisms that control ion movement across the membrane and the biochemistry of ion-sensitive proteins within the cell. Since Ca^{2+} is the most dynamic second messenger known, measurements of this ion were the subject of widespread interest. In time, other probes became available and attentions diverged to other intracellular ions. Indicators for intracellular free Mg^{2+} have been in use for around 5 years since their synthesis (Raju *et al.*, 1989) and studies are beginning to demonstrate that $[Mg^{2+}]_i$ may be more dynamic then was once thought. Hormonal regulation of free Mg^{2+} has been shown in murine lymphoma cells (Grubbs and Maguire, 1987), light is known to affect the total Mg content of retinal rod outer segments (Somlyo and Walz, 1985) and glucose modifies Mg^{2+} fluxes in pancreatic islet cells (Henquin *et al.*, 1983). The results of this study cautiously suggest that glutamate may also stimulate increases in $[Mg^{2+}]_i$. The implications of this on cellular functions are that neuronal excitability may be regulated by environmental stimuli or chemical mediators via an effect of Mg^{2+} on ion channels. Secondly, a number of chronic diseases are associated with altered levels of Mg^{2+}. Hypomagnesemia is associated with diabetes, alcoholism and essential hypertension, and hypermagnesemia is associated with renal vascular disease and circulatory shock (Altura and Altura, 1981). Symptoms of these and other diseases involving changes in Mg levels may be consequences of an effect on ion channels and may be treatable by opposing their effect through the intervention of drugs.

The current climate surrounding research into Ca^{2+} channels is one of great excitement. Structure-function studies and molecular cloning will undoubtedly lead to a more complete map relating each region of the protein to a specific function. Ca^{2+} channel interactions with the molecular components of the presynaptic machinery for neurosecretion will also be the subject of future interest following the observation that syntaxin and synaptotagmin are functionally linked to N-type Ca^{2+} channels (Bennett *et al.*, 1992).

For cerebellar granule neurones, the continued assessment of Ca^{2+} channel species using new pharmacological agents as they become available and studies of single-channel properties in combination with a molecular biological approach will

undoubtedly lead to a more comprehensive picture of Ca^{2+} channel diversity in the future. There is a clear need for a detailed description of the expression of all Ca^{2+} channel subunits in these cells both in vivo and in cell culture. This may also reveal developmental patterns of expression that are altered when cells are maintained in culture.

A more thorough look at the effect of DHP antagonists on α_{1E} Ca^{2+} channel currents would be recommended since it was not determined whether or not inhibition of α_{1E} currents was a property of all DHP antagonists or specific to nicardipine. It may be that binding of the drug molecule to the channel pore occurs at a different receptor site for L-type and α_{1E} Ca^{2+} channels.

Manipulation of $[Mg^{2+}]_i$ has shown that Mg^{2+} can regulate currents through Ca^{2+} channels and certain channel types may be regulated over different concentration ranges. Expression of a single class of Ca^{2+} channel clone would be required to demonstrate type-specific differences in the sensitivity of Ca^{2+} channels to block by Mg^{2+}. Single-channel studies employing outside-out patches would also be of use in examining the blocking mechanism of Mg^{2+}.

Abstracts and publications

Huston, E., Cullen, G.P., Burley, J.R. and Dolphin, A.C. (1995) The involvement of multiple calcium channel sub-types in glutamate release from cerebellar granule cells and its modulation by GABAB receptor activation. *Neuroscience* **68**, 465-478.

Burley, J.R., and Dolphin, A.C. (1995) Inhibition of whole-cell calcium channel currents in rat cerebellar granule neurones by nicardipine and the conus peptide ω-conotoxin-MVIIC. *Brit. J. Pharm.* **117**, 315P (Abstract).

Stephens, G.J., Berrow, N., Burley, J.R., Page, K., Tedder, I., Fitzgerald, E. and Dolphin, A.C. (1996) Comparison of properties of cloned α1A and α1E calcium channels transiently expressed in the COS-7 cell line. *Soc. Neurosci.* **22**, 495.6 (Abstract).

Stephens, G.J., Page, K.M., Burley, J.R., Berrow, N.S. and Dolphin, A.C. (1997) Functional expression of rat brain cloned a_{1E} calcium channels in COS-7 cells. *Pflugers Archives* **433**, 523-532.

Acknowledgements

I wish to thank Annette Dolphin for help and supervision throughout, and Maureen Docherty, Alistair Mathie, and Talvinder Sihra for inspiration and encouragement.

For technical assistance I would like to thank Elaine Huston whose instructions in cell culture technique were of great benefit, and Nick Berrow and Karen Page for kindly supplying cDNA. Adeola Oodunlami helped with preparation and transfection of COS-7 cells. Due credit should also be given to Brian Amos and Alistair Mathie who provided guidance concerning the use of fluorescent indicators. I also wish to thank Chris Wyatt, Jeff Allen, Gary Stephens and Kathy Sutton for occasional gems of electrophysiological experience.

I am especially appreciative to Chris Watkins for his keen interest and constant availability for discussion.

Finally, my gratitude extends to all those, past and present who have helped provide a relaxed and friendly working environment over the past three years.

This work was funded by a Wellcome studentship.

References

Abraham, A.S., Rosenmann, D., Kramer, M., Balkin, J., Zion, M.M., Farbstien, H. and Eylath, U. (1987) Magnesium in the prevention of lethal arrhythmias in acute myocardial infarction. *Archives of Internal Medicine* **147**, 753-755.

Adams, M.E., Myers, R.A., Imperial, J.S. and Olivera, B.M. (1993) Toxityping rat brain calcium channels with omega-toxins from spider and cone snail venoms. *Biochemistry* **32**, 12566-12570.

Agus, Z.S., Kelepouris, E., Dukes, I. and Morad, M. (1989) Cytosilic magnesium modulates calcium channel activity in mammalian ventricular cells. *Am. J. Physiol.* **256**, C452-C455.

Ahlijanian, M.K., Westenbroek, R.E. and Catterall, W.A. (1990) Subunit structure and localization of dihydropyridine-sensitive calcium channels in mammalian brain, spinal cord, and retina. *Neuron* **4**, 819-832.

Ahlijanian, M.K., Striessnig, J. and Catterall, W.A. (1991) Phosphorylation of an alpha 1-like subunit of an omega-conotoxin-sensitive brain calcium channel by cAMP-dependent protein kinase and protein kinase. *J. Biol. Chem.* **266**, 20192-20197.

Akaike, N., Kostyuk, P.G. and Osipchuk, Y.V. (1989) Dihydropyridine-sensitive low-threshold calcium channels in isolated rat hypothalamic neurones. *J. Physiol.* **412**, 181-195.

Allen, T.G., Sim, J.A. and Brown, D.A. (1993) The whole-cell calcium current in acutely dissociated magnocellular cholinergic basal forebrain neurones of the rat. *J. Physiol.* **460**, 91-116.

Almers, W., McCleskey, E. and Palade, P. (1985) Rubin, R.P., Weiss, J.B. and Putney, J.W. (Eds.) *Calcium in Biological Systems*, pp. 321-330. New York, London: Plenum Publishing Corp.]

Almers, W. and McCleskey, E.W. (1984) Non-selective conductance in calcium channels of frog muscle: calcium selectivity in a single-file pore. *J. Physiol.* **353**, 585-608.

Altman, J. (1972a) Postnatal development of the cerebellar cortex in the rat. I. The external germinal layer and the transitional molecular layer. *Journal of Comparative Neurology* **145**, 353-397.

Altman, J. (1972b) Postnatal development of the cerebellar cortex in the rat. II. Phases in the maturation of Purkinje cells and of the molecular layer. *Journal of Comparative Neurology* **145**, 399-463.

Altman, J. and Bayer, S.A. (1982) Development of the cranial nerve ganglia and related nuclei in the rat. *Advances in Anatomy, Embryology & Cell Biology* **74**, 1-90.

Altura, B.M. and Altura, B.T. (1981) Magnesium ions and contraction of vascular smooth muscles: relationship to some vascular diseases. [Review]. *Federation Proceedings* **40**, 2672-2679.

Aniksztejn, L. and Ben-Ari, Y. (1991) Novel form of long-term potentiation produced by a K+ channel blocker in the hippocampus. *Nature* **349**, 67-69.

Aosaki, T. and Kasai, H. (1989) Characterization of two kinds of high-voltage-activated Ca-channel currents in chick sensory neurons. Differential sensitivity to dihydropyridines and omega-conotoxin GVIA. *Pflugers Archiv - European Journal of Physiology* **414**, 150-156.

Armstrong, C.M. and Gilly, W.F. (1992) Access resistance and space clamp problems associated with whole-cell patch clamping. In: Anonymous *Methods in Enzymology: Vol 207: Electrophysiological Techniques*, pp. 100-122. Academic Press Inc.]

Artalejo, C.R., Ariano, M.A., Perlman, R.L. and Fox, A.P. (1990) Activation of facilitation calcium channels in chromaffin cells by D1 dopamine receptors through a cAMP/protein kinase A-dependent mechanism [see comments]. *Nature* **348**, 239-242.

Artalejo, C.R., Dahmer, M.K., Perlman, R.L. and Fox, A.P. (1991a) Two types of Ca2+ currents are found in bovine chromaffin cells: facilitation is due to the recruitment of one type [published erratum appears in J Physiol (Lond) 1991 Jun;437:765]. *J. Physiol.* **432**, 681-707.

Artalejo, C.R., Mogul, D.J., Perlman, R.L. and Fox, A.P. (1991b) Three types of bovine chromaffin cell Ca2+ channels: facilitation increases the opening probability of a 27 pS channel. *J. Physiol.* **444**, 213-240.

Artalejo, C.R., Perlman, R.L. and Fox, A.P. (1992) Omega-conotoxin GVIA blocks a Ca2+ current in bovine chromaffin cells that is not of the "classic" N type. *Neuron* **8**, 85-95.

Ashcroft, F.M. (1988) Adenosine 5'-triphosphate-sensitive potassium channels. [Review]. *Annu. Rev. Neurosci.* **11**, 97-118.

Auld, V.J., Goldin, A.L., Krafte, D.S., Catterall, H.A., Lester, H.A., Davidson, N. and Dunn, R.J. (1987) A neutral amino acid change in segment IIS4 dramatically alters the gating properties of the voltage-dependent sodium channel. *Proceedings of the National Academy of Science USA* 323-327.

Baker, P.F. and Crawford, A.C. (1972) Mobility and transport of magnesium in squid giant axons. *J. Physiol.* **227**, 855-874.

Bara, M., Guiet-Bara, A. and Durlach, J. (1993) Regulation of sodium and potassium pathways by magnesium in cell membranes. [Review]. *Magnesium Research* **6**, 167-177.

Barhanin, J., Coppola, T., Schmid, A., Borsotto, M. and Lazdunski, M. (1987) The calcium channel antagonists receptor from rabbit skeletal muscle. Reconstitution after purification and subunit characterization. *Eur. J. Biochem.* **164**, 525-531.

Bean, B.P., Sturek, M., Puga, A. and Hermsmeyer, K. (1986) Calcium channels in muscle cells isolated from rat mesenteric arteries: modulation by dihydropyridine drugs. *Circ. Res.* **59**, 229-235.

Bechem, M., Gross, R., Hebisch, S. and Schramm, M. (1989) Ca-agonists: a new class of inotropic drugs. *Basic Research in Cardiology* **84 Suppl 1**, 105-116.

Bennett, M.K., Calakos, N. and Scheller, R.H. (1992) Syntaxin: a synaptic protein implicated in docking of synaptic vesicles at presynaptic active zones. *Science* **257**, 255-259.

Berjukow, S., Doring, F., Froschmayr, M., Grabner, M., Glossman, H. and Hering, S. (1996) Endogenous calcium channels in human embryonic kidney (HEK293) cells. *Br. J. Pharmacol.* **118**, 748-754.

Bernheim, L., Beech, D.J. and Hille, B. (1991) A diffusible second messenger mediates one of the pathways coupling receptors to calcium channels in rat sympathetic neurons. *Neuron* **6**, 859-867.

Bernstein, J. (1902) Untersuchungen zur Thermodynamik der bioelektrishen Strome. Erster Theil. *Pflugers Archives* **92**, 521-562.

Bernstein, J. (1912) *Elektrobiologie*, Vieweg, Braunschweig.

Berridge, M.J. (1993) Inositol trisphosphate and calcium signalling. [Review]. *Nature* **361**, 315-325.

Berrow, N.S., Campbell, V., Fitzgerald, E.M., Brickley, K. and Dolphin, A.C. (1995) Antisense depletion of beta-subunits modulates the biophysical and pharmacological properties of neuronal calcium channels. *J. Physiol.* **482**, 481-491.

Berrow, N.S., Brice, N.L., Tedder, I., Page, K. and Dolphin, A.C. (1997) Properties of cloned rat a_{1A} calcium channels transiently expressed in the COS-7 cell line. *Eur. J. Neurosci.* **in press**,

Biel, M., Ruth, P., Bosse, E., Hullin, R., Stuhmer, W., Flockerzi, V., Hofmann and F. (1990) Primary structure and functional expression of a high voltage activated calcium channel from rabbit lung. *FEBS Lett.* **269**, 409-412.

Biel, M., Hullin, R., Freundner, S., Singer, D., Dascal, N., Flockerzi, V. and Hofmann, F. (1991) Tissue-specific expression of high-voltage-activated dihydropyridine-sensitive L-type calcium channels. *Eur. J. Biochem.* **200**, 81-88.

Biton, B., Granger, P., Depoortere, H., Scatton, B. and Avenet, P. (1995) Block of P-type Ca2+ channels by the NMDA receptor antagonist eliprodil in acutely dissociated rat Purkinje cells. . *Eur. J. Pharmacol.* **294**, 91-100.

Bley, K.R. and Tsien, R.W. (1990) Inhibition of Ca2+ and K+ channels in sympathetic neurons by neuropeptides and other ganglionic transmitters. *Neuron* **4**, 379-391.

Boland, L.M., Allen, A.C. and Dingledine, R. (1991) Inhibition by bradykinin of voltage-activated barium current in a rat dorsal root ganglion cell line: role of protein kinase C. *J. Neurosci.* **11**, 1140-1149.

Borchgrevink, P.C., Oksendal, A.N. and Jynge, P. (1987) Acute extracellular magnesium deficiency and myocardial tolerance to ischemia. *Journal of the American College of Nutrition* **6**, 125-130.

Borsotto, M., Norman, R.I., Fosset, M. and Lazdunski, M. (1984) Solubilization of the nitrendipine receptor from skeletal muscle transverse tubule membranes. Interactions with specific inhibitors of the voltage-dependent Ca2+ channel. *Eur. J. Biochem.* **142**, 449-455.

Bosse, E., Regulla, S., Biel, M., Ruth, P., Meyer, H.E., Flockerzi, V., Hofmann and F. (1990) The cDNA and deduced amino acid sequence of the gamma subunit of the L-type calcium channel from rabbit skeletal muscle. *FEBS Lett.* **267**, 153-156.

Bossu, J.-L., Dupont, J.-L. and Feltz, A. (1989) Calcium currents in rat cerebellar Purkinje cells maintained in culture. *Neuroscience* **30**, 605-617.

Bossu, J.L., De Waard, M., Fagni, L., Tanzi, F. and Feltz, A. (1994) Characteristics of calcium channels responsible for voltage-activated calcium entry in rat cerebellar granule cells. *Eur. J. Neurosci.* **6**, 335-344.

Bourinet, E., Fournier, F., Nargeot, J. and Charnet, P. (1992) Endogenous Xenopus-oocyte Ca-channels are regulated by protein kinases A and C. *FEBS Lett.* **299**, 5-9.

Bourinet, E., Charnet, P., Tomlinson, W.J., Stea, A., Snutch, T.P. and Nargeot, J. (1994) Voltage-dependent facilitation of a neuronal alpha 1C L-type calcium channel. *EMBO J.* **13**, 5032-5039.

Brice, N.L., Berrow, N.S., Campbell, V., Page, K.M., Brickley, K., Tedder, I. and Dolphin, A.C. (1997) Importance of the different b subunits in the membrane expression of the a_{1A} and a_2 calcium channel subunits: studies using a depolarisation-sensitive a_{1A} antibody. *Eur. J. Neurosci.* **in press**,

Brickley, K., Campbell, V., Berrow, N., Leach, R., Norman, R.I., Wray, D., Dolphin, A.C. and Baldwin, S.A. (1995) Use of site-directed antibodies to probe

the topography of the alpha 2 subunit of voltage-gated Ca2+ channels. *FEBS Lett.* **364**, 129-133.

Brinley, F.J., Jr. and Scarpa, A. (1975) Ionized magnesium concentration in axoplasm of dialyzed squid axons. *FEBS Lett.* **50**, 82-85.

Brocard, J.B., Rajdev, S. and Reynolds, I.J. (1993) Glutamate-induced increases in intracellular free Mg2+ in cultured cortical neurons. *Neuron* **11**, 751-757.

Brust, P.F., Simerson, S., McCue, A.F., Deal, C.R., Schoonmaker, S., Williams, M.E., Velicelebi, G., Johnson, E.C., Harpold, M.M. and Ellis, S.B. (1993) Human neuronal voltage-dependent calcium channels: studies on subunit structure and role in channel assembly. *Neuropharmacology* **32**, 1089-1102.

Caffrey, J.M., Josephson, I.R. and Brown, A.M. (1986) Calcium channels of amphibian stomach and mammalian aorta smooth muscle cells. *Biophys. J.* **49**, 1237-1242.

Caldwell-Violich, M. and Requena, J. (1979) Magnesium content and net fluxes in squid giant axons. *J. Gen. Physiol.* **74**, 739-752.

Campbell, V., Berrow, N. and Dolphin, A.C. (1993) GABAB receptor modulation of Ca2+ currents in rat sensory neurones by the G protein G(0): antisense oligonucleotide studies. *Journal of Physiology - London* **470**, 1-11.

Campbell, V., Berrow, N., Brickley, K., Page, K., Wade, R. and Dolphin, A.C. (1995) Voltage-dependent calcium channel beta-subunits in combination with alpha 1 subunits, have a GTPase activating effect to promote the hydrolysis of GTP by G alpha o in rat frontal cortex. *FEBS Lett.* **370**, 135-140.

Carbone, E. and Lux, H.D. (1984a) A low voltage-activated, fully inactivating Ca channel in vertebrate sensory neurones. *Nature* **310**, 501-502.

Carbone, E. and Lux, H.D. (1984b) A low voltage-activated calcium conductance in embryonic chick sensory neurons. *Biophys. J.* **46**, 413-418.

Catterall, W.A., de Jongh, K., Rotman, E., Hell, J., Westenbroek, R., Dubel, S.J. and Snutch, T.P. (1993) Molecular properties of calcium channels in skeletal muscle and neurons. *Ann. NY Acad. Sci.* **681**, 342-355.

Cavalie, A., Pelzer, D. and Trautwein, W. (1986) Fast and slow gating behaviour of single calcium channels in cardiac cells. Relation to activation and inactivation of calcium-channel current. *Pflugers Archiv - European Journal of Physiology* **406**, 241-258.

Ceccarelli, B., Fesce, R., Grohovaz, F. and Haimann, C. (1988) The effect of potassium on exocytosis of transmitter at the frog neuromuscular junction. *J. Physiol.* **401**, 163-183.

Cena, V., Stutzin, A. and Rojas, E. (1989) Effects of calcium and Bay K-8644 on calcium currents in adrenal medullary chromaffin cells. *Journal of Membrane Biology* **112**, 255-265.

Chad, J.E. and Eckert, R. (1986) An enzymatic mechanism for calcium current inactivation in dialysed Helix neurones. *J. Physiol.* **378**, 31-51.

Chin, H., Smith, M.A., Kim, H.L. and Kim, H. (1992) Expression of dihydropyridine-sensitive brain calcium channels in the rat central nervous system. *FEBS Lett.* **299**, 69-74.

Cohen, L., Vereault, D., Wasserstrom, J.A., Retzinger, G.S. and Kezdy, F.J. (1987) Evidence that uncharged verapamil inhibits myocardial contractility. *Journal of Pharmacology & Experimental Therapeutics* **242**, 721-725.

Connor, J.A., Tseng, H.Y. and Hockberger, P.E. (1987) Depolarization- and transmitter-induced changes in intracellular Ca2+ of rat cerebellar granule cells in explant cultures. *J. Neurosci.* **7**, 1384-1400.

Cukierman, S., Zinkand, W.C., French, R.J. and Krueger, B.K. (1988) Effects of membrane surface charge and calcium on the gating of rat brain sodium channels in planar bilayers [published erratum appears in J Gen Physiol 1989 Apr;93(4):following 760]. *J. Gen. Physiol.* **92**, 431-447.

Cull-Candy, S.G., Howe, J.R. and Ogden, D.C. (1988) Noise and single channels activated by excitatory amino acids in rat cerebellar granule neurones. *Journal of Physiolgy* **400**, 189-222.

Cull-Candy, S.G. and Usowicz, M.M. (1989) Whole-cell current noise produced by excitatory and inhibitory amino acids in large cerebellar neurones of the rat. *J. Physiol.* **415**, 533-553.

Curtis, B.M. and Catterall, W.A. (1984) Purification of the calcium antagonist receptor of the voltage-sensitive calcium channel from skeletal muscle transverse tubules. *Biochemistry* **23**, 2113-2118.

Curtis, B.M. and Catterall, W.A. (1986) Reconstitution of the voltage-sensitive calcium channel purified from skeletal muscle transverse tubules. *Biochemistry* **25**, 3077-3083.

Dani, J.A. (1986) Ion-channel entrances influence permeation. Net charge, size, shape, and binding considerations. *Biophys. J.* **49**, 607-618.

De Lean, A., Munson, P.J. and Rodbard, D. (1978) Simultaneous analysis of families of sigmoidal curves: application to bioassay, radioligand assay, and physiological dose-response curves. *Am. J. Physiol.* **235**, E97-E102.

De Waard, M., Feltz, A. and Bossu, J.L. (1991) Properties of a High-threshold Voltage-activated Calcium Current in Rat Cerebellar Granule Cells. *Eur. J. Neurosci.* **3**, 771-777.

De Waard, M., Seagar, M., Feltz, A. and Couraud, F. (1992) Inositol phosphate regulation of voltage-dependent calcium channels in cerebellar granule neurons. *Neuron* **9**, 497-503.

De Waard, M., Pragnell, M. and Campbell, K.P. (1994) Ca2+ channel regulation by a conserved beta subunit domain. *Neuron* **13**, 495-503.

De Waard, M. and Campbell, K.P. (1995) Subunit regulation of the neuronal alpha 1A Ca2+ channel expressed in Xenopus oocytes. *J. Physiol.* **485**, 619-634.

De Waard, M., Liu, H., Walker, D., Scott, V.E.S., Gurnett, C.A. and Campbell, K.P. (1997) Direct binding of G-protein beta gamma complex to voltage-dependent calcium channels. *Nature* **385**, 446-450.

DeLean, A., Munson, P.J. and Rodbard, D. (1978) Simultaneous analysis of families of sigmoidal curves: application to bioassay, radioligand assay, and physiological dose-response curves. *Am. J. Physiol.* **235**, E97-102.

Deyo, R.A., Straube, K.T., Moyer, J.R., Jr. and Disterhoft, J.F. (1989) Nimodipine ameliorates aging-related changes in open-field behaviors of the rabbit. *Experimental Aging Research* **15**, 169-175.

Diochot, S., Richard, S., Baldy-Moulinier, M., Nargeot, J. and Valmier, J. (1995) Dihydropyridines, phenylalkylamines and benzothiazepines block N-, P/Q- and R-type calcium currents. *Pflugers Archiv European Journal of Physiology* **431**, 10-19.

Diverse-Pierluissi, M., Goldsmith, P.K. and Dunlap, K. (1995) Transmitter-mediated inhibition of N-type calcium channels in sensory neurons involves multiple GTP-binding proteins and subunits. *Neuron* **14**, 191-200.

Doerner, D., Abdel-Latif, M., Rogers, T.B. and Alger, B.E. (1990) Protein kinase C-dependent and -independent effects of phorbol esters on hippocampal calcium channel current. *J. Neurosci.* **10**, 1699-1706.

Dubel, S.J., Starr, T.V., Hell, J., Ahlijanian, M.K., Enyeart, J.J., Catterall, W.A. and Snutch, T.P. (1992) Molecular cloning of the alpha-1 subunit of an omega-conotoxin-sensitive calcium channel. *Proc. Natl. Acad. Sci. U. S. A.* **89**, 5058-5062.

Ebel, H. and Gunther, T. (1980) Magnesium metabolism: a review. [Review]. *Journal of Clinical Chemistry & Clinical Biochemistry* **18**, 257-270.

Ellinor, P.T., Zhang, J.F., Randall, A.D., Zhou, M., Schwarz, T.L. and Tsien, R.W. (1993) Functional expression of a rapidly inactivating neuronal calcium channel. *Nature* **363**, 455-458.

Ellis, S.B., Williams, M.E., Ways, N.R., Brenner, R., Sharp, A.H., Leung, A.T., Campbell, K.P., McKenna, E., Koch, W.J., Hui, A. and et al. (1988) Sequence and expression of mRNAs encoding the alpha 1 and alpha 2 subunits of a DHP-sensitive calcium channel. *Science* **241**, 1661-1664.

Elmslie, K.S., Kammermeier, P.J. and Jones, S.W. (1994) Reevaluation of Ca2+ channel types and their modulation in bullfrog sympathetic neurons. *Neuron* **13**, 217-228.

Ewald, D.A., Sternweis, P.C. and Miller, R.J. (1988) Guanine nucleotide-binding protein Go-induced coupling of neuropeptide Y receptors to Ca2+ channels in sensory neurons. *Proc. Natl. Acad. Sci. U. S. A.* **85**, 3633-3637.

Fatt, P. and Ginsborg, B.L. (1958) The ionic requirements for the production of action potentials in crustacean muscle fibres. *J. Physiol.* **142**, 516-543.

Fatt, P. and Katz, B. (1953) The electrical properties of crustacean muscle fibres. *J. Physiol.* **120**, 171-204.

Feldmeyer, D., Melzer, W., Pohl, B. and Zollner, P. (1992) Modulation of calcium current gating in frog skeletal muscle by conditioning depolarization. *J. Physiol.* **457**, 639-653.

Fenwick, E.M., Marty, A. and Neher, E. (1982) A patch-clamp study of bovine chromaffin cells and of their sensitivity to acetylcholine. *J. Physiol.* **331**, 577-597.

Ferguson, W.B. (1991) Competitive Mg2+ block of a large-conductance, Ca(2+)-activated K+ channel in rat skeletal muscle. Ca2+, Sr2+, and Ni2+ also block. *J. Gen. Physiol.* **98**, 163-181.

Finch, E.A., Turner, T.J. and Goldin, S.M. (1991) Calcium as a coagonist of inositol 1,4,5-trisphosphate-induced calcium release. *Science* **252**, 443-446.

Fischmeister, R. and Hartzell, H.C. (1990) Regulation of calcium current by low-Km cyclic AMP phosphodiesterases in cardiac cells. *Molecular Pharmacology* **38**, 426-433.

Fisher, R.E., Gray, R. and Johnston, D. (1990) Properties and distribution of single voltage-gated calcium channels in adult hippocampal neurons. *Journal of Neurophysiology* **64**, 91-104.

Flatman, P.W. (1984) Magnesium transport across cell membranes. [Review]. *Journal of Membrane Biology* **80**, 1-14.

Flockerzi, V., Oeken, H.J. and Hofmann, F. (1986) Purification of a functional receptor for calcium-channel blockers from rabbit skeletal-muscle microsomes. *Eur. J. Biochem.* **161**, 217-224.

Forscher, P. and Oxford, G.S. (1985) Modulation of calcium channels by norepinephrine in internally dialyzed avian sensory neurons. *J. Gen. Physiol.* **85**, 743-763.

Forti, L., Tottene, A., Moretti, A. and Pietrobon, D. (1994) Three novel types of voltage-dependent calcium channels in rat cerebellar neurons. *J. Neurosci.* **14**, 5243-5256.

Forti, L. and Pietrobon, D. (1993) Functional diversity of L-type calcium channels in rat cerebellar neurons. *Neuron* **10**, 437-450.

Fox, A.P., Nowycky, M.C. and Tsien, R.W. (1987a) Single-channel recordings of three types of calcium channels in chick sensory neurones. *J. Physiol.* **394**, 173-200.

Fox, A.P., Nowycky, M.C. and Tsien, R.W. (1987b) Kinetic and pharmacological properties distinguishing three types of calcium currents in chick sensory neurones. *J. Physiol.* **394**, 149-172.

Frankenhaeuser, B. and Hodgkin, A.L. (1957) The action of calcium on the electrical properties of squid axons. *J. Physiol.* **137**, 218-244.

Fuchs, E. and Hanukoglu, I. (1983) Unraveling the structure of the intermediate filaments. [Review]. *Cell* **34**, 332-334.

Fujita, Y., Mynlieff, M., Dirksen, R.T., Kim, M.S., Niidome, T., Nakai, J., Friedrich, T., Iwabe, N., Miyata, T., Furuichi, T. and et al. (1993) Primary structure and functional expression of the omega-conotoxin-sensitive N-type calcium channel from rabbit brain. *Neuron* **10**, 585-598.

Fukushima, Y. and Hagiwara, S. (1985) Currents carried by monovalent cations through calcium channels in mouse neoplastic B lymphocytes. *J. Physiol.* **358**, 255-284.

Galizzi, J.P., Fosset, M. and Lazdunski, M. (1984) Properties of receptors for the Ca2+-channel blocker verapamil in transverse-tubule membranes of skeletal muscle. Stereospecificity, effect of Ca2+ and other inorganic cations, evidence for two categories of sites and effect of nucleoside triphosphates. *Eur. J. Biochem.* **144**, 211-215.

Gallo, V., Kingsbury, A., Balazs, R. and Jorgensen, O.S. (1987) The role of depolarization in the survival and differentiation of cerebellar granule cells in culture. *J. Neurosci.* **7**, 2203-2213.

Garcia, A.G., Artalejo, C.R., Borges, R., Reig, J.A. and Sala, F. (1986) Pharmacological properties of the chromaffin cell calcium channel. *Advances in Experimental Medicine & Biology* **211**, 139-157.

Glossmann, H., Ferry, D.R. and Boschek, C.B. (1983) Purification of the putative calcium channel from skeletal muscle with the aid of [3H]-nimodipine binding. *Naunyn-Schmiedebergs Archives of Pharmacology* **323**, 1-11.

Glossmann, H., Ferry, D.R., Goll, A., Striessnig, J. and Schober, M. (1985) Calcium channels: basic properties as revealed by radioligand binding studies. *J. Card. Pharmac.* **7 Suppl 6**, S20-30.

Grabner, M., Wang, Z., Hering, S., Striessnig, J. and Glossmann, H. (1996) Transfer of 1,4-dihydropyridine sensitivity from L-type to class A (BI) calcium channels. *Neuron* **16**, 207-218.

Grover, L.M. and Teyler, T.J. (1990) Two components of long-term potentiation induced by different patterns of afferent activation. *Nature* **347**, 477-479.

Grubbs, R.D. and Maguire, M.E. (1987) Magnesium as a regulatory cation: criteria and evaluation. [Review]. *Magnesium* **6**, 113-127.

Grynkiewicz, G., Poenie, M. and Tsien, R.Y. (1985) A new generation of Ca2+ indicators with greatly improved fluorescence properties. *J. Biol. Chem.* **260**, 3440-3450.

Gunther, T. (1993) Mechanisms and regulation of Mg2+ efflux and Mg2+ influx. [Review]. *Mineral & Electrolyte Metabolism* **19**, 259-265.

Gunther, T. and Vormann, J. (1990) Characterization of Na(+)-independent Mg2+ efflux from erythrocytes. *FEBS Lett.* **271**, 149-151.

Gurnett, C.A., De Waard, M. and Campbell, K.P. (1996) Dual function of the voltage-dependent Ca^{2+} channel a_2d subunit in current stimulation and subunit interaction. *Neuron* **16**, 431-440.

Guy, H.R. and Conti, F. (1990) Pursuing the structure and function of voltage-gated channels. [Review]. *TiNS* **13**, 201-206.

Hagiwara, S. and Byerly, L. (1981) Calcium channel. [Review]. *Annu. Rev. Neurosci.* **4**, 69-125.

Hamill, O.P., Marty, A., Neher, E., Sakmann, B. and Sigworth, F.J. (1981) Improved patch-clamp techniques for high-resolution current recording from cells and cell-free membrane patches. *Pflugers Archiv - European Journal of Physiology* **391**, 85-100.

Hamilton, S.L., Yatani, A., Brush, K., Schwartz, A. and Brown, A.M. (1987) A comparison between the binding and electrophysiological effects of dihydropyridines on cardiac membranes. *Molecular Pharmacology* **31**, 221-231.

Harman, A.W., Nieminen, A.L., Lemasters, J.J. and Herman, B. (1990) Cytosolic free magnesium, ATP and blebbing during chemical hypoxia in cultured rat hepatocytes. *Biochemical & Biophysical Research Communications* **170**, 477-483.

Hartzell, H.C. and White, R.E. (1989) Effects of Magnesium on INactivation of the Voltage-gated Calcium Current in Cardiac Myocytes. *J. Gen. Physiol.* **94**, 745-767.

Heinemann, S.H., Terlau, H., Stuhmer, W., Imoto, K. and Numa, S. (1992) Calcium channel characteristics conferred on the sodium channel by single mutations. *Nature* **356**, 441-443.

Hell, J.W., Westenbroek, R.E., Warner, C., Ahlijanian, M.K., Prystay, W., Gilbert, MM, Snutch, T.P. and Catterall, W.A. (1993) Identification and differential subcellular localization of the neuronal class C and class D L-type calcium channel alpha 1 subunits. *J. Cell. Biol.* **123**, 949-962.

Hell, J.W., Appleyard, S.M., Yokoyama, C.T., Warner, C. and Catterall, W.A. (1994a) Differential phosphorylation of two size forms of the N-type calcium channel alpha 1 subunit which have different COOH termini. *J. Biol. Chem.* **269**, 7390-7396.

Hell, J.W., Westenbroek, R.E., Elliott, E.M. and Catterall, W.A. (1994b) Differential phosphorylation, localization, and function of distinct a_1 subunits of neuronal calcium channels. Two size forms for class B, C, and D a_1 subunits with different COOH-termini. *Ann. NY Acad. Sci.* **747**, 282-293.

Henquin, J.C., Tamagawa, T., Nenquin, M. and Cogneau, M. (1983) Glucose modulates Mg2+ fluxes in pancreatic islet cells. *Nature* **301**, 73-74.

Hering, S., Hughes, A.D., Timin, E.N. and Bolton, T.B. (1993) Modulation of calcium channels in arterial smooth muscle cells by dihydropyridine enantiomers. *J. Gen. Physiol.* **101**, 393-410.

Herlitze, S., Garcia, D.E., Mackie, K., Hille, B., Scheuer, T. and Catterall, W.A. (1996) Modulation of Ca2+ channels by G-protein beta gamma subunits. *Nature* **380**, 258-262.

Hescheler, J., Pelzer, D., Trube, G. and Trautwein, W. (1982) Does the organic calcium channel blocker D600 act from inside or outside on the cardiac cell membrane? *Pflugers Archiv - European Journal of Physiology* **393**, 287-291.

Hescheler, J., Rosenthal, W., Trautwein, W. and Schultz, G. (1987) The GTP-binding protein, Go, regulates neuronal calcium channels. *Nature* **325**, 445-447.

Hescheler, J. and Trautwein, W. (1988) Modification of L-type calcium current by intracellularly applied trypsin in guinea-pig ventricular myocytes. *J. Physiol.* **404**, 259-274.

Hess, P., Lansman, J.B. and Tsien, R.W. (1984) Different modes of Ca channel gating behaviour favoured by dihydropyridine Ca agonists and antagonists. *Nature* **311**, 538-544.

Hess, P., Lansman, J.B. and Tsien, R.W. (1986) Calcium channel selectivity for divalent and monovalent cations. Voltage and concentration dependence of single channel current in ventricular heart cells. *J. Gen. Physiol.* **88**, 293-319.

Hess, P., Prod'hom, B. and Pietrobon, D. (1989) Mechanisms of interaction of permeant ions and protons with dihydropyridine-sensitive calcium channels. *Ann. NY Acad. Sci.* **560**, 80-93.

Hess, P. and Tsien, R.W. (1984) Mechanism of ion permeation through calcium channels. *Nature* **309**, 453-456.

Hille, B., Woodhull, A.M. and Shapiro, B.I. (1975) Negative surface charge near sodium channels of nerve: divalent ions, monovalent ions, and pH. *Philosophical Transactions of the Royal Society of London - Series B: Biological Sciences* **270**, 301-318.

Hille, B. (1977) Local anesthetics: hydrophilic and hydrophobic pathways for the drug-receptor reaction. *J. Gen. Physiol.* **69**, 497-515.

Hille, B. (1992) *Ionic Channels of Excitable Membranes.* Second edn. Sunderland, Massachusetts: Sinauer.

Hillyard, D.R., Monje, V.D., Mintz, I.M., Bean, B.P., Nadasdi, L., Ramachandran, J., Miljanich, G., Azimi-Zoonooz, A., McIntosh, J.M., Cruz, L.J. and et al. (1992) A new Conus peptide ligand for mammalian presynaptic Ca2+ channels. *Neuron* **9**, 69-77.

Hirano, T., Kubo, Y. and Wu, M. (1986) Cerebellar granule cells in culture: Monosynaptic connections with Purkinje cells and ionic currents. *Proceedings of the National Academy of Sciences USA* **83**, 4957-4961.

Hirano, T. and Hagiwara, S. (1988) Synaptic transmission between rat cerebellar granule and Purkinje cells in dissociated cell culture: Effects of excitatory-amino acid transmitter antagonists. *Proceedings of the National Academy of Sciences USA* **85**, 934-938.

Hockberger, P.E., Tseng, H. and Connor, J.A. (1987) Immunocytochemical and electrophysiological differentiation of rat cerebellar granule cells in explant cultures. *The journal of neuroscience* **7(5)**, 1370-1383.

Hockberger, P., Toselli, M., Swandulla, D. and Lux, H.D. (1989) A diacylglycerol analogue reduces neuronal calcium currents independently of protein kinase C activation. . *Nature* **338**, 340-342.

Hodgkin, A.L. and Huxley, A.F. (1952a) The components of membrane conductance in the giant axon of *Loligo*. *J. Physiol.* **116**, 473-496.

Hodgkin, A.L. and Huxley, A.F. (1952b) A quantitative description of membrane current and its application to conduction and excitation in nerve. *J. Physiol.* **117**, 500-544.

Hodgkin, A.L. and Huxley, A.F. (1952c) Currents carried by sodium and potassium ions through the membrane of the giant axon of *Loligo*. *J. Physiol.* **116**, 449-472.

Hodgkin, A.L. and Huxley, A.F. (1952d) The dual effect of membrane potential on sodium conductance in the giant axon of *Loligo*. *J. Physiol.* **116**, 497-506.

Holmes, G. (1939) The cerebellum of man. *Brain* **62**, 11-30.

Holz, G.G., 4th, Rane, S.G. and Dunlap, K. (1986) GTP-binding proteins mediate transmitter inhibition of voltage-dependent calcium channels. *Nature* **319**, 670-672.

Hondeghem, L.M. and Katzung, B.G. (1977) Time- and voltage-dependent interactions of antiarrhythmic drugs with cardiac sodium channels. [Review]. *BBA* **472**, 373-398.

Horne, W.A., Hawrot, E. and Tsien, R.W. (1991) omega-Conotoxin GVIA receptors of Discopyge electric organ. Characterization of omega-conotoxin binding to the nicotinic acetylcholine receptor. *J. Biol. Chem.* **266**, 13719-13725.

Horne, W.A., Ellinor, P.T., Inman, I., Zhou, M., Tsien, R.W. and Schwarz, T.L. (1993) Molecular diversity of Ca2+ channel alpha 1 subunits from the marine ray Discopyge ommata. *Proc. Natl. Acad. Sci. U. S. A.* **90**, 3787-3791.

Hovda, D.A., Fu, K., Badie, H., Samii, A., Pinanong, P. and Becker, D.P. (1994) Administration of an omega-conopeptide one hour following traumatic brain injury reduces 45calcium accumulation. *Acta Neurochirurgica - Supplementum* **60**, 521-523.

Huguenard, J.R. (1996) Low-threshold calcium currents in central nervous system neurones. *Ann. Rev. Physiol.* **58**, 329-348.

Huguenard, J.R. and Prince, D.A. (1992) A novel T-type current underlies prolonged Ca(2+)-dependent burst firing in GABAergic neurons of rat thalamic reticular nucleus. *J. Neurosci.* **12**, 3804-3817.

Hui, A., Ellinor, P.T., Krizanova, O., Wang, J.J., Diebold, R.J. and Schwartz, A. (1991) Molecular cloning of multiple subtypes of a novel rat brain isoform of the alpha 1 subunit of the voltage-dependent calcium channel. *Neuron* **7**, 35-44.

Huston, E., Scott, R.H. and Dolphin, A.C. (1990) A comparison of the effect of calcium channel ligands and GABAB agonists and antagonists on transmitter release and somatic calcium channel currents in cultured neurons. *Neuroscience* **38**, 721-729.

Huston, E., Cullen, G., Sweeney, M.I., Pearson, H., Fazeli, M.S. and Dolphin, A.C. (1993) Pertussis toxin treatment increases glutamate release and dihydropyridine binding sites in cultured rat cerebellar granule neurons. *Neuroscience* **52**, 787-798.

Huston, E., Cullen, G.P., Burley, J.R. and Dolphin, A.C. (1995) The involvement of multiple calcium channel sub-types in glutamate release from cerebellar granule cells and its modulation by GABAB receptor activation. *Neuroscience* **68**, 465-478.

Hymel, L., Striessnig, J., Glossmann, H. and Schindler, H. (1988) Purified skeletal muscle 1,4-dihydropyridine receptor forms phosphorylation-dependent oligomeric calcium channels in planar bilayers. *Proc. Natl. Acad. Sci. U. S. A.* **85**, 4290-4294.

Iino, M. and Endo, M. (1992) Calcium-dependent immediate feedback control of inositol 1,4,5-triphosphate-induced Ca2+ release. *Nature* **360**, 76-78.

Ikeda, S.R. (1996) Voltage-dependent modulation of N-type calcium channels by G-protein beta gamma subunits. *Nature* **380**, 255-258.

Isenberg, G. and Klockner, U. (1985) The electrophysiological properties of the isolated adult heart cell: an overview. *Basic Research in Cardiology* **80 Suppl 2**, 51-54.

Ishijima, S., Sonoda, T. and Tatibana, M. (1991) Mitogen-induced early increase in cytosolic free Mg2+ concentration in single Swiss 3T3 fibroblasts. *Am. J. Physiol.* **261**, C1074-80.

Jalonen, T., Johansson, S., Holopainen, I., Oja, S.S. and Arhem, P. (1990) Single-channel and whole-cell currents in rat cerebellar granule cells. *Brain Res.* **535**, 33-38.

Jay, S.D., Sharp, A.H., Kahl, S.D., Vedvick, T.S., Harpold, M.M. and Campbell, K.P. (1991) Structural characterization of the dihydropyridine-sensitive calcium channel alpha 2-subunit and the associated delta peptides. *J. Biol. Chem.* **266**, 3287-3293.

Jones, S.W. and Marks, T.N. (1989) Calcium currents in bullfrog sympathetic neurons. II. Inactivation. *J. Gen. Physiol.* **94**, 169-182.

Josephson, I.R. and Sperelakis, N. (1990) Fast activation of cardiac Ca++ channel gating charge by the dihydropyridine agonist, BAY K 8644. *Biophys. J.* **58**, 1307-1311.

Kanneganti, M. and Halpern, N.A. (1996) Acute hypertension and calcium-channel blockers. [Review]. *New Horizons* **4**, 19-25.

Kasai, H., Aosaki, T. and Fukuda, J. (1987) Presynaptic Ca-antagonist omega-conotoxin irreversibly blocks N-type Ca-channels in chick sensory neurons. *Neurosci. Res.* **4**, 228-235.

Kass, R.S. and Arena, J.P. (1989) Influence of pHo on calcium channel block by amlodipine, a charged dihydropyridine compound. Implications for location of the dihydropyridine receptor. *J. Gen. Physiol.* **93**, 1109-1127.

Kass, R.S. and Krafte, D.S. (1987) Negative surface charge density near heart calcium channels. Relevance to block by dihydropyridines. *J. Gen. Physiol.* **89**, 629-644.

Katz, B. and Miledi, R. (1967) The timing of calcium action during neuromuscular transmission. *J. Physiol.* **189**, 535-544.

Kim, H.L., Kim, H., Lee, P., King, R.G. and Chin, H. (1992) Rat brain expresses an alternatively spliced form of the dihydropyridine-sensitive L-type calcium channel alpha 2 subunit [published erratum appears in Proc Natl Acad Sci U S A 1992 Jun 15;89(12):5699]. *Proc. Natl. Acad. Sci. U. S. A.* **89**, 3251-3255.

Kokubun, S. and Reuter, H. (1984) Dihydropyridine derivatives prolong the open state of Ca channels in cultured cardiac cells. *Proc. Natl. Acad. Sci. U. S. A.* **81**, 4824-4827.

Kostyuk, P.G. (1983) The main principles of the organization of ionic channels which determine the excitability of the neuronal membrane. *Acta Morphologica Hungarica* **31**, 63-72.

Kostyuk, P.G., Shuba, Y.M. and Savchenko, A.N. (1986) Single channels of low- and high-threshold calcium currents in the membrane of the mouse sensory neurones. *Neurophysiology (Kiev)* **18**, 412-416.

Kostyuk, P.G., Shuba YaM and Savchenko, A.N. (1988) Three types of calcium channels in the membrane of mouse sensory neurons. *Pflugers Archiv - European Journal of Physiology* **411**, 661-669.

Kristipati, R., Nadasdi, L., Tarczy-Hornoch, K., Lau, K., Miljanich, G.P., Ramachandran, J. and Bell, J.R. (1994) Characterization of the binding of omega-conopeptides to different classes of non-L-type neuronal calcium channels. *Molecular & Cellular Neurosciences* **5**, 219-228.

Kuga, T., Sadoshima, J.I., Tomoike, H., Kanaide, H., Akaike, N. and Nakamura, M. (1990) Actions of Ca^{2+} antagonists on two types of Ca^{2+} channels in rat aorta smooth muscle cells in primary culture. *Circ. Res.* **67**, 469-480.

Lacerda, A.E., Rampe, D. and Brown, A.M. (1988) Effects of protein kinase C activators on cardiac Ca2+ channels. *Nature* **335**, 249-251.

Lacerda, A.E., Kim, H.S., Ruth, P., Perez-Reyes, E., Flockerzi, V., Hofmann, F., Birnbaumer, L. and Brown, A.M. (1991) Normalization of current kinetics by interaction between the alpha 1 and beta subunits of the skeletal muscle dihydropyridine-sensitive Ca2+ channel. *Nature* **352**, 527-530.

Lacerda, A.E., Perez-Reyes, E., Wei, X., Castellano, A. and Brown, A.M. (1994) T-type and N-type calcium channels of Xenopus oocytes: evidence for specific interactions with beta subunits. *Biophys. J.* **66**, 1833-1843.

Lacerda, A.E. and Brown, A.M. (1989) Nonmodal gating of cardiac calcium channels as revealed by dihydropyridines. *J. Gen. Physiol.* **93**, 1243-1273.

Lai, F.A., Anderson, K., Rousseau, E., Liu, Q.Y. and Meissner, G. (1988) Evidence for a Ca2+ channel within the ryanodine receptor complex from cardiac sarcoplasmic reticulum. *Biochemical & Biophysical Research Communications* **151**, 441-449.

Lansman, J.B., Hess, P. and Tsien, R.W. (1986) Blockade of current through single calcium channels by Cd2+, Mg2+, and Ca2+. Voltage and concentration dependence of calcium entry into the pore. *J. Gen. Physiol.* **88**, 321-347.

Lee, K.S., Marban, E. and Tsien, R.W. (1985) Inactivation of calcium channels in mammalian heart cells: joint dependence on membrane potential and intracellular calcium. *J. Physiol.* **364**, 395-411.

Lemos, J.R. and Nowycky, M.C. (1989) Two types of calcium channels coexist in peptide-releasing vertebrate nerve terminals. *Neuron* **2**, 1419-1426.

Leveque, C., el Far, O., Martin-Moutot, N., Sato, K., Kato, R., Takahashi, M. and Seagar, M.J. (1994) Purification of the N-type calcium channel associated with syntaxin and synaptotagmin. A complex implicated in synaptic vesicle exocytosis. *J. Biol. Chem.* **269**, 6306-6312.

Lin, F., Conti, F. and Moran, O. (1991) Competitive blockage of the sodium channel by intracellular magnesium ions in central mammalian neurones. *European Biophysics Journal* **19**, 109-118.

Llinas, R., Sugimori, M., Lin, J.W. and Cherksey, B. (1989) Blocking and isolation of a calcium channel from neurons in mammals and cephalopods utilizing a toxin fraction (FTX) from funnel-web spider poison. *Proc. Natl. Acad. Sci. U. S. A.* **86**, 1689-1693.

Llinas, R.R. (1982) Calcium in synaptic transmission. *Scientific American* **247**, 56-65.

London, R.E. (1991) Methods for measurement of intracellular magnesium: NMR and fluorescence. [Review]. *Ann. Rev. Physiol.* **53**, 241-258.

Lopatin, A.N., Makhina, E.N. and Nichols, C.G. (1994) Potassium channel block by cytoplasmic polyamines as the mechanism of intrinsic rectification. *Nature* **372**, 366-369.

Malenka, R.C., Ayoub, G.S. and Nicoll, R.A. (1987) Phorbol esters enhance transmitter release in rat hippocampal slices. *Brain Res.* **403**, 198-203.

Manev, H., Favaron, M., Guidotti, A. and Costa, E. (1989) Delayed increase of Ca2+ influx elicited by glutamate: role in neuronal death. *Molecular Pharmacology* **36**, 106-112.

Marchetti, C., Carignani, C. and Robello, M. (1991) Voltage-dependent calcium currents in dissociated granule cells from rat cerebellum. *Neuroscience* **43**, 121-133.

Marchetti, C., Amico, C. and Usai, C. (1995) Functional characterization of the effect of nimodipine on the calcium current in rat cerebellar granule cells. *Journal of Neurophysiology* **73**, 1169-1180.

Marks, T.N. and Jones, S.W. (1992) Calcium currents in the A7r5 smooth muscle-derived cell line. An allosteric model for calcium channel activation and dihydropyridine agonist action. *J. Gen. Physiol.* **99**, 367-390.

Marshall, J., Molloy, R., Moss, G.W., Howe, J.R. and Hughes, T.E. (1995) The jellyfish green fluorescent protein: a new tool for studying ion channel expression and function. *Neuron* **14**, 211-215.

Matsuda, H., Saigusa, A. and Irisawa, H. (1987) Ohmic conductance through the inwardly rectifying K channel and blocking by internal Mg2+. *Nature* **325**, 156-159.

McCarthy, R.T. and Cohen, C.J. (1989) Nimodipine block of calcium channels in rat vascular smooth muscle cell lines. Exceptionally high-affinity binding in A7r5 and A10 cells. *J. Gen. Physiol.* **94**, 669-692.

McCleskey, E.W., Fox, A.P., Feldman, D.H., Cruz, L.J., Olivera, B.M., Tsien, R.W. and Yoshikami, D. (1987) Omega-conotoxin: direct and persistent blockade of specific types of calcium channels in neurons but not muscle. *Proc. Natl. Acad. Sci. U. S. A.* **84**, 4327-4331.

McCormack, K., Tanouye, M.A., Iverson, L.E., Lin, J.W., Ramaswami, M., McCormack, T, Campanelli, J.T., Mathew, M.K. and Rudy, B. (1991) A role for

hydrophobic residues in the voltage-dependent gating of Shaker K+ channels. *Proc. Natl. Acad. Sci. U. S. A.* **88**, 2931-2935.

McDonald, T.F., Pelzer, S., Trautwein, W. and Pelzer, D.J. (1994) Regulation and modulation of calcium channels in cardiac, skeletal, and smooth muscle cells. [Review]. *Physiological Reviews* **74**, 365-507.

McDonough, S.I., Swartz, K.J., Mintz, I.M., Boland, L.M. and Bean, B.P. (1996) Inhibition of calcium channels in rat central and peripheral neurons by omega-conotoxin MVIIC. *J. Neurosci.* **16**, 2612-2623.

McEnery, M.W., Snowman, A.M., Sharp, A.H., Adams, M.E. and Snyder, S.H. (1991) Purified omega-conotoxin GVIA receptor of rat brain resembles a dihydropyridine-sensitive L-type calcium channel [published erratum appears in Proc Natl Acad Sci U S A 1992 Apr 1;89(7):3164]. *Proc. Natl. Acad. Sci. U. S. A.* **88**, 11095-11099.

Meldolesi, J., Clementi, E., Fasolato, C., Zacchetti, D. and Pozzan, T. (1991) Ca2+ influx following receptor activation [see comments]. [Review]. *TiPS* **12**, 289-292.

Menon-Johansson, A.S., Berrow, N. and Dolphin, A.C. (1993) G(o) transduces GABAB-receptor modulation of N-type calcium channels in cultured dorsal root ganglion neurons. *Pflugers Archiv - European Journal of Physiology* **425**, 335-343.

Mikami, A., Imoto, K., Tanabe, T., Niidome, T., Mori, Y., Takeshima, H., Narumiya, S. and Numa, S. (1989) Primary structure and functional expression of the cardiac dihydropyridine-sensitive calcium channel. *Nature* **340**, 230-233.

Miller, R.J. (1987) Multiple calcium channels and neuronal function. [Review]. *Science* **235**, 46-52.

Mintz, I.M., Adams, M.E. and Bean, B.P. (1992a) P-type calcium channels in rat central and peripheral neurons. *Neuron* **9**, 85-95.

Mintz, I.M., Venema, V.J., Swiderek, K.M., Lee, T.D., Bean, B.P. and Adams, M.E. (1992b) P-type calcium channels blocked by the spider toxin omega-Aga-IVA. *Nature* **355**, 827-829.

Mintz, I.M. (1994) Block of Ca channels in rat central neurons by the spider toxin omega-Aga-IIIA. *J. Neurosci.* **14**, 2844-2853.

Mintz, I.M. and Bean, B.P. (1993a) Block of calcium channels in rat neurons by synthetic omega-Aga-IVA. *Neuropharmacology* **32**, 1161-1169.

Mintz, I.M. and Bean, B.P. (1993b) GABAB receptor inhibition of P-type Ca2+ channels in central neurons. *Neuron* **10**, 889-898.

Monje, V.D., Haack, J.A., Naisbitt, S.R., Miljanich, G., Ramachandran, J., Olivera, B.M., Hillyard, D.R. and Gray, W.R. (1993) A new Conus peptide ligand for Ca channel subtypes. *Neuropharmacology* **32**, 1141-1149.

Mori, Y., Friedrich, T., Kim, M., Mikami, A., Nakai, J., Ruth, P., Bosse, E., Hofmann, F., Flockerzi, V., Furuichi, T., Mikoshiba, K., Imoto, K., Tanabe, T. and Numa, S. (1991) Primary structure and functional expression from complementary DNA of a brain calcium channel. *Nature* **350**, 398-402.

Muller, R.U. and Finkelstein, A. (1974) The electrostatic basis of Mg++ inhibition of transmitter release. *Proc. Natl. Acad. Sci. U. S. A.* **71**, 923-926.

Murphy, E., Freudenrich, C.C., Levy, L.A., London, R.E. and Lieberman, M. (1989) Monitoring cytosolic free magnesium in cultured chicken heart cells by use of the fluorescent indicator Furaptra. *Proc. Natl. Acad. Sci. U. S. A.* **86**, 2981-2984.

Murphy, E., Freudenrich, C.C. and Lieberman, M. (1991) Cellular magnesium and Na/Mg exchange in heart cells. [Review]. *Ann. Rev. Physiol.* **53**, 273-287.

Murphy, T.H., Worley, P.F. and Baraban, J.M. (1991) L-type voltage-sensitive calcium channels mediate synaptic activation of immediate early genes. *Neuron* **7**, 625-635.

Mynlieff, M. and Beam, K.G. (1992) Characterization of voltage-dependent calcium currents in mouse motoneurons. *Journal of Neurophysiology* **68**, 85-92.

Nakayama, H., Taki, M., Striessnig, J., Glossmann, H., Catterall, W.A., Kanaoka and Y. (1991) Identification of 1,4-dihydropyridine binding regions within the alpha 1 subunit of skeletal muscle Ca2+ channels by photoaffinity labeling with diazipine. *Proc. Natl. Acad. Sci. U. S. A.* **88**, 9203-9207.

Neely, A., Wei, X., Olcese, R., Birnbaumer, L. and Stefani, E. (1993) Potentiation by the beta subunit of the ratio of the ionic current to the charge movement in the cardiac calcium channel. *Science* **262**, 575-578.

Neher, E. (1992) Correction for liquid junction potentials in patch clamp experiments. *Methods in Enzymology* **207**, 123-131.

Neher, E. and Sakmann, B. (1976) Single-channel currents recorded from membrane of denervated frog muscle fibres. *Nature* **260**, 799-802.

Nernst, E. (1888) Zur Kinetik der in Losung befindlichen Korper: Theorie der Diffusion. *Z. Phys. Chem.* 613-637.

Neveu, D., Nargeot, J. and Richard, S. (1993) Two high-voltage-activated, dihydropyridine-sensitive Ca2+ channel currents with distinct electrophysiological and pharmacological properties in cultured rat aortic myocytes. *Pflugers Archiv - European Journal of Physiology* **424**, 45-53.

Niidome, T., Kim, M.S., Friedrich, T. and Mori, Y. (1992) Molecular cloning and characterization of a novel calcium channel from rabbit brain. *FEBS Lett.* **308**, 7-13.

Nowycky, M.C., Fox, A.P. and Tsien, R.W. (1985a) Long-opening mode of gating of neuronal calcium channels and its promotion by the dihydropyridine calcium agonist Bay K 8644. *Proc. Natl. Acad. Sci. U. S. A.* **82**, 2178-2182.

Nowycky, M.C., Fox, A.P. and Tsien, R.W. (1985b) Three types of neuronal calcium channel with different calcium agonist sensitivity. *Nature* **316**, 440-443.

Nunoki, K., Florio, V. and Catterall, W.A. (1989) Activation of purified calcium channels by stoichiometric protein phosphorylation. *Proc. Natl. Acad. Sci. U. S. A.* **86**, 6816-6820.

Okabe, K., Terada, K., Kitamura, K. and Kuriyama, H. (1987) Selective and long-lasting inhibitory actions of the dihydropyridine derivative, CV-4093, on calcium currents in smooth muscle cells of the rabbit pulmonary artery. *Journal of Pharmacology & Experimental Therapeutics* **243**, 703-710.

Olcese, R., Qin, N., Schneider, T., Neely, A., Wei, X., Stefani, E., Birnbaumer and L. (1994) The amino terminus of a calcium channel beta subunit sets rates of channel inactivation independently of the subunit's effect on activation. *Neuron* **13**, 1433-1438.

Olivera, B.M., Miljanich, G.P., Ramachandran, J. and Adams, M.E. (1994) Calcium channel diversity and neurotransmitter release: the omega-conotoxins and omega-agatoxins. [Review]. *Ann. Rev. Biochem.* **63**, 823-867.

Ono, K. and Fozzard, H.A. (1992) Phosphorylation restores activity of L-type calcium channels after rundown in inside-out patches from rabbit cardiac cells. *Journal of Physiology - London* **454**, 673-688.

Pearson, H.A., Sutton, K.G., Scott, R.H. and Dolphin, A.C. (1993) Ca2+ currents in cerebellar granule neurones: role of internal Mg2+ in altering characteristics and antagonist effects. *Neuropharmacology* **32**, 1171-1183.

Pearson, H.A., Sutton, K.G., Scott, R.H. and Dolphin, A.C. (1995) Characterization of Ca2+ channel currents in cultured rat cerebellar granule neurones. *J. Physiol.* **482**, 493-509.

Pearson, H.A. and Dolphin, A.C. (1993a) Inhibition of omega-conotoxin-sensitive Ca2+ channel currents by internal Mg2+ in cultured rat cerebellar granule neurones. *Pflugers Archives* **425**, 518-527.

Pearson, H.A. and Dolphin, A.C. (1993b) Internal Mg/nucleotide levels alter Ca2+ channel characteristics and responses to (-)-baclofen in cultures rat cerebellar granule neurones. *J. Physiol.* **459**, 402P

Pelzer, D., Trautwein, W. and McDonald, T.F. (1982) Calcium channel block and recovery from block in mammalian ventricular muscle treated with organic channel inhibitors. *Pflugers Archiv - European Journal of Physiology* **394**, 97-105.

Perez-Reyes, E., Kim, H.S., Lacerda, A.E., Horne, W., Wei, X.Y., Rampe, D., Campbell, K.P., Brown, A.M. and Birnbaumer, L. (1989) Induction of calcium currents by the expression of the alpha 1-subunit of the dihydropyridine receptor from skeletal muscle. *Nature* **340**, 233-236.

Perez-Reyes, E., Wei, X.Y., Castellano, A. and Birnbaumer, L. (1990) Molecular diversity of L-type calcium channels. Evidence for alternative splicing of the transcripts of three non-allelic genes. *J. Biol. Chem.* **265**, 20430-20436.

Perez-Reyes, E., Castellano, A., Kim, H.S., Bertrand, P., Baggstrom, E., Lacerda, AE, Wei, X.Y. and Birnbaumer, L. (1992) Cloning and expression of a cardiac/brain beta subunit of the L-type calcium channel. *J. Biol. Chem.* **267**, 1792-1797.

Perez-Reyes, E. and Schneider, T. (1994) Calcium Channels: Structure, Function, and Classification. *Drug Development Research* **33**, 295-318.

Plummer, M.R., Logothetis, D.E. and Hess, P. (1989) Elementary properties and pharmacological sensitivities of calcium channels in mammalian peripheral neurons. *Neuron* **2**, 1453-1463.

Plummer, M.R. and Hess, P. (1991) Reversible uncoupling of inactivation in N-type calcium channels. *Nature* **351**, 657-659.

Pragnell, M., De Waard, M., Mori, Y., Tanabe, T., Snutch, T.P. and Campbell, K.P. (1994) Calcium channel beta-subunit binds to a conserved motif in the I-II cytoplasmic linker of the alpha 1-subunit [see comments]. *Nature* **368**, 67-70.

Pusch, M., Conti, F. and Stuhmer, W. (1989) Intracellular magnesium blocks sodium outward currents in a voltage- and dose-dependent manner. *Biophys. J.* **55**, 1267-1271.

Pusch, M. (1990a) Divalent cations as probes for structure-function relationships of cloned voltage-dependent sodium channels. *European Biophysics Journal* **18**, 327-333.

Pusch, M. (1990b) Open-channel block of Na+ channels by intracellular Mg2+. *European Biophysics Journal* **18**, 317-326.

Rajdev, S., Rothermund, K. and Reynolds, I.J. (1991) Relationship between changes in intracellular free calcium ($[Ca^{2+}]_i$) and neurotoxicity. *Society for Neuroscience* **17**, (Abstract)

Raju, B., Murphy, E., Levy, L.A., Hall, R.D. and London, R.E. (1989) A fluorescent indicator for measuring cytosolic free magnesium. *Am. J. Physiol.* **256**, C540-8.

Ramon y Cajal, S. (1911) *Histologie due systeme nerveux de l'homme et des vertebres.* Paris: Maloine.

Randall, A. and Tsien, R.W. (1995) Pharmacological dissection of multiple types of Ca2+ channel currents in rat cerebellar granule neurons. *J. Neurosci.* **15**, 2995-3012.

Rane, S.G., Walsh, M.P., McDonald, J.R. and Dunlap, K. (1989) Specific inhibitors of protein kinase C block transmitter-induced modulation of sensory neuron calcium current. *Neuron* **3**, 239-245.

Regan, L.J., Sah, D.W. and Bean, B.P. (1991) Ca2+ channels in rat central and peripheral neurons: high-threshold current resistant to dihydropyridine blockers and omega-conotoxin. *Neuron* **6**, 269-280.

Regan, R.F. and Choi, D.W. (1994) The effect of NMDA, AMPA/kainate, and calcium channel antagonists on traumatic cortical neuronal injury in culture. *Brain Res.* **633**, 236-242.

Regulla, S., Schneider, T., Nastainczyk, W., Meyer, H.E. and Hofmann, F. (1991) Identification of the site of interaction of the dihydropyridine channel blockers nitrendipine and azidopine with the calcium-channel alpha 1 subunit. *EMBO J.* **10**, 45-49.

Richard, S., Diochot, S., Nargeot, J., Baldy-Moulinier, M. and Valmier, J. (1991) Inhibition of T-type calcium currents by dihydropyridines in mouse embryonic dorsal root ganglion neurons. *Neurosci. Letts.* **132**, 229-234.

Ringer, S. (1882) Concerning the influence exerted by each of the constituents of the blood on the contraction of the ventricle. *J. Physiol.* **2**, 380-393.

Ringer, S. (1883a) A further contribution regarding the influence of the different constituents of the blood on the contraction of the heart. *J. Physiol.* **4**, 29-42.

Ringer, S. (1883b) An investigation regarding the action of rubidium and caesium salts compared with the action of potassium salts on the ventricle of the frog's heart. *J. Physiol.* **4**, 371-379.

Robbins, J., Cloues, R. and Brown, D.A. (1992) Intracellular Mg2+ inhibits the IP3-activated IK(Ca) in NG108-15 cells. [Why intracellular citrate can be useful for recording IK(Ca)]. *Pflugers Archiv - European Journal of Physiology* **420**, 347-353.

Robello, M., Carignani, C. and Marchetti, C. (1989) A transient voltage-dependent outward current in cultured cerebellar granules. *Bioscience Reports* **9**, 451-457.

Rohrkasten, A., Meyer, H.E., Nastainczyk, W., Sieber, M. and Hofmann, F. (1988) cAMP-dependent protein kinase rapidly phosphorylates serine- 687 of the skeletal muscle receptor for calcium channel blockers. *J. Biol. Chem.* **263**, 15325-15329.

Romani, A. and Scarpa, A. (1992) Regulation of cell magnesium. [Review]. *Archives of Biochemistry & Biophysics* **298**, 1-12.

Rossi, P., D'Angelo, E., Magistretti, J., Toselli, M. and Taglietti, V. (1994) Age-dependent expression of high-voltage activated calcium currents during cerebellar granule cell development in situ. *Br. J. Pharmacol.* **99**, 629-630.

Roux, M.J., Tareilus, E., Qin, N., Birnbaumer, L. and Stefani, E. (1996) Molecular cloning of a functional *Xenopus* oocyte calcium channel b subunit. *Biophysics Journal* **70**, A317(Abstract)

Rubin, H. (1976) Magnesium deprivation reproduces the coordinate effects of serum removal or cortisol addition on transport and metabolism in chick embryo fibroblasts. *Journal of Cellular Physiology* **89**, 613-625.

Ruth, P., Rohrkasten, A., Biel, M., Bosse, E., Regulla, S., Meyer, H.E., Flockerzi, V. and Hofmann, F. (1989) Primary structure of the beta subunit of the DHP-sensitive calcium channel from skeletal muscle. *Science* **245**, 1115-1118.

Sanchez, J.A. and Stefani, E. (1978) Inward calcium current in twitch muscle fibres of the frog. *J. Physiol.* **283**, 197-209.

Sather, W.A., Tanabe, T., Zhang, J.-F., Mori, Y., Adams, M.E. and Tsien, R.W. (1993) Distinctive Biophysical and Pharmacological Properties of Class A (BI) Calcium Channel a1 Subunits. *Neuron* **11**, 291-303.

Schneider, T., Wei, X., Olcese, R., Costantin, J.L., Neely, A., Palade, P., Perez-Reyes, E., Qin, N., Zhou, J., Crawford, G.D. and et al. (1994) Molecular analysis and functional expression of the human type E neuronal Ca2+ channel alpha 1 subunit. *Receptors & Channels* **2**, 255-270.

Schramm, M., Thomas, G., Towart, R. and Franckowiak, G. (1983) Novel dihydropyridines with positive inotropic action through activation of Ca2+ channels. *Nature* **303**, 535-537.

Schroeder, J.E., Fischbach, P.S. and McCleskey, E.W. (1990) T-type calcium channels: heterogeneous expression in rat sensory neurons and selective modulation by phorbol esters. *J. Neurosci.* **10**, 947-951.

Schuurman, T. (1993) Effect of calcium antagonists on memory and sensorimotor functions of aged animals. *Neuroscience Research Communications* **13**, 59-62.

Schuurman, T. and Traber, J. (1994) Calcium antagonists in aging brain. *Ann. NY Acad. Sci.* **747**, 467-474.

Sciancalepore, M., Forti, L. and Moran, O. (1989) Changes of N-methyl-D-aspartate activated channels of cerebellar granule cells with days in culture. *Biochemical & Biophysical Research Communications* **165**, 481-487.

Scott, R.H., Dolphin, A.C., Bindokas, V.P. and Adams, M.E. (1990) Inhibition of neuronal Ca2+ channel currents by the funnel web spider toxin omega-Aga-IA. *Molecular Pharmacology* **38**, 711-718.

Scott, R.H., Pearson, H.A. and Dolphin, A.C. (1991) Aspects of vertebrate neuronal voltage-activated calcium currents and their regulation. [Review]. *Prog. Neurobiol.* **36**, 485-520.

Sculptoreanu, A., Scheuer, T. and Catterall, W.A. (1993) Voltage-dependent potentiation of L-type Ca2+ channels due to phosphorylation by cAMP-dependent protein kinase. *Nature* **364**, 240-243.

Seino, S., Chen, L., Seino, M., Blondel, O., Takeda, J., Johnson, J.H. and Bell, G.I. (1992) Cloning of the alpha 1 subunit of a voltage-dependent calcium channel expressed in pancreatic beta cells. *Proc. Natl. Acad. Sci. U. S. A.* **89**, 584-588.

Shimono, T., Nosaka, S. and Sasaki, K. (1976) Electrophysiological study on the postnatal development of neuronal mechanisms in the rat cerebellar cortex. *Brain Res.* **108**, 279-294.

Sinton, C.M., Krosser, B.I., Walton, K.D. and Llinas, R.R. (1989) The effectiveness of different isomers of octanol as blockers of harmaline-induced tremor. *Pflugers Archives* **414**, 31-36.

Skryma, R., Prevarskaya, N., Vacher, P. and Dufy, B. (1994) Voltage-dependent ionic conductances in Chinese hamster ovary cells. *Am. J. Physiol.* **267**, C544-53.

Slesinger, P.A. and Lansman, J.B. (1991a) Inactivating and non-inactivating dihydropyridine-sensitive Ca2+ channels in mouse cerebellar granule cells. *Journal of Physiology - London* **439**, 301-323.

Slesinger, P.A. and Lansman, J.B. (1991b) Inactivation of calcium currents in granule cells cultured from mouse cerebellum. *J. Physiol.* **435**, 101-121.

Slesinger, P.A. and Lansman, J.B. (1991c) Reopening of Ca2+ channels in mouse cerebellar neurons at resting membrane potentials during recovery from inactivation. *Neuron* **7**, 755-762.

Slesinger, P.A. and Lansman, J.B. (1996) Reopening of single L-type Ca^{2+} channels in mouse cerebellar granule cells: dependence on voltage and ion concentration. *J. Physiol.* **491**, 335-345.

Smith, J.S., Coronado, R. and Meissner, G. (1986) Single Channel Measurements of the Calcium Release Channel from Skeletal Muscle Sarcoplasmic Reticulum. *J. Gen. Physiol.* **88**, 573-588.

Snutch, T.P., Tomlinson, W.J., Leonard, J.P. and Gilbert, M.M. (1991) Distinct calcium channels are generated by alternative splicing and are differentially expressed in the mammalian CNS. *Neuron* **7**, 45-57.

Somlyo, A.P. and Walz, B. (1985) Elemental distribution in Rana pipiens retinal rods: quantitative electron probe analysis. *J. Physiol.* **358**, 183-195.

Soong, T.W., Stea, A., Hodson, C.D., Dubel, S.J., Vincent, S.R. and Snutch, T.P. (1993) Structure and functional expression of a member of the low voltage-activated calcium channel family. *Science* **260**, 1133-1136.

Starr, T.V., Prystay, W. and Snutch, T.P. (1991) Primary structure of a calcium channel that is highly expressed in the rat cerebellum. *Proc. Natl. Acad. Sci. U. S. A.* **88**, 5621-5625.

Stea, A., Dubel, S.J., Pragnell, M., Leonard, J.P., Campbell, K.P. and Snutch, T.P. (1993) A beta-subunit normalizes the electrophysiological properties of a cloned N-type Ca2+ channel alpha 1-subunit. *Neuropharmacology* **32**, 1103-1116.

Stea, A., Tomlinson, W.J., Soong, T.W., Bourinet, E., Dubel, S.J., Vincent, S.R. and Snutch, T.P. (1994) Localization and functional properties of a rat brain alpha 1A calcium channel reflect similarities to neuronal Q- and P-type channels. *Proc. Natl. Acad. Sci. U. S. A.* **91**, 10576-10580.

Stephens, G.J., Page, K.M., Burley, J.R., Berrow, N.S. and Dolphin, A.C. (1997) Functional expression of rat brain cloned a_{1E} calcium channels in COS-7 cells. *Pflugers Archives* **433**, 523-532.

Stewart, R.R., Bossu, J.L., Muzet, M., Dupont, J.L. and Feltz, A. (1995) Voltage-activated ionic currents in differentiating rat cerebellar granule neurons cultured from the external germinal layer. *Journal of Neurobiology* **28**, 419-432.

Striessnig, J., Moosburger, K., Goll, A., Ferry, D.R. and Glossmann, H. (1986) Stereoselective photoaffinity labelling of the purified 1,4-dihydropyridine receptor of the voltage-dependent calcium channel. *Eur. J. Biochem.* **161**, 603-609.

Striessnig, J., Murphy, B.J. and Catterall, W.A. (1991) Dihydropyridine receptor of L-type Ca2+ channels: identification of binding domains for [3H](+)-PN200-110 and [3H]azidopine within the alpha 1 subunit. *Proc. Natl. Acad. Sci. U. S. A.* **88**, 10769-10773.

Strong, J.A. and Scott, S.A. (1992) Divalent-selective voltage-independent calcium channels in Lymnaea neurons: permeation properties and inhibition by intracellular magnesium. *J. Neurosci.* **12**, 2993-3003.

Stuhmer, W., Ruppersberg, J.P., Schroter, K.H., Sakmann, B., Stocker, M., Giese, KP, Perschke, A., Baumann, A. and Pongs, O. (1989) Molecular basis of functional diversity of voltage-gated potassium channels in mammalian brain. *EMBO J.* **8**, 3235-3244.

Takahashi, K. and Akaike, N. (1991) Calcium antagonist effects on low-threshold (T-type) calcium current in rat isolated hippocampal CA1 pyramidal neurons. *Journal of Pharmacology and Experimental Therapeutics* **256**, 169-175.

Takahashi, M., Seagar, M.J., Jones, J.F., Reber, B.F. and Catterall, W.A. (1987) Subunit structure of dihydropyridine-sensitive calcium channels from skeletal muscle. *Proc. Natl. Acad. Sci. U. S. A.* **84**, 5478-5482.

Tanabe, T., Takeshima, H., Mikami, A., Flockerzi, V., Takahashi, H., Kangawa, K., Kojima, M., Matsuo, H., Hirose, T. and Numa, S. (1987) Primary structure of the receptor for calcium channel blockers from skeletal muscle. *Nature* **328**, 313-318.

Tanabe, T., Beam, K.G., Powell, J.A. and Numa, S. (1988) Restoration of excitation-contraction coupling and slow calcium current in dysgenic muscle by dihydropyridine receptor complementary DNA. *Nature* **336**, 134-139.

Tang, C.M., Presser, F. and Morad, M. (1988) Amiloride selectively blocks the low threshold (T) calcium channel. *Science* **240**, 213-215.

Tang, S., Mikala, G., Bahinski, A., Yatani, A., Varadi, G. and Schwartz, A. (1993a) Molecular localization of ion selectivity sites within the pore of a human L-type cardiac calcium channel. *J. Biol. Chem.* **268**, 13026-13029.

Tang, S., Yatani, A., Bahinski, A., Mori, Y. and Schwartz, A. (1993b) Molecular localization of regions in the L-type calcium channel critical for dihydropyridine action. *Neuron* **11**, 1013-1021.

Thibault, O., Porter, N.M. and Landfield, P.W. (1993) Low Ba2+ and Ca2+ induce a sustained high probability of repolarization openings of L-type Ca2+ channels in hippocampal neurons: physiological implications. *Proc. Natl. Acad. Sci. U. S. A.* **90**, 11792-11796.

Tottene, A., Moretti, A. and Pietrobon, D. (1996) Functional diversity of P-type and R-type calcium channels in rat cerebellar neurones. *The journal of neuroscience* **16**, 6353-6363.

Traynelis, S.F., Silver, R.A. and Cull-Candy, S.G. (1993) Estimated conductance of glutamate receptor channels activated during EPSCs at the cerebellar mossy fiber-granule cell synapse. *Neuron* **11**, 279-289.

Triggle, D.J. and Swamy, V.C. (1983) Calcium antagonists. Some chemical-pharmacologic aspects. [Review]. *Circ. Res.* **52**, I17-28.

Tsien, R.W., Hess, P., McCleskey, E.W. and Rosenberg, R.L. (1987) Calcium channels: mechanisms of selectivity, permeation, and block. [Review]. *Annual Review of Biophysics & Biophysical Chemistry* **16**, 265-290.

Tsien, R.W., Lipscombe, D., Madison, D.V., Bley, K.R. and Fox, A.P. (1988) Multiple types of neuronal calcium channels and their selective modulation. *Trends in Neuroscience* **11(10)**, 431-438.

Tsien, R.Y., Pozzan, T. and Rink, T.J. (1982) Calcium homeostasis in intact lymphocytes: cytoplasmic free calcium monitored with a new, intracellularly trapped fluorescent indicator. *J. Cell. Biol.* **94**, 325-334.

Tsien, R.Y. and Poenie, M. (1986) Fluorescence ratio imaging: a new window into intracellular ionic signalling. *Trends in Biological Sciences* **11**, 450-455.

Usowicz, M.M., Sugimori, M., Cherksey, B. and Llinas, R. (1992) P-type calcium channels in the somata and dendrites of adult cerebellar Purkinje cells. *Neuron* **9**, 1185-1199.

Vaghy, P.L., Striessnig, J., Miwa, K., Knaus, H.G., Itagaki, K., McKenna, E., Glossmann, H. and Schwartz, A. (1987) Identification of a novel 1,4-dihydropyridine- and phenylalkylamine-binding polypeptide in calcium channel preparations. *J. Biol. Chem.* **262**, 14337-14342.

Valdivia, H.H. and Coronado, R. (1990) Internal and external effects of dihydropyridines in the calcium channel of skeletal muscle. *J. Gen. Physiol.* **95**, 1-27.

Valentino, K., Newcomb, R., Gadbois, T., Singh, T., Bowersox, S., Bitner, S., Justice, A., Yamashiro, D., Hoffman, B.B., Ciaranello, R. and et al. (1993) A selective N-type calcium channel antagonist protects against neuronal loss after global cerebral ischemia. *Proc. Natl. Acad. Sci. U. S. A.* **90**, 7894-7897.

Varadi, G., Mikala, G., Lory, P., Varadi, M., Drouet, B., Pincon-Raymond, M. and Schwartz, A. (1995) Endogenous cardiac Ca2+ channels do not overcome the E-C coupling defect in immortalized dysgenic muscle cells: evidence for a missing link. *FEBS Lett.* **368**, 405-410.

Venema, V.J., Swiderek, K.M., Lee, T.D., Hathaway, G.M. and Adams, M.E. (1992) Antagonism of synaptosomal calcium channels by subtypes of omega-agatoxins. *J. Biol. Chem.* **267**, 2610-2615.

Vicini, S., Wroblewski, J.T. and Costa, E. (1986) Pharmacological modulation of gabaergic transmission in cultured cerebellar neurons. *Neuropharmacology* **25(2)**, 207-211.

Vivaudou, M.B., Clapp, L.H., Walsh, J.V., Jr. and Singer, J.J. (1988) Regulation of one type of Ca2+ current in smooth muscle cells by diacylglycerol and acetylcholine. *FASEB Journal* **2**, 2497-2504.

Wacker, W.E. (1969) The biochemistry of magnesium. *Ann. NY Acad. Sci.* **162**, 717-726.

Wacker, W.E.C. (1980) *Magnesium and Man.* Cambridge, Massachusetts: Harvard University Press.

Wakade, A.R., Malhotra, R.K. and Wakade, T.D. (1985) Phorbol ester, an activator of protein kinase C, enhances calcium-dependent release of sympathetic neurotransmitter. *Naunyn-Schmiedebergs Archives of Pharmacology* **331**, 122-124.

Wakamori, M., Niidome, T., Furutama, D., Furuichi, T., Mikoshiba, K., Fujita, Y., Tanaka, I., Katayama, K., Yatani, A., Schwartz, A. and et al. (1994) Distinctive functional properties of the neuronal BII (class E) calcium channel. *Receptors & Channels* **2**, 303-314.

Wei, X.Y., Perez-Reyes, E., Lacerda, A.E., Schuster, G., Brown, A.M., Birnbaumer and L. (1991) Heterologous regulation of the cardiac Ca2+ channel alpha 1 subunit by skeletal muscle beta and gamma subunits. Implications for the structure of cardiac L-type Ca2+ channels. *J. Biol. Chem.* **266**, 21943-21947.

Weiss, J.H., Hartley, D.M., Koh, J. and Choi, D.W. (1990) The calcium channel blocker nifedipine attenuates slow excitatory amino acid neurotoxicity. *Science* **247**, 1474-1477.

Westenbroek, R.E., Hell, J.W., Warner, C., Dubel, S.J., Snutch, T.P. and Catterall, W.A. (1992) Biochemical properties and subcellular distribution of an N-type calcium channel alpha 1 subunit. *Neuron* **9**, 1099-1115.

Westenbroek, R.E., Sakurai, T., Elliott, E.M., Hell, J.W., Starr, T.V., Snutch, T.P. and Catterall, W.A. (1995) Immunochemical identification and subcellular distribution of the alpha 1A subunits of brain calcium channels. *J. Neurosci.* **15**, 6403-6418.

Wheeler, D.B., Randall, A. and Tsien, R.W. (1994) Roles of N-type and Q-type Ca2+ channels in supporting hippocampal synaptic transmission [see comments]. *Science* **264**, 107-111.

White, R.E. and Hartzell, H.C. (1988) Effects of Intracellular Free Magnesium on Calcium Current in Isolated Cardiac Myocytes. *Science* **239**, 778-780.

White, R.E. and Hartzell, H.C. (1989) Magnesium ions in cardiac function. Regulator of ion channels and second messengers. [Review]. *Biochemical Pharmacology* **38**, 859-867.

White, W.F., Nadler, J.V. and Cotman, C.W. (1979) The effect of acidic amino acid antagonists on synaptic transmission in the hippocampal formation in vitro. *Brain Res.* **164**, 177-194.

Wickens, J.R. and Abraham, W.C. (1991) The involvement of L-type calcium channels in heterosynaptic long-term depression in the hippocampus. *Neurosci. Letts.* **130**, 128-132.

Williams, M.E., Brust, P.F., Feldman, D.H., Patthi, S., Simerson, S., Maroufi, A., McCue, A.F., Velicelebi, G., Ellis, S.B. and Harpold, M.M. (1992a) Structure and functional expression of an omega-conotoxin-sensitive human N-type calcium channel. *Science* **257**, 389-395.

Williams, M.E., Feldman, D.H., McCue, A.F., Brenner, R., Velicelebi, G., Ellis, S.B. and Harpold, M.M. (1992b) Structure and functional expression of alpha 1, alpha 2, and beta subunits of a novel human neuronal calcium channel subtype. *Neuron* **8**, 71-84.

Williams, M.E., Marubio, L.M., Deal, C.R., Hans, M., Brust, P.F., Philipson, L.H., Miller, R.J., Johnson, E.C., Harpold, M.M. and Ellis, S.B. (1994) Structure and functional characterization of neuronal alpha 1E calcium channel subtypes. *J. Biol. Chem.* **269**, 22347-22357.

Wiser, O., Trus, M., Tobi, D., Halevi, S., Giladi, E. and Atlas, D. (1996) The alpha 2/delta subunit of voltage sensitive Ca2+ channels is a single transmembrane extracellular protein which is involved in regulated secretion. *FEBS Lett.* **379**, 15-20.

Witcher, D.R., De Waard, M. and Campbell, K.P. (1993) Characterization of the purified N-type Ca2+ channel and the cation sensitivity of omega-conotoxin GVIA binding. *Neuropharmacology* **32**, 1127-1139.

Worley, J.F., Quayle, J.M., Standen, N.B. and Nelson, M.T. (1991) Regulation of single calcium channels in cerebral arteries by voltage, serotonin, and dihydropyridines. *Am. J. Physiol.* **261**, H1951-60.

Yaney, G.C., Wheeler, M.B., Wei, X., Perez-Reyes, E., Birnbaumer, L., Boyd, A.E., 3d and Moss, L.G. (1992) Cloning of a novel alpha 1-subunit of the voltage-dependent calcium channel from the beta-cell. *Molecular Endocrinology* **6**, 2143-2152.

Yang, J. and Tsien, R.W. (1993) Enhancement of N- and L-type calcium channel currents by protein kinase C in frog sympathetic neurons. *Neuron* **10**, 127-136.

Yokoyama, C.T., Westenbroek, R.E., Hell, J.W., Soong, T.W., Snutch, T.P., Catterall and WA. (1995) Biochemical properties and subcellular distribution of the neuronal class E calcium channel alpha 1 subunit. *J. Neurosci.* **15**, 6419-6432.

Yoshida, A., Oho, C., Omori, A., Kuwahara, R., Ito, T. and Takahashi, M. (1992) HPC-1 is associated with synaptotagmin and omega-conotoxin receptor. *J. Biol. Chem.* **267**, 24925-24928.

Yoshikami, D., Bagabaldo, Z. and Olivera, B.M. (1989) The inhibitory effects of omega-conotoxins on Ca channels and synapses. *Ann. NY Acad. Sci.* **560**, 230-248.

Yu, C., Lin, P.X., Fitzgerald, S. and Nelson, P. (1992) Heterogeneous calcium currents and transmitter release in cultured mouse spinal cord and dorsal root ganglion neurons. *Journal of Neurophysiology* **67**, 561-575.

Zamponi, G.W., Bourinet, E., Nelson, D., Nargeot, J. and Snutch, T.P. (1997) Crosstalk between G proteins and protein kinase C mediated by the calcium channel a_1 subunit. *Nature* **385**, 442-445.

Zhang, J.F., Randall, A.D., Ellinor, P.T., Horne, W.A., Sather, W.A., Tanabe, T. and Tsien, R.W. (1993) Distinctive pharmacology and kinetics of cloned neuronal Ca2+ channels and their possible counterparts in mammalian CNS neurons. [Review]. *Neuropharmacology* **32**, 1075-1088.